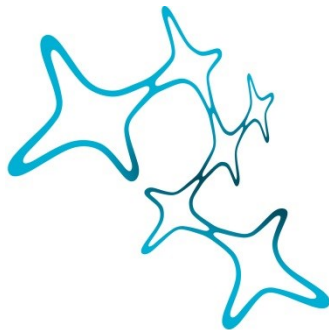

MOLECULAR MECHANISMS OF TAU AND TDP-43 CO-PATHOLOGY IN ALZHEIMER'S DISEASE

Francesca Simonetti



Graduate School of
Systemic Neurosciences
LMU Munich



Dissertation at the
Graduate School of Systemic Neurosciences
Ludwig-Maximilians-Universität München

July, 2024

Supervisor
Prof. Dr. Dieter Edbauer
Graduate School of Systemic Neurosciences GSN-LMU
Deutsches Zentrum für Neurodegenerative Erkrankungen (DZNE)

First Reviewer: Prof. Dr. Dieter Edbauer
Second Reviewer: Prof. Dr. Carmen Nussbaum
External Reviewer: Prof. Dr. Konstanze Winkelhofer

Date of Submission: 30th July, 2024
Date of Defense: 8th November, 2024

TABLE OF CONTENTS

1 ABSTRACT.....	5
2 INTRODUCTION	7
2.1 Neurodegenerative diseases	7
2.1.1 Amyloidosis	9
2.1.2 Tauopathies	9
2.1.3 Synucleinopathies	10
2.1.4 TDP-43 proteinopathies	10
2.2 ALS and FTD	11
2.2.1 Genetic causes of ALS and FTD	12
2.2.2 Neuropathology of ALS and FTD.....	13
2.2.3 TDP-43 pathology.....	14
2.3 Alzheimer’s Disease	15
2.3.1 Genetic cause of AD	16
2.3.2 Neuropathology of AD	16
2.3.3 Tau pathology	18
2.4 Tau/TDP-43 co-pathology in AD.....	18
2.4.1 Tau/TDP-43 pathology in other neurodegenerative diseases.....	20
2.5 Tau and TDP-43.....	23
2.5.1 Tau protein: structure, functions and PTMs.....	23
2.5.2 TDP-43 protein: structure, functions and PTMs	26
2.5.3 Recruitment of Tau and TDP-43 to Stress Granules.....	29
2.6 Phase separation: basic biophysical principles.....	30
2.6.1 Phase separation in cells	31
2.6.2 Regulation of phase separation	32
2.6.3 Role of Tau and TDP-43 phase separation in health and disease	32
2.7 Spreading of Tau and TDP-43 pathology	36
2.8 Strategies to target Tau and TDP-43 pathology.....	38

3 PUBLICATION I.....	41
3.1 Aim of the project.....	41
4 PUBLICATION II.....	65
4.1 Aim of the project.....	65
5 PUBLICATION III.....	92
5.1 Aim of the project.....	92
6 DISCUSSION.....	130
6.1 Potential implications of the Tau and TDP-43 interaction ..	131
6.2 The presence of TDP-43 may exacerbate Tau pathology.....	132
6.3 Protein condensation: Protective mechanism or precursor to aggregate formation?	133
6.4 Cellular events that potentially favor Tau and TDP-43 interaction.....	136
6.5 Potential domains of Tau and TDP-43 involved in their interaction.....	138
6.6 Molecular commonalities and cellular crosstalks between Tau and TDP-43	139
6.7 Future directions to study Tau/TDP-43 interactions.....	141
7 REFERENCES	143
8 ACKNOWLEDGEMENTS.....	171
9 CURRICULUM VITAE.....	172
10 LIST OF PUBLICATIONS.....	173
11 DECLARATION OF AUTHOR CONTRIBUTION	175

1 ABSTRACT

Neurodegenerative diseases are classified by characteristic protein aggregates. However, it is now widely recognized that many patients show a mixed pathology, which can accelerate disease progression. For example, recent studies have shown that up to 60% of Alzheimer's disease (AD) patients exhibit not only the hallmark amyloid- β ($A\beta$) plaques and Tau tangles but also TDP-43 aggregates, predominantly located in the limbic system, particularly the amygdala and hippocampus. In fact, AD patients with TDP-43 pathology exhibit more severe cognitive decline, greater memory loss, and increased hippocampal atrophy compared to those without these inclusions.

TDP-43 pathology was first identified in Amyotrophic Lateral Sclerosis (ALS) and Frontotemporal Dementia (FTD), two neurodegenerative diseases, where TDP-43 inclusions are mainly found in the motor cortex, spinal cord, and frontotemporal cortex, respectively.

One characteristic feature of TDP-43 aggregates is their disease-specific hyperphosphorylation, which was long considered pathogenic. However, emerging evidence suggests that this modification may also play a protective role in TDP-43 pathology, potentially counteracting the harmful effects of its aggregation. This dual role of hyperphosphorylation underscores the complexity of TDP-43's behavior in different neurodegenerative diseases, including its role in AD.

Adding to this complexity, recent studies in AD patients have shown that Tau and TDP-43 aggregates can colocalize within the same cells, and occasionally even within the same inclusions. However, the frequency and significance of this colocalization are still debated.

Nevertheless, an increasing number of studies support the idea of a critical interaction between Tau and TDP-43, suggesting that this relationship plays an important role in the progression of AD and other proteinopathies. Despite increasing clinical evidence of Tau/TDP-43 co-pathology, the molecular mechanisms behind the interaction of these two proteins remain largely unexplored.

Finally, another important emerging therapeutic approach in the field of neurodegeneration is active and passive antibody therapy targeting protein aggregates. Several studies demonstrating the protective effects of different antibodies recognizing hallmark proteins, such as Tau and TDP-43.

In this thesis, I present the findings of three studies I contributed to.

In my main project, I explored the interplay between Tau and TDP-43 *in vitro*, investigating how these proteins influence each other's behavior and whether they interact directly (Simonetti et al., in revision). Additionally, I contributed in examining the role of TDP-43 hyperphosphorylation to determine whether this post-translational modification (PTM) serves as a protective mechanism or promotes TDP-43 aggregation and phase separation (Grujts da Silva et al., 2022). Lastly, I participated in a study aimed at identifying immunogenic epitopes in TDP-43, with the goal of generating monoclonal antibodies for safe and effective, active and future passive immunization (Riemenschneider et al., 2023).

The main methods I used for these projects were *in vitro* phase separation and aggregation assays using both recombinant Tau and TDP-43 proteins, alongside cellular assays to study protein seeding, sequestration in stress granules, and cellular uptake.

Using classical TDP-43 phase separation assay, I showed that Tau induces the formation of large, irregular TDP-43 condensates, and by using the semi-denaturing detergent gel electrophoresis I showed that Tau also promotes TDP-43 aggregation *in vitro*. Furthermore, TDP-43 significantly influenced Tau's *in vitro* behavior, promoting the formation of multiphasic Tau/TDP-43 co-condensates with intra-Tau droplets. Additionally, TDP-43 suppresses Tau fibril formation, likely by binding Tau's protofibril (PHF) core region via its N-terminal domain, and generates smaller structures with reduced seeding capacity.

Further, I transfected two reporter cell lines designed to study Tau and TDP-43 seeding, using aggregates from AD and FTLD patient samples. I found that brain extracts from AD patients without visible TDP-43 pathology still induced intracellular TDP-43 aggregation, indicating the presence of seeding-competent TDP-43 species. Similarly, brain extracts from FTLD-TDP patients, promoted Tau seeding, suggesting the presence of Tau seeding-competent species without visible inclusions.

Although further research is needed to determine whether Tau and TDP-43 consistently colocalize in patient aggregates, my study suggests that even in the absence of visible inclusions, one protein can influence the seeding activity of the other. This supports the idea that Tau and TDP-43 may enhance each other's aggregation in pathological conditions, amplifying their pathogenic roles in disease progression.

Additionally, I contributed in identifying a potential protective role for TDP-43 hyperphosphorylation. We showed that kinase-mediated hyperphosphorylation or phosphomimetic mutations reduce TDP-43 phase separation and aggregation, both *in vitro* and in primary neurons.

Finally, I also helped in demonstrating that targeting TDP-43's glycine-rich domain with peptide antigens prevents its condensation and aggregation *in vitro*, and reduced TDP-43 cellular uptake. In a mouse model of ALS/FTD, immunization with these peptides lowered serum neurofilament light chain levels, suggesting a protective effect also *in vivo*.

In conclusion, my main project provides new insights into the molecular mechanisms of Tau and TDP-43 co-pathology in AD. For the first time, I present evidence of a potential direct interaction between these two proteins, which may contribute to AD progression.

We also propose a novel protective role for TDP-43 phosphorylation, and highlight the therapeutic potential of targeting the glycine-rich domain of TDP-43.

Together, these findings advance our understanding of two key proteins in neurodegeneration, offering new directions for research and potential treatment strategies for AD, ALS, and FTD.

2 INTRODUCTION

2.1 Neurodegenerative diseases

Neurodegenerative diseases (NDs) are one of the most common pathologies worldwide, affecting more than 50 million people, with an incidence expected to increase in our society as the population ages (Van Schependom and D'haeseleer, 2023; Wilson et al., 2023). Although age is the main contributing factor to the development of NDs, genetic causes and environmental influences also play an important role (Brown et al., 2005; Chin-Chan et al., 2015; Inoue, 2015).

The main phenomenon occurring in patients with NDs is the progressive loss of neurons in the central nervous system (CNS) and/or peripheral nervous system (PNS). However, this process represents just one facet of the pathophysiology of these disorders. Multiple additional pathological events contribute to the underlying causes of neurodegeneration; recently, Wilson and colleagues listed the hallmarks of NDs that synergistically contribute to the development of the pathology (Fig. 1) (Wilson et al., 2023):

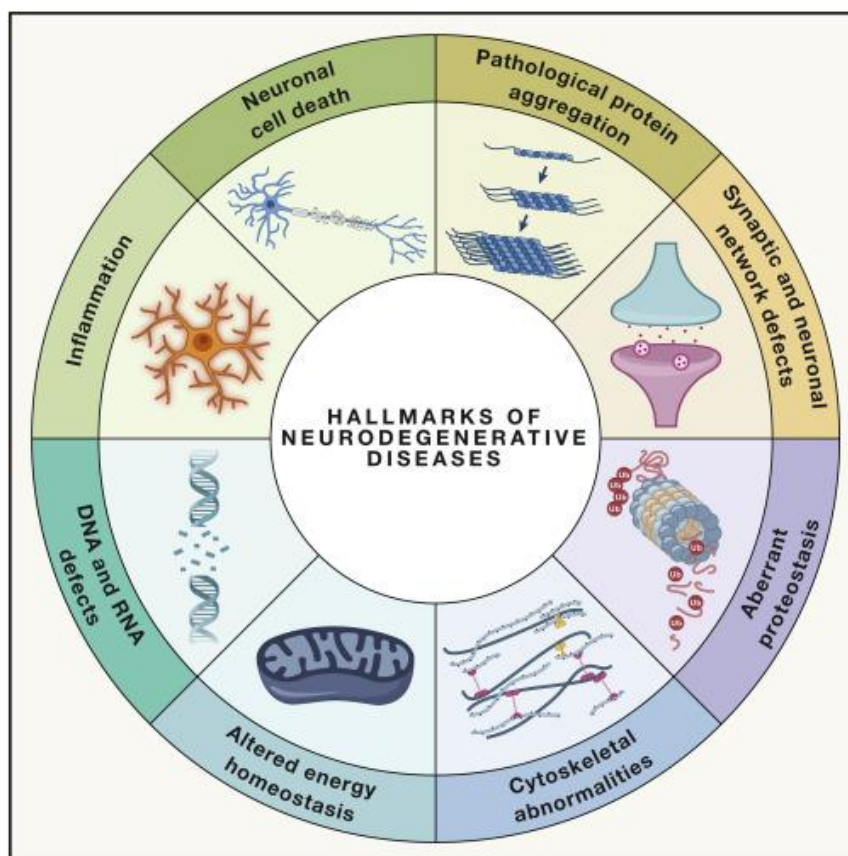


Figure 1 - Hallmarks of Neurodegenerative diseases (NDs)

Scheme depicting the 8 hallmarks of NDs – (Wilson et al., 2023), with permission to reuse with CC BY license.

- *neuronal cell death*. Neurons, as post-mitotic cells, lack the ability to replicate, rendering them long-lived and prone to accumulate damage, which ultimately makes them vulnerable to death. Neuronal death is a complex pathway, posing challenges in

identifying precise mechanisms across different neuropathologies (Fricker et al., 2018);

- *pathological protein aggregation*. In NDs, several proteins undergo misfolding and aggregation within different cell types and compartments; this phenomenon can lead to loss of physiological functions of the protein, and/or can induce toxic protein behavior that significantly contributes to the pathology (Taylor et al., 2002);
- *aberrant proteostasis*. This pathomechanism is highly associated with the accumulation of aggregated proteins, resulting from malfunctions in the proteostasis system. These defects can include aberrant functions of chaperones, which ensure proper protein folding, the ubiquitin-proteasome system (UPS), responsible of eliminating ubiquitin-marked proteins caused by abnormal functioning, and the autophagy-lysosome pathway (ALP), which is involved in the clearance of aggregates and deficient organelles (Hipp et al., 2019; Pohl and Dikic, 2019);
- *altered energy homeostasis*. Energy metabolism defects arise as a direct consequence of mitochondrial dysfunction, as these organelles are responsible for energy generation via ATP production; given that neurons have a high energy demands due to their electrical signalling, any impairment in mitochondrial activity can significantly impact neuronal function and viability (Li and Sheng, 2022);
- *synaptic and neuronal network defects*. The dysfunction of synapses has been described as an event that precedes neuronal loss, with altered synaptic regulation disrupting neuronal networks; these abnormalities are closely linked with other ND hallmarks, such as defective energy metabolism, oxidative stress (Li and Sheng, 2022), and early protein aggregation that can further contribute to synaptic failure (Henstridge et al., 2016);
- *cytoskeletal abnormalities*. Alterations in the cytoskeleton organization can derive either from mutations in genes involved in the structural integrity of the cytoskeleton or from the aggregation of cytoskeletal proteins; these disruptions impair the efficient transport of cargo, such as mitochondria, vesicles and ribonucleoprotein (RNP) granules along neuronal axons, ultimately resulting in altered energy metabolism and synaptic dysfunction (Millecamps and Julien, 2013);
- *DNA and RNA defects*. DNA damage and RNA dysregulation, caused by numerous endogenous and exogenous factors, exert significant effects on various cellular functions, ultimately culminating in cell death; genomic and transcriptomic defects, alongside with other hallmarks described above, have now been firmly established as key contributors to neurodegeneration (Madabhushi et al., 2014; Nussbacher et al., 2019);
- *inflammation*. Inflammation in NDs includes both microgliosis and astrogliosis; these responses initially emerge with a protective intent, aimed at mitigating cellular damage, but in the context of pathology, these inflammatory reactions fail to resolve, exacerbating the disease process and accelerating neurodegeneration (Hickman et al., 2018; Phatnani and Maniatis, 2015).

NDs are typically classified according to one of three different categories: 1) genetic versus sporadic, 2) molecular hallmarks and 3) clinical and anatomical manifestation (Kovacs, 2018;

Menéndez-González, 2023). However, the second category is the most frequent way to classify these diseases; in fact, the most common neurodegenerative disorders are described as amyloidoses, tauopathies, α -synucleinopathies and TAR DNA binding protein 43 (TDP-43) proteinopathies, characterized by the abnormal accumulation in the brain of amyloids (such as β -amyloid (A β) or prion protein (PrP)), and proteins named Tau, α -synuclein and TDP-43, respectively (Dugger and Dickson, 2017; Kovacs, 2018; Taylor et al., 2002).

Other NDs not mentioned in the classification above but also defined by hallmark proteins are Huntington's disease and spinocerebellar ataxia, both caused by a genetic expansion of cytosine-adenine-guanine (CAG) repeats in the genes coding for the huntingtin (Htt) and ataxin proteins, respectively.

2.1.1 Amyloidoses

The distinctive feature of amyloidoses is the abnormal extracellular accumulation of protein aggregates known as amyloids, which are insoluble filamentous protein aggregates characterized by a β -sheet secondary structure (Westermarck et al., 2005). Alzheimer's disease (AD) is the most common amyloidosis, marked by the deposition of A β peptides into amyloid-plaques within the brain's neuronal and glial cytoplasm. These plaques disrupt synaptic function and trigger neuroinflammation, ultimately leading to progressive cognitive decline and neuronal loss (Palop and Mucke, 2010). Additionally, other very well-known amyloidosis are prion diseases, such as the familial and sporadic Creutzfeldt-Jakob disease (CJD) in humans, as well as bovine spongiform encephalopathy (BSE) and scrapie in animals. These prion disorders involve the misfolding of normal prion protein (PrP^C) into a pathological form (PrP^{Sc}), which accumulates as aggregate and spreads within the CNS, perpetuating the pathological cascade and causing widespread neurodegeneration (Nafe et al., 2023; Prusiner, 1998). Despite differences in etiology and clinical manifestations, both AD and prion diseases highlight the devastating consequences on the brain of amyloid accumulation.

2.1.2 Tauopathies

Tauopathies are all disorders characterized by the abnormal aggregation of hyperphosphorylated Tau protein in different inclusions, such as neurofibrillary tangles (NFTs), neuropil threads and glial fibrillary tangles. Tau is encoded by the *MAPT* gene and serves as a microtubule-binding protein, crucial for the assembly, stability and transport regulation of axonal microtubules (Dugger and Dickson, 2017; Mandelkow and Mandelkow, 2012).

The discovery of mutations in the *MAPT* gene linked to the chromosome 17 (FTDP-17T) in frontotemporal dementia (FTD) and parkinsonism underscored Tau's involvement in the pathogenesis of these diseases (Yoshiyama et al., 2001). In addition to FTDP-17T, other familial tauopathies are AD, Progressive Supranuclear Palsy (PSP), that involves the degeneration of several brain areas, and is often present with atypical parkinsonism (Williams and Lees, 2009), Corticobasal Degeneration (CBD), a disease that spreads in the cerebral cortex and basal ganglia and can show also atypical parkinsonism (Wilson et al., 2021), and Pick's Disease, described as a specific type of FTD (Tamvaka et al., 2023). However, most

cases of these diseases are sporadic, alongside with Chronic Traumatic Encephalopathy (CTE), a disease associated with chronic repetitive head injury leading to behavioral and cognitive changes (Montenigro et al., 2015).

Noteworthy, splicing mutations on the *MAPT* gene change the relative ratio of different Tau isoforms (Wang and Mandelkow, 2016). Alternative mRNA splicing generates multiple Tau isoforms which are cell-type specific and modulate different functions (Andreadis, 2005; Buée et al., 2000); for instance, the splicing of exon 10 (E10) produces two isoforms of Tau, one with four repeats (4R) and another with three repeats (3R), all of which are located within the microtubule-binding domain of the Tau sequence. The ratio of these isoforms is 50:50 in healthy brain, but this condition can be substantially altered in diseases: 4R only isoform is present in PSP, CBD and some forms of FTDP-17T, the 3R isoform appears in Pick's disease and forms of FTDP-17T, and finally an abnormal 4R:3R ratio (approximately 2:1) is found in AD, CTE and forms of FTD-17T (Chen et al., 2010; Dugger and Dickson, 2017).

2.1.3 Synucleinopathies

Another big class of NDs are those marked by the accumulation of α -synuclein, a protein encoded by the *SNCA* gene and present in neurons at the presynaptic terminals where its main function is to regulate vesicle trafficking and overall synaptic activity (Burré et al., 2010; Lashuel et al., 2013).

α -synuclein is characterized by an amphipathic lysine-rich N-terminal domain responsible of protein interactions with membranes, the non-amyloid- β component of AD amyloid plaques (NAC) region, which is a highly hydrophobic sequence crucial for its aggregation, and lastly, a disordered acidic C-terminal involved in interactions with proteins and other molecules (Lashuel et al., 2013).

Similar to Tau and TDP-43, α -synuclein can undergo physiological phase separation both *in vitro* and in cells, behavior that can progress into a pathological condition, leading to aberrant protein aggregation. Pathological oligomerization and fibrillization of α -synuclein are associated with the formation of inclusions found in synucleinopathies. Furthermore, seeds of α -synuclein can propagate from cell to cell, spreading the pathology to different brain regions (Zbinden et al., 2020).

The major hallmarks of synucleinopathies are the Lewy bodies, Lewy neurites and glial inclusions, which are α -synuclein aggregates found in Parkinson's disease, Dementia with Lewy Bodies (DLB) and Multiple System Atrophy (MSA) (Dugger and Dickson, 2017).

Parkinson's disease, the second most common neurodegenerative pathology, correlates with loss of dopaminergic neurons in the substantia nigra of the midbrain. It typically initiates with motor symptoms that progress to dementia alongside with changes in mood and behavior (DeMaagd and Philip, 2015). DLB is distinguished by an unusual accumulation of α -synuclein in the brain, and it is characterized by additional cognitive, neuropsychiatric and sleep-related symptoms (Prasad et al., 2023). Lastly, MSA is an autonomic disorder and can be described as MSA-C with cerebellar ataxia, and MSA-P with atypical parkinsonism; both subtypes present glial Lewy bodies, specifically in oligodendrocytes (Dugger and Dickson, 2017).

2.1.4 TDP-43 proteinopathies

TDP-43 proteinopathies represent a group of NDs characterized by the abnormal accumulation of TDP-43 protein within neurons and glial cells.

TDP-43 is a multifunctional protein that belongs to the family of heterogeneous nuclear ribonucleoproteins (hnRNPs); it is an evolutionarily conserved protein, ubiquitously expressed and predominantly located in the nucleus (Berning and Walker, 2019), but also shuttles to the cytoplasm where it performs specific functions, including regulation of RNA metabolism, and stress responses (Ratti and Buratti, 2016). In pathological conditions, TDP-43 loses its nuclear localization and accumulates and aggregates in the cytoplasm of neurons and glial cells, resulting in the loss of its normal cellular functions and detrimental misregulation of mRNA processing (Ling et al., 2013). This aberrant TDP-43 aggregation is implicated in the pathogenesis of diseases such as amyotrophic lateral sclerosis (ALS), which affects both upper and lower motor neurons, and FTD, which is caused by an atrophy of the frontal and temporal lobe of the brain (Nelson et al., 2018; Neumann et al., 2006).

2.2 ALS and FTD

Initially, ALS and FTD were considered two separate diseases, but increasing evidence has changed this conception showing an association between ALS and FTD (Van Langenhove et al., 2012). Research efforts have focused in elucidating the connections between these two diseases, revealing that ALS is a multisystem neurodegenerative disorder, that not only impacts the motor areas of the brain, but also affects cortical regions associated with behavior and personality, as occurs in patients with FTD (Couratier et al., 2017).

ALS, with an incidence on a global scale of almost 3 cases per 100,000 persons annually (Wolfson et al., 2023) is characterized by two aspects: the degeneration of cortico spinal motor neurons projecting their axons in the lateral spinal cord (lateral sclerosis), and the loss of spinal motor neurons, leading to secondary muscle wasting (amyotrophy) (Taylor et al., 2016).

This disease is often diagnosed in middle age, with 90% of cases being sporadic and the remaining 10% familial. Characterized by its progressive nature, symptoms usually begin with weakness as muscle flaccidity, or cramping in the limbs or bulbar, and eventually progresses to paralysis, affecting nearly all skeletal muscles (Cicardi et al., 2021; Taylor et al., 2016). Typically, clinical symptoms start to manifest in a focal manner, often arising from a localized lesion; over time, these symptoms intensify and propagate, amplifying through a combination of contiguous and non-contiguous mechanisms, involving cell-to-cell contacts and long-range interactions, respectively (Kanouchi et al., 2012).

As mentioned above, overall 50% of ALS patients also manifest cognitive impairment, and about 15-20% of ALS patients have concomitant FTD (Ling et al., 2013; Taylor et al., 2016; Couratier et al., 2017).

FTD is the third most common type of dementia, with an annual incidence of up to 4 cases per 100,000 persons, typically aged 40-60 years (Hogan et al., 2016); contrary to ALS, almost 50% of FTD cases are heritable (Rohrer et al., 2009).

As the name suggests, FTD is characterized by the progressive degeneration of the frontal and temporal lobes of the brain, resulting in changes in behavior, personality, and language skills.

In fact, the disease can be classified into three clinical subtypes: behavioral-variant FTLN (bv-FTLD) with changes in behavior and personality, progressive non-fluent aphasia (PNFA) with loss of motor speech fluency, and semantic dementia (SD) with deficits in semantic knowledge (Van Langenhove et al., 2012). As the disease progresses, individuals may experience difficulties with social interactions, emotional regulation, and executive functioning, ultimately leading to significant impairment in daily activities. Similarly as described above for ALS, this convergence of symptoms arises from the disease's progression, starting in a localized area of the brain and then spreading to other regions of the frontal and temporal lobes. (Bang et al., 2015).

Based on the hallmark protein found in patient aggregates, FTLN can be classified in FTLN-TDP-43, FTLN-Tau, FTLN-FUS and FTLN-UPS, which stands for ubiquitin-proteasome system and referred to protein deposits consisting solely of ubiquitin and p62 (Ling et al., 2013; I. R. A. Mackenzie et al., 2010).

For both ALS and FTLN not all the causes are fully understood, but genetic factors are known to play a significant role in familial forms of these diseases.

2.2.1 Genetic causes of ALS and FTLN

Familial ALS (fALS) and FTLN can be caused by mutations in different genes: while each disease can be uniquely associated with specific genes, there is also overlap, with mutations in certain genes contributing to the pathology of both disorders (Fig. 2).

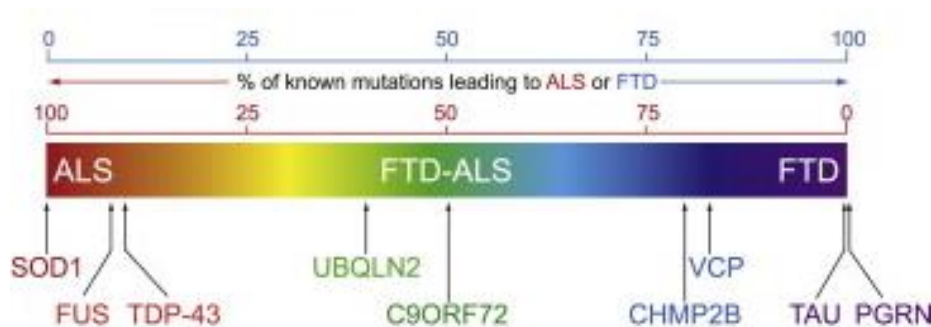


Figure 2 - Genetic spectrum in ALS and FTLN

Genes involved in the pathogenesis of ALS and FTLN can be represented as a spectrum, with some genes being specifically associated with one disease (left: ALS; right: FTLN), and other genes being involved in both diseases (middle: FTLN-ALS) – modified from (Ling et al., 2013), with permission to reuse under license number 5797110476427.

Familial ALS is distinguished by mutations in the *superoxide dismutase 1* (*SOD1*), *TAR DNA binding protein* (*TARDBP*) and *fused in sarcoma* (*FUS*) genes, whereas FTLN is hallmarked by mutations in the *microtubule-associated protein tau* (*MAPT*) and *granulin* (*GRN*) genes. Notably, the majority of hereditary ALS or FTLN cases are caused by mutations in the *chromosome 9 open reading frame 72* (*C9ORF72*) gene; additionally, mutations associated with clearance pathway-related genes, such as *ubiquilin-2* (*UBQLN2*) and *valosin-containing protein* (*VCP*), have also been identified as causative factors in both ALS and FTLN pathologies (Ling et al., 2013).

Furthermore, these mutated genes can be divided into two functional groups: genes encoding proteins with RNA processing functions, *TARDBP* and *FUS*, and those involved in protein degradation pathways, *UBQLN2* and *VCP* (Couratier et al., 2017).

TDP-43 and FUS are RNA-binding proteins that, in a disease scenario, shift from their normal nuclear localization to the cytoplasm, where they form aggregates; this phenomenon is associated with loss of their nuclear functions and subsequent RNA processing defects, which are considered significant pathomechanisms (Ling et al., 2013).

The clearance of aggregates is probably strongly countered by protein degradation pathways, namely the ubiquitin-proteasome system and the autophagy-lysosomal system, as supported by the fact that TDP-43 and FUS aggregates always contain ubiquitin and p62/SQSTM1 (Budini et al., 2017). Whether impairment in protein degradation precedes RNA-binding protein aggregation or *vice versa* is not entirely clear, but, these phenomena highlight a complex interplay of key pathomechanisms common to both ALS and FTD (Ng et al., 2015).

The genetic mutations in ALS and FTD are mainly missense substitutions, with the exception of the long GGGGCC hexanucleotide repeat expansion in the *C9ORF72* gene (Taylor et al., 2016). In case of pathology, the number of the GGGGCC repeats in the *C9ORF72* gene is dramatically increased, leading to the translation of RNA repeats into dipeptide repeat (DPR) proteins, which ultimately aggregate and form cytoplasmic DPR inclusions in neurons (Gallo and Edbauer, 2022).

2.2.2 Neuropathology of ALS and FTD

ALS and FTD exhibit common neuropathological aspects, mirroring the shared clinical and genetic features observed in these conditions.

The hallmark of ALS is motor neuron loss, leading to muscle atrophy, but in patients with dementia, due to the overlap with FTD, there is also a brain atrophy in the frontal and temporal cortex (Saberri et al., 2015). In fact, the classic neuropathological sign in FTD is the extensive atrophy of the bilateral frontal and anterior temporal lobes, as well as of limbic regions, including the hippocampus and amygdala (Wang et al., 2022).

Moreover, a common pathological factor linking both diseases is the TDP-43 deposition (neuronal cytoplasmic inclusions and dystrophic neurites) found in both ALS and FTD patients; these pathological protein aggregates frequently exhibit positivity for ubiquitin and p62, markers for the proteasome and autophagy degradation systems (Arai et al., 2006; Neumann et al., 2006). In addition, FUS inclusions are also a hallmark of both diseases, but in only 9% of FTD patients and less than 1% of ALS cases (I. R. Mackenzie et al., 2010) (Fig. 3).

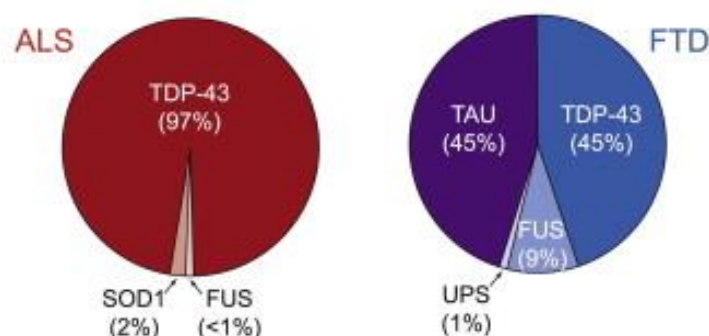


Figure 3 – Different pathological inclusions in ALS and FTD

Pie graphs illustrating the different prevalence of the distinct pathological protein inclusions found in ALS and FTD – modified from (Ling et al., 2013), with permission to reuse under license number 5797110476427.

Finally, the neuropathological manifestation of C9ORF72-associated disease is also recognized as a shared feature of ALS and FTD. Hallmarks of C9orf72-ALS/FTD include RNA foci and cytoplasmic DPRs, which form from unconventional translation of expanded (G₄C₂)_n nucleotide repeats, and consist of five different dipeptide repeat proteins: glycine-arginine (GR), proline-arginine (PR), glycine-alanine (GA), glycine-proline (GP), and proline-alanine (PA) (Gendron et al., 2013; Gitler and Tsuiji, 2016).

2.2.3 TDP-43 pathology

Pathological TDP-43 was first identified in ALS and FTD, establishing it as the hallmark protein in both disorders and highlighting that these diseases have shared features (Arai et al., 2006; Neumann et al., 2006). Subsequently, TDP-43 pathology has been linked to other neurodegenerative diseases, including AD (Arai et al., 2009; Josephs et al., 2014a), PD and Huntington's disease (HD) (Gao et al., 2018). More recently limbic-predominant age-related TDP-43 encephalopathy (LATE) has been described as a disease that affects elderly individuals with clinical manifestation similar to Alzheimer's-type dementia, featuring neuroanatomical TDP-43 pathology restricted to limbic regions of the brain (Nelson et al., 2018).

In these neurodegenerative diseases, the aberrant cytoplasmic accumulation and mislocalization of TDP-43 disrupts its normal activities, leading to cellular dysfunction and neuronal loss (Lee et al., 2011; Ling et al., 2013; Neumann et al., 2006).

Inclusions of TDP-43 in the cytoplasm of neurons and glia are major neuropathological markers, specifically in the frontotemporal neocortex and hippocampus in FTLD-TDP, and in the primary motor cortex, brainstem motor nuclei, spinal cord, and associated white matter tracts in ALS (Fig. 4) (I. R. Mackenzie et al., 2010). The morphology of these TDP-43-positive aggregates include small granules, Lewy-body-like inclusions, and filamentous skeins; additionally, rare lentiform intranuclear inclusions of TDP-43 can be found mainly in familial cases of FTLD-TDP (I. R. Mackenzie et al., 2010).

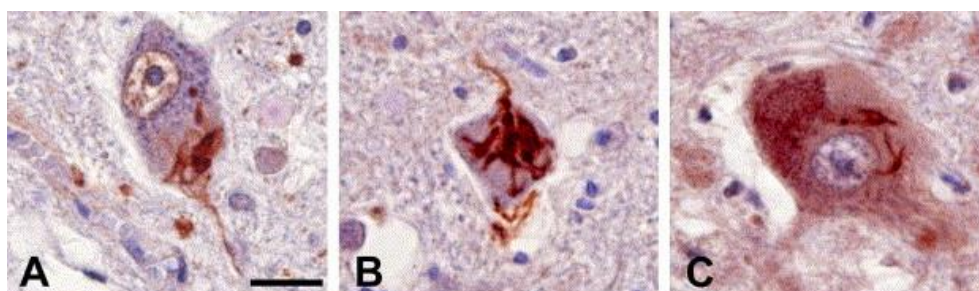


Figure 4 – Examples of TDP-43 inclusions in spinal cord of ALS cases

Immunostaining of skein-like inclusions of TDP-43 in motoneurons of the lumbar spinal cord using anti-ubiquitin (A), polyclonal anti-TDP-43 (B) and monoclonal anti-TDP-43 (C) antibodies – modified from (Arai et al., 2006), with permission to reuse under license number 5797120060968.

These aberrant TDP-43 aggregates are typically hyperphosphorylated, mainly at Ser403/404 and Ser409/410 (Hasegawa et al., 2008), and are composed of truncated C-terminal fragments of TDP-43, which are prone to aggregation and readily form inclusions (Arai et al., 2010). A prominent example of these CTFs is the ~25kDa CTF (TDP-25), which represents the most abundant form of TDP-43 inclusions observed in patients with ALS and FTD (Igaz et al., 2008). This fragment lacks the nuclear localization signal, the RRM1, and a portion of the RRM2. Additionally, there is another fragment, TDP-35, which lacks only the N-terminus containing the NLS (Chhangani et al., 2021).

Furthermore, TDP-43-positive inclusions can be also identified by several markers, including ubiquitin and p62 (Arai et al., 2006; Neumann et al., 2006), indicating failed degradation processes, and SGs markers, since TDP-43 is recruited to these compartments under cellular stress, and in case of pathology SGs become reservoirs for protein aggregation, making them typically associated with deposits of protein inclusions in neurodegenerative diseases (Bentmann et al., 2012; Dormann et al., 2010; Wolozin and Ivanov, 2019).

2.3 Alzheimer’s Disease

The predominant form of amyloidosis is Alzheimer’s disease (AD), which is also the most common cause of dementia with an incidence of more than 100 patients per 100,000 population (Li et al., 2022). The majority of cases (95%) are sporadic and occur after the age of 65, known as late-onset AD (LOAD); the remaining cases (5%) are familial and named early-onset AD (EOAD) since they begin at early age (Chin-Chan et al., 2015; Long and Holtzman, 2019).

As for other neurodegenerative diseases, AD has a progressive course characterized by different disease stages: i) the early stage, with mild impairment in learning and memory, ii) the middle stage, with progressive cognitive decline, and iii) the final late stage, with significant functional impairment and eventual loss of ability to perform daily activities independently (Breijyeh and Karaman, 2020; Sperling et al., 2011; Vermunt et al., 2019).

As the disease advances, individuals may also experience language difficulties (aphasia), disorientation, and challenges with reasoning and judgment. Behavioral changes such as agitation, aggression, and mood swings can also occur. In later stages, individuals may lose awareness of their surroundings, developing agnosia, failure to recognize people or objects, and apraxia, inability to perform motor act (Brown et al., 2005; Long and Holtzman, 2019).

Early diagnosis and intervention are crucial for managing symptoms and improving outcomes. Nowadays, antemortem neuropathologic diagnoses are possible, using cerebrospinal fluid (CSF) or positron emission tomography (PET) imaging to detect pathological protein deposition in patients up to 10-20 years before disease onset (Long and Holtzman, 2019).

However, while not all the causes of AD are known, there are four risk factors that are firmly recognized: aging, inheritance of one or two $\epsilon 4$ alleles of the apolipoprotein E gene (*APOE*), familial association and Down syndrome (McDowell, 2001; Selkoe, 2024). In addition, environmental risk factors, such as diet, heavy metals and pesticides are also recognized as contributors to the development of AD (Brown et al., 2005; Chin-Chan et al., 2015).

2.3.1 Genetic causes of AD

Genetic factors play a significant role in the development of AD, with both rare familial mutations and common genetic variants implicated in its pathogenesis. Rare familial forms of AD are typically associated with autosomal dominant mutations in one of three genes: amyloid precursor protein (*APP*), presenilin 1 (*PSEN1*) and presenilin 2 (*PSEN2*) (Breijyeh and Karaman, 2020). *APP* encodes for APP, a transmembrane protein present in neuronal synapses that upon proteolysis serves as a precursor to $A\beta$, one of the hallmark proteins of AD; *PSEN1* and *PSEN2* encode critical components of γ -secretase, an enzyme crucial for APP cleavage. Mutations in these genes increase pathological $A\beta$ production and promote $A\beta$ fibril and plaque formation, thereby facilitating the development of AD (Inoue, 2015).

Furthermore, it is noteworthy to highlight that the *APP* gene is situated on chromosome 21. This genetic positioning amplifies the susceptibility to AD in individuals with Down syndrome (trisomy 21), as almost all Down syndrome patients manifest symptoms of AD by the age of 40 years (Lott and Head, 2019).

The *APOE* gene is the most common genetic risk factor for AD. This gene has three polymorphic alleles ($\epsilon 2$, $\epsilon 3$ and $\epsilon 4$), with the $\epsilon 4$ allele corresponding to the well-established genetic risk factor for LOAD, influencing the age of onset and severity of the disease. This gene encodes for the APOE protein, a major cholesterol carrier involved in lipid transport and in the regulation of lipid homeostasis (Liu et al., 2013). This protein directly binds to $A\beta$ and enhances its proteolytic cleavage, but the APOE- $\epsilon 4$ isoform is less efficient at clearing $A\beta$ aggregates, resulting in increased pathological $A\beta$ deposition and subsequent $A\beta$ plaque formation in patients carrying this allele (Jiang et al., 2008).

Finally, other common genetic variants associated with an increased risk of AD have also been identified by genome-wide association studies (Bellenguez et al., 2022; Breijyeh and Karaman, 2020).

2.3.2 Neuropathology of AD

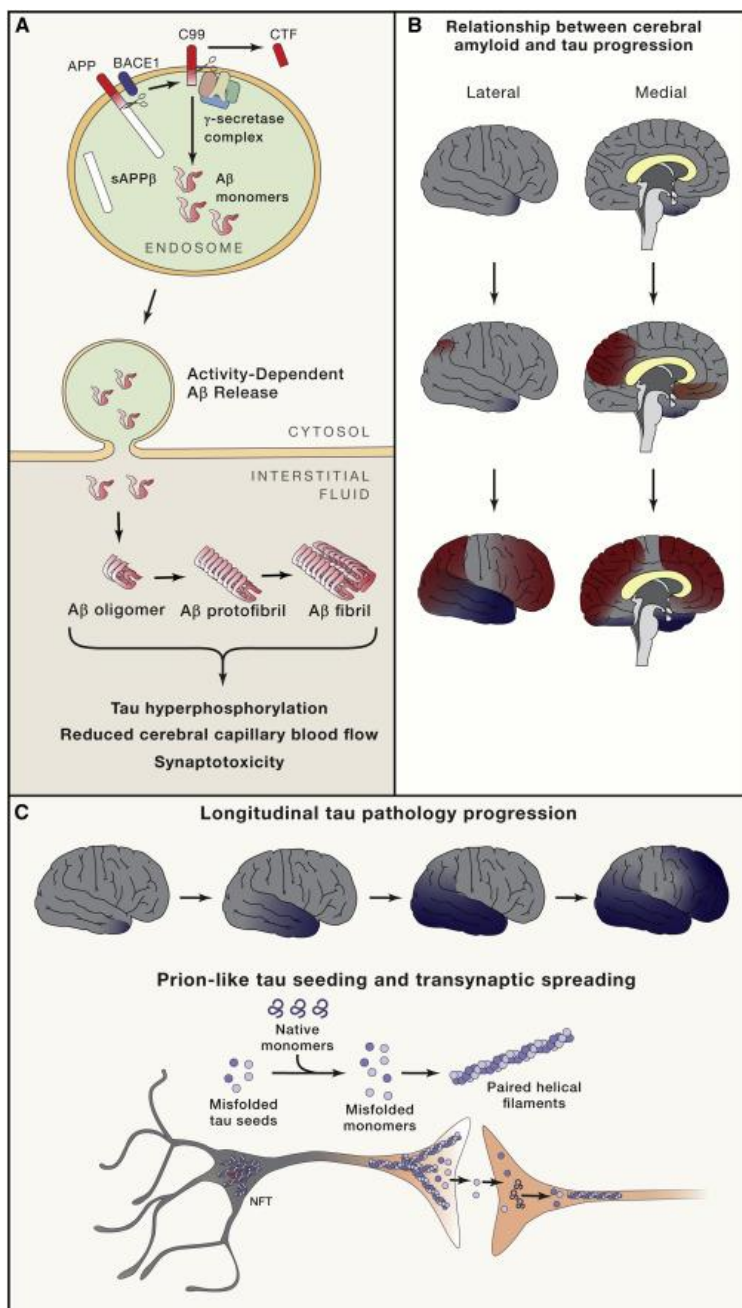
Alzheimer's disease brains typically reveal significant atrophy, particularly in regions crucial for memory and cognition, such as the hippocampus and cortex. This atrophy often manifests as pronounced cortical thinning and enlargement of the ventricles, reflecting neuronal loss and tissue degeneration; overall, a decreased brain weight is observed in most affected patients (DeTure and Dickson, 2019).

Furthermore, AD is characterized by the extracellular deposition of $A\beta$ in the form of amyloid plaques, and the intraneuronal accumulation of the phosphorylated Tau protein in NFTs (Breijyeh and Karaman, 2020; Dugger and Dickson, 2017; Long and Holtzman, 2019).

The 37-43 amino acids $A\beta$ peptide derives from the cleavage of the β -amyloid precursor protein (APP) by the β -secretase and γ -secretase, described as the amyloidogenic pathway

(Haass et al., 2012). Once the A β peptide is generated, it is prone to aggregate into higher molecular structures, forming oligomers, protofibrils and fibrils which are then released by the cells, often due to cell death caused by their accumulation, and they finally deposit extracellularly where they form pathological A β plaques (Fig. 5A) (Friedrich et al., 2010; Hu et al., 2009; Long and Holtzman, 2019).

In addition in AD brains the Tau protein aggregates and accumulates within neurons, forming NFTs (Fig. 5C, lower part) (DeTure and Dickson, 2019).



The A β and Tau pathologies serve as indicators of the underlying neurodegenerative processes of AD and how the disease progresses (Fig. 5B and C, upper part). In 1991 Braak defined the Braak staging system, based on the distribution and progression of NFTs throughout the brain; in brief, it delineates six stages, with early stages primarily affecting the entorhinal cortex and hippocampus before spreading to neocortical regions (Braak and Braak, 1991).

A few years later, the Thal phases were introduced, focusing on the accumulation of A β plaques across different brain regions. This staging system identifies five phases, with A β deposition beginning in the basal portions of the neocortex before advancing to more widespread cortical areas (Thal et al., 2002).

Both Braak and Thal staging systems serve as essential tools in characterizing the neuropathological progression of Alzheimer's disease.

Figure 5 - A β and Tau pathophysiology

A. Scheme of the amyloidogenic pathway; B. A β (in red) and Tau (in blue) deposition in the brain along the course of the disease; C. Progression of Tau pathology (in blue) in the brain (upper part), and Tau fibril formation and seeding (lower part) – from (Long and Holtzman, 2019), with permission to reuse under license number 5797120901757.

2.3.3 Tau pathology

Tau is a highly expressed neuronal protein known for its primary role in binding and stabilizing microtubules. Under physiological situations, Tau is soluble and natively unfolded; additionally, it undergoes various post-translational modifications (PTMs) both under normal homeostasis and during stress events. However, in pathological conditions, abnormal phosphorylation diminishes Tau binding affinity to microtubules, causing the protein to lose its main axonal localization and undergo aberrant aggregation in the cytoplasm (Long and Holtzman, 2019). Tau then begins to aggregate into cross β -sheet-containing amyloid structures, forming paired helical filaments (PHFs) that further mature into proto-fibrils (Scheres et al., 2023). Ultimately, Tau aggregation culminates in long fibrillar structures within the brain, giving rise to NFTs (Fig. 5C) (Guo et al., 2017; Medeiros et al., 2010).

Tau pathology in AD correlates with neurodegeneration, and the spreading of Tau appears to be linked to Tau oligomers (Guo et al., 2017; Lasagna-Reeves et al., 2011; Spires-Jones et al., 2011; Ward et al., 2012). Recent findings have highlighted the importance of oligomeric, misfolded, phosphorylated Tau species as the seeding entities of the protein, located at the terminals of neuronal synapses (Gerson and Kaye, 2013). These species have been implicated in the propagation of disease within the brain, even when the burden of NFTs is low (Colom-Cadena et al., 2023). This discovery aligns with a previous study by Devos and colleagues, which suggested that pathogenic Tau seeding precedes the onset of Tau pathology (DeVos et al., 2018).

Nevertheless, how A β accumulation in senile plaques is linked to Tau aggregation and deposition in AD brains it is still under debate (Musiek and Holtzman, 2015). Unraveling these intricate relationships, along with the involvement of other proteins involved in AD pathogenesis, such as TDP-43, may provide fundamental insights into the mechanisms underlying this and other neurodegenerative disorders.

2.4 Tau/TDP-43 co-pathology in AD

It is now widely recognized that protein aggregation in a particular neurodegenerative disease is not always confined to a single protein pathology; instead, several different hallmark proteins are sometimes co-deposited.

Widely recognized examples include the co-aggregation of α -synuclein and Tau in Lewy Bodies of PD patients (Ishizawa et al., 2003), and the co-localization of A β and phospho-Tau (pTau) at the synaptic terminals in AD brains (Fein et al., 2008). Furthermore, intracellular accumulation of TDP-43 has also been observed in patients with DLB (Higashi et al., 2007; McAleese et al., 2017; Nakashima-Yasuda et al., 2007), and other α -synucleinopathies, where partial colocalization between TDP-43 and α -synuclein may occur within the same cellular aggregates (Kokoulina and Rohn, 2010; Yamashita et al., 2014). Additionally, another example of comorbidity is the Tau/TDP-43 co-pathology observed in tauopathies, FTD and ALS (Kim et al., 2018; Stevens et al., 2019; Takeda, 2018).

However, the most common protein co-pathology is the one between Tau and TDP-43 found in Alzheimer's disease. Since 2007, it has become clear that up to 60% of AD patients present not only the classical deposition of A β and Tau aggregates, but also additional cytosolic

deposits of TDP-43 (Amador-Ortiz et al., 2007; Arai et al., 2009; Josephs et al., 2014b; Latimer and Liachko, 2021; Meneses et al., 2021; Tomé et al., 2020).

TDP-43 deposition in AD brains is mainly found in the amygdala (Nelson et al., 2018), hippocampus (Josephs et al., 2017), and to a lower extent in the cortex regions of the brain (Kadokura et al., 2009). As a consequence of this, AD patients with TDP-43 pathology manifest a more significant hippocampus atrophy, memory loss, and high cognitive impairment usually paired with dementia, in comparison to AD patients without TDP-43 pathology (Fig. 6) (Josephs et al., 2014b, 2015, 2017; Thomas et al., 2020). Thus, there is a substantial increase in neurodegeneration among AD subjects with TDP-43 pathology compared to AD patients lacking TDP-43 deposition (Josephs et al., 2014b; Wilson et al., 2013), suggesting an important contribution of TDP-43 to AD pathogenesis.

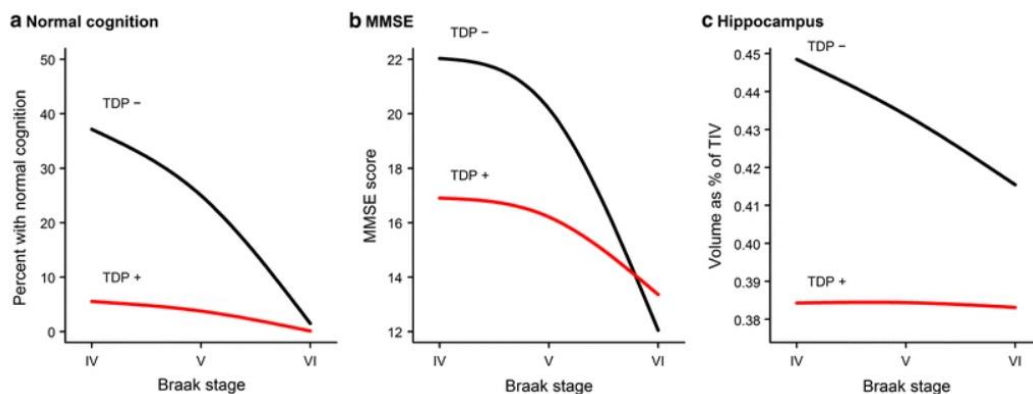


Figure 6 - Neurodegeneration in AD patients with and without TDP-43 pathology

Graphs show a stronger decrease in normal cognition, mini-mental state examination (MMSE) score and hippocampus volume in AD patients presenting TDP-43 pathology (TDP+, red line) in comparison with AD patients without TDP-43 pathology (TDP-, black line) – from (Josephs et al., 2014b), with permission to reuse under license number 5797140912624.

In addition, it has been demonstrated that TDP-43 aggregates often colocalize with Tau NFTs in neurons of the entorhinal cortex and dentate gyrus (Amador-Ortiz et al., 2007), or in the amygdala and hippocampus of AD patients (Fig. 7) (Higashi et al., 2007; Smith et al., 2018; Tomé et al., 2021), and proximity ligation and co-immunoprecipitation experiments have suggested that TDP-43 and Tau interact in the AD brain (Tomé et al., 2021).

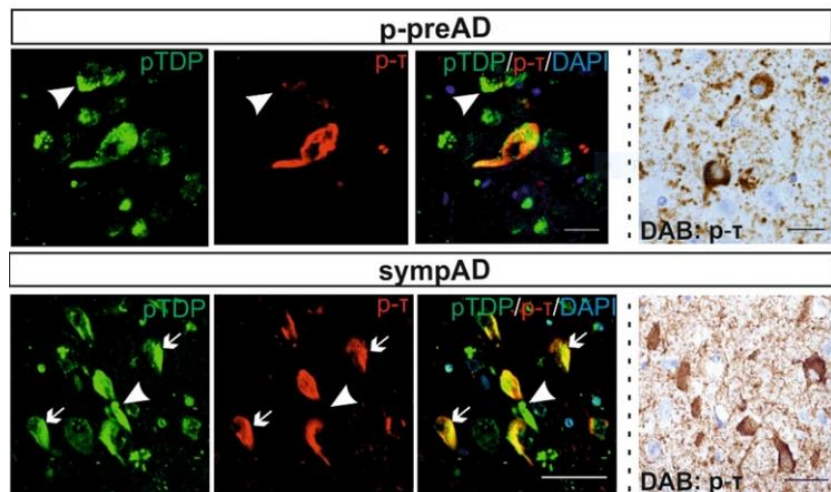


Figure 7 - TDP-43 aggregates colocalizes with Tau in AD

Immunostaining of the hippocampal CA1 region with phospho-TDP (pTDP) (in green) and phospho-Tau (pT) antibody (in red) of pre-clinical AD cases (p-preAD) and symptomatic AD cases (sympAD). Arrows indicate colocalization of pT and pTDP in the same neurons, arrowheads point to inclusions only positive for pTDP, and asterisks shows inclusions only positive for pT – modified from (Tomé et al., 2021), with permission to reuse under license number 5822460798651.

However, whether they influence each other's oligomerization, aggregation or seeding behavior is still unknown. There has been much speculation on this subject, yet no clear conclusion has been reached. What is known is that these two proteins share similar pathological cascades in their respective proteinopathies. Some of the causes that can lead to their aggregation, such as different types of stress or defects in autophagy, are common factors in these diseases, and therefore it is not surprising that the two proteins may be reciprocally involved in the pathogenesis of different disorders (Chornenkyy et al., 2019).

Several studies support the hypothesis of a crucial interplay between Tau and TDP-43, critical for the pathogenesis of AD and other proteinopathies (Montalbano et al., 2020; Tomé et al., 2021). However, little is known about the interaction of TDP-43 and Tau on the molecular level. Thus, further investigation is required and such insights will be fundamental for unraveling disease mechanisms and subsequently developing specific therapeutic interventions.

2.4.1 Tau/TDP-43 pathology in other neurodegenerative diseases

Evidence of Tau/TDP-43 co-pathology has been found not only in AD, but also in other neurodegenerative diseases, such as FTLN, ALS and Lewy body disorders (Chornenkyy et al., 2019; Higashi et al., 2007; Kim et al., 2018; Koga et al., 2022; McAleese et al., 2017; Nakashima-Yasuda et al., 2007; Stevens et al., 2019; Takeda et al., 2015).

FTLN is typically categorized into different subtypes based on the specific protein accumulation (e.g. FTLN-TDP, FTLN-Tau, FTLN-FUS), i.e. they mostly feature one dominant protein pathology (I. R. A. Mackenzie et al., 2010). In the past, only rare cases of "mixed FTLN" have been observed, such as a patient with primary progressive aphasia (PPA)

reported by Flanagan and colleagues, who exhibited both tauopathy and TDP-43 proteinopathy (Flanagan et al., 2016).

Although the co-occurrence of TDP-43 and Tau pathologies in FTLD patients remains uncommon, recent studies have discovered more cases of FTLD with both Tau and TDP-43 co-pathologies (Bieniek et al., 2013; Freeman et al., 2008; Kim et al., 2018; Koga et al., 2022).

For example, Kim and colleagues identified mixed TDP-43 and Tau pathology in 3.6% of FTLD cases. Furthermore, they presented FTLD-corticobasal degeneration (CBD) as the most common tauopathy with concomitant TDP-43 pathology. This mixed FTLD variant exhibits the typical clinical outcomes of FTLD but the more severe type, with pronounced atrophy in the affected brain regions, and with TDP-43 pathology observed not only in the limbic area, but also in the frontal and temporal gyrus (Kim et al., 2018).

Another study confirmed the presence of TDP-43 pathology in CBD subjects, but not in progressive supranuclear palsy (PSP) and Pick's disease cases. They observed TDP-43 inclusions similar to those seen in FTLD-TDP, as well as a distinct type of glial TDP-43 pathology, all possibly found in the same neurons with Tau aggregates, although they did not colocalize (Uryu et al., 2008).

These results contrast with the 33% Pick's disease cases analyzed by Freeman and colleagues, which presented TDP-43 aggregates partially colocalized with both Tau and ubiquitin in small cytoplasmic inclusions and in Pick's bodies (Freeman et al., 2008).

These discrepancies among different studies may be due to several reasons, including varying technical approaches and the heterogeneity of tissue samples; nevertheless, it is possible to conclude that TDP-43 pathology is present not only in AD but also in other tauopathies.

Similarly, a study which analyzed different FTLD-TDP cases, with and without motor neuron disease (MND), confirmed the presence of Tau pathology in these subjects, especially primary age-related tauopathy (PART) and ageing-related tau astroglipathy (ARTAG), occurring at a rate of 30-40%; this result suggests a more common frequency of the co-occurrence of the two pathologies in FTLD subjects (Koga et al., 2022).

Moreover, there is also substantial evidence of Tau pathology in ALS.

A few years ago, phosphorylated Tau was identified in both upper and lower motor neurons of sporadic ALS patients, suggesting a role for Tau phosphorylation in the pathogenesis of this disease (Stevens et al., 2019). Specifically, they found that Tau phosphorylated at serine 396 (pS396) was present in both the nucleus and cytoplasm of lower and upper motor neurons, whereas Tau pS214 and pS404 was found only in the cytoplasm of upper and lower motor neurons. Additionally, they observed a distinct Tau phosphorylation progression in the motor cortex and spinal cord, which differently influences the number of affected neurons and the duration of the disease (Stevens et al., 2019).

Moreover, insoluble and hyperphosphorylated Tau was present in ALS patients with cognitive impairment (ALSci), with both intraneuronal and extracellular inclusions. Tau aggregates were also significantly present in astrocytes of amygdala, entorhinal cortex, frontal cortex, cingulate gyrus and basal ganglia of ALS patients (Yang et al., 2003; Strong et al., 2006; Yang and Strong, 2012).

Furthermore, harmful 17 kDa Tau fragments generated by calpain-mediated cleavage and previously observed in AD and other tauopathies (Ferreira and Bigio, 2011), have also been detected in the spinal cord and in the upper motor neurons of ALS subjects, presenting a possible role of Tau neurotoxic fragmentation in the pathogenesis of ALS (Vintilescu et al., 2016).

Another example of TDP-43 and Tau co-pathology is the one observed in cerebral age-related TDP-43 with sclerosis (CARTS), described in patients of old age with TDP-43 pathology but lacking AD. In these patients a high incidence of dentate granule NFTs have been detected in the hippocampus. This study supports the hypothesis that in the later stages of the disease, multiple protein pathologies can coexist in the brain (Smith et al., 2018)

Lastly, it is known that patients can simultaneously present clinical signs of AD and either PD or DLB (McKeith et al., 2005). Given that TDP-43 pathology commonly occurs in AD, several studies have identified the co-occurrence of TDP-43 and Tau in Lewy bodies disorders (Arai et al., 2009; Higashi et al., 2007; McAleese et al., 2017; Nakashima-Yasuda et al., 2007).

When analyzing cases of concomitant AD and DLB, 30-50% were positive for TDP-43 pathology, which was found in the hippocampus and entorhinal cortex (Nakashima-Yasuda et al., 2007; McAleese et al., 2017). Double fluorescent immunohistochemistry revealed high colocalization between cytoplasmic and neuritic TDP-43 inclusions with ubiquitin; in contrast, co-presence of TDP-43 with Tau or α -synuclein aggregates was only rarely observed in the cytoplasm of the same cells, although there was some correlation between the deposition of these proteins (Nakashima-Yasuda et al., 2007).

Another study identified TDP-43 inclusions in AD and DLB brains. These aggregates were located in the amygdala and hippocampus in AD and DLB, whereas they are normally located in frontal cortex of FTLTDP patients, suggesting different TDP-43 pathology distribution in different diseases. In contrast, the morphology of TDP-43 inclusions was similar among the different disorders. Additionally, TDP-43-positive inclusions were found in the same neurons with Tau NFTs and α -synuclein LBs, with a higher colocalization with the latter protein (Higashi et al., 2007).

It is also worth mentioning animal experiments that support the idea of the presence of Tau/TDP-43 co-pathology in synucleinopathies. Specifically, mice injected with recombinant α -synuclein fibrils start to accumulate both pTau and TDP-43 after one month, although there is no or little colocalization of these proteins with α -synuclein. These results reflect observations found in patients and suggest a synergistic effect on the accumulation of these three proteins (Masuda-Suzukake et al., 2014).

Taken together, the evidence for a high prevalence of co-pathologies in neurodegenerative diseases is supported by a growing body of *in vitro*, *in vivo* and clinical studies. Tau/TDP-43 co-pathology is particularly frequent and has been observed in different diseases, such as AD, FTLTDP, ALS and DLB (Josephs et al., 2014b; Latimer et al., 2022; Nonaka et al., 2018; Takeda et al., 2015; Tomé et al., 2020).

2.5 Tau and TDP-43

As introduced above, Tau and TDP-43 are among the key players in various neurodegenerative diseases. Despite being associated with distinct physiological functions, they share some similarities, while also possessing evident differences (Fig. 8). Structural and functional aspects of Tau and TDP-43 are a fascinating topic and examining them more closely will help to unravel the intricate mechanisms underlying neurodegeneration.

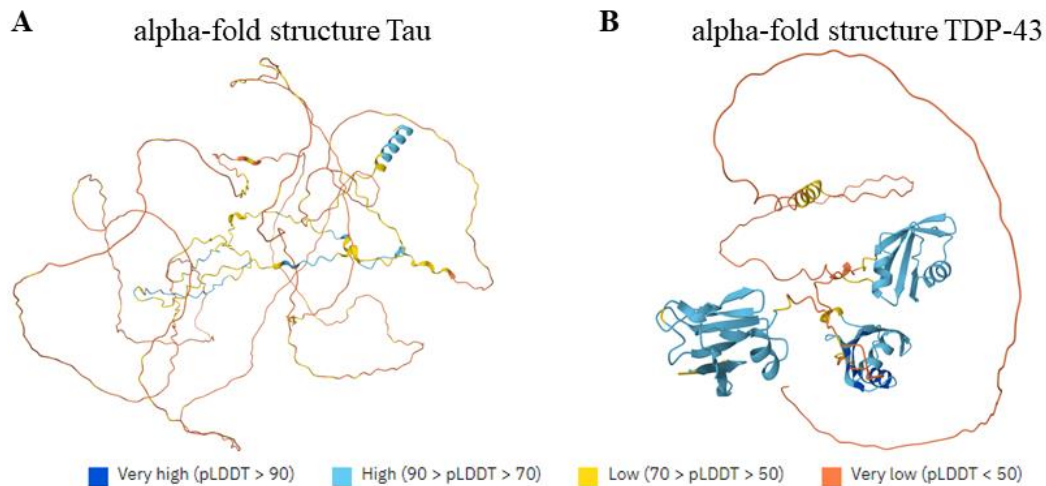


Figure 8 - Scheme of Tau and TDP-43 structures and their natural disordered regions

A and B: alpha-fold structures of Tau and TDP-43 created using AlphaFold Protein Structure Database (AFDB) (Varadi et al., 2024); pLDDT is a per-residue model confidence score between 0 and 100.

2.5.1 Tau protein: structure, functions and PTMs

Tau is encoded by the *MAPT* gene, which undergoes alternative splicing mRNA of exons E2, E3 and E10. This leads to the generation of six different splice isoforms (Fig. 9) of the protein that exhibit differential expression patterns during development and in various brain regions (Andreadis, 2005).

Tau consists of four major domains (Fig. 9): the N-terminal projection domain (NTD), the proline-rich region (PRD), the microtubule-binding domain (MTBD), and the C-terminal domain (CTD). The N-terminal projection domain projects from the microtubule surface to interact with cellular components and is characterized by acidic residues and several phosphorylation sites. The proline-rich region facilitates protein-protein interactions, while the MTBD, comprising microtubule-binding repeats, is responsible for Tau's crucial role in stabilizing microtubules. Lastly, the C-terminal assembly domain plays a role in regulating Tau aggregation (Kolarova et al., 2012).

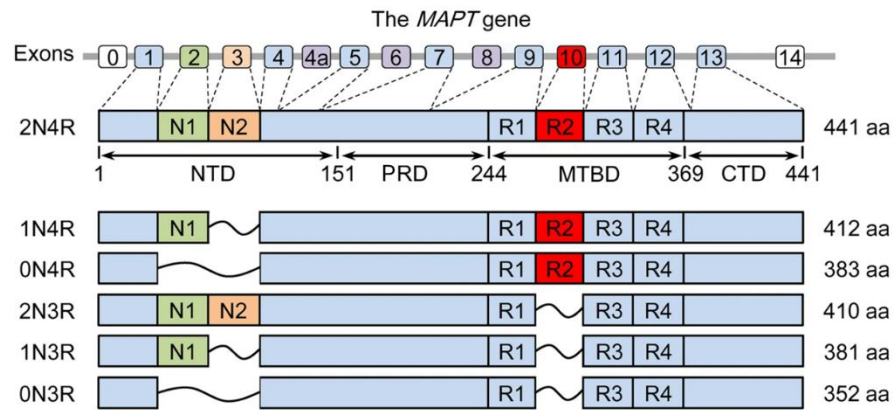


Figure 9 - Structure of Tau and its 6 isoforms

Scheme of Tau encoded by 13 exons, showing its different domains; N-terminal domain (NTD), proline-rich domain (PRD), microtubule binding domain (MTBD) and C-terminal domain (CTD) (upper part). Alternative splicing leads to the generation of 6 isoforms 2N4R, 1N4R, 0N4R, 2N3R, 1N3R and 0N3R (lower part) – from (Ye et al., 2022), with permission to reuse under license number 5797151088945.

Tau is a hydrophilic and basic protein and it is natively unfolded, i.e. it is of intrinsically disordered nature (Mukrasch et al., 2009), with its sequence exhibiting different charges. This distinctive charge distribution not only governs Tau's interaction with microtubules and other molecules, but also its aggregation processes (Wang and Mandelkow, 2016).

Primarily localized in axons, Tau's key functions are stabilizing microtubules and promoting their assembly via tubulin polymerization (Fig. 10). Microtubules are essential components of the neuronal cytoskeleton involved in intracellular transport and structural support. Given its functions, Tau facilitates proper axonal transport of cellular cargoes, including organelles and proteins. This critical role underscores its significance in maintaining neuronal structure and function, highlighting its indispensability in ensuring proper cellular integrity and communication within the nervous system (Feinstein and Wilson, 2005; Mandelkow and Mandelkow, 2012).

Emerging evidence suggests that Tau may have additional functions, which still need to be investigated. For instance, Tau is also found in small amounts in dendrites, where it may play a role in regulating synaptic plasticity, and in neuronal nuclei, where it maintains the integrity of DNA and RNA (Fig. 10). Moreover, Tau influences neurite outgrowth and interacts with actin, modulating the cytoskeletal network and thereby affecting neuronal connectivity and communication; these functions further highlight its complex role in neuronal physiology (Wang and Mandelkow, 2016).

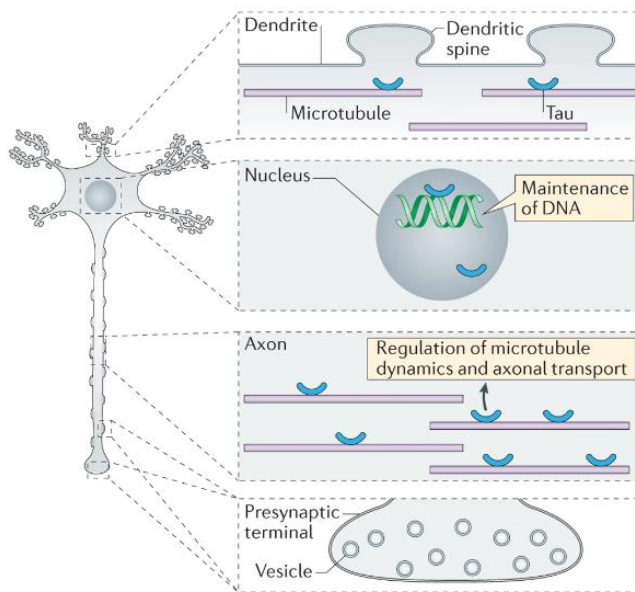


Figure 10 – Physiological functions of Tau

Cartoon on physiological functions of Tau in the different neuronal compartments: in the dendrites Tau binds and stabilizes the microtubules (MTs), in the nucleus it is involved in the maintenance of DNA, in the axons Tau regulates MT dynamics and axonal transport, and it also modulates vesicle deposition at the synaptic level – modified from (Wang and Mandelkow, 2016), with permission to reuse under license number 5797150553287.

Post-translational modifications (PTMs) play a crucial role in modulating the structure and physiological function of various proteins, however aberrant modifications have been found in proteins implicated in neurodegenerative diseases (Li et al., 2024; Sternburg et al., 2022).

Tau undergoes a myriad of PTMs (Fig. 11), including phosphorylation, acetylation, glycosylation, ubiquitination, and truncation, among others. Phosphorylation is the most extensively studied protein modification; for instance, it is intricately involved in regulating Tau's physiological functions, such as its binding to microtubules (Kolarova et al., 2012).

Hyperphosphorylation of Tau remarkably disrupts its functionality: it triggers detachment of Tau from microtubules and alters its interactions with other partners (Martin et al., 2011); additionally, it can lead to the protein's translocation to the somatodendritic compartment, ultimately contributing to synaptic dysfunction (Hoover et al., 2010). Furthermore, hyperphosphorylation alters Tau's susceptibility to proteases and its recognition by complexes involved in protein degradation, consequently enhancing Tau aggregation (Wang and Mandelkow, 2016).

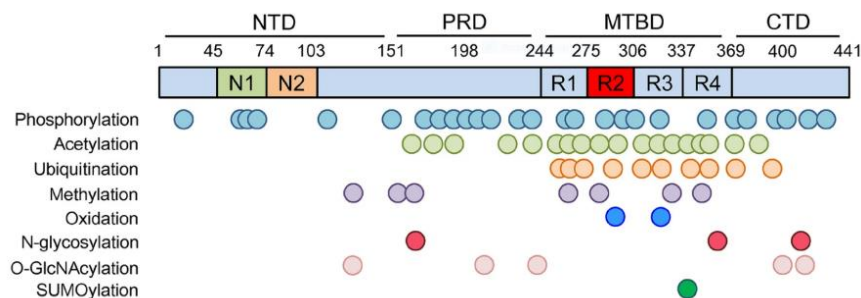


Figure 11 – PTMs in Tau

Scheme showing different PTMs identified in physiological and disease conditions, both in vitro and in vivo, and their location on the Tau protein – modified from (Ye et al., 2022), with permission to reuse under license number 5797151088945.

Collectively, there is evidence that Tau hyperphosphorylation precedes and drives the processes of Tau aggregation and cleavage (Martin et al., 2011; Mondragón-Rodríguez et al.,

2008), however there are also examples of site-specific phosphorylation of Tau that inhibits its fibrillization and seeding capacity (Haj-Yahya et al., 2020).

Consistent with this, there are also other PTMs that exert contrasting effects on Tau degradation and aggregation, depending on the specific sites of modification (Yuzwa et al., 2014). For example, acetylation can either facilitate or inhibit Tau degradation, while glycosylation on specific sites can promote hyperphosphorylation and maintenance of Tau PHFs. Furthermore, ubiquitination marks Tau for degradation via the proteasome or autophagy pathways, whereas truncation generates Tau fragments with increased neurotoxicity (Martin et al., 2011; Min et al., 2010; Wang and Mandelkow, 2016).

The debate on the role of PTMs on proteins implicated in neurodegenerative diseases is still ongoing, and additional studies are necessary to elucidate whether PTMs exert protective effects or directly contribute to pathological mechanisms (Sternburg et al., 2022).

2.5.2 TDP-43 protein: structure, functions and PTMs

TAR DNA-binding protein 43 is encoded by the *TARDBP* gene and is crucially involved in various cellular processes, particularly due to its binding to RNA and occasionally to DNA (Ayala et al., 2005).

Structurally, TDP-43 comprises several distinct domains, including the two folded RNA recognition motifs (RRM1 and RRM2) in the N-terminal region, which also contains the nuclear localization signal (NLS), followed by an intrinsically disordered region (IDR) in the C-terminal domain, which is also called low complexity domain (LCD) or prion-like domain (PrLD) (Fig. 12) (Asakawa et al., 2021).

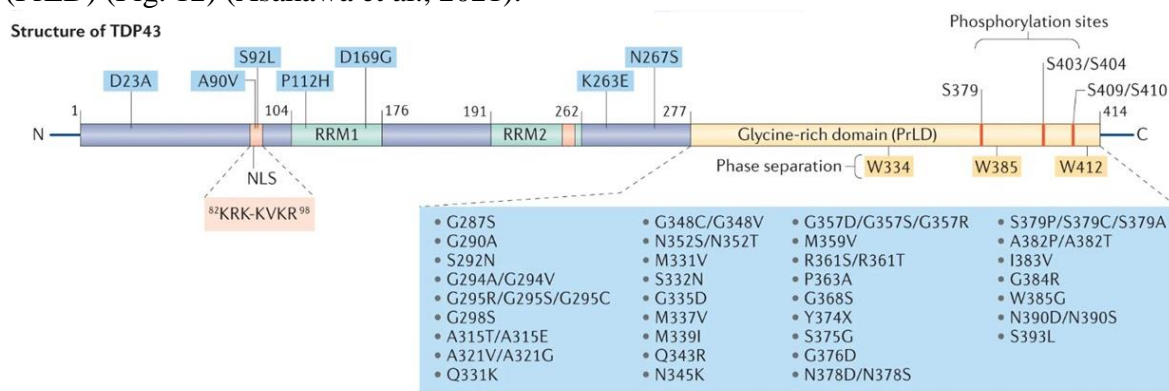


Figure 12 - Structure of TDP-43 with its disease-causing mutations

TDP-43 sequence consists of: the N-terminal domain (in violet) harboring a bipartite nuclear localization signal (NLS), two RNA recognition motif (RRM1 and RRM2) domains (in green), and the C-terminal domain, also called glycine-rich prion like domain (PrLD) (in yellow), which has three tryptophan residues (highlighted in yellow) that are crucial for *TDP-43*'s phase separation; blue boxes depict all ALS/FTD-linked mutations found on *TDP-43*, some of the disease-linked serine phosphorylation sites are also highlighted – modified from (Tziortzouda et al., 2021), with permission to reuse under license number 5797160155970.

The RNA recognition motifs mediate the interaction of TDP-43 with DNA/RNA molecules, in particular through RRM1 which is necessary and sufficient for the binding process; this

recognition involves binding of TDP-43 to UG repeats present in the target RNA sequences, and the binding affinity increases with the number of these repeats (Buratti and Baralle, 2001). In contrast to the folded RRM domains, the LCD is intrinsically disordered, i.e. it does not adopt a stable secondary or tertiary structure, with exception of a short α -helix (amino acids 321 – 340) (Conicella et al., 2016, 2020) which contributes to protein-protein interactions and phase separation of TDP-43 (Conicella et al., 2016, 2020; Hallegger et al., 2021); additionally, the C-terminal PrLD harbors three tryptophan residues, which are crucial for TDP-43's phase separation (Fig. 12) (Conicella et al., 2020; Li et al., 2018b; Tziortzouda et al., 2021).

Furthermore, under physiological conditions, the N-terminal folded domain (amino acids 1-80) drives the homo-oligomerization of TDP-43, which is crucial for the protein's physiological function in regulating splicing, and appears to protect against cytoplasmic TDP-43 aggregation, possibly by spatially separating the aggregation-prone C-terminal domains of individual protein monomers (Afroz et al., 2017; Oiwa et al., 2023).

Another crucial sequence element in the N-terminal region of TDP-43 is the nuclear localization signal (NLS), which directs TDP-43 to the nucleus, where it primarily resides under normal cellular conditions (Winton et al., 2008). Defects in nuclear import, e.g. due to impaired function of nuclear import receptors, have been implicated in the mislocalization and cytoplasmic aggregation of TDP-43 in neurodegenerative diseases, such as ALS and FTD (Hutten & Dormann 2020).

TDP-43 is a ubiquitously expressed nuclear RNA-binding protein, primarily recognized for its role in RNA metabolism, regulating all steps of the mRNA life cycle (Fig. 13) (Ratti and Buratti, 2016). Notably, one of the RNA target of TDP-43 is its own transcript, thereby the protein regulates its own expression in an autoregulatory mechanism to maintain the cellular TDP-43 levels at a physiological concentration (Ayala et al., 2011).

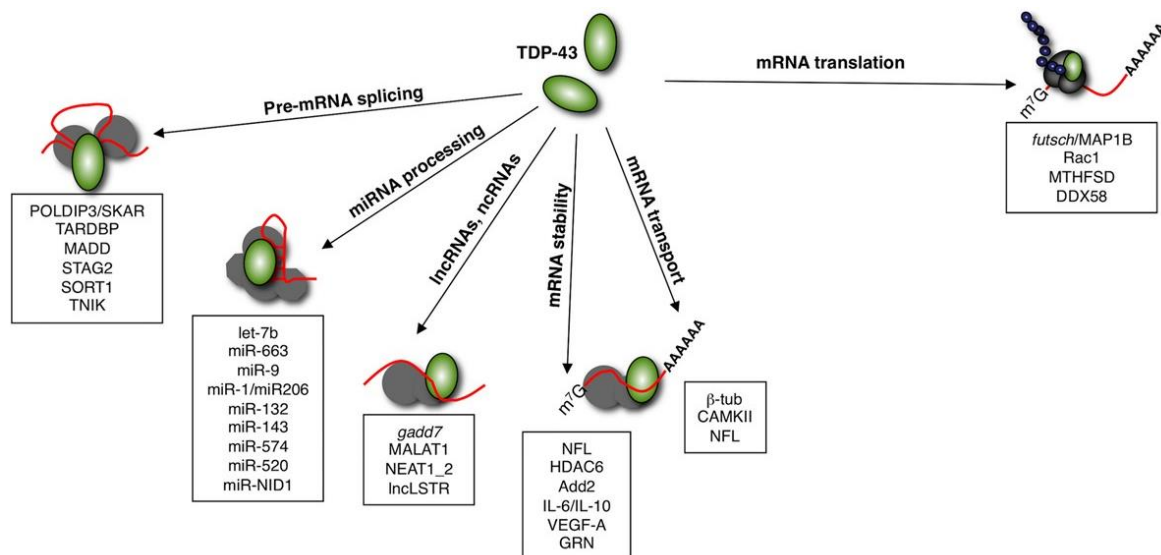


Figure 13 - Physiological functions of TDP-43

Scheme depicting the different physiological functions of TDP-43, both in the nucleus and in the cytoplasm; boxes list the names of the RNA targets – modified from (Ratti and Buratti, 2016), with permission to reuse under license number 5820810117151.

Moreover, TDP-43 is also implicated in DNA repair mechanisms, highlighting the critical nature of its nuclear localization and its broader impact on cellular integrity and genomic stability (Mitra et al., 2019).

Recent findings have shown that TDP-43 plays a crucial role in the repression of cryptic exons. The latter are alternatively spliced exons that, if incorporated, can cause aberrant changes to the resulting mRNA. While they are typically skipped during normal splicing, they can be erroneously incorporated under certain conditions, and it has been shown that loss of TDP-43 in mouse embryonic stem cells results in the incorporation of cryptic exons into certain mRNAs, leading to disruptions of their translation and nonsense-mediated decay (Ling et al., 2015). An example of this phenomenon is observed in the variants of *UNC13A*, a gene critical for synapse function; this has been linked to increased susceptibility to ALS and FTD, as the loss of nuclear TDP-43 results in the inclusion of a cryptic exon in the *UNC13A* transcript, leading to the loss of UNC13A protein (Brown et al., 2022).

Beyond its nuclear localization, TDP-43 can shuttle into the cytoplasm by passive diffusion (Ederle et al., 2018), where it plays essential roles in mRNA stability, trafficking and translation (Ederle and Dormann, 2017). Additionally, TDP-43 has been shown to form mRNP transport granules with targeted mRNA to facilitate their anterograde transport from the soma to the axons of neurons via microtubules (Alami et al., 2014)

As described above for Tau, TDP-43 also undergoes several PTMs, such as phosphorylation, acetylation, oxidation and nitrosylation, ubiquitination, O-GlcNAcylation and proteolysis (Fig. 14) (Sternburg et al., 2022). These modifications modulate TDP-43 subcellular localization, its interactions with RNA and other proteins, and ultimately its propensity for aggregation and subsequent toxicity.

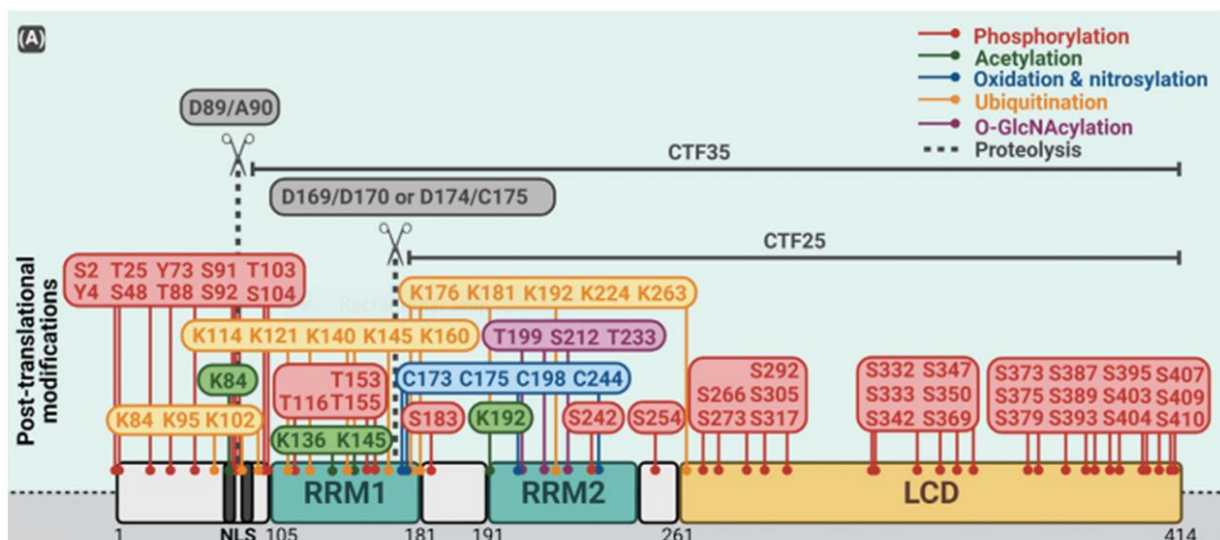


Figure 14 - PTMs in TDP-43

PTMs on the different domains of TDP-43 - modified from (Sternburg et al., 2022), with permission to reuse under license number 5821171181135.

The most common PTM of TDP-43 is phosphorylation, typically targeting serines in the case of this protein (Buratti, 2018).

The debate on its protective or pathological implications is ongoing. On one side, it has been widely described that in pathological situations, TDP-43 can become hyperphosphorylated, with findings indicating that this PTM can promote protein aggregation. For instance, studies utilizing a *C. elegans* TDP-43 proteinopathy model have demonstrated that phosphorylation contributes to protein aggregation (Liachko et al., 2010); moreover, experiments involving overexpression of various TDP-43 kinases promotes TDP-43 aggregation and subsequent neurotoxicity (Nonaka et al., 2016; Taylor et al., 2018). Furthermore, hyperphosphorylation is observed in the cleaved C-terminal fragments (CTFs) of TDP-43, which have been extensively implicated in neurodegenerative processes (Arai et al., 2010).

On the other side, phosphorylation can also be considered as a protective mechanism. Mimicking the phosphorylation pattern of ALS and FTD on TDP-43 has been shown to strongly suppress its phase separation and aggregation (Grujjs da Silva et al., 2022).

Thus, TDP-43 phosphorylation, initially described only as a pathological mechanism, can now be also considered as a protective event that counteracts TDP-43 aggregation (Grujjs da Silva et al., 2022).

Furthermore, TDP-43 frequently undergoes proteolysis and ubiquitination, PTMs also implicated in disease-link modifications. Proteolysis of TDP-43 results in the formation of C-terminal fragments (CTF), already described in chapter 1.2.3 (Sternburg et al., 2022); ubiquitination, instead, is the process which attaches ubiquitin molecules primarily to lysine residues of a protein or aggregate to signal its degradation via the ubiquitin-proteasome pathway (Buratti, 2018); in diseases, this pathway is impaired leading to the accumulation of ubiquitinated TDP-43.

All the aforementioned PTMs have been observed in TDP-43 inclusions found in the brains of ALS and FTD patients (Sternburg et al., 2022); in most cases of AD with TDP-43 proteinopathy, phosphorylation and the generation of CTFs of TDP-43 are the predominant modifications observed (Meneses et al., 2021).

While PTMs may initially be physiological, over time, they can eventually become the opposite, driving the progression of the pathology and accelerating the deposition of protein aggregates in the brain of patients affected by neurodegenerative diseases.

2.5.3 Recruitment of Tau and TDP-43 to Stress Granules

Another important aspect of Tau and TDP-43 is their recruitment to stress granules (SGs), cytoplasmic assemblies composed of proteins and mRNA that form in response to various stress conditions. Their primary function is to stop translation and protect mRNA molecules from degradation during cellular stress. Their assembly is a dynamic and reversible process: upon the resolution of stress, SGs disassemble, allowing the translation machinery to resume normal function and mRNAs to be re-engaged in translation (Protter and Parker, 2016; Riback et al., 2017).

Dysregulation of stress granule dynamics has been implicated in various neurodegenerative disorders like ALS and FTD, where persistent stress granules can contribute to cellular dysfunction and disease progression (Alberti et al., 2019; Wolozin and Ivanov, 2019). In fact, chronic stress that prevents the dissolution of SGs leads to the formation of stable stress

compartments, which serve as nuclei for the aggregation of disease-related proteins (Fakim and Vande Velde, 2024; Li et al., 2013; Wolozin and Ivanov, 2019).

The composition of SGs has been extensively studied, and among the different associated proteins, Tau is one of them (Wolozin and Ivanov, 2019). In fact, research indicates that Tau interacts with key SG components, such as TIA1 (Ash et al., 2021) and GRBP2 (Wang et al., 2023).

Furthermore, under stress conditions TDP-43 translocates to the cytoplasm (Dewey et al., 2011), where it is also recruited to SGs and likely contributes to their formation (Colombrita et al., 2009), regulating their dynamics by stabilizing mRNAs and modulating their trafficking (Gao et al., 2018; Lee et al., 2011). Notably, SGs are also widely recognized as initial sites for TDP-43 aggregation, particularly due to the high concentration of the protein in these compartments when the stress persists (Ratti and Buratti, 2016). Additionally, several SG markers have been found in aggregates of patients with ALS and FTD, further confirming their role in disease pathology (Bentmann et al., 2012; Dormann et al., 2010)

2.6 Phase separation: basic biophysical principles

Phase separation (PS) is a fascinating phenomenon in which biomolecules, particularly proteins and nucleic acids, segregate into distinct liquid-like compartments within the cellular environment; these compartments are known as membraneless organelles (MLOs) and describe different cellular structures, such as SGs (Alberti, 2017).

PS is a biophysical process in which polymeric molecules undergo separation into two distinct phases: a dilute phase devoid of molecules and a dense phase that is highly enriched in these molecules; thus, PS is a condensation process, in which biopolymers form a network of interacting molecules giving rise to “biomolecular condensates”.

The formation of the biomolecular condensates is driven by multivalent interactions such as electrostatic interactions, between folded domains or intrinsically disordered regions (IDRs) of proteins, which can also involve nucleic acids (Fig. 15) (Alberti and Hyman, 2021; Boeynaems et al., 2018). Multidomain proteins can undergo multivalent protein-protein interactions; their multidomain composition provide them with high valency, enabling them to form extensive molecular networks and undergo phase separation (Li et al., 2012). Also IDRs, which constitute ~30% of our proteome and lack a fixed structure, often engage in multivalent protein-protein or protein-nucleic acid interactions, facilitating the formation of molecular networks and phase separation processes (Fig. 15) (Alberti and Dormann, 2019; Boeynaems et al., 2018; Borchers et al., 2021).

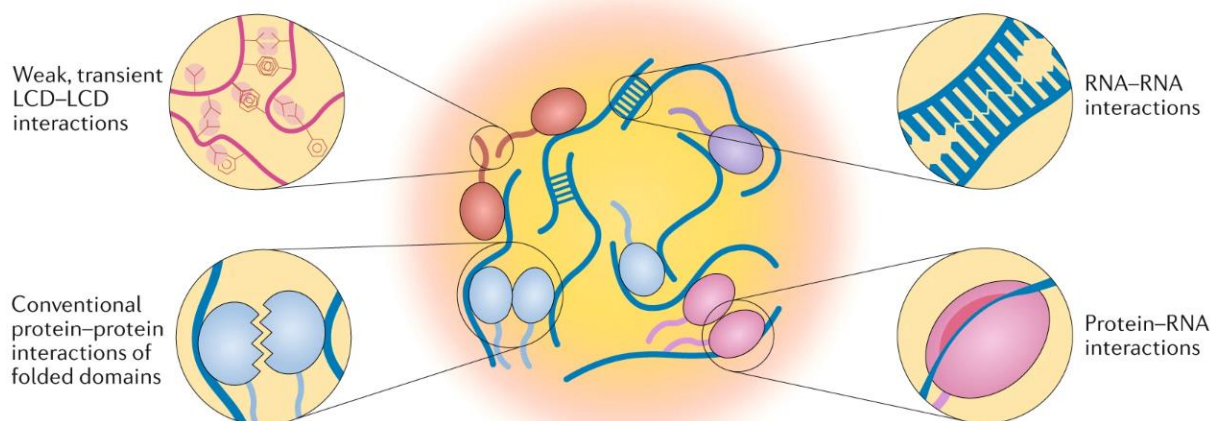


Figure 15 – Multivalent interactions that drives phase separation

Examples of multivalent interactions that drive PS: transient interactions between low complexity domains (LCDs), protein-protein interactions, RNA-RNA interactions and protein-RNA interactions - from (Nedelsky and Taylor, 2019), with permission to reuse under license number 5821341415203.

The PS of IDRs can be described by the “stickers and spacers” model: stickers facilitate multivalent interactions between polymeric chains, while spacers provide flexibility of the network, thus promoting a dynamic, liquid-like behavior of the dense phase (J. Wang et al., 2018). Examples of IDRs that drive PS contain arginine- and glycine-rich (RGG/RG) repeats (Chong et al., 2018), and prion-like low-complexity sequences with predominantly polar residues which promote multivalent interactions (Alberti et al., 2019).

Lastly, RNAs are ideal molecules for driving PS processes due to their multivalent nature; they have been found to be key components of biomolecular condensates in cells, which assemble through RNA-RNA and RNA-protein interactions (Langdon et al., 2018).

2.6.1 Phase separation in cells

Traditionally, cellular organization was thought to be governed only by compartments with lipid membranes (such as mitochondria, the endoplasmic reticulum or the Golgi apparatus), however it is now widely recognized that there is another layer of intracellular organization, defined by MLOs that arise through phase separation (Alberti, 2017).

The MLOs play critical roles in various cellular processes, including formation of cytoskeletal structures, signaling, transcription, and stress response (Jalihal et al., 2021). Examples of cytoplasmic biomolecular condensates are SGs and P granules, bodies containing RNAs and proteins with liquid-like properties (Brangwynne et al., 2009). In contrast, nuclear MLOs are the nucleolus with its multilayered compartments formed by spontaneous PS (Feric et al., 2016), and other bodies such as Cajal bodies and paraspeckles (Boeynaems et al., 2018; Forman-Kay et al., 2022). While all of these aforementioned MLOs are RNA-protein condensates (RNP granules), there are also non-RNA-protein MLOs, such as condensates involved in DNA repair, signaling condensates, or MLOs involved in the formation of the nuclear pore complex.

There are two types of molecules within cellular condensates: scaffolds and clients. Scaffolds have a high valence, meaning they form numerous interactions and drive the PS process, also setting the threshold concentration; clients, on the other hand, have a lower valence and are the one recruited by the scaffolds to become part of the condensate (Alberti and Dormann, 2019; Alberti and Hyman, 2021).

Importantly, phase separation of these molecules provides a means for the spatial organization and concentration of biomolecules, allowing for efficient biochemical reactions and regulation of cellular activities (Alberti et al., 2019; Shin and Brangwynne, 2017).

Finally, the MLOs can adapt to different physical states and properties, adjusting to cellular needs and responding to environmental cues such as temperature, pH, molecular concentrations, and salt composition (Alberti, 2017; Alberti et al., 2019).

2.6.2 Regulation of phase separation

Overall, a variety of parameters and mechanisms govern cellular phase separation, and the synergy of these factors allows cells to control and modulate the assembly and dynamics of MLOs (Snead and Gladfelter, 2019).

For instance, PS is not only regulated by the concentration of molecules involved in the condensation, but also by the changes in temperature, pH and ionic strength within the cellular environment (Alberti, 2017; Alberti et al., 2019).

Additionally, both genetic mutations and environmental factors can affect the formation of cellular condensates, for example, by altering protein properties. These changes can lead to shifts in compartment localization or solubility, ultimately resulting in loss- or gain-of-function mutations (Alberti and Dormann, 2019; Alberti and Hyman, 2021).

PTMs also play a crucial role in regulating PS, as they induce structural changes, create or eliminate binding sites, or alter the charge and hydrophobicity of amino acids, therefore affecting the propensity of a protein to undergo PS. Depending on the context, PTMs can either enhance or reduce phase separation (Borcherds et al., 2021; Liu et al., 2024).

For instance, phosphorylation, one of the most common protein modifications, introduces negatively charged phosphoryl groups to the hydroxyl groups of serine, threonine and tyrosine residues, and this modification can either positively or negatively affect phase separation (Hofweber et al., 2018; Sternburg et al., 2022).

Additionally, arginine methylation, which adds one or more methyl group to an arginine residue, alters the bulkiness and hydrophobicity of the modified arginine side-chain, mostly resulting in a decrease of PS (Hofweber et al., 2018; Sternburg et al., 2022). Another example is lysine acetylation, which reduces positive charges on proteins and thus can disfavor protein condensation processes (Saito et al., 2019).

Therefore, controlling PS is critical for the maintenance of normal cellular functions. However, dysregulation of phase separation has been implicated in various diseases, highlighting the importance of understanding the underlying principles of this process for both physiological functions and pathological implications.

2.6.3 Role of Tau and TDP-43 phase separation in health and disease

Intrinsically disordered regions (IDRs) of prion-like domain (PrLD) nature are crucial for driving PS of proteins; notably, both Tau and TDP-43 possess a disordered nature in their sequences and can undergo PS (Fig. 16) (Zbinden et al., 2020).

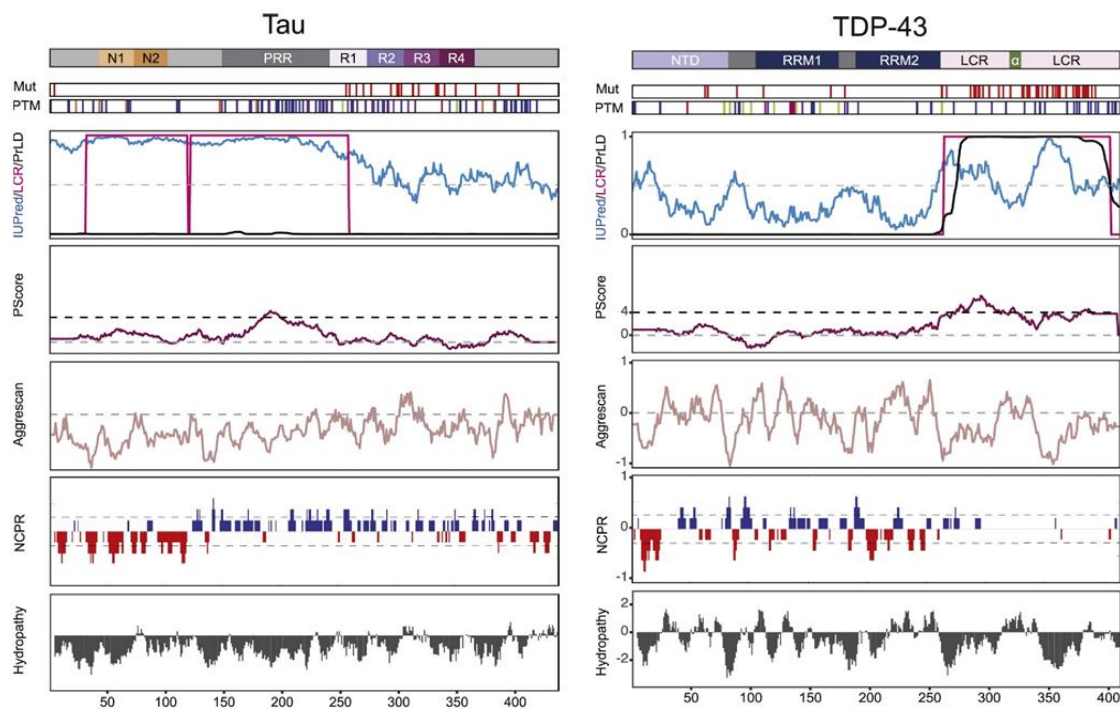


Figure 16 - Features of Tau and TDP-43 sequences

Scheme of Tau (on the left) and TDP-43 (on the right) of their sequence properties. First row: protein domains; second row: disease-associated mutations; third row: post-translational modifications (PTMs); fourth row: prediction of natural disordered regions; fifth row: propensity Score (pScore) assessing phase separating properties; sixth row: prediction of aggregation; seventh row: net charge per residue (NCPR), with positive charges in blue and negative charges in red; eighth row: prediction of hydrophobicity – modified from (Zbinden et al., 2020), with permission to reuse under license number 5820680216471.

Although Tau lacks a typical low-complexity domain (LCD) and its IDR is not prion-like, its intrinsic disorder allows the protein to PS (Ambadipudi et al., 2017; Zhang et al., 2017) and this process is governed by electrostatic interactions between its oppositely charged domains, i.e. the negatively charged N-terminal and the positively charged (lysine-rich) C-terminal domains (Fig. 16, left panel) (Boyko et al., 2019).

As mentioned before, PTMs play a key role in regulating protein PS; for instance, phosphorylation at lysine K18 and at serines S119 and S202 promotes Tau phase separation (Ambadipudi et al., 2017; Wegmann et al., 2018), whereas acetylation decreases it (Ferreon et al., 2018).

Additionally, the P301L mutation in the R2 domain of Tau also enhances PS, as well as the presence of RNA in the crowded environment (Hochmair et al., 2022; Lin et al., 2019).

PS of Tau has a big physiological relevance. For instance, it has been shown that Tau droplet formation promotes the local nucleation of microtubules by concentrating tubulin in the condensed phase, therefore facilitating the creation of microtubule bundles (Hernández-Vega et al., 2017a).

Contrarily to Tau, TDP-43 contains an extensive disordered LCD with PrLD that promotes various forms of self-assembly, including oligomers and droplet-like condensates through PS (Fig. 16, right panel) (Li et al., 2018a; A. Wang et al., 2018). Its IDRs are enriched in aromatic residues which drive TDP-43 condensation through π - π interactions (Li et al., 2018a); additionally, the transient α -helix in the C-terminal domain (CTD) also facilitate TDP-43 PS (Conicella et al., 2016, 2020; Hallegger et al., 2021), along with the three aromatic tryptophans (Fig. 12, highlighted in yellow), and the newly recognized phenylamine and methionine residues of the CTD (Mohanty et al., 2023).

Furthermore, phosphorylation at serine 48 disrupts TDP-43 oligomerization and PS (A. Wang et al., 2018), as well as C-terminal phosphomimetic mutations (serine-to-aspartate) suppresses its PS (Gruijs da Silva et al., 2022). Similarly, most ALS-associated mutations in the α -helix region also decrease TDP-43 PS (Conicella et al., 2016); instead, RNA binding oppositely modulates TDP-43 condensation, with specific RNA binding to the RRM decreasing and unspecific RNA binding to the LCR increasing PS of TDP-43 (Zbinden et al., 2020).

Physiologically, condensation of TDP-43 driven by homomeric CTD interactions is essential for efficient RNA regulation, including autoregulation of its own mRNA (Hallegger et al., 2021; Koehler et al., 2022). Additionally, PS and RNA-mediated self-assembly of TDP-43 are crucial mechanisms for its nuclear retention, preventing the mislocalization of the protein to the cytoplasm (Dos Passos et al., 2024).

Collectively, protein PS is an important physiological mechanism which governs several fundamental cellular functions. Due to its significance, disruptions of this process can cause detrimental defects. In fact, increasing evidence highlights the role of phase separation in different diseases such as cancer, age-related conditions, and neurodegeneration (Alberti and Dormann, 2019; Alberti and Hyman, 2021; de Oliveira et al., 2019). In the case of neurodegenerative diseases, the exact relevance of phase separation for the formation of protein inclusions in the brain is still under investigation, but it has been postulated that protein condensation may promote their pathological aggregation, representing an early event in the pathogenesis of different proteinopathies (Babinchak et al., 2019; Kanaan et al., 2020; A. Wang et al., 2018; Wegmann et al., 2018).

PS governs the dynamicity of several proteins implicated in neurodegeneration; in pathological conditions, these proteins undergo changes in their physical properties, transitioning from a liquid-to-solid state, phenomenon which is believed to drive the formation of pathological protein aggregates (Fig. 17) (Alberti and Dormann, 2019).

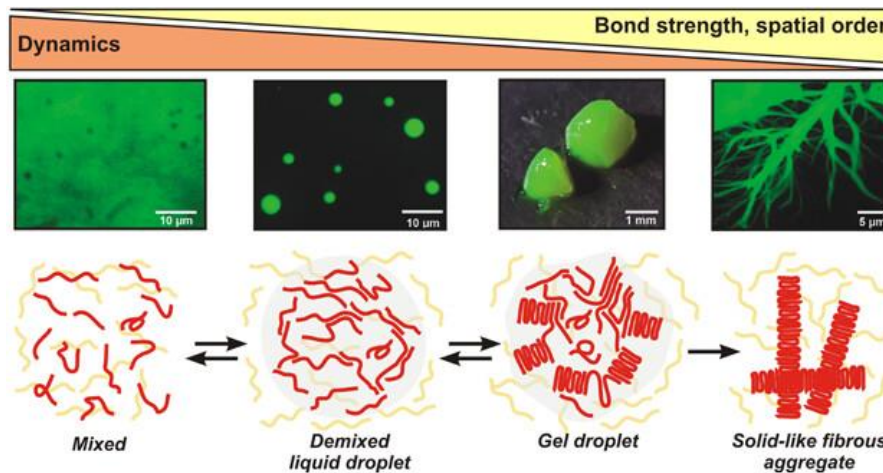


Figure 17 - Phase separation: from liquid molecules to solid-like structures

Scheme of phase separation events, from mixed molecules to the demixed liquid droplet, that turn into a gel-like structure and ultimately form solid aggregates. On top of the figure the purified protein FUS in Sarcoma (FUS) is shown as an example undergoing these different structural transitions – modified from (Alberti and Hyman, 2016), with permission to reuse with CC BY license.

The initial findings that led to this hypothesis were observed by researchers who studied purified hnRNPA1 and FUS *in vitro* (Molliex et al., 2015; Patel et al., 2015).

Molliex and colleagues showed that the RNA-binding protein hnRNPA1 can phase separate into liquid droplets and through this mechanism the protein is recruited by SGs. Since hnRNPA1 is prone to fibrillization, they hypothesized that the increased protein concentration found in the condensed liquid droplets could favor the nucleation of new fibrils (Molliex et al., 2015). Similarly, the other research group demonstrated that liquid droplets of FUS can convert over time to an aggregated state *in vitro*, describing an aberrant phase transition that proteins may undergo in disease-related conditions (Patel et al., 2015).

Subsequently, anomalous phase separation of Tau and TDP-43 were also described, both *in vitro* and in cells.

In the case of Tau, aberrant phosphorylation alters the protein's ability to condense into droplets, which may promote Tau aggregation and formation of solid fibrils (Ambadipudi et al., 2017; Wegmann et al., 2018). Additionally, prolonged phase separation of Tau has been shown to give rise to toxic conformers and favor its oligomerization, both phenomena exacerbated by disease-linked mutations (Kanaan et al., 2020).

Similarly, elevated cytoplasmic level of TDP-43 form long-lived liquid droplets; it has been demonstrated that under arsenite stress, these condensates rapidly convert into solid structures, recruiting additional phosphorylated TDP-43 and molecules of the nucleocytoplasmic transport, thereby promoting TDP-43 mislocalization and cell death (Gasset-Rosa et al., 2019). Moreover, a recent study also showed that upon increased TDP-43 concentration and during oxidative stress, TDP-43 phase separates and de-mixes with SGs components, forming dynamic granules that transition into pathological aggregates over time (Yan et al., 2024).

These observations highlight the importance of understanding the structural dynamics of Tau and TDP-43, which can be further elucidated through advanced techniques such as high-resolution protein structural analysis, crucial in order to study protein structures and to infer and predict their assembly in pathology (Zbinden et al., 2020).

Analyzing the atomic structure of amyloids from post mortem brain tissues with cryo-electron microscopy (cryo-EM) represent a significant advancement in the field, providing critical insights into protein folding and behavior (Scheres et al., 2023).

Both Tau and TDP-43 pathological structures have been extensively described (Arseni et al., 2022, 2023, 2024; Fitzpatrick et al., 2017).

In AD, NFTs of Tau consist of paired helical filaments (PHFs) and straight filaments (SFs), which present different protofilament packing; the core of the amyloid filaments is formed by two identical protofilaments made of Tau residues 306-378, which fold into a combined cross- β / β -helix structure. This core is sufficient and essential to initiate Tau fibrillization and seeding (Fitzpatrick et al., 2017).

For TDP-43 pathological aggregates, Arseni and colleagues described different aggregate structures for the various FTLD subtypes. In patients with ALS and type B FTLD-TDP, they identified amyloid-like filament structures formed by a single protofilament consisting of residues 282-360 of the CTD of TDP-43; this filament folds into a double-spiral shape (Arseni et al., 2022). In patients presenting type A FTLD-TDP, they described TDP-43 aggregates as chevron badge amyloid filaments, highlighting structural differences across diseases (Arseni et al., 2023). Finally, in type C FTLD-TDP patients, they found that the inclusions are formed not only by TDP-43 but also by annexin A11 (ANXA11), which co-assemble via their LCDs to form an extensive hydrophobic core (Arseni et al., 2024).

This latter research paves the way for further cryo-EM studies of protein structures involving multiple proteins, expanding the knowledge of co-pathologies in neurodegenerative diseases.

2.7 Spreading of Tau and TDP-43 pathology

Neurodegenerative diseases typically begin in a specific brain region and at later stages progress to other areas of the brain. Both tauopathies and TDP-43 proteinopathies are characterized by this phenomenon (Ayers et al., 2018; Jo et al., 2020; Polymenidou and Cleveland, 2011), which is governed by the prion-like propagation of pathological aggregates (Jucker and Walker, 2013). Prions are composed of misfolded prion protein (PrP) molecules that aggregate and induce aberrant conformational changes in native PrPs, acting as seeds and initiating a chain reactions of misfolding and spreading (Jucker and Walker, 2013).

Later, these events have been associated with several other proteins involved in neurodegenerative diseases, all of which can act as seeds and spread from cell to cell, causing the normal protein counterparts to misfold and become pathological (Aguzzi, 2009; Polymenidou and Cleveland, 2012)..

Usually, it is not the final large aggregates that act as seeds, but rather the pathological species at the beginning of the aggregation cascade; their small size allows them to be easily released and taken up by cells. For instance, numerous studies have demonstrated that Tau oligomers are the potent seeding species responsible for propagation (Berger et al., 2007; Takeda, 2018; Usenovic et al., 2015).

However, fragmentation of large aggregates into smaller, highly seed-competent particles can also occur (Nachman et al., 2020; Tittelmeier et al., 2020).

The spread of pathological proteins has been extensively studied and can be described as two sequential events: the release of the pathological seed from the donor cell, and its uptake by the recipient cell (Fig. 18) (Guo and Lee, 2014; Peng et al., 2020).

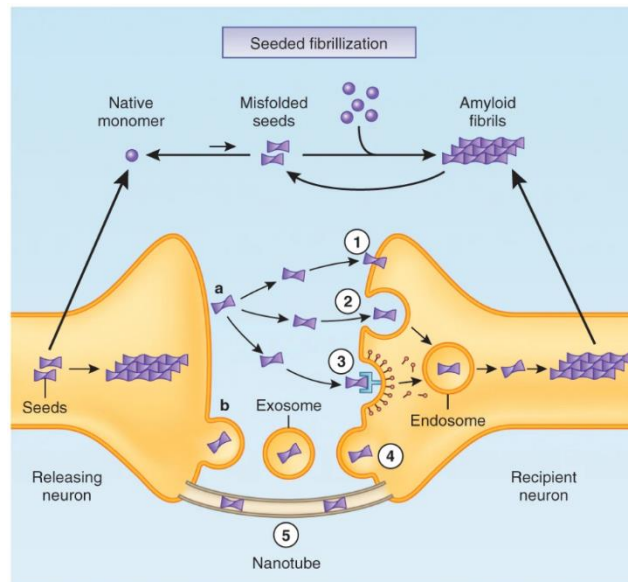


Figure 18 - Potential mechanisms of release and uptake of pathological seeds between two cells

Scheme showing the formation of pathological seeds from native monomer, and potential mechanisms how seeds can spread from a donor cell to a recipient cell. The seed can be released in the extracellular space either “naked” (a) or via exosome formation (b); once it reaches the recipient cell it can directly penetrate the plasma membrane (1), enter the cell via endocytosis (2) or receptor-mediated endocytosis (3), alternatively the exosome can fuse with the plasma membrane of the recipient cell (4). Finally nanotubes that connect the cytoplasm of the two cells can facilitate the seeding event (5) – (Guo and Lee, 2014), with permission to reuse under license number 5797170171199.

Seeds can be released extracellularly via diffusion after cell death, or through tunneling nanotubes that create direct contact between two cellular compartments allowing protein transfer. However, the most described and accepted release event is the exosome-based secretion, in which the released seed is packaged in vesicles, which are then internalized by recipient cells, either via receptor-mediated endocytosis or through simple fusion (Fig. 18) (Guo and Lee, 2014; Peng et al., 2020). Once internalized, the seeds can cause the vesicles to rupture in order to release their cargo into the recipient cells. This initiates the pathological amplification process by recruiting the natural counterpart of the protein and ultimately spread the disease (Fig. 18) (Flavin et al., 2017).

In the case of Tau, its release occurs through synaptic connectivity, and its internalization takes place by heparan sulfate proteoglycans (HSPGs) binding, specifically via the low-density lipoprotein receptor-related protein 1 (LRP1) (Holmes et al., 2013; Rauch et al., 2020, 2018). Moreover, phosphorylated Tau has been found in exosomes isolated from

cerebrospinal fluid (CSF) of AD patients (Saman et al., 2012; Wang et al., 2017), providing additional evidences for Tau exosome-based secretion.

The pathological spread of TDP-43 is also thought to occur via exosomes. It has been demonstrated that TDP-43 packed in microvesicles/exosome (MVEs) can be exchanged both horizontally (between neuronal somas) and vertically (between axons) (Feiler et al., 2015).

Additionally, several *in vitro* and cellular experiments have shown that aggregated forms of TDP-43, particularly aggregated CTFs, can seed physiological TDP-43 to aggregate (Furukawa et al., 2011; Jo et al., 2020; Nonaka et al., 2013; Pesiridis et al., 2011).

Nevertheless, further investigation is needed to elucidate the precise molecular mechanisms that underlines TDP-43 propagation in disease (Jo et al., 2020).

In conclusion, seeding plays a crucial role in neurodegenerative diseases, explaining the propagation of protein pathology across different brain regions. Nowadays, it is widely recognized that the synergistic effect of different protein inclusions contributes significantly to disease progression, highlighting the concept of co-pathology. As a matter of fact, there is growing interest in the phenomenon of cross-seeding, whereby the aggregation and propagation cascade of pathological proteins involves multiple proteins (Lim, 2019; Subedi et al., 2022). For instance, one type of amyloid can act as seed for another type of protein, favoring the formation of heterologous amyloids (Subedi et al., 2022). The review article by Subedi and colleagues thoroughly discusses various examples of proteins associated with neurodegenerative diseases that can undergo cross-seeding, including A β and Tau, A β and α -synuclein, and Tau and α -synuclein (Subedi et al., 2022).

Cross-seeding offers a novel perspective for understanding the comorbidities associated with the deposition of different proteins in patients, and exploring how these proteins interact and influence each other's aggregation pathways is an important strategy to gain deeper insights into the pathogenesis of neurodegenerative diseases.

2.8 Strategies to target Tau and TDP-43 pathology

Therapeutic approaches for NDs aim to halt or slow the progression of these debilitating conditions by targeting their underlying mechanisms. The complex nature of these diseases highlights the need to develop a range of treatments that address these conditions from multiple angles (Mortada et al., 2021).

Although NDs are not yet fully curable, advances in research have led to significant progress in slowing disease progression (Gan et al., 2018; Guo and Lee, 2014; Peng et al., 2020).

Immunotherapy has recently gained significant attention as a promising approach to treat neurodegenerative disorders. A crucial mechanism of this approach is to target aggregated proteins for degradation, and thereby offering a potential pathway to mitigate disease progression.

A type of immunotherapy is vaccination, which can be divided in active and passive immunization. In active immunization specific antigens are administered *in vivo* to trigger an immune response, including a strong humoral immune response. In contrast, passive immunization involves the direct injection of monoclonal antibodies to mimic the effects of

active immunization, while avoiding potential side effects due to cellular immune responses (Brody and Holtzman, 2008).

In 1999, the first study on active immunization against A β was published, using a transgenic animal model that mimicked AD pathology. Vaccination before and after plaque deposition reduced A β levels in these animals (Schenk et al., 1999).

Nowadays, passive immunization used in the treatment of AD is the most advanced immunotherapy. Aducanumab, a monoclonal antibody approved by the Food and Drug Administration (FDA) in 2021, can penetrate different brain regions and binds to the N-terminal of A β with high affinity, targeting pathogenic aggregate forms of the protein (Budd Haeberlein et al., 2017). However, production of Aducanumab has been now discontinued in favor of another monoclonal antibody, Lecanemab, FDA-approved in 2023; this drug shows a lower incidence of amyloid-related imaging abnormalities, mainly because it targets A β protofibrils, and has demonstrated efficacy in reducing amyloid markers in the early stages of AD (Jucker and Walker, 2023; van Dyck et al., 2023).

Antibody therapy is also promising for intracellular aggregates, such as Tau. For example, the 43D monoclonal antibody targeting the N-terminal segment of Tau significantly reduces Tau burden in transgenic mice (Dai et al., 2018). Moreover, targeting hyperphosphorylated Tau is another valid approach currently under development in animal models, along with research into anti-tau oligomer antibodies (Mortada et al., 2021). In addition, promising clinical studies have been reported also in patients with a peptide-conjugate vaccine that targets pathological Tau (Novak et al., 2021).

In the field of TDP-43 proteinopathies, passive immunization has also emerged as a potential treatment approach. A monoclonal antibody, recognizing the RRM1 domain of the protein, has demonstrated efficacy in reducing cytoplasmic accumulation of TDP-43 both *in vitro* and in mouse models (Pozzi et al., 2019, 2020). Building on this foundation, a recent study, to which I contributed, was published by (Riemenschneider et al., 2023), investigating both active immunization in TDP-43 transgenic mice and monoclonal antibody therapy *in vitro*. This study highlights the potential benefits of targeting the C-terminal pS409/410 epitope, showing reduced levels of Neurofilament light chain (NfL) in a mouse model of ALS/FTD; additionally, monoclonal antibodies directed against epitopes in the RRM2 and LCD of TDP-43 were shown to reduce phase separation, aggregation, and uptake of TDP-43 *in vitro* (Riemenschneider et al., 2023).

In addition to immunotherapy, another potential advancement in drug discovery for NDs involves targeting aberrant biomolecular condensates, developing the so-called condensate-modifying therapeutics (c-mods) (Mitrea et al., 2022). Unlike traditional drugs that target single macromolecules, c-mods aim to modulate all components of cellular condensates, thus altering their physical properties and network dynamics (Mitrea et al., 2022).

A c-mod can employ three different approaches: 1) removing an aberrant condensate or restoring its normal behavior, 2) altering the functions of an aberrant condensate; and 3) inactivating a specific target or make it de-partitioning from a condensate (Mitrea et al., 2022).

C-mods can also be considered in the context of modulating aberrant PS of proteins like Tau and TDP-43: this strategy aims to inhibit their pathological condensation or phase transitions into solid aggregates, without altering their healthy native forms (Wheeler, 2020).

For instance, c-mods are compounds that can alter the interactions between proteins, nucleic acids and protein-nucleic acids complexes within condensates; these include short RNAs composed of TDP-43 target sequences, which prevent the generation of TDP-43 inclusions (Mann et al., 2019), or small molecules with planar aromatic moieties that inhibit the recruitment of RNA-binding proteins, such as TDP-43, into SGs, thereby preventing their pathological accumulation (Fang et al., 2019).

Additionally, c-mods can modulate the composition of condensates by promoting or impeding specific protein recruitment by directly targeting protein IDRs, and therefore modulating their ability to interact (or not interact) with other molecules in the condensates (Mitrea et al., 2022).

C-mods can also efficiently degrade proteins within condensates using methods like proteolysis-targeting chimera (PROTAC), which involves the formation of a complex between the protein to degrade and an E3 ligase. Molecular glues work similarly to PROTACs but are smaller in size, and hydrophobic tagging (HyT), which requires the attachment of hydrophobic tags to the target protein, favors the recognition and degradation by the UPS machinery (Hyun and Shin, 2021).

These methods have been applied to both Tau and TDP-43. Specifically, TH006, a peptide-based PROTAC compound has been shown to target Tau for degradation in cells and regulate Tau levels in the brain of an AD mouse model (Chu et al., 2016). Additionally, the hydrophobic Tau conjugated peptide, HyT-Tau-CPP, has been shown to efficiently degrade Tau in cells (Gao et al., 2017).

Similarly, Gao and colleagues developed different single and double HyT-conjugated peptides to target TDP-43 degradation, identifying D4 as the most effective in reducing TDP-43 level and cytotoxicity in cells and in a *Drosophila* model (Gao et al., 2019).

Together, these multi-faceted approaches represent interesting new strategies to target Tau and TDP-43 pathologies. As the mechanism of neurodegenerative diseases are highly complex, diverse strategies might have to be combined to effectively combat them.

3 PUBLICATION I

Disease-linked TDP-43 hyperphosphorylation suppresses TDP-43 condensation and aggregation

Published in The EMBO Journal, 2022 as

Lara A Gruijs da Silva, **Francesca Simonetti**, Saskia Hutten, Henrick Riemenschneider, Erin L Sternburg, Lisa M Pietrek, Jakob Gebel, Volker Dötsch, Dieter Edbauer, Gerhard Hummer, Lukas S Stelzl & Dorothee Dormann


3.1 Aim of the project

The aim of this project is to investigate the role of TDP-43 hyperphosphorylation in neurodegenerative diseases, such as ALS and FTD, being inclusions of hyperphosphorylated TDP-43 a hallmark of these pathologies.

By exploring how Casein kinase 1 δ -mediated TDP-43 hyperphosphorylation or phosphomimetic mutations affect its phase separation and aggregation *in vitro*, and function in neurons, this study seeks to determine whether this post-translational modification acts as a protective or causal mechanism in TDP-43 aggregation and phase separation.



Disease-linked TDP-43 hyperphosphorylation suppresses TDP-43 condensation and aggregation

Lara A Gruijs da Silva^{1,2} , Francesca Simonetti^{1,2,3} , Saskia Hutten¹, Henrick Riemenschneider³, Erin L Sternburg¹, Lisa M Pietrek⁴, Jakob Gebel⁵ , Volker Dötsch⁵, Dieter Edbauer^{2,3,6} , Gerhard Hummer^{4,7} , Lukas S Stelzl^{1,4,8,9}  & Dorothee Dormann^{1,6,9,*} 

Abstract

Post-translational modifications (PTMs) have emerged as key modulators of protein phase separation and have been linked to protein aggregation in neurodegenerative disorders. The major aggregating protein in amyotrophic lateral sclerosis and frontotemporal dementia, the RNA-binding protein TAR DNA-binding protein (TDP-43), is hyperphosphorylated in disease on several C-terminal serine residues, a process generally believed to promote TDP-43 aggregation. Here, we however find that Casein kinase 1 δ -mediated TDP-43 hyperphosphorylation or C-terminal phosphomimetic mutations reduce TDP-43 phase separation and aggregation, and instead render TDP-43 condensates more liquid-like and dynamic. Multi-scale molecular dynamics simulations reveal reduced homotypic interactions of TDP-43 low-complexity domains through enhanced solvation of phosphomimetic residues. Cellular experiments show that phosphomimetic substitutions do not affect nuclear import or RNA regulatory functions of TDP-43, but suppress accumulation of TDP-43 in membrane-less organelles and promote its solubility in neurons. We speculate that TDP-43 hyperphosphorylation may be a protective cellular response to counteract TDP-43 aggregation.

Keywords neurodegeneration; phase separation; phosphorylation; RNA-binding protein; TDP-43

Subject Categories Neuroscience; RNA Biology

DOI 10.15252/embj.2021108443 | Received 15 April 2021 | Revised 23

December 2021 | Accepted 4 January 2022 | Published online 3 February 2022

The EMBO Journal (2022) 41: e108443

See also: **GM Ginell & AS Holehouse** (April 2022)

Introduction

TAR DNA-binding protein (TDP-43) is the major aggregating protein in amyotrophic lateral sclerosis (ALS) and frontotemporal dementia (FTD) patients and also forms pathological aggregates in up to 50% of Alzheimer's disease patients (Neumann *et al*, 2006; Josephs *et al*, 2014). It is a ubiquitously expressed RNA-binding protein (RBP) with key functions in RNA processing, e.g., regulation of alternative splicing and polyadenylation, miRNA processing, mRNA stability and localization (Ratti & Buratti, 2016). In the affected brain regions of ALS and FTD patients, the physiological diffuse nuclear localization of TDP-43 is lost. Instead the protein forms cytoplasmic and occasionally nuclear inclusions in neurons and glial cells (Mackenzie *et al*, 2010). TDP-43 pathology closely correlates with neurodegeneration, and both loss-of-function mechanisms, e.g., misregulation of nuclear RNA targets, and gain-of-function mechanisms, e.g., aberrant interactions of the TDP-43 aggregates, are believed to contribute to neuronal dysfunction and eventually neurodegeneration (Ling *et al*, 2013; Tziortzouda *et al*, 2021).

Similar to other prion-like RBPs, TDP-43 is thought to aggregate through aberrant liquid–liquid phase separation (LLPS), i.e., the transition of liquid-like RBP condensates into a solid-like state (Nedelsky & Taylor, 2019). Aberrant phase transitions may occur in stress granules (SGs) or other membrane-less organelles (MLOs), where aggregation-prone RBPs are highly concentrated and exceed the critical concentration for LLPS (Alberti & Dormann, 2019; Alberti & Hyman, 2021). Subsequent liquid-to-solid phase transition, as demonstrated for various disease-linked RBPs *in vitro* (Molliex *et al*, 2015; Patel *et al*, 2015), may then cause formation of pathological RBP inclusions. LLPS is often driven by intrinsically disordered low complexity domains (LCDs), that tend to engage in weak multivalent interactions with other molecules (Alberti, 2017). TDP-43 harbors a long C-terminal LCD enriched in glycine, serine, asparagine and

1 Biocenter, Institute of Molecular Physiology, Johannes Gutenberg-Universität (JGU), Mainz, Germany

2 Graduate School of Systemic Neurosciences (GSN), Planegg-Martinsried, Germany

3 German Center for Neurodegenerative Diseases (DZNE), Munich, Germany

4 Department of Theoretical Biophysics, Max Planck Institute of Biophysics, Frankfurt am Main, Germany

5 Institute for Biophysical Chemistry, Goethe-Universität, Frankfurt am Main, Germany

6 Munich Cluster for Systems Neurology (SyNergy) Munich, Munich, Germany

7 Institute for Biophysics, Goethe-Universität, Frankfurt am Main, Germany

8 KOMET1, Institute of Physics, Johannes Gutenberg-Universität (JGU), Mainz, Germany

9 Institute of Molecular Biology (IMB), Mainz, Germany

*Corresponding author. Tel: +49 6131 39 36206; E-mail: ddormann@uni-mainz.de

glutamine residues, which drives intermolecular TDP-43 interactions and assembly by phase separation (Conicella *et al*, 2016; Babinchak *et al*, 2019). The LCD is also the region that harbors numerous ALS-linked point mutations (Buratti, 2015), suggesting that small chemical changes to the TDP-43 LCD can cause neurodegeneration.

Liquid–liquid phase separation and MLO dynamics are often regulated by post-translational modifications (PTMs) in LCDs, as the introduction of small chemical groups or proteins changes the chemical nature of amino acids, e.g., their charge or hydrophobicity, which can alter their molecular interactions and LLPS behavior (Bah & Forman-Kay, 2016; Hofweber & Dormann, 2019). A highly disease-specific PTM on deposited TDP-43 inclusions is hyperphosphorylation on C-terminal serine residues in the LCD (Hasegawa *et al*, 2008; Inukai *et al*, 2008; Neumann *et al*, 2009; Kametani *et al*, 2016). Antibodies specific for C-terminal TDP-43 phosphorylation sites (e.g., S409/S410 and S403/S404) detect inclusion pathology in patients, without cross-reactivity with physiological nuclear TDP-43. Therefore, C-terminal TDP-43 hyperphosphorylation is considered a pathological hallmark and is generally believed to promote TDP-43 aggregation (Buratti, 2018). This view is largely based on the observations that C-terminal TDP-43 phosphorylation correlates with inclusion pathology and that overexpression of kinases that can phosphorylate TDP-43 enhance TDP-43 aggregation and neurotoxicity (Choksi *et al*, 2014; Liachko *et al*, 2014; Nonaka *et al*, 2016; Taylor *et al*, 2018). Based on these studies, inhibition of TDP-43 phosphorylation by specific kinase inhibitors has even been proposed as a potential therapeutic strategy for ALS (Liachko *et al*, 2013; Salado *et al*, 2014; Martinez-Gonzalez *et al*, 2020). However, the molecular consequences of this disease-linked PTM are still poorly understood, and its effects on TDP-43 LLPS and aggregation are still unknown.

Using *in vitro*, *in silico* and cellular experiments, we now demonstrate that disease-linked C-terminal hyperphosphorylation of TDP-43 suppresses TDP-43 condensation and insolubility. We show this through (i) *in vitro* phase separation and aggregation assays with recombinant, full-length TDP-43; (ii) coarse-grained and atomistic molecular dynamics (MD) simulations of condensates of TDP-43 LCDs, elucidating molecular driving forces; and (iii) experiments in HeLa cells, stable inducible U2OS cells and primary rat neurons, where C-terminal phosphomimetic mutations do not disturb nuclear import or

RNA processing functions of TDP-43, but abrogate TDP-43 condensation into MLOs and enhance its solubility. Based on our findings, we speculate that C-terminal TDP-43 hyperphosphorylation may be a protective cellular response to counteract TDP-43 solidification, rather than being a driver of TDP-43 pathology, as has so far been assumed.

Results

In vitro phosphorylation with Casein kinase 1δ reduces condensation of TDP-43

To examine how phosphorylation affects TDP-43 phase transitions, we expressed and purified unphosphorylated full-length TDP-43 with a solubilizing MBP tag and a His₆-tag in *Escherichia coli* (Wang *et al*, 2018) (Appendix Fig S1A–E). We then *in vitro* phosphorylated the purified protein with casein kinase 1 delta (CK1δ), a kinase previously reported to phosphorylate TDP-43 at disease-associated sites (Kametani *et al*, 2009), and confirmed phosphorylation of C-terminal serines (S403/S404; S409/S410) with phospho-specific antibodies (Fig EV1A). Mass spectrometric analysis detected phosphorylation on several additional serine/threonine sites (Fig EV1B), and the running behavior in SDS–PAGE suggests hyperphosphorylation on multiple sites (Figs 1B and EV1A). We then induced phase separation of the unphosphorylated vs *in vitro* phosphorylated TDP-43 by cleaving off the MBP tag with TEV protease (Wang *et al*, 2018) and used centrifugation to separate the condensates (C) from the cleared supernatant (S; Fig 1A). Cleaved TDP-43 was mostly in the condensate fraction (S/[S + C] ratio ~0.25), whereas *in vitro* phosphorylated TDP-43 was predominantly in the supernatant (S/[S + C] ratio > 0.6; Fig 1B and C). Reduced sedimentation of TDP-43 was not seen upon addition of adenosine triphosphate (ATP) or CK1δ alone, suggesting that it is indeed caused by the addition of phospho-groups to TDP-43.

C-terminal phosphomimetic substitutions mimicking disease-linked phosphorylation suppress TDP-43 phase separation

To study defined disease-linked phosphorylation sites, we generated phosphomimetic proteins harboring different numbers of

Figure 1. TDP-43 phosphorylation by CK1δ and C-terminal phosphomimetic substitutions reduce TDP-43 condensation *in vitro*.

- Scheme of sedimentation assay (created in BioRender.com): phase separation of TDP-43 was induced by TEV protease cleavage of TDP-43-MBP-His₆, and condensates were pelleted by centrifugation.
- Sedimentation assay to quantify condensation of unmodified TDP-43 versus *in vitro* phosphorylated TDP-43 (+CK1δ, +ATP) and controls (CK1δ or ATP only); TDP-43 detected by Western blot (rabbit anti-TDP-43 N-term). Due to incomplete TEV cleavage, some TDP-43-MBP-His₆ remains present and co-fractionates with cleaved TDP-43, due to TDP-43 self–self interaction.
- Quantification of band intensities of cleaved TDP-43 shown as mean of Supernatant/(Supernatant + Condensate) (S/[S + C]) ratio of three independent experimental replicates ($n = 3$) ± SD. *** $P < 0.0002$ by one-way ANOVA with Dunnett's multiple comparison test to Wt.
- Schematic diagram of TDP-43 and sequence of C-terminal region (aa. 370–414) for Wt, phosphomimetic (S-to-D) variants and control (S-to-A) variants. NTD, N-terminal domain; RRM, RNA recognition motif; LCD, low complexity domain with α -helical structure.
- Turbidity measurements (optical density [OD] at 600 nm) to quantify phase separation of the indicated TDP-43 variants at three different concentrations (in Hepes buffer). Values represent mean of three independent experimental replicates ($n = 3$) ± SD. * $P < 0.0332$, ** $P < 0.0021$ and *** $P < 0.0002$ by one-way ANOVA with Dunnett's multiple comparison test to Wt, comparing the respective concentration condition (5, 10 and 20 μ M).
- Representative bright field microscopic images of TDP-43 condensates (in Hepes buffer), Bar, 25 μ m (F) and quantification of condensate number (G), size (H) and roundness (I). Box plots show the comparison of median and inter-quartile range (upper and lower quartiles) of all fields of view (FOV) from Min to Max (whiskers) of two replicates (≥ 22 FOV per condition). * $P < 0.0332$, ** $P < 0.0021$ and *** $P < 0.0002$ by one-way ANOVA with Dunnett's multiple comparison test to Wt, comparing the respective concentration condition (5, 10 and 20 μ M).

Source data are available online for this figure.

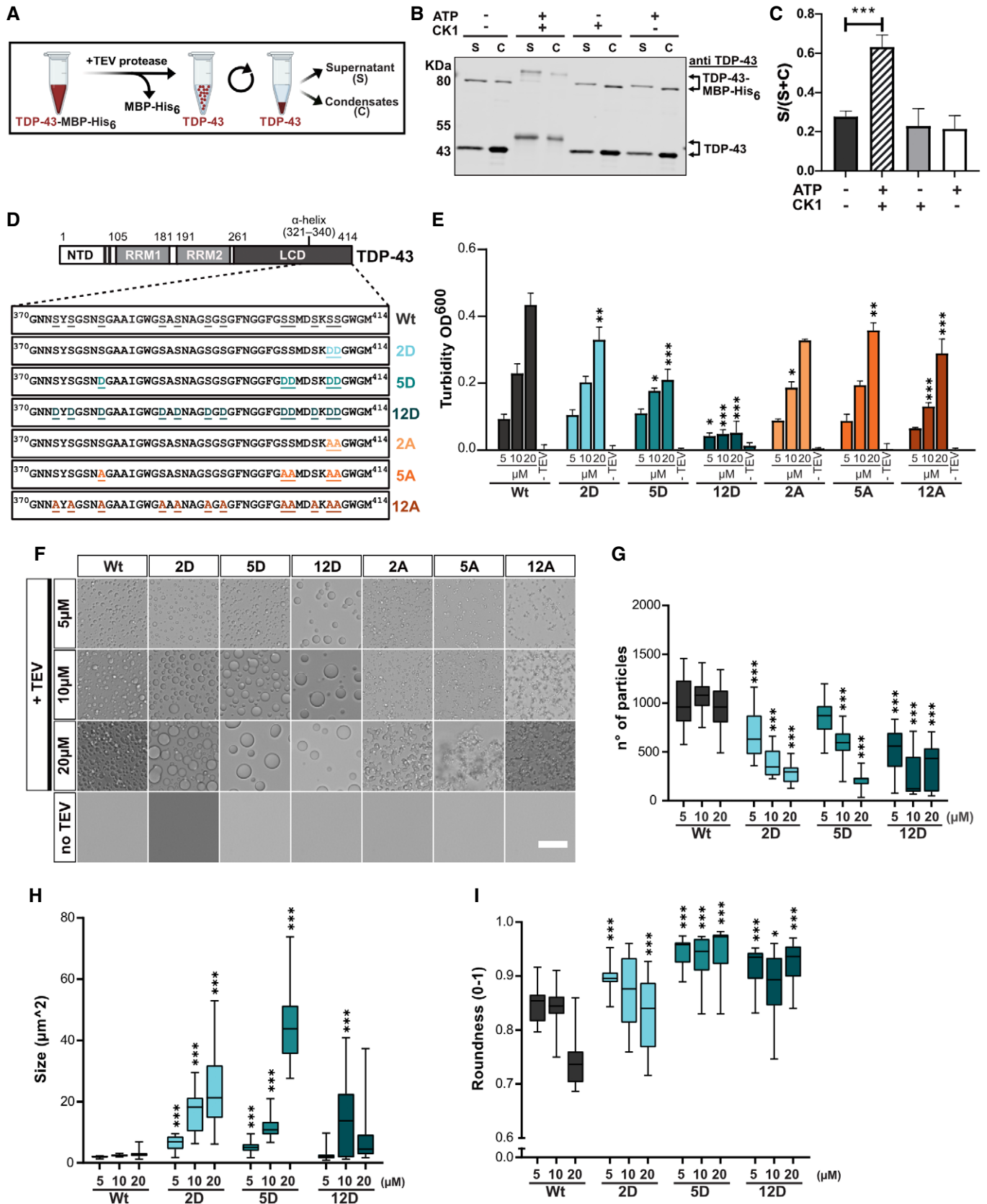


Figure 1.

phosphomimetic serine-to-aspartate (S-to-D) mutations or corresponding serine-to-alanine (S-to-A) mutations as control. Phosphomimetic substitutions rely on the replacement of a phosphorylated serine or threonine with a negatively charged amino acid (D or E), thus mimicking the negative charge of the phospho group. Even though they under-appreciate the charge change (net charge of aspartate = -1 instead of -2 for a phospho-group) and do not always accurately mimic the chemistry of a phospho group, phosphomimetics have been successfully used to probe the biological function of phosphorylated residues (Martin *et al*, 2014). Phosphorylation on S409/S410 is a highly specific and consistent feature of aggregated TDP-43 in all ALS/FTD subtypes (Inukai *et al*, 2008; Neumann *et al*, 2009), and five phosphorylation sites (S379, S403, S404, S409 and S410) were detected with phosphorylation site-specific antibodies in human post-mortem tissue (Hasegawa *et al*, 2008). Therefore, we mutated these serines to create "2D" and "5D" variants as well as the corresponding "2A" and "5A" controls (Fig 1 D). Based on a mass spectrometric study that found phosphorylation on 12 out of 14 serines in the C-terminal LCD of TDP-43 in ALS spinal cord (Kametani *et al*, 2016), we also mutated these 12 sites (S373, S375, S379, S387, S389, S393, S395, S403, S404, S407, S409 and S410) to create "12D" or "12A" variants (Fig 1D). Interestingly, the PLAAC web tool (<http://plaac.wi.mit.edu/>) that allows prediction of probable prion subsequences using a hidden-Markov model (HMM) algorithm (Lancaster *et al*, 2014), predicted a reduced prion-like character of the C-terminal region in the phosphomimetic 12D variant compared with the wild-type (Wt) and 12A protein (Appendix Fig S2).

To study phase separation experimentally, all variants were expressed and purified as TDP-43-MBP-His₆ fusion proteins (Appendix Fig S1A–E), and phase separation induced by TEV protease-mediated cleavage of the MBP tag was examined by turbidity, sedimentation or microscopic condensate assays. Turbidity measurements revealed a concentration-dependent increase in phase separation for TDP-43 Wt, as expected, whereas the increase was less pronounced for the 2D and 5D variants and no concentration-dependent increase was seen for the 12D mutant (Fig 1E). The gradual decrease in turbidity caused by the phosphomimetic mutations (Wt > 2D > 5D > 12D) was not seen to the same extent for the corresponding S-to-A control mutations (Fig 1E), hence suppression of phase separation is not due to the loss of serines at these positions, but can be attributed to the additional negative charges introduced by the D substitutions. Turbidity assays in phosphate buffer instead of Hepes buffer gave similar results (Fig EV2A), and sedimentation assays confirmed that TDP-43 condensation is gradually suppressed by increasing numbers of phosphomimetic mutations (Fig EV2B and C).

Phosphomimetic S-to-D substitutions lead to rounder TDP-43 condensates, whereas S-to-A mutations cause an amorphous, aggregate-like morphology

Interestingly, bright field microscopy revealed that TDP-43 Wt formed relatively small, amorphous condensates, suggestive of solid-like material properties (Fig 1F). In contrast, the phosphomimetic S-to-D proteins formed fewer, but much larger and rounder condensates (Fig 1F, see G–I for quantification), suggesting a more liquid-like behavior and therefore fusion of condensates into larger

droplets. Again, the observed changes were correlated with the number of phosphomimetic mutations, i.e., they were most pronounced for the 12D mutant, which formed very few, but large and perfectly circular protein droplets. (Note that these few large condensates most likely escape detection in the turbidity assay due to rapid sedimentation during the assay.) In contrast, the S-to-A control variants formed numerous small, amorphous condensates and had a more irregular, aggregate-like appearance than TDP-43 Wt (Fig 1F). This phenotype suggests that the OH groups in the respective serines influence the material properties of TDP-43 and contribute to preventing its aggregation. Similar results were obtained when the assay was carried out in phosphate buffer instead of Hepes buffer, except that 12D formed only very few, small condensates in phosphate buffer (Fig EV2D), possibly because the ions in phosphate buffer may screen certain attractive interactions between TDP-43 molecules and disfavor phase separation. Together, these results demonstrate that phosphomimetic substitutions mimicking disease-linked C-terminal TDP-43 phosphorylation reduce the tendency of TDP-43 to phase separate into amorphous condensates and suggest a more dynamic, liquid-like behavior of C-terminally phosphorylated TDP-43.

C-terminal phosphomimetic substitutions yield more liquid-like, dynamic TDP-43 condensates

To test whether the phosphomimetic mutations indeed render TDP-43 more liquid-like, we performed live imaging of Alexa488-labeled Wt, 5D and 12D condensates by spinning disc confocal microscopy. For TDP-43 Wt, no fusion events were observed over a time course of several minutes. Instead the small condensates stuck to each other in a chain-like arrangement (Movie EV1, Fig 2A). In contrast, 5D condensates occasionally and slowly fused with each other, and 12D condensates readily fused upon contact and relaxed into perfectly round spheres, indicating a liquid droplet-like nature (Movies EV2 and EV3, Fig 2A). To assess the mobility of TDP-43 molecules in condensates, we performed half-bleaches of condensates and analyzed fluorescent recovery after photobleaching (FRAP) in the bleached half. In TDP-43 Wt condensates, fluorescence recovered very slowly, indicating a low mobility of TDP-43 molecules, whereas recovery was faster in 5D and even faster in 12D condensates (Fig 2B and C), in line with an increased mobility of phosphomimetic TDP-43 compared with "unmodified" TDP-43. Taken together, phosphomimetic S-to-D substitutions in the C-terminal region enhance the liquidity of TDP-43 condensates, suggesting that phosphorylation in this region might counteract TDP-43's tendency to form solid, irreversible aggregates.

C-terminal phosphomimetic substitutions reduce TDP-43 aggregation

To address whether phosphorylation indeed counteracts TDP-43 aggregation, we performed *in vitro* aggregation assays modified from published protocols (Halfmann & Lindquist, 2008; French *et al*, 2019). Under the assay conditions, TEV cleavage of fluorescently labeled TDP-43-MBP-His₆ yields amorphous TDP-43 aggregates that can be visualized by confocal microscopy. In contrast to Wt or 12A, the phosphomimetic 5D or 12D proteins formed much smaller and fewer aggregates, respectively (Fig 2D), suggesting that C-terminal

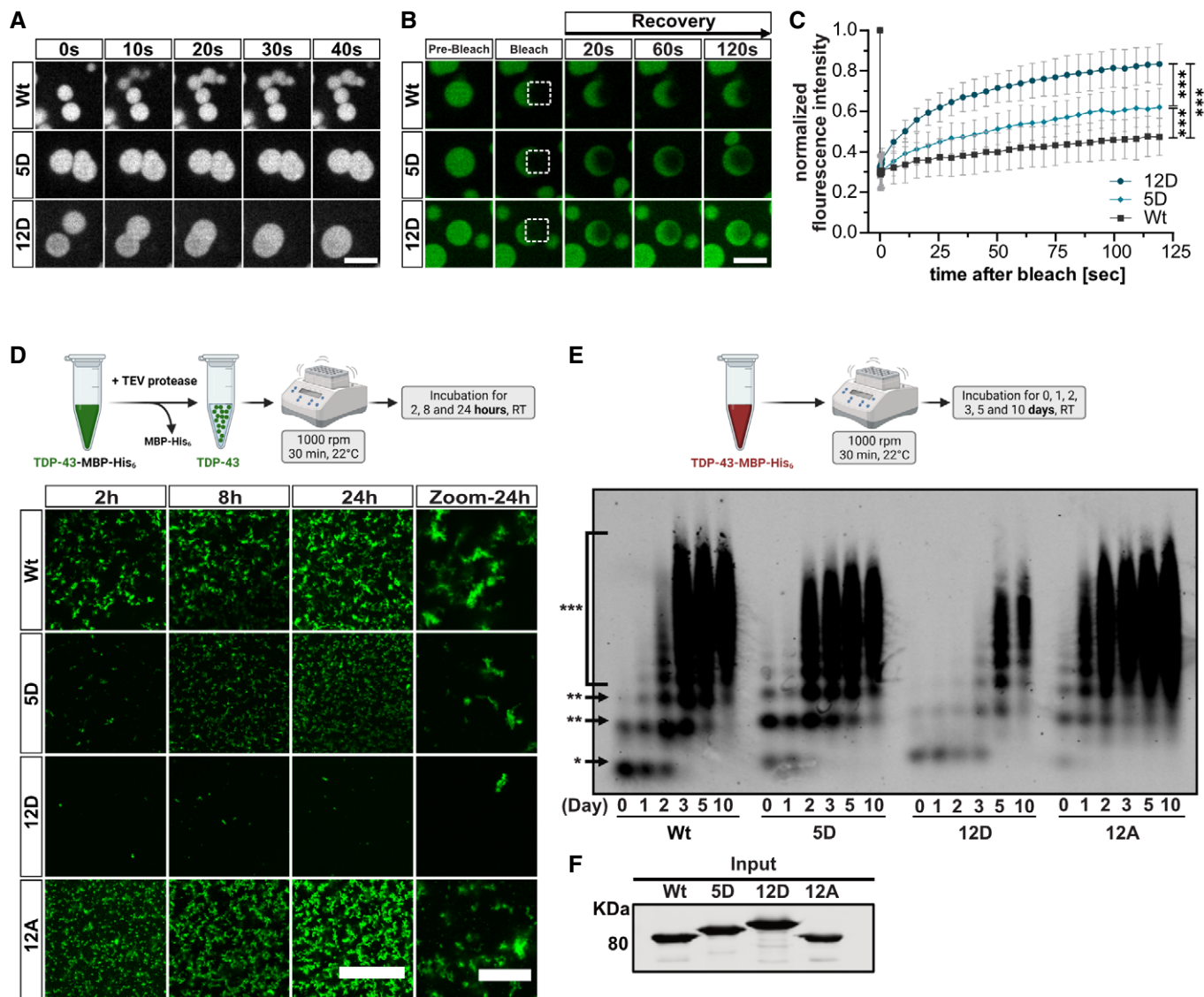


Figure 2. C-terminal phosphomimetic substitutions enhance liquidity of TDP-43 condensates and reduce TDP-43 aggregation *in vitro*.

- A Representative still images of Alexa488-labeled TDP-43 condensates by spinning disc timelapse confocal microscopy. Wt condensates do not fuse, 5D condensates fuse slowly and 12D condensates readily fuse upon contact and relax into spherical droplets. Bar, 5 μ m.
- B Representative images of FRAP experiments at indicated time-points. Boxes indicate bleached area (half-bleach of condensate). Bar, 5 μ m.
- C FRAP curves after half-bleach of freshly formed Alexa488-labeled TDP-43 condensates. Values represent mean \pm SD of three independent experimental replicates ($n = 3$) of ≥ 9 droplets analyzed per condition. $***P < 0.0002$ by one-way ANOVA with Tukey's multiple comparison test for area under the curve (AUC) of individual droplets.
- D Confocal images of Alexa488-labeled TDP-43 aggregates formed in an *in vitro* aggregation assay (with TEV protease cleavage). Bar, 100 μ m. Zoom shows magnified view of aggregates at the 24 h time point. Bar, 20 μ m.
- E SDD-AGE followed by TDP-43 Western blot to visualize SDS-resistant oligomers/high-molecular-weight species of TDP-43-MBP-His₆ in an *in vitro* aggregation assay (without TEV protease cleavage). Asterisks represent monomeric (*), oligomeric (**), and polymeric (***) species.
- F Input of TDP-43-MBP-His₆ variants used in the SDD-AGE assay, detected by Western blot (anti-TDP-43 N-term).

Source data are available online for this figure.

TDP-43 phosphorylation can efficiently suppress TDP-43 aggregation. For biochemical characterization of the formed aggregates, we performed semi-denaturing detergent-agarose gel electrophoresis (SDD-AGE) under the same assay conditions, just in the absence of TEV, as MBP-tagged TDP-43 aggregates slower than TDP-43 and distinct oligomeric/polymeric species resistant to 0.5% SDS can be

visualized under these conditions (Appendix Fig S3). In comparison to TDP-43 Wt and 5D, 12D showed reduced and delayed oligomerization and formation of high-molecular-weight species (Fig 2E, equal protein input shown in Fig 2F). In contrast, 12A formed SDS-resistant oligomers/high-molecular-weight species at a higher rate, which together with our microscopic images of TDP-43 condensates

(Fig 1F), suggests that C-terminal alanine substitutions make TDP-43 more aggregation-prone. Taken together, C-terminal phosphomimetic substitutions that mimic the phosphorylation pattern in ALS patients reduce the formation of SDS-resistant high-molecular-weight oligomers and TDP-43 aggregates *in vitro*.

Multi-scale simulations of the TDP-43 LCD reveal reduced protein-protein interactions through enhanced solvation of phosphomimetic residues

To understand the effect of C-terminal TDP-43 phosphorylation on phase separation at the molecular level, we used coarse-grained and atomistic MD simulations of the disordered TDP-43 LCD (aa. 261–414) with and without phosphomimetic substitutions. In coarse-grained simulations, we can access the relevant long time and large length scales to characterize phase behavior, while in atomistic simulations we can resolve the interactions of condensates with high resolution and high accuracy (Dignon *et al*, 2018; Pietrek *et al*, 2020; Benayad *et al*, 2021). We found that phosphomimetic substitutions locally reduce protein–protein interactions (Fig EV3) and increase protein–solvent interactions (Fig 3). In the coarse-grained simulations, the LCD of both TDP-43 Wt and 12D phase separated spontaneously to form condensates (shown for Wt in Fig 3A and Movie EV4). Yet, phosphomimicking residues are less prone to interact with protein in the phase-separated condensates and are somewhat more solvated than the corresponding serine residues (Figs 3B and EV3A and B). The aspartate side chains in 12D LCDs engage in partially compensatory interactions with arginines, showing that introduction of charged side chains gives rise to both stabilizing and destabilizing interactions in condensates. Importantly, our simulations are in line with previous studies that have highlighted the importance of aromatic sticker–sticker interactions in driving phase separation of prion-like domains and the TDP-43 LCD (Li *et al*, 2018; Schmidt *et al*, 2019; Martin *et al*, 2020).

To characterize the interactions of TDP-43 LCDs further, we performed atomistic MD simulations of dense protein condensates (Fig 3C, Movie EV5) assembled with hierarchical chain growth (HCG; Pietrek *et al*, 2020) to enhance the sampling of polymeric degrees of freedom. In microsecond dynamics with explicit solvent and a highly accurate atomistic description of molecular interactions

(Robustelli *et al*, 2018), we again found serine residues in the Wt protein to be more prone to interact with other protein residues than interacting with solvent (Fig 3D). By contrast, phosphomimicking aspartate side chains bind comparably more water molecules and show an overall reduced tendency for protein–protein interactions (Fig 3D and E, Appendix Fig S4A). Enhanced side chain solvation is consistent across the 12 phosphomimetic substitution sites (Appendix Fig S4B). The atomistic simulations are consistent with an increase in charge favoring solvated states and thus weakening TDP-43 condensates.

Effects of phosphomimicking mutations and phosphorylation on TDP-43 LCD phase behavior

To characterize possible differences between phosphomimicking mutations and phosphorylation, we employed the highly efficient hydrophobicity scale (HPS) coarse-grained model (Dignon *et al*, 2018). The HPS implicit solvent model enabled us to quantify differences in the phase behavior of TDP-43 LCD variants. In line with experiments on full-length TDP-43 (Fig 1), 12D LCD phase-separated, but more protein remained in the dilute phase compared with Wt (Fig 3F–H). Indeed, computing the excess free energy of transfer ΔG_{trans} from the density profile (Appendix Fig S5D), which reports how favorable it is to move one chain from dilute solution at the saturation density to the dense phase of the condensate, showed that 12D LCDs are less prone to interact with each other in a condensate than Wt LCDs (Appendix Table S1). Loss of local contacts in the C-terminal region due to phosphomimetic substitutions was only partially compensated by new protein–protein interactions with arginines (Appendix Fig S5A–C), in accordance with coarse-grained simulations with explicit solvent (Fig EV3C). The 12A substitutions stabilized the TDP-43 LCD condensates, as expected based on our experiments, with little protein remaining in the dilute phase (Fig 3F). Phosphorylation modulates the stability of LCD condensates in a dose-dependent way. Attaching five phospho groups (5pS) led to a somewhat less-dense LCD condensate, but overall the excess free energy of transfer is on par with Wt (Appendix Table S1, Appendix Fig S5D). By contrast, fully phosphorylating all twelve sites (12pS) dissolved the LCD condensate in our simulations, with no clear peak in the density profile (Fig 3F).

Figure 3. Atomistic and coarse-grained simulations of TDP-43 LCD: phosphomimicking residues form fewer protein–protein interactions and more protein–solvent interactions.

- A TDP-43 LCD phase separates in coarse-grained simulations with explicit solvent. Condensate of TDP-43 Wt LCD is shown, protein colored according to chain identity. Water omitted for clarity. Ions shown in cyan.
- B Normalized probability of protein–protein contacts by phosphomimicking aspartates in 12D and serines in Wt resolved by amino acid type from coarse-grained simulations. Error bars smaller than symbols. Inset: Distributions of the number of water molecules within 5 Å of side chains of phosphomimicking aspartates of 12D and corresponding serines in Wt from 15 μs of coarse-grained molecular dynamics simulations.
- C Atomistic simulation setup of 32 TDP-43 LCDs. Different LCD chains shown in different colors in space-filling representation. For one chain (lower left), a transparent surface reveals its atomic structure as sticks.
- D Normalized probability of protein–protein contacts by phosphomimicking aspartates in 12D and serines in Wt resolved by amino acid type from atomistic simulations. Two 1 μs simulations are distinguished by color intensity. Inset: distributions of the number of water molecules within 5 Å of the side chains of phosphomimicking aspartates of 12D and the corresponding serines in Wt from atomistic simulations.
- E Representative snapshots of atomistic simulations showing water within 3 Å of (left) Wt S407, S409 and S410 with nearby LCDs in surface representation and (right) 12D D407, D409 and D410. Protein surfaces are colored according to chain identity.
- F Density profiles in TDP-43 LCD condensates (peak at center) coexisting with dilute solutions for Wt, 12D, 5pS, 12pS and 12A from coarse-grained simulations with the implicit solvent coarse-grained HPS model.
- G, H Snapshots of 12D condensate (G) and fragmented 12pS clusters (H) in simulations with the coarse-grained HPS model. Side view on elongated boxes (blue lines).

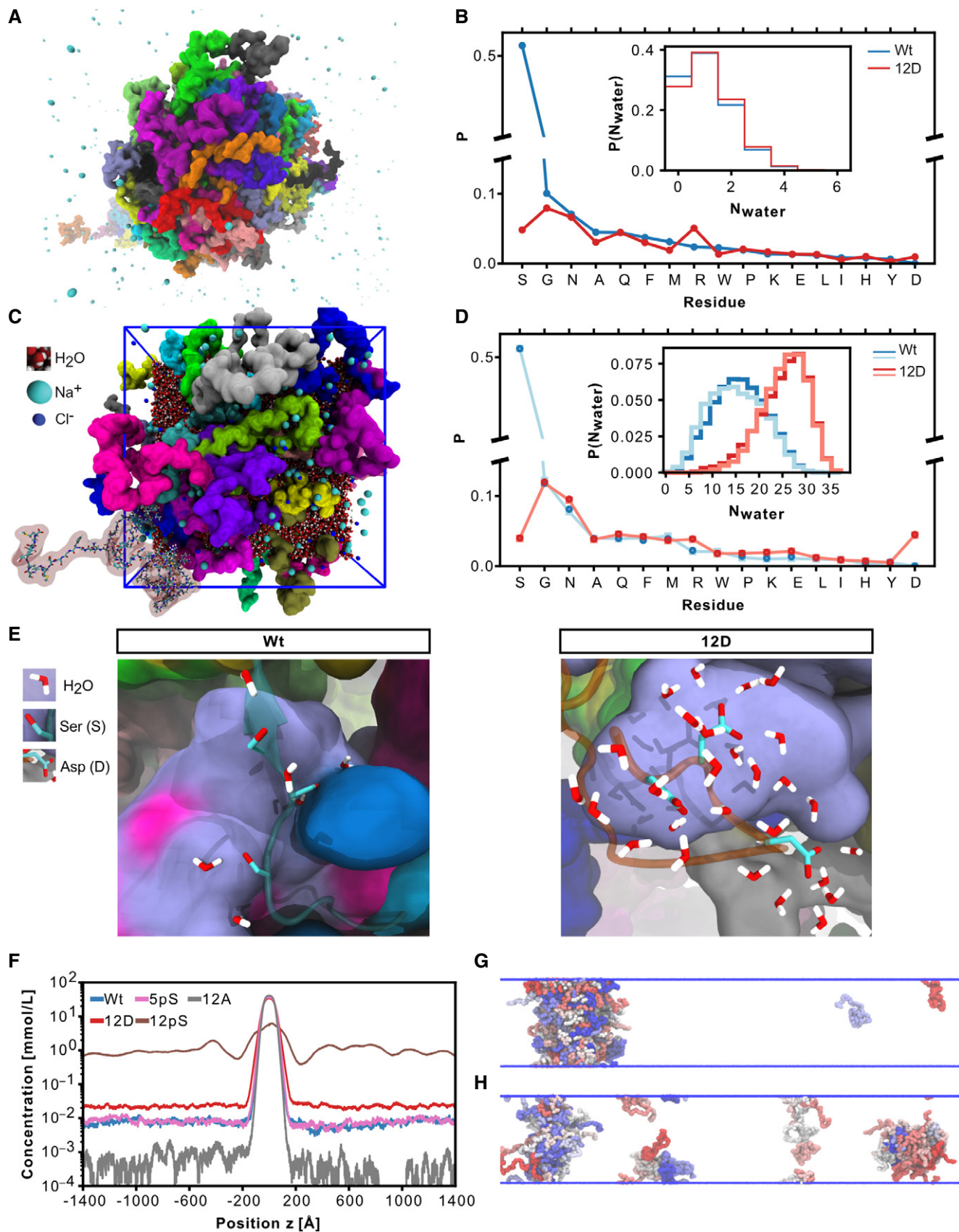


Figure 3.

Overall, the simulations with the HPS model rank the saturation density to form condensates as $12A \gg Wt \sim 5pS > 12D \gg 12pS$. The calculations thus predict that (i) phosphorylation may indeed dissolve condensates, and (ii) that phosphorylation may have an even stronger effect than phosphomimicking substitutions, due to the larger negative charge of phospho-serine compared with aspartate.

C-terminal phosphomimetic substitutions do not impair nuclear import and RNA regulatory functions of TDP-43

Next, we turned to cellular experiments to investigate how C-terminal TDP-43 phosphorylation affects the behavior and function of TDP-43 in cells. As TDP-43 hyperphosphorylation is found in the disease state, it seems possible that this PTM has detrimental effects on the protein and contributes to mislocalization and/or malfunction of TDP-43, thus driving neurodegeneration. To address this possibility, we transiently expressed different myc-tagged TDP-43 variants (Wt, 12D, 12A) in HeLa cells and analyzed their intracellular localization, nuclear import and RNA processing functions. All three TDP-43 variants showed a predominantly nuclear steady-state localization (Fig EV4A). We also compared their nuclear import rates in a hormone-inducible reporter assay by live cell imaging (Hutten *et al.*, 2020). In this assay, a protein-of-interest harboring a nuclear localization signal (NLS) is fused to a tandem EGFP and two hormone binding domains of the glucocorticoid receptor (GCR), which retains the reporter protein in the cytoplasm. Upon addition of a steroid hormone (dexamethasone), the reporter protein is released from the cytoplasm and imported into the nucleus, by virtue of the NLS in the protein-of-interest. We examined reporters containing the different TDP-43 variants (Wt, 12D, 12A) and found that their import rates were indistinguishable (Fig 4A and B).

To assess whether hyperphosphorylated TDP-43 shows functional impairments in RNA processing, we first assessed its ability to autoregulate its own levels when transiently overexpressed in HeLa cells (Ayala *et al.*, 2011; Avendano-Vazquez *et al.*, 2012). However, endogenous TDP-43 was downregulated to the same degree by all three myc-TDP-43 variants (Fig 4C), indicating that hyperphosphorylated TDP-43 can normally bind to its own 3'UTR and autoregulate its own levels. In line with these findings, recombinant TDP-43 Wt, 12D and 12A showed comparable RNA binding in electrophoretic mobility shift assays (EMSAs) with *in vitro* transcribed RNA comprised of the autoregulatory TDP-43 binding site

(Fig 4D) or synthetic (UG)₁₂ RNA (Fig EV4B). Second, we examined splicing of two known TDP-43 splice targets that get mis-spliced upon loss of TDP-43 (Tollervey *et al.*, 2011; Fiesel *et al.*, 2012). After siRNA-mediated silencing of endogenous TDP-43 expression and re-expression of siRNA-resistant myc-TDP-43 Wt, 12D or 12A (Appendix Fig S6A), splicing of *SKAR* and *Bim* exon 3 were fully restored by all three TDP-43 variants (Fig 4E), indicating normal function of phosphomimetic TDP-43 in splicing regulation. Normal nuclear localization and autoregulation of TDP-43 were also replicated in a cellular system that avoids high overexpression and has homogenous expression levels, namely stable inducible Flp-In U2OS cell lines that express the different myc-TDP-43 variants (Wt, 12D and 12A) after overnight doxycycline addition (Fig EV4C–E, in Fig EV4C endogenous TDP-43 was silenced with siRNAs, see Appendix Fig S6C). In conclusion, even though an effect on other RNA targets/RNA processing events or intracellular transport in other cell types cannot be excluded, our data suggest that C-terminal TDP-43 hyperphosphorylation is not primarily responsible for cytosolic mislocalization or impaired RNA regulatory functions of TDP-43 in disease.

Phosphorylation suppresses recruitment of TDP-43 into stress-induced MLOs

Finally, we investigated how C-terminal TDP-43 phosphorylation affects TDP-43 condensation in cellular MLOs. First, we used a quantitative assay to measure SG association of recombinant proteins under controlled conditions in semi-permeabilized HeLa cells (Hutten & Dormann, 2020) (Fig 5A). In line with our *in vitro* condensation experiments, increasing the number of phosphomimetic S-to-D substitutions caused a gradual decrease in SG association of TDP-43 (Fig EV5A and B). *In vitro* phosphorylated TDP-43 showed a similar or even stronger reduction in SG association as the 12D protein (Fig 5B and C), demonstrating that the phosphomimetic substitutions and phospho-groups introduced by a kinase have similar effects on SG association of TDP-43. Second, we expressed the different TDP-43 variants in intact HeLa cells to analyze their recruitment into stress-induced MLOs. To this end, we silenced endogenous TDP-43 expression using siRNA (Appendix Fig S6A and B) and then re-introduced siRNA-resistant myc-tagged TDP-43 Wt, 12D or 12A, thus avoiding oligomerization with endogenous TDP-43 via the N-terminal domain (Afroz *et al.*, 2017). Short term oxidative stress treatment with H₂O₂ caused a partially cytosolic relocalization

Figure 4. Phosphomimetic substitutions do not alter the rate of TDP-43 nuclear import and do not impair TDP-43 autoregulation, RNA-binding or alternative splicing function.

- A Hormone-inducible nuclear import assay, representative still images of GCR₂-EGFP₂-TDP-43 Wt, 12D and 12A before and during import triggered by addition of dexamethasone. Images were live recorded by spinning disc confocal microscopy. Bar, 20 μm.
- B Quantification of the hormone-inducible nuclear import measured during a total time course of 50 min. Values represent the mean fluorescence intensity of GCR₂-EGFP₂-TDP-43 in the cytoplasm for three independent replicates ± SEM (≥ 42 cells per condition).
- C Phosphomimetic 12D TDP-43 is competent in autoregulating TDP-43 expression. SDS-PAGE followed by TDP-43 Western blot showing downregulation of endogenous TDP-43 through autoregulation (60) after 48 h expression of Wt, 12D and 12A variants in HeLa cells. TDP-43 was detected using rabbit anti-TDP-43 C-term antibody (Proteintech), Histone H3 (rabbit anti-Histone H3 antibody, Abcam) was visualized as a loading control. * denotes an unspecific band.
- D Electrophoretic mobility shift assays (EMSA) of TDP-43-MBP-His₆ variants (Wt, 12D and 12A) in a complex with TDP-43 autoregulatory RNA binding site (60). All TDP-43 variants form TDP-43-RNA complexes equally well.
- E Splicing analysis by RT-PCR of known TDP-43 splice targets (*SKAR* exon 3 and *Bim* exon 3) in HeLa cells. Silencing of endogenous TDP-43 by siRNA leads to altered splice isoforms of *SKAR* and *Bim* (second vs first lane). These splicing alterations can be rescued by re-expression of TDP-43 Wt, but also 12D or 12A variants, demonstrating that phosphomimetic TDP-43 is fully competent in regulation splicing of these TDP-43 splice targets.

Source data are available online for this figure.

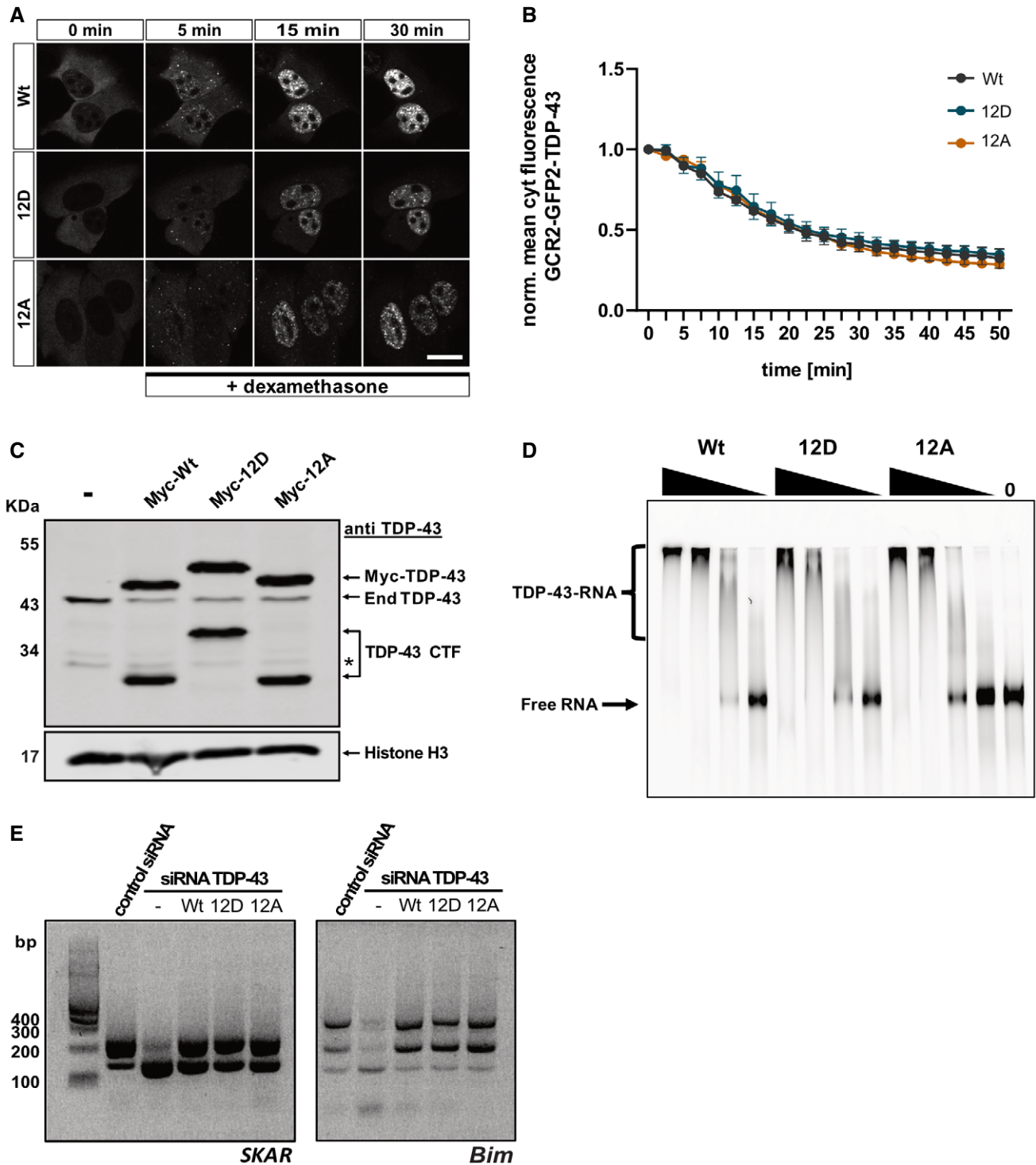


Figure 4.

of TDP-43 and led to recruitment of TDP-43 Wt and 12A, but significantly reduced recruitment of the 12D mutant into TIA-1-positive SGs (Fig 5D and E, see Appendix Fig S6D for control staining of untransfected cells). Similar results were obtained for nuclear import-deficient TDP-43 (Fig 5F and G) that was strongly mislocalized to the cytoplasm due to point mutations in the nuclear

localization signal (NLSmut; Appendix Fig S7). Finally, we examined recruitment of TDP-43 into arsenite-induced nuclear bodies (NBs) (Wang *et al*, 2020) and found that TDP-43 Wt and 12A were readily recruited into stress-induced NBs, while the phosphomimetic 12D protein remained dispersed in the nucleoplasm (Fig 5H–J, see Appendix Fig S6E for control staining of untransfected cells). TDP-

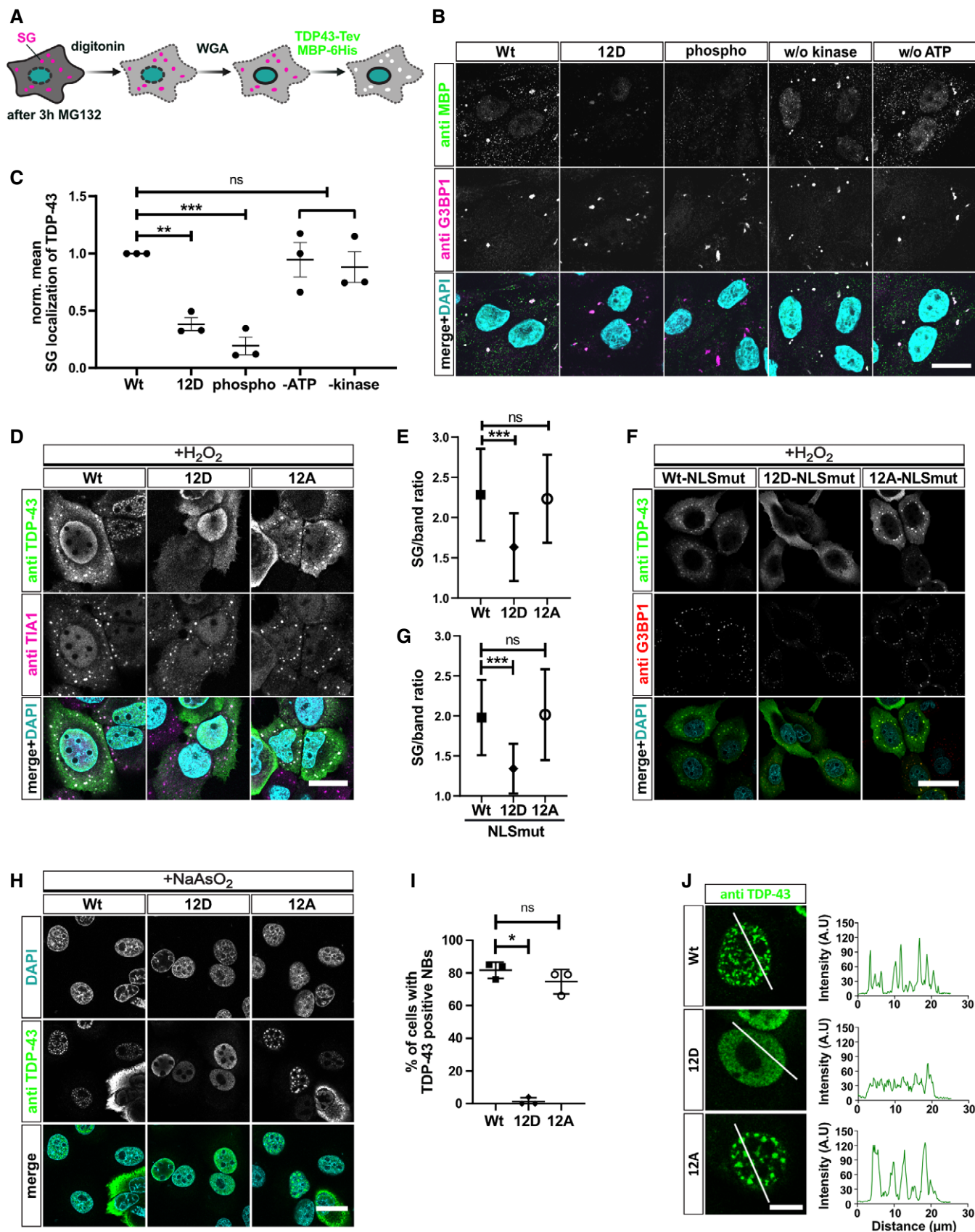


Figure 5.

Figure 5. Phosphorylation and phosphomimetic substitutions reduce recruitment of TDP-43 into stress-induced membrane-less organelles.

- A Scheme of stress granule (SG) recruitment assay in semi-permeabilized cells.
- B Reduced SG association of TDP-43 by 12D mutations or *in vitro* phosphorylation. Bar, 20 μ m.
- C Quantification of TDP-43-MBP-His₆ mean fluorescence intensity in SGs normalized to Wt \pm SEM of three independent experimental replicates ($n = 3$; ≥ 10 cells; ≥ 46 SGs each). ** $P < 0.0021$ and *** $P < 0.0002$ by one-way ANOVA with Dunnett's multiple comparison test to Wt.
- D SG recruitment of TDP-43 variants in intact HeLa cells in absence of endogenous TDP-43. After TDP-43 silencing and expression of myc-TDP-43 Wt, 12D and 12A variants, SGs were induced by H₂O₂ treatment and SG recruitment of TDP-43 was monitored by TDP-43 and TIA1 immunostaining. For clarity, signals were converted to grey values in the individual channels (upper two rows). In the merge (lower row), nuclei were stained in DAPI (turquoise), TDP-43 (green) and TIA-1 (magenta). Bar, 25 μ m.
- E Quantification of TDP-43 in SGs versus cytoplasm \pm SD of two independent experimental replicates ($n = 2$; ≥ 62 cells; ≥ 234 SGs each). *** $P < 0.0002$ by Kruskal–Wallis test with Dunn's multiple comparison test to Wt.
- F SG recruitment of different TDP-43-NLSmut variants in intact HeLa cells in the absence of endogenous TDP-43. After TDP-43 silencing and expression of NLSmut Wt, 12D and 12A variants, SGs were induced by H₂O₂ treatment and SG recruitment of TDP-43 was monitored by TDP-43 and G3BP1 immunostaining. For clarity, signals were converted to grey values in the individual channels (upper two rows). In the merge (lower row), nuclei were stained in DAPI (turquoise), TDP-43 (green) and G3BP1 (red). Bar, 40 μ m.
- G Quantification of TDP-43-NLS mutants in SGs versus band around SGs of two independent replicates \pm SD. *** $P < 0.0002$ by Kruskal–Wallis test with Dunn's multiple comparison test to Wt (≥ 56 cells; ≥ 315 SGs per condition).
- H Recruitment of TDP-43 into arsenite-induced nuclear bodies (NBs) in HeLa cells. After TDP-43 silencing and expression myc-TDP-43 Wt, 12D and 12A, NBs were induced by sodium arsenite treatment and NB recruitment of TDP-43 was monitored by TDP-43 immunostaining. Bar, 20 μ m.
- I Percentage of cells with TDP-43 in NBs \pm SD of three independent experimental replicates ($n = 3$). * $P < 0.0332$ by Kruskal–Wallis test with Dunn's multiple comparison test to Wt.
- J Intensity profiles (right) of TDP-43 Wt, 12D and 12A variants (green) along white lines (left). Bar, 10 μ m.

43 12D also remained completely dispersed in the stable inducible U2OS cell lines treated with arsenite, whereas TDP-43 WT and 12A localized in NBs upon arsenite treatment (Fig EV5C and D). Taken together, phosphomimetic substitutions that mimic disease-linked phosphorylation of TDP-43 suppress the localization of TDP-43 in phase-separated MLOs that could be condensation sites for pathological TDP-43 aggregation.

Phosphomimetic substitutions enhance TDP-43 solubility and suppress SG recruitment in primary neurons

To further support the idea that phosphorylation enhances the solubility of TDP-43 and counteracts its aggregation propensity in cells, we expressed the different myc-tagged TDP-43 variants in HeLa cells and performed a biochemical fractionation into a RIPA-soluble (S) and RIPA-insoluble (I) fraction. Indeed, the 12D protein had a significantly higher S/(S + I) ratio compared with the Wt and 12A proteins (Fig 6A and B). We also expressed EGFP-tagged TDP-43 Wt, 12D, 12A or the corresponding NLS-mutant cytosolic versions in primary rat neurons (see Appendix Fig S8 and Fig 6D for subcellular localization, which was unaltered by the phosphomimetic mutations). We

then probed for RIPA-insoluble high-molecular-weight material in a filter trap assay. Both the nuclear and the cytosolic 12D proteins showed a strong reduction in the amount of RIPA-insoluble TDP-43 in the transduced neurons (Fig 6C). Confocal microscopy of transduced neurons revealed a completely dispersed localization of the NLS-mutant 12D protein, whereas TDP-43 Wt and 12A showed a more granular, condensed pattern in the neuronal cytoplasm (Fig 6D). Moreover, NLS mutant TDP-43 Wt and 12A were readily recruited into G3BP1-positive SGs induced by heat shock in primary rat neurons, whereas TDP-43 12D was not (Fig 6E). Thus, we conclude that phosphomimetic substitutions mimicking disease-linked C-terminal hyperphosphorylation reduce TDP-43's tendency to condense into MLOs and to become insoluble in neurons. Based on these findings, we speculate that TDP-43 phosphorylation might be a cellular response to counteract pathological TDP-43 aggregation.

Discussion

C-terminal TDP-43 phosphorylation is a long-recognized pathological hallmark in ALS and FTD (Hasegawa *et al*, 2008; Inukai *et al*,

Figure 6. Phosphomimetic substitutions enhance TDP-43 solubility in HeLa cells and primary neurons.

- A Biochemical fractionation into RIPA-soluble (S) and RIPA-insoluble (I) fractions to analyze solubility of the different myc-TDP-43 variants (Wt, 12D and 12A) expressed in HeLa cells for 48 h. TDP-43 was detected by TDP-43 Western blot (upper blot, rabbit anti-TDP-43 C-term, Proteintech) and Myc Western blot (lower blot, mouse anti-Myc 9E10).
- B Quantification of myc-TDP-43 variants (Wt, 12D and 12A) in (S) versus (I) fractions extracted from TDP-43 Western blots of four independent replicates \pm SD, plotted as S/(S + I). * $P < 0.0332$ by one way ANOVA with Dunnett's multiple comparison test to Wt.
- C RIPA-insoluble material of the indicated EGFP-tagged TDP-43 variants (\pm NLS mutation) expressed in primary cortical neurons analyzed by filter-trap assay.
- D Primary hippocampal neurons expressing EGFP-TDP-43 Wt, 12D or 12A with additional NLS mutation. Bar, 80 μ m. Right: zoomed images of white squares (TDP-43 signal). Bar, 10 μ m.
- E SG recruitment of EGFP-TDP-43 NLS mutant variants (Wt, 12D, 12A) in primary hippocampal neurons. SG formation was induced by 1 h heat shock at 42°C. SGs and TDP-43 were monitored by G3BP1 antibody staining and EGFP fluorescence, respectively. For clarity, signals were converted to grey values in the individual channels (first two columns). In the merge (third column), EGFP-TDP-43 shown in green, G3BP1 in red and nuclei (DAPI staining) in turquoise. Bar, 20 μ m.

Source data are available online for this figure.

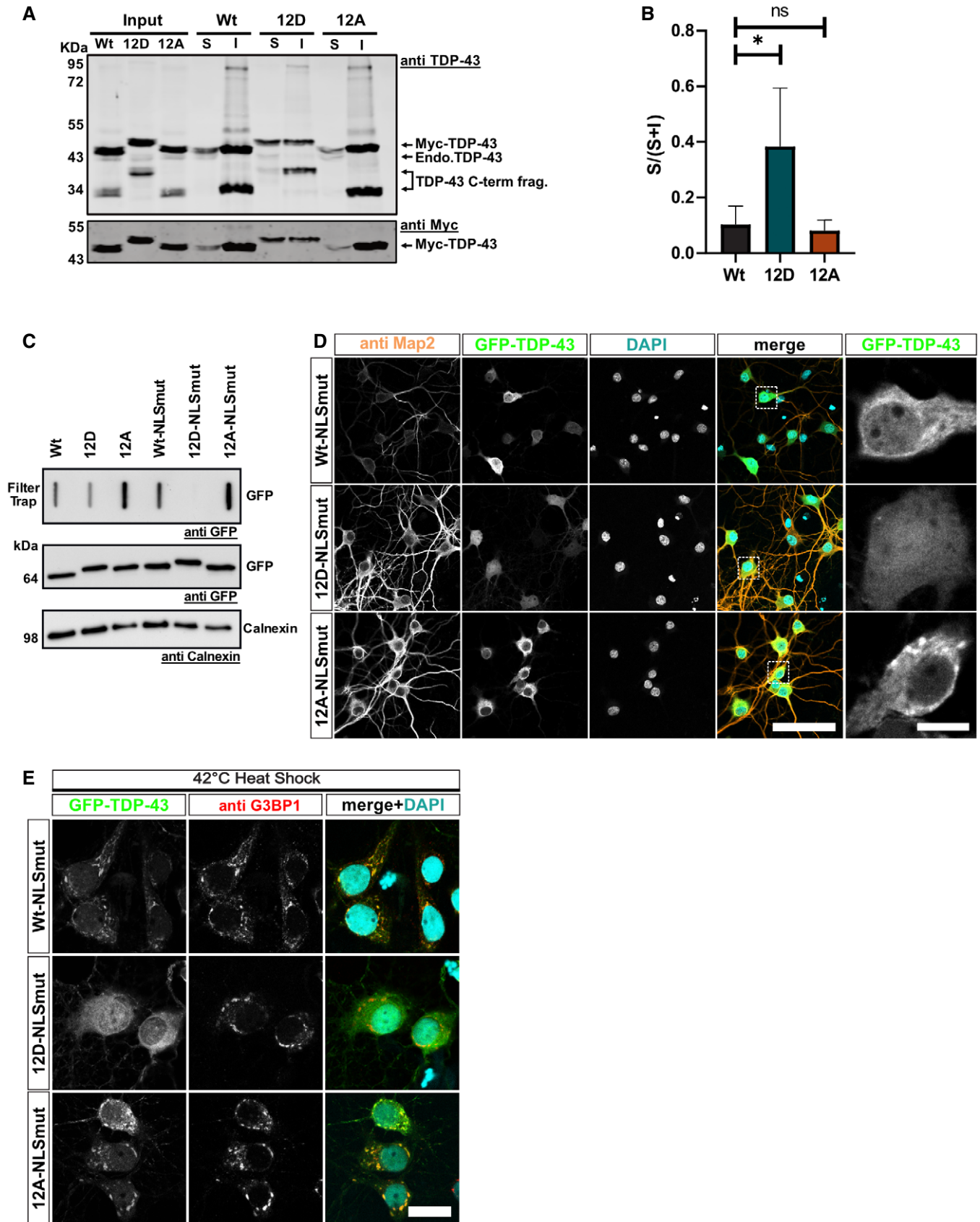


Figure 6.

2008; Neumann *et al*, 2009; Kametani *et al*, 2016). Against previous expectations, we now show that TDP-43 phosphorylation, and in particular phosphomimetic mutations mimicking the phosphorylation pattern in ALS/FTD (Hasegawa *et al*, 2008; Kametani *et al*, 2016), strongly suppress TDP-43 phase separation and aggregation both *in vitro* and in cells. Our data are in line with two previous studies that examined C-terminal fragments of TDP-43 with phosphomimetic 2D or 5D/E mutations and observed a reduced aggregation propensity and toxicity in cell lines and *Drosophila* (Brady *et al*, 2011; Li *et al*, 2011). Even though phosphomimetic mutations do not always recapitulate the effects of phosphorylation on protein-protein interactions (Yaffe *et al*, 1997; Durocher *et al*, 1999), our *in vitro* data with purified proteins show that the phosphomimetic 12D variant has a similar condensation behavior as CK18-phosphorylated TDP-43. We would like to point out that phosphomimetic mutations are an experimental under-appreciation of true charge, as aspartate has a net charge of -1 , whereas phosphorylation has a net charge of -2 . In line, our simulations show that 12S-p disrupts phase separation of the TDP-43 LCD more strongly than the phosphomimetic 12D mutations (Fig 3F–H). It seems possible that the number of phosphorylation sites, but not their exact position, is critical for the suppression of TDP-43 condensation, which would indicate that multisite phosphorylation may regulate TDP-43 phase separation through bulk electrostatics, as previously shown for other proteins (Serber & Ferrell, 2007; Strickfaden *et al*, 2007). Indeed, two recent studies showed that the net charge of IDR-containing RBPs tunes their driving force for assembly (preprint: Crabtree *et al*, 2020; preprint: Bremer *et al*, 2021). For instance, reducing the net charge of the disordered region of Ddx4 promotes its phase separation (preprint: Crabtree *et al*, 2020), and increasing the net charge of the low complexity region of hnRNP-A1 reduces its phase separation, likely due to repulsive electrostatic long-range interactions (preprint: Bremer *et al*, 2021). At physiological pH, TDP-43 has a net charge of -4.1 , phosphomimetic 12D TDP-43 has a net charge of -16.1 and 12 \times phosphorylated TDP-43 has a net charge of -28.1 . In line with the aforementioned studies, it seems likely that the strong increase in negative net charge in phosphomimetic/phosphorylated TDP-43 is responsible for the reduced propensity to self-assemble into condensates.

Various modes of TDP-43 assembly have been proposed, including homotypic interactions of an α -helical structure in the conserved region (CR) of the LCD (Conicella *et al*, 2016, 2020) and interactions between aromatic/aliphatic residues in the LCD (Li *et al*, 2018; Schmidt *et al*, 2019; Laurents *et al*, 2021). All phosphomimetic mutations examined in our study are outside of the α -helix/CR (aa. 321–360; Fig 1D), hence they are unlikely to interfere with helix-helix interactions. In line with this hypothesis, the contact maps extracted from the simulations of the TDP-43 LCD show that most interactions, including aromatic interactions, are not strongly affected by C-terminal phosphomimetics and that mainly interactions of serines with nearby residues are reduced. However, more work is required to understand how PTMs on TDP-43 affect aromatic “sticker”–“sticker” interactions on the molecular scale. C-terminal phosphorylation may also affect amyloid-like fibril formation: A recent cryo-EM structure of solid TDP-43 LCD fibrils showed that several C-terminal serines are buried inside the fibril structure (Li *et al*, 2021), hence phosphorylation could disrupt the amyloid fibril structure, in line with our experimental findings that TDP-43

aggregate formation is strongly reduced by phosphomimetic substitutions. We therefore speculate that TDP-43 phosphorylation might be a protective cellular mechanism that counteracts aberrant TDP-43 phase transitions and renders TDP-43 more dynamic and liquid-like by reducing C-terminal LCD-LCD interactions through negatively charged, highly hydrated phospho-groups.

Under what conditions C-terminal TDP-43 phosphorylation arises in cells and which form of TDP-43 (soluble, phase separated, aggregated) is phosphorylated is still unknown. Interestingly, we and others previously found that C-terminal TDP-43 phosphorylation follows TDP-43 insolubility, suggesting that phosphorylation arises downstream of TDP-43 aggregation (Dormann *et al*, 2009; Brady *et al*, 2011; Zhang *et al*, 2019). In line with these findings, treatment of neuron-like cells with amyloid-like particles triggers a solidification of initially liquid-like cytoplasmic TDP-43 droplets, along with C-terminal TDP-43 phosphorylation (Gasset-Rosa *et al*, 2019). Why phosphorylated TDP-43 aggregates nevertheless persist and are not readily disassembled after phosphorylation remains to be investigated. Further research into the functional consequences of C-terminal TDP-43 phosphorylation, e.g., how it affects global protein or RNA interactions, TDP-43 stability or the introduction of additional PTMs, is needed to understand the role of TDP-43 phosphorylation in physiology and pathology.

Several other studies on TDP-43 phosphorylation at first glance contrast our findings. Overexpression of various TDP-43 kinases in cell or animal models was shown to promote TDP-43 aggregation and neurotoxicity (Choksi *et al*, 2014; Liachko *et al*, 2014; Nonaka *et al*, 2016; Taylor *et al*, 2018). Based on these studies, inhibition of TDP-43 phosphorylation by kinase inhibitors has been proposed as a potential therapeutic strategy for ALS (Liachko *et al*, 2013; Salado *et al*, 2014; Martinez-Gonzalez *et al*, 2020). A possible explanation for the discrepant findings could be that kinase overexpression has pleiotropic effects that may cause TDP-43 aggregation and neurotoxicity independent of TDP-43 phosphorylation. Our data exclude such indirect effects, as they rely on experiments with purified components, MD simulations and defined phosphomimetic constructs rather than modulation of kinase levels/activity. Furthermore, our results suggest that beneficial effects seen with kinase inhibitors are likely not the direct consequence of reduced TDP-43 phosphorylation, but rather mediated by other mechanisms.

An alternative scenario that we cannot exclude is that reduced TDP-43 condensation due to hyperphosphorylation may have negative consequences by disturbing essential functions of TDP-43 that depend on its capacity to phase separate or solidify, e.g., certain DNA/RNA processing steps or recruitment of TDP-43 into cytoprotective NBs (Wang *et al*, 2020) or other MLOs. In support of this hypothesis, a deep mutagenesis study recently found that aggregating TDP-43 variants decrease toxicity in yeast, whereas dynamic, liquid-like variants enhance toxicity (Bolognesi *et al*, 2019), so further work is needed to investigate this possible scenario. However, our data clearly show that some essential RNA processing functions (autoregulation and regulation of certain splicing events), RNA-binding and nuclear localization/import of TDP-43 are not affected by C-terminal hyperphosphorylation, at least in HeLa and U2OS cells, and therefore do not depend on TDP-43's phase separation and solidification capacity. In line with our findings, an earlier study found that phase separation-deficient TDP-43 remains competent in splicing regulation (Schmidt *et al*, 2019).

Of note, abnormal PTMs are a common theme in neurodegenerative disorders, e.g., Tauopathies linked to pathological Tau aggregation (Morris *et al*, 2015; Alquezar *et al*, 2020). Interestingly, even though hyperphosphorylation is generally believed to trigger Tau aggregation, site-specific phosphorylation in the microtubule-binding region of Tau was recently shown to inhibit, rather than promote Tau fibrillization and seeding (Haj-Yahya *et al*, 2020). We now show that C-terminal TDP-43 phosphorylation as detected on ALS/FTD inclusions has a similar inhibitory effect on TDP-43 aggregation, underscoring the idea that aberrant PTMs detected on pathological inclusions may not necessarily all be drivers of protein aggregation, but could also have protective, anti-aggregation effects that are later-on overruled by other pathogenic mechanisms.

Materials and Methods

cdNA constructs

Bacterial expressing constructs

TDP-43 carrying mutations in serine 409 and 410, either to aspartate (2D) or to alanine (2A), were generated by site-directed mutagenesis using Q5 high fidelity DNA polymerase (NEB) using primers containing the mutations S409D/410D and S409A/410A and pJ4M TDP-43-TEV-MBP-His₆ vector as a template. Expression constructs with 5 or 12 serine substitutions (5D, 5A, 12D and 12A) were generated using synthetic double-stranded DNA fragments (gBlocks Gene Fragments, IDT) containing the respective mutations, cloned into PstI and XhoI sites of the pJ4M TDP-43-TEV-MBP-His₆-backbone.

Mammalian expressing constructs

To generate an expressing construct coding for Myc-hTDP-43, the coding sequence of hTDP-43 was PCR amplified from pEGFP-C1-hTDP-43 (Ederle *et al*, 2018), including a Myc coding sequence in the forward PCR primer, and cloned into a pcDNA5-FRT-TO-backbone using XhoI and BamHI restriction sites. Note, that the hTDP-43 template includes a resistance to TARDBPHSS118765 siRNA (Invitrogen) used to silence endogenous TDP-43 (see “siRNA-mediated knockdown of TDP-43”). For generation of the TDP-43 12D and 12A constructs, synthetic gBlocks (IDT) harboring the respective mutations were previously cloned into the NdeI and BamHI sites of the pEGFP-C1-hTDP-43 vector. In constructs carrying mutations in the NLS of TDP-43 (mNLS), amino acids 82–84 as well as 95, 97 and 98 were exchanged for alanine (pEGFP-hTDP-43 mNLS). Then, the mNLS region was transferred from the pEGFP-TDP-43 mNLS template to the pcDNA5-FRT-TO-Myc-hTDP-43, 12D and 12A vectors via the restriction enzymes XhoI and NdeI. To generate the GCR₂-EGFP₂-TDP-43 12D and 12A constructs, the respective coding sequences were PCR amplified and inserted into GCR₂-EGFP₂-backbone using EcoRV and BamHI. To allow for lentiviral packaging and subsequent neuronal transduction, coding sequences of TDP-43 Wt, 12D and 12A were subcloned into the FhSynW backbone in frame with mEGFP (May *et al*, 2014).

HeLa cell culture, transient transfection and stress treatment

HeLa cells were grown in DMEM high glucose GlutaMAX (Invitrogen) supplemented with 10% fetal bovine serum (FBS) and 10 µg/

ml gentamicin and incubated in a humidified chamber with 5% CO₂ at 37°C. cDNA transfections were performed using Lipofectamine 2000 (Thermo) in culture medium without gentamicin and medium was exchanged after 4 to 6 h to avoid cellular stress by the transfection reagent. Note, that for equal transfection efficiency different amounts of DNA were transfected for the different constructs (for 12D: 100%; for Wt and 12A: 75% + 25% empty vector DNA). For immunostaining cells were fixed after ~24 h, hydrogen peroxide (H₂O₂; 1 mM) treatment was carried out for 2 h, MG132 (10 µM) treatment for 2.5–3 h and sodium arsenite (0.5 mM) treatment for 45 min.

Flp-In T-Rex U2OS cell culture and stress treatment

Inducible U2OS cell lines stably expressing myc-hTDP-43 variants (Wt, 12D and 12A) were generated using the Flp-In T-Rex system. Flp-In T-Rex U2OS cells (gift from A. Lamond lab) were cotransfected with pcDNA5-FRT-TO-hTDP-43 (Wt, 12D or 12A) and pOG44 Flp recombinase expression plasmids, followed by selection with Hygromycin (150 µg/ml) and Blasticidin (15 µg/ml). After expansion of surviving single cell colonies, myc-TDP-43 expression was induced by doxycycline (dox) addition for 24 h, using 0.005 µg/ml dox for myc-TDP-43 Wt and 0.25 µg/ml dox for TDP-43 12D and 12A, in order to yield similar protein expression levels. To induce nuclear stress bodies, cells were treated with sodium arsenite (0.5 mM) for 2 h.

Neuronal cell culture, lentiviral packaging and stress treatment

Primary hippocampal and cortical neuronal cultures were prepared from embryonic day 19 rats as described in detail previously (Guo *et al*, 2018). In brief, neocortex and hippocampus were dissected, followed by enzymatic dissociation and gentle trituration. For immunofluorescence experiments, hippocampal neurons (85,000 cells/ml) were plated on poly-D-lysine-coated glass coverslips (VWR) in 12-well plates (Thermo Fisher) and cultured in Neurobasal medium (Thermo Fisher) supplemented with 2% B27 (Thermo Fisher), 1% Penicillin–Streptomycin (Thermo Fisher), 0.5 mM L-glutamine (Thermo Fisher) and 12.5 µM glutamate (Thermo Fisher). Both, cortical and hippocampal neurons, were transduced on day *in vitro* (DIV) 5.

Cortical neurons (250,000 cells/ml) used for filter trap assays were plated on poly-D-lysine-coated six-well plates and cultured in Neurobasal medium containing 2% B27, 1% Penicillin–Streptomycin and 0.5 mM L-glutamine.

Lentiviral packaging was performed by seeding HEK293FT cells (Thermo Fisher) of low passage number into three 10 cm dishes per construct (5 × 10⁶ cells/dish). Cells were plated in DMEM, high glucose, GlutaMAX (Thermo Fisher) supplemented with 10% FBS (Sigma), 1% Penicillin–Streptomycin (Thermo Fisher) and 1% non-essential amino acids (Thermo Fisher). On the following day, cells were co-transfected with 18.6 µg transfer vector (FhSynW-mEGFP-hTDP-43, FhSynW-mEGFP-hTDP-43 [12D], FhSynW-mEGFP-hTDP-43 [12A]), 11 µg pSPAX2 and 6.4 µg pVSVG using Lipofectamine 2000 (Thermo Fisher). The transfection media was replaced by plating media supplemented with 13 mg/ml bovine serum albumin (BSA, Sigma)

on the next day. Lentivirus from the cell supernatant was collected 24 h later by ultracentrifugation with a Sw28 rotor (Beckman Coulter; 64,100 g, 2 h, 4°C). Finally, lentiviral particles were resuspended in Neurobasal media (Thermo Fisher), stored at –80°C and used for lentiviral transduction by adding to neuronal culture media upon thawing. Neurons were kept in culture for 4 additional days after transduction on DIV5 (DIV5 + 4). To induce SGs, heat shock was carried out by incubating neurons for 1 h at 42°C in a cell culture incubator.

Recombinant protein expression and purification

TDP-43-TEV-MBP-His₆

All TDP-43-MBP-His₆ variants were purified according to (Wang *et al*, 2018) with minor adaptations. First, expression of proteins was performed in *E. coli* BL21-DE3 Rosetta 2 using 0.5 mM IPTG and grown overnight at 16°C. Next, cells were resuspended in lysis buffer (20 mM Tris pH 8, 1 M NaCl, 10 mM imidazole, 10% (v/v) glycerol, 4 mM β-mercaptoethanol and 1 μg/ml each of aprotinin, leupeptin hemisulfate and pepstatin A) supplemented with 0.1 mg/ml RNase A, and lysed using lysozyme and sonication. Subsequently, the protein was purified by Ni-NTA agarose (Qiagen) and eluted with lysis buffer containing 300 mM imidazole. For all TDP-43-MBP-His₆ variants, a final size exclusion chromatography (SEC; Hiload 16/600 Superdex 200 pg, GE Healthcare) purification step was performed in purification buffer (20 mM Tris pH 8, 300 mM NaCl, 10% (v/v) glycerol supplemented with 2 mM TCEP), in order to separate TDP-43-MBP-His₆ from protein aggregates and contaminants. Purified monomeric TDP-43-MBP-His₆ was collected by pooling the fractions corresponding to peak B in the SEC profile (Appendix Fig S1D). All purified proteins were concentrated using Amicon ultra centrifugal filters and then flash frozen and stored at –80°C. To determine protein concentration, absorbance at 280 nm was measured using the respective extinction coefficient (ϵ) predicted by the ProtParam tool. Additionally, for all purified proteins, the A260/280 ratio was determined and found to be between 0.5 and 0.7.

CK1δ

The kinase domain of CSNK1D was expressed as an N-terminal MBP-tagged fusion in *E. coli* Rosetta 2 cells, co-expressing λ-phosphatase to guarantee a completely unphosphorylated protein. The cells were grown to an OD of 0.45 and subsequently the temperature was reduced to 18°C. Then the cells were induced (generally at OD 0.7–0.8) with 0.5 mM IPTG and expression was performed overnight. Cells were harvested and resuspended in AC-A buffer (25 mM Bis-Tris, 500 mM NaCl, 10 mM β-mercaptoethanol, pH 7.0), supplemented with DNase, RNase, lysozyme and protease inhibitor cocktail (selfmade) for cell disruption. Lysis was done by sonication on ice (5 × 30 s with breaks of 1 min between each pulse). Cell debris was pelleted by centrifugation (SS34 rotor, 34,541 g, 30 min). The supernatant was filtered and subsequently loaded on a Dextrin Sepharose column (cytiva), previously equilibrated with AC-A buffer. The column was washed for 5 column volumes with AC-A buffer. Elution was done with MBP-B buffer (25 mM Bis-Tris, 500 mM NaCl, 10 mM β-mercaptoethanol, 20 mM maltose, pH 7.0). The eluted protein was subject to TEV protease cleavage overnight at 4°C. On the next day the buffer was

exchanged to IEX-A buffer (25 mM Bis-Tris, 50 mM NaCl, 10 mM β-mercaptoethanol) by ultra-filtration (Amicon Ultra-15 30 kDa, Merck Millipore) and subject to cation-exchange chromatography by a linear to IEX-B buffer (25 mM Bis-Tris, 500 mM NaCl, 10 mM β-mercaptoethanol). Eluted protein was concentrated and gel-filtered over a Superdex 75 (cytiva) into SEC buffer (25 mM Bis-Tris, 50 mM NaCl, 10 mM MgCl₂, 1 mM DTT). Fractions were collected, concentrated and aliquots of 200 μl were flash frozen and stored at –80°C until use.

His₆-TEV protease

His₆-TEV protease expression and purification was performed as described in Hutten *et al* (2020).

In vitro phosphorylation

TDP-43-MBP-His₆ was *in vitro* phosphorylated with CK1δ and 200 μM ATP in phosphorylation buffer (50 mM Tris-HCl, pH 7.5, 10 mM MgCl₂, 1 mM DTT) for 2 h at RT, using a two-fold molar excess of TDP-43-MBP-His₆ over CK1δ. Subsequently, the reaction was used for sedimentation and SG association assays. As negative controls, either the kinase or the ATP was omitted and also included as controls in subsequent assays.

Enzymatic digestion, enrichment for phospho-peptides and mass spectrometric analysis

TDP-43-MBP-His₆ was *in vitro* phosphorylated as described above, separated on a 10% SDS-PAGE gel and visualized by Coomassie staining. The gel band corresponding to the phosphorylated TDP-43-MBP-His₆ was excised and destained twice for 30 min at 37°C with 50% acetonitrile in 50 mM Tris-HCl, pH 8. The gel piece was dehydrated with 100% acetonitrile, reduced and alkylated, and finally digested overnight at 37°C with 375 ng trypsin (Promega). The peptides were extracted from the gel twice using 100 μl of 50% acetonitrile and 0.25% TFA buffer. Both extractions were merged and evaporated in a vacuum evaporator. In order to enrich the phospho-peptides, 10 μl of 0.5 mg/μl TiO₂ beads (GL Sciences Cat. No.: 5010-21315) in loading buffer (80% ACN, 5% TFA and 1 M glycolic acid) were added to the dried samples in a ratio of 0.3 mg of beads to 5 pmol of protein. Samples were incubated for 10 min at RT on a shaker at 270 g and spun down at 100 g for 1 min. The supernatant was removed and kept for further analysis, while beads were sequentially washed with loading buffer, washing buffer 1 (80% ACN, 1% TFA) and washing buffer 2 (10% ACN, 0.2% TFA). Next, the beads were dried in the hood for 10 min and resuspended with 50 μl elution buffer (28% ammonia solution in H₂O). Finally, the samples were speed vacuum evaporated and resuspended with 15 μl 0.1% FA. For LC-MS purposes, desalted peptides were injected in an Ultimate 3000 RSLCnano system (Thermo) and separated in a 25-cm analytical column (75 μm ID, 1.6 μm C18, IonOpticks) with a 30-min gradient from 3 to 30% acetonitrile in 0.1% formic acid. The effluent from the HPLC was directly electrosprayed into a Qexactive HF (Thermo) operated in data-dependent mode to automatically switch between full scan MS and MS/MS acquisition. Survey full scan MS spectra (from *m/z* 300–1,600) were acquired with resolution $R = 60,000$ at *m/z* 400 (AGC target of 3×10^6). The 10 most intense peptide ions with charge states between 2 and 5 were

sequentially isolated to a target value of 1×10^5 with resolution $R = 15,000$ and isolation window 1.6 Th and fragmented at 27% normalized collision energy. Typical mass spectrometric conditions were: spray voltage, 1.5 kV; no sheath and auxiliary gas flow; heated capillary temperature, 250°C; ion selection threshold, 33,000 counts.

Fluorescent labeling of purified TDP-43

TDP-43-MBP-His₆ variants were labeled with Alexa Fluor 488 C5 maleimide (Thermo Fisher) at a low (~0.01–0.05) labeling efficiency in order to avoid interference with condensate formation. Labeling was performed according to the manufacturer's protocol using a 1:100 or 1:20 protein:fluorescent dye mole ratio. Briefly, the Alexa Fluor reagent, previously dissolved in DMSO, was mixed with the protein and kept in the dark for 2 h at RT. Excess dye was removed by consecutive washes with TDP-43 purification buffer using Amicon ultra centrifugal filters. Subsequently, labeled protein was used for spinning disc confocal microscopy, FRAP and aggregation assays, respectively.

In vitro phase separation and aggregation assays

Sedimentation assay

For sedimentation analysis, 1 μM TDP-43-TEV-MBP-His₆ variants or *in vitro* phosphorylated TDP-43-TEV-MBP-His₆ was cleaved by addition of 20 μg/ml His₆-TEV protease in 50 or 25 μl Hepes buffer (20 mM Hepes, pH 7.5, 150 mM NaCl, 1 mM DTT), respectively, to remove the MBP-His₆ tag and induce phase separation. Samples were incubated for 60 min at 30°C, followed by centrifugation for 15 min at 21,000 g at 4°C to pellet the formed condensates. Equal amounts of supernatant (S) and condensate (C) fractions were loaded onto an SDS-PAGE gel and TDP-43 was detected by Western Blot (rabbit TDP-43 N-term, Proteintech, Cat. No.: 10782-2-AP).

Microscopic condensate assay

For all microscopic condensate assays, uncoated μ-Slide 18 Well-Flat chambers (Cat. No.: 81821, Ibidi) were pretreated with 10% Pluronic F-127 solution for 1 h and 5 times washed with MilliQ water. The water remained in the chamber until just before the experiment, as described in Ceballos *et al* (2018).

Purified TDP-43-TEV-MBP-His₆ variants were buffer exchange to Hepes buffer or phosphate buffer (20 mM Na₂HPO₄/NaH₂PO₄, pH 7.5, 150 mM NaCl, 2.5% glycerol, 1 mM DTT). Proteins were then centrifuged at 21,000 g for 10 min at 4°C to remove any preformed protein precipitates. For condensates formation, the reaction was setup directly in Pluronic-coated μ-Slide 18 Well-Flat chambers, where proteins were diluted to the indicated concentrations and phase separation was induced by addition of 100 μg/ml His₆-TEV protease at RT. After ~20 min, imaging was performed by bright field microscopy using a widefield microscope.

For fusion events and FRAP analysis, condensates were formed directly in Pluronic-coated μ-Slide 18 Well - Flat chambers as described above using 20 μM of each Al.488-labeled TDP-43 protein variants (Wt, 5D and 12D) in Hepes buffer and incubated for 10 min at RT before imaging. Note that experiments were performed until maximally 1 h after adding the TEV protease, in order to avoid *in vitro* aging of condensates.

Turbidity assay

Phase separation of TDP-43-TEV-MBP-His₆ variants was induced as described earlier for the microscopic condensate assay. Reactions of 20 μl samples were prepared at the indicated concentrations in 384-well plates and incubated for 30 min at RT after adding TEV protease. Subsequently, a BioTek Power Wave HT plate reader was used to measure turbidity at 600 nm. Turbidity measurements were performed in triplicates.

Semi-denaturing detergent agarose gel electrophoresis

SDD-AGE experiments were performed based on protocols published by French *et al* (2019) and Halfmann and Lindquist (2008). First, 2 μM purified TDP-43-MBP-His₆ variants (WT, 5D, 12D and 12A) were set up in low binding tubes (Eppendorf) in 35 μl aggregation buffer (50 mM Tris pH 8.0, 250 mM NaCl, 5% glycerol, 5% sucrose, 150 mM imidazole pH 8.0) and supplemented with 1× protease inhibitor (Sigma). Samples were shaken for 30 min on a thermomixer at 1,000 rpm at RT (~22°C) and then incubated at RT for the indicated time period. 5 μl of each sample was collected and diluted in SDD-AGE buffer (40 mM Tris-HCl pH 6.8, 5% glycerol, 0.5% SDS, 0.1% bromphenol-blue) and analyzed by SDD-AGE by horizontal 1.5% agarose gel electrophoresis (gel: 1.5% agarose in 20 mM Tris, 200 mM glycine and 0.1% SDS) in running buffer (60 mM Tris, 20 mM acetate, 200 mM glycine, 1 mM EDTA and 0.1% SDS) for ~6 h at 60 V. Detection of TDP-43 monomers, oligomers and high-molecular-weight species was performed after overnight capillary transfer in TBS (50 mM Tris pH 7.6, 150 mM NaCl) to a nitrocellulose membrane and by standard Western Blot using rabbit anti TDP-43 N-term antibody (Proteintech, Cat. No.: 10782-2-AP).

Formation of Alexa 488-labeled TDP-43 aggregates

In order to visualize TDP-43 (wt, 5D, 12D and 12A) aggregates formed under the above described assay conditions, 10 μM Al.488-labeled TDP-43-MBP-His₆ was set up in low binding tubes (Eppendorf) in aggregation buffer and incubated with or without 100 μg/ml His₆-TEV protease. Samples were shaken at 1,000 rpm at RT for 30 min and then transferred into a 384-well black plate (Greiner Bio-One), incubated at RT and imaged by confocal microscopy after 2, 8 and 24 h.

Cellular TDP-43 solubility assays

Fractionation in RIPA-Benzonase buffer

HeLa cells (~ 1×10^6) were washed twice in PBS, harvested by scraping and pelleted at 1,100 g for 5 min. Cell pellets were incubated on ice for 15 min in 200 μl RIPA buffer (50 mM Tris-HCl, pH 8.0, 150 mM NaCl, 1% NP-40, 0.5% deoxycholate, 0.1% SDS) with freshly added 1× protease inhibitor cocktail (Sigma), 1× phosphatase inhibitors (final concentration: 10 mM NaF, 1 mM β-glycerophosphate, 1 mM Na₃VO₄) and 0.05 unit/μl Benzonase (Sigma). Samples were sonicated in a BioRuptorPico (Diagenode) for 45 sec and 20 μl of sample was collected as "Input". The remaining sample was then centrifuged at 13,000 g for 30 min at 4°C. The resulting supernatants (S) were collected and the remaining pellets were washed in RIPA buffer with inhibitors, resonicated for 45 sec and recentrifuged for 30 min at 4°C at 13,000 g. Finally, the RIPA

insoluble pellets (I) were resuspended in 36 μ l urea buffer (7 M urea, 2 M thiourea, 4% CHAPS, 30 mM Tris-HCl, pH 8.5) and sonicated. All samples were supplemented with 4 \times Lämmli buffer (250 mM Tris-HCl, pH 6.8, 40% glycerol, 8% SDS, 0.1% bromophenol-blue, 4% β -mercaptoethanol) and input and supernatant (S) samples were boiled prior to SDS-PAGE and Western Blot against TDP-43 (rabbit anti TDP-43 C-term, Proteintech, Cat. No.: 12892-1-AP) and Myc (mouse anti-myc 9E10 antibody, Helmholtz Center Munich). Note that for detection reasons, the (I) fractions were 4 \times more concentrated than the (S) fractions, so they are represented in a 1:5 ratio.

Filter trap assay

Cortical neurons expressing the indicated EGFP-tagged TDP-43 variants (DIV5 + 4 days expression) were washed two times with PBS and lysed on ice in RIPA buffer (50 mM Tris-HCl, pH 8.0, 150 mM NaCl, 1% NP-40, 0.5% deoxycholate, 0.1% SDS) freshly supplemented with 1 \times protease inhibitor cocktail (Sigma), 1 \times phosphatase inhibitor cocktail (Sigma) and 0.125 Units/ μ l benzoylase (Sigma) for 20 min. Cell lysates were collected and centrifuged at 1,000 g, 4°C for 30 min. Two-third of the resulting supernatant (RIPA-insoluble fraction) was filtered through a nitrocellulose membrane (0.2 μ m pore size, Merck) using a filter trap slot blot (Hoefer Scientific Instruments). After washing with PBS for three times, membranes were blocked for 1 h with 2% I-Block (Thermo Fisher) prior to immuno-detection with mouse anti-GFP (UC Davis/NIH Neuromab Facility, Cat. No.: N86/8) and rabbit anti Calnexin antibody (Enzo Life Sciences, Cat. No.: ADI-SPA-860). The remaining 1/3 of the lysates was diluted with 3 \times loading buffer (200 mM Tris-HCl pH 6.8, 6% SDS, 20% glycerol, 0.1 g/ml DTT, 0.1 mg bromophenol blue), boiled at 95°C and used for subsequent standard Western Blot analysis.

Multi-scale MD simulations

Explicit solvent coarse-grained MD simulations

Coarse-grained MD simulations with explicit solvent to investigate protein phase separation and phase-separated protein condensates were run with a rescaled version of the Martini forcefield (Marrink *et al*, 2007; Monticelli *et al*, 2008) as described by Benayad *et al* (2021). A similar approach was shown to describe the conformational ensembles of proteins with disordered domains very well (Larsen *et al*, 2020; Martin *et al*, 2021), and we recently showed that such approaches can be extended to simulations of LLPS of disordered proteins (Benayad *et al*, 2021). Protein-protein interactions were thus scaled to 0.8 of the default value. Chloride and sodium ions were added to neutralize the system in simulations of Wt and 12D proteins. 10% of the water beads were replaced by WF anti-freeze beads. Coarse-grained simulations were run with GROMACS 2018 (Abraham *et al*, 2015). Simulations boxes measured 450 \times 450 \times 600 Å. Simulations systems were energy minimized and equilibrated in MD simulations with and without position restraints. 118 Wt and 12D C-terminal LCDs (aa. 261–414) were simulated for 20 μ s each. The coarse-grained simulations systems consist of roughly one million particles. Equations of motions were integrated with a 20-fs time step. Simulations were conducted in the NPT ensemble at 1 bar and 300 K using the Parrinello-Rahman barostat (Parrinello & Rahman, 1981) and the

Bussi-Donadio-Parrinello velocity-rescaling thermostat (Bussi *et al*, 2007).

Note that in the coarse-grained approach we employed, four atoms are typically grouped together to a coarse-grained particle. For example, a coarse-grained water molecule would correspond to four water molecules in an atomistic simulation.

Implicit solvent coarse-grained MD simulations

The HPS coarse-grained model provides a coarser and thus computationally very efficient description of disordered proteins and their phase behavior (Dignon *et al*, 2018). Parameters for PTMs, such as phosphorylation, are available (Perdikari *et al*, 2021). Solvent is treated implicitly and electrostatics is described by Debye-Hückel theory. We simulated 100 C-terminal LCDs (aa. 261–414) in slab geometry (212 Å \times 212 Å \times 2800 Å) following the protocol of Mittal and co-workers (https://bitbucket.org/jeetain/hoomd_slab_builder/src/master/) (Dignon *et al*, 2018; Regy *et al*, 2020). Simulations were started with all proteins concentrated and equilibrated in a small sub volume so that the proteins formed an initial condensate. We studied the phase behavior of Wt, 12D, 12A, 5pS and 12pS TDP-43 LCDs. Production simulations ($T = 310$ K) were run for at least 5.8 μ s and up to 6.5 μ s for each LCD variant.

Atomistic MD simulations

HCG (Pietrek *et al*, 2020) enables us to generate statistically independent and chemically-meaningful conformations of a biomolecular condensate with atomic resolution, which serve as starting points for atomistic MD simulations. Atomic-resolution models of clusters of the C-terminal disordered domain of TDP-43 (aa. 261–414) were generated for both Wt protein and the 12D mutant. To assemble the disordered proteins into a condensate, we first assemble pairs of disordered domains, then pairs of pairs, pairs of quadruplets, and so forth, following the logic set out in (Pietrek *et al*, 2020). HCG Monte Carlo manifestly satisfies detailed balance and thus we generate representative ensembles. Finally, we arrive at densely packed disordered domains, while retaining atomic resolution at each modeling step. Periodic boundary conditions were employed during the assembly.

Clusters of Wt and 12D LCDs were solvated in a 150 Å \times 150 Å \times 150 Å simulation box, the system charge was neutralized and 150 mM NaCl was added. We employed the Amber-disp protein force field developed by Robustelli *et al* (2018), including the modified TIP4P-D water model (Piana *et al*, 2015) that accompanies the Amber-disp protein force field. Temperature was maintained at 300 K by the Bussi-Donadio-Parrinello velocity-rescaling thermostat (Bussi *et al*, 2007). We employed the Parrinello-Rahman barostat (Robustelli *et al*, 2018) to set the pressure to 1 bar. Equations of motions were integrated with a 2-fs time step. Production simulations were prepared by energy minimization with and without soft-core potentials. To start production simulations, we equilibrated the atomistic simulations systems, running at least 5,000 steps with a 1-fs time step and position restraints and for 1.5 ns with a 2-fs time step also with position restraints. Equilibrium simulations of the clusters of the disordered domains were conducted with GROMACS 2019 (Abraham *et al*, 2015). For both wild-type and 12D, clusters of 32 chains with 154 residues were simulated for just over 1 μ s, with two repeats each started from independently generated HCG structures.

Simulations were analyzed with the MDAnalysis (Michaud-Agrawal *et al*, 2011; Gowers *et al*, 2016) and the MDtraj Python libraries (McGibbon *et al*, 2015). Contact analysis was performed with the Contact Map Explorer Python library (https://github.com/dwhswenson/contact_map).

Analysis of MD simulations

Simulations were analyzed with the MDAnalysis (Michaud-Agrawal *et al*, 2011; Gowers *et al*, 2016) and the MDtraj Python libraries (McGibbon *et al*, 2015). Contact analysis of the coarse-grained simulations with the explicit solvent Martini model was performed with the Contact Map Explorer Python library (https://github.com/dwhswenson/contact_map). For simulations with the HPS implicit solvent coarse-grained model, contacts were computed with MDAnalysis. Two amino acids were deemed in contact in the simulations with the HPS model when their inter-bead distance was $< 2^{1/6}\sigma_{ij}$ where $\sigma_{ij} = \frac{1}{2}(\sigma_i + \sigma_j)$ is the average of bead diameter of the respective amino acids i and j . The concentrations c_{dilute} and c_{dense} of dilute and dense phases, respectively, were determined by adapting the workflow of Tesei *et al* (<https://github.com/KULL-Centre/papers/tree/main/2021/CG-IDPs-Tesei-et-al>) from the simulations of the HPS model (preprint: Tesei *et al*, 2021). The excess free energy of transfer from the dilute to the dense phase was then computed as $\Delta G_{trans} = -RT \ln (c_{dense}/c_{dilute})$, where R is the gas constant and T is the absolute temperature.

Nuclear transport assay

To analyze import of GCR₂-EGFP₂ tagged TDP-43 reporters, HeLa cells were grown for at least two passages in DMEM supplemented with 10% dialyzed FBS and were transiently transfected with the different GCR₂-EGFP₂-TDP-43 variants as described earlier. Import of the GCR₂-EGFP₂-TDP-43 reporters was induced by adding dexamethasone (5 μ M final concentration) in imaging medium (fluorobrite) and followed by live cell imaging using a spinning disk confocal microscope (see below).

SG association assay

HeLa cells were grown on high precision (No. 1.5) poly-L-lysine coated 12 mm coverslips, and after SG induction with MG132 (10 μ M for 2.5–3 h), cells were permeabilized for 2 \times 2 min with 0.004–0.005% digitonin in KPB (20 mM potassium phosphate pH 7.4, 5 mM Mg(OAc)₂, 200 mM KOAc, 1 mM EGTA, 2 mM DTT and 1 mg/ml each aprotinin, pepstatin and leupeptin). Soluble proteins were removed by several, stringent washes (4 \times 4 min in KPB on ice) before blocking nuclear pores by 15 min incubation with 200 mg/ml wheat germ agglutinin (WGA) on ice. Cells were then incubated for 30 min at RT with 100 nM TDP-43-MBP-His₆. For comparison of *in vitro* phosphorylated TDP-43 with controls, proteins were either subjected to the *in vitro* phosphorylation reaction or mock treated (Wt, 12D) in absence of kinase or ATP before exchanging the buffer to KPB using 40K Zeba spin desalting columns (Thermo). Subsequently, cells were washed (3 \times 5 min in KPB on ice) to remove unbound TDP-43-MBP-His₆ and processed by immunostaining to visualize SGs. SGs and TDP-43-MBP-His₆ were visualized by G3BP1 immunostaining (rabbit anti G3BP1 antibody, Proteintech, Cat. No.: 13057-2-AP) and MBP immunostaining (by

mouse anti MBP antibody, Proteintech, Cat. No.: 66003-1-Ig), respectively. On Fig 4B for clarity, signals were converted to grey values in the individual channels (upper two rows). In the merge (lower row), G3BP1 is shown in magenta, TDP-43-MBP-His₆ in green, white pixels indicate colocalization. Nuclei were counterstained with DAPI (turquoise).

siRNA-mediated knockdown of TDP-43

TDP-43 knockdown was achieved using the pre-designed TARDBPHSS118765 siRNA (Invitrogen) as described in Dormann *et al* (2009). Briefly, 20 nM siRNA was transfected into HeLa or U2OS cells using RNAimax (Thermo) transfection reagent. Knockdown was analyzed 48 h post transfection by immunohistochemistry using mouse anti TDP-43 antibody (Proteintech, Cat. No.: 60019-2-Ig) and immunoblotting using rabbit anti TDP-43 C-Term antibody (Proteintech, Cat. No.: 12892-1-AP) to detect TDP-43 and mouse anti alpha-Tubulin antibody (Proteintech, Cat. No.: 66031-1-Ig) for detection of α -Tubulin as a control.

RNA extraction and RT-PCR to analyze TDP-43 splice targets

TDP-43 expression was silenced in HeLa cells by siRNA as described earlier and 24 h later cells were transfected with siRNA-resistant pcDNA5-FRT-TO-Myc-hTDP43 constructs (Wt, 12D and 12A). 48 h after transfection, cells were harvested and total RNA was extracted using an RNeasy mini kit from Qiagen. cDNA was synthesized using 500 ng of total RNA, M-MLV reverse transcriptase polymerase (Invitrogen), and 6 μ M of random hexamer primer (NEB). cDNA was amplified with Taq DNA polymerase (NEB) using the forward (FW) and reverse (RV) primers targeting the SKAR gene (FW—5'CCTTCATAAACCCACCCATTGGGACAG3'; RV—5'GTGGTGGAGA AAGCCGCCTGAG3') (Fiesel *et al*, 2012) and the BIM gene (FW—5'TCTGAGTGTGACCGAGAAGG3'; RV—5'TCTTGGGCGATCCATAT CTC 3') (Tollervy *et al*, 2011). PCR products were separated by electrophoresis on a 2.5% agarose gel containing GelRed (Sigma).

Electrophoretic mobility shift assays

The TDP-43 autoregulatory RNA site (Ayala *et al*, 2011) located in the TARDBP 3'UTR (5'UCACAGGCCGCGUCUUUGACGGUGGGUGU CCCAUUUUUUAUCCGCUACUCUUUUUAUUUCAUGGAGUCGUAUCAAC GCUAUGAACGCAAGGUCUGUGAUUAUGGAACAGAAAGGCGUGUCUGA ACUUUUUGAAACCUUGUGUGGGAUUGAUGGUGGUGCCGAGGCAUG AAAGGCUAGUAUGAGCGAGAAAAGGAGAGAGCGCGUGCAGAGAC UUGGUGGUGCAUUAUGGAUUAUUUUUUUAACUUGGCGAGAUGUGU CUCUCAAUCCUGUGGCUUUGGUGAGAGAGUGUGCAGAGAGCAAU GAUAGCAAUUAUGUACGAAUGUUUUUUUGCAUUAAGGACAUC CACAUCUGUUGGAAGACUUUUUAAGUGAGUUUUUGUUCUUAAGUA ACCCAUUAAGAUGAAUGUGUUAAGUGAAUGAUACUUGUACUC CCCCACCCUUUGUCAACUGCUGUG) was *in vitro* transcribed from double-stranded DNA templates and Cy5-labeled using the HyperScribe™ T7 High Yield Cy5 RNA Labeling Kit (APEXIO, Cat. No.: K1062) per manufacturer's instructions. (UG)₁₂ RNA (5' UGU GUGUGUGUGUGUGUGUGUG) was chemically synthesized with the addition of a 5' Cy5-label (Metabion). 16 nM of Cy5-labeled RNA was mixed with varying amounts of TDP-43 Wt, 12A, and 12D (0–1.6 μ M). Binding reactions (20 μ l) were incubated in binding

buffer (20 mM NaPO₄ [pH 8], 150 mM NaCl, 1 mM DTT, 5 mM MgCl₂, 0.5 mg/ml BSA, 0.1 mg/ml yeast tRNA, 5% glycerol and 1 U/μl RNase inhibitor [NEB]) for 20 min at RT before loading onto a 1-mm thick non-denaturing polyacrylamide gel (6%) in 0.5× TBE. Gels were run at 100 V for 1 h at RT. Gels were imaged with a Typhoon™ FLA 9500 laser scanner.

Immunostaining

All steps were performed at RT. HeLa and Flp-In T-Rex U2OS cells were fixed in 4% formaldehyde in PBS for 10 min, permeabilized for 5 min using 0.2% (v/v) Triton X-100 in PBS and subsequently blocked in blocking buffer (5% goat or donkey serum in 0.1% saponine in PBS) for 30 min. Primary and secondary antibodies were diluted in blocking buffer and applied each for 1 h and washed three times using 0.1% saponine in PBS. Myc-TDP-43 was stained using mouse anti TDP-43 antibody (Proteintech) or mouse anti-myc 9E10 antibody (IMB protein production core facility), SGs were stained using goat anti TIA1 antibody (Santa Cruz, Cat. No.: sc-48371) or rabbit anti G3BP1 antibody (Proteintech) and DNA was stained with DAPI at 0.5 μg/ml in PBS for 5 min. Coverslips were then mounted on glass slides with ProLong™ Diamond Antifade reagent (Life Technologies) and dried overnight at RT.

Hippocampal neurons cultured on glass coverslips were washed twice with PBS and fixed for 10 min at RT using 4% paraformaldehyde and 4% sucrose in PBS. Primary antibody as well as secondary antibody (1:400) were diluted in GDB buffer (0.1% gelatin, 0.3% Triton X-100, 450 mM NaCl, 16 mM sodium phosphate pH 7.4). Primary antibodies (Mouse anti Map2, Sigma, Cat. No.: M1406; Rabbit anti G3BP1, Abcam, Cat. No.: ab181150) were incubated overnight at 4°C while secondary antibodies was applied for 1 h at RT, each followed by three times washing with PBS. Coverslips were mounted using Vectashield Vibrance with DAPI (Biozol) to counterstain nuclei.

Microscopy

Bright and wide-field microscopy

Imaging of unlabeled TDP-43 condensates was done by bright-field microscopy on an Axio Observer.Z1 wide-field fluorescence microscope, using a 63×/1.40 Oil objective and an AxioCam 506 (Zeiss, Oberkochen, Germany).

Confocal microscopy

Confocal microscopy of TDP-43 aggregates and HeLa cells was performed using an inverted Leica SP8 microscope and the LAS X imaging program (Leica), provided by the Bioimaging core facility of the Biomedical Center (LMU Munich), which included the excitation lasers for 405, 488, 552 and 638 nm. Images were acquired using two-fold frame averaging with a 63×1.4 oil objective, with an image pixel size of 180 nm for Al488-TDP-43 aggregates and fixed cells, and 59 nm for images of cells subjected to the SG association assay. Confocal images of U2OS cells were obtained using an inverted Leica SP5 microscope and the LASAF imaging program (Leica), provided by the Light Microscopy core facility of the Biocenter (JGU Mainz). Images were acquired using two-fold frame averaging with a 100× 1.4 oil objective, with an image pixel size of 151 nm.

The following fluorescence settings were used for detection: DAPI: 419–442 nm, GFP: 498–533 nm, Alexa 555: 562–598 nm and Alexa 647: 650–700 nm. Recording was performed sequentially using a conventional photomultiplier tube to avoid bleed-through.

Spinning disc confocal microscopy

a Nuclear transport assay imaging: Images were acquired for a duration of 50 min in 2.5 min intervals at 36.5°C and 5% CO₂ (EMBLEM environmental chamber) using an inverted microscope (Axio Observer.Z1; Carl Zeiss, Oberkochen, Germany) equipped with a confocal spinning disc (CSU-X1; Yokogawa, Tokyo, Japan) and a 63×/1.4 oil immersion lens. Images were acquired using the 488 nm SD laser line and an EM-CCD camera (EvolveDelta; Photomoetrics) at bin 1 × 1.

b Fusion events and FRAP: Experiments were performed on an inverted microscope (Axio Observer.Z1; Carl Zeiss, Oberkochen, Germany) equipped with a confocal spinning disk unit (CSU-X1; Yokogawa, Tokyo, Japan) and an oil immersion lens of 100×/1.46 Oil Ph3. Images recording the dynamics of TDP-43 condensates were obtained using a EM-CCD camera (EvolveDelta; Photomoetrics), with a bin 1 × 1 in a recording mode of 5 s intervals in a block of 3 min. Images of TDP-43 condensates after bleaching were acquired with bin 1 × 1 in streaming mode for 1.5 s followed by a block of 2 min where images were recorded in intervals of 5 sec. Experiments were performed at RT and ≥ 11 condensates were analyzed per condition in three independent experiments. Localized photobleaching (“half-bleach”) was obtained using a laser scanning device (UGA-42 Geo; Rapp OptoElectronic, Hamburg, Germany). The “Geo” module allowed for simultaneous laser illumination within hardware-defined shapes of different sizes. For this experiment, an illumination size of ~4 μm in a square-like shape was used. The targeting structure was half bleached to approximately 70% of the initial intensity using a 473-nm diode laser (DL-473/75; Rapp OptoElectronic, Hamburg, Germany).

Quantification and analysis

Droplet quantification

Wide-field images of droplets were processed and quantified and measured using Image J/Fiji software. First, a bandpass filter of 20 pixels was applied to all images in order to reveal some details and thresholds were adjusted to optimally include all droplets. Finally, droplets were counted and measured by their size and roundness [$4 \times \text{area} / (\pi \times \text{major_axis}^2)$], or the inverse of the aspect ratio] using the command Analyze Particles, excluding the detection of particles with a circularity below 0.3 and/or an area smaller than 3 pixels. Statistical analyses were performed using GraphPad Prism 8.

Analysis of cellular images

Analysis of the nuclear transport assay was performed using Image J/Fiji software by measuring loss in cytoplasmic fluorescence over time and normalizing $t = 0$ min to 1.

Images of cells from the SG association assay (Hutten & Dormann, 2020) were processed and analyzed using Image J/Fiji software, applying linear enhancement for brightness and contrast and implemented plugins for measurement of pixel intensities in SGs.

Quantification of Myc-hTDP-43 recruitment into SGs was performed using Image J/Fiji software. First, SGs from TDP-43-positive cells were selected using the Wand tracing tool and a band of 1 μm representing a proxy for the cytosol was drawn around all selected SGs using the “Make Band” command. Then, all pixel intensities for both SG and band selections was extracted for the TDP-43 channel. After subtraction of the background signal from all measured values, calculation of the SG/band ratio was performed for each SG.

Analysis of Myc-hTDP-43 recruitment into NBs was performed by counting the number of cells with positive TDP-43 nuclear condensates, excluding cells expressing TDP-43 staining only in the cytoplasm. Profile of TDP-43 nuclear staining was performed using Image J/Fiji software by using the “Plot Profile” command, which quantifies the gray values along the indicated lines.

All statistical analyses were performed using GraphPad Prism 8.

WB analysis

WB analysis was performed by extracting the optical densities of each band using the software Image Studio Lite (LI-COR), using the top and bottom average background option, to obtain the signal value, in which local background is automatically subtracted.

Analysis of Sedimentation assays and Fractionation in RIPA-Benzamide buffer experiments was performed by dividing the signal values of (S) by the total (S + C) or (S + I) signal values, to obtain a S/(S + C) or S/(S + I) ratio, respectively.

Analysis of TDP-43 autoregulation levels in the Flp-In T-Rex U2OS cell line was performed by comparing the signal values of endogenous TDP-43 protein between induced (+Dox) and non-induced (–Dox) expression conditions of myc-hTDP-43 variants. After housekeeping protein normalization using Histone H3, endogenous TDP-43 protein expression levels were normalized to 1 in the myc-TDP-43 Wt (–Dox) condition.

All statistical analyses were performed using GraphPad Prism 8.

FRAP analysis

FRAP analysis were performed using Image J/Fiji software by calculating the fluorescence intensity over time ($I(t)$) using the macro Time Series Analyzer command and the following formula:

$$I(t) = \frac{[\text{ROI1}(t) - \text{ROI3}(t)]}{[\text{ROI2}(t) - \text{ROI3}(t)]}$$

ROI1 corresponds to the averaged gray values of the bleached area, and ROI2 to the averaged gray values of the total droplet. ROI3 corresponds to the averaged background values. Values were further normalized to the initial fluorescence by dividing $I(t)$ by the mean gray value of the initial 1 time step before bleaching $\langle I(1) \rangle$. This way bleached areas were corrected for background noise and bleaching due to imaging over time. Statistical analyses were performed using GraphPad Prism 8.

Data availability

This study includes no data deposited in external repositories.

Expanded View for this article is available online.

Acknowledgements

We thank Bettina Schmid, Magdalini Polymenidou, Sören von Bülow, Kumar Gaurav and Zakarya Benayad for insightful discussions and Ignasi Forné, Tobias Straub, Fridolin Kielisch and Arya Changiarath Sivasadan for technical support and discussion. We thank Angus Lamond for gift of the Flp-In U2OS cell line. We acknowledge support by the Core Facilities Proteomics, Bioimaging and Bioinformatics of the BioMedical Center, LMU Munich, the Light Microscopy Core Facility of the Biocenter, JGU Mainz and the Bioinformatics Core Facility of IMB Mainz. We thank Peter Becker and Michael Kiebler for infrastructure and access to the spinning disc confocal microscope (DFG, INST 86/1581-1 FUGG) and are grateful to Edward Lemke for generously sharing lab space and infrastructure. The authors gratefully acknowledge the computing time granted on the supercomputer Mogen II at Johannes Gutenberg University Mainz (hpc.uni-mainz.de). This work was supported by the Deutsche Forschungsgemeinschaft (DFG, German Research Foundation), specifically by project DO1804/4-1 within the Priority Programme SPP2191 - ID 402723784 (to D.D.), projects DO1804/1-1 and DO1804/1-2 within the Emmy Noether Programme (to D.D.), project DO1804/5-1 within the Heisenberg Programme (to D.D.), the Paul Ehrlich and Ludwig Darmstädter Award for Young Researchers 2019 (to D.D.), the Munich Cluster for Systems Neurology (EXC2145 SyNergy—ID 390857198 to D.D. and D.E.) and the NOMIS foundation (D.E.). G.H. acknowledges financial support from the German Research Foundation (CRC 902: Molecular Principles of RNA Based Regulation) and the Max Planck Society. L.S.S. acknowledges support by ReALity (Resilience, Adaptation and Longevity), M³ODEL and Forschungsinitiative des Landes Rheinland-Pfalz, and D.D. acknowledges support by ReALity and the Gutenberg Forschungskolleg (GFK). Open access funding enabled and organized by ProjektDEAL.

Author contributions

Lara A Grujics da Silva: Investigation; Visualization; Methodology; Writing—original draft; Writing—review and editing. **Francesca Simonetti:** Investigation; Visualization; Methodology; Writing—review and editing. **Saskia Hutten:** Investigation; Visualization; Methodology; Writing—review and editing. **Henrick Riemenschneider:** Investigation; Visualization; Methodology; Writing—review and editing. **Erin L Sternburg:** Investigation; Visualization; Methodology; Writing—review and editing. **Lisa M Pietrek:** Methodology. **Jakob Gebel:** Resources; Investigation; Methodology. **Volker Dötsch:** Resources. **Dieter Edbauer:** Resources; Supervision; Methodology; Writing—review and editing. **Gerhard Hummer:** Resources; Methodology; Writing—review and editing. **Lukas D Stelzl:** Investigation; Visualization; Methodology; Writing—original draft; Writing—review and editing. **Dorothee Dormann:** Conceptualization; Supervision; Funding acquisition; Writing—original draft; Writing—review and editing.

In addition to the CRediT author contributions listed above, the contributions in detail are:

Conceptualization: DD, LAGS; Methodology: all authors; Investigation: LAGS, FS, SH, HR, ELS, LMP, JG, LSS; Resources: DD, GH, LSS, DE, VD; Writing—original draft: DD, LAGS; Writing—review and editing: all authors; Visualization: LAGS, FS, SH, HR, ELS, JG, LSS; Supervision: DD, GH, DE, VD, LSS; Project administration: DD; Funding acquisition: DD, DE, GH, LSS, VD.

Disclosure and competing interests statement

The authors declare that they have no conflict of interest.

References

Abraham MJ, Murtola T, Schulz R, Páll S, Smith JC, Hess B, Lindahl E (2015) GROMACS: high performance molecular simulations through multi-level parallelism from laptops to supercomputers. *SoftwareX* 1–2: 19–25

- Afroz T, Hock E-M, Ernst P, Foglieni C, Jambeau M, Gilhespy LAB, Laferriere F, Maniecka Z, Plückthun A, Mittl P et al (2017) Functional and dynamic polymerization of the ALS-linked protein TDP-43 antagonizes its pathologic aggregation. *Nat Commun* 8: 45
- Alberti S (2017) Phase separation in biology. *Curr Biol* 27: R1097–R1102
- Alberti S, Dormann D (2019) Liquid-liquid phase separation in disease. *Annu Rev Genet* 53: 171–194
- Alberti S, Hyman AA (2021) Biomolecular condensates at the nexus of cellular stress, protein aggregation disease and ageing. *Nat Rev Mol Cell Biol* 22: 196–213
- Alquezar C, Arya S, Kao AW (2020) Tau post-translational modifications: dynamic transformers of tau function, degradation, and aggregation. *Front Neurol* 11: 595532
- Avendano-Vazquez SE, Dhir A, Bembich S, Buratti E, Proudfoot N, Baralle FE (2012) Autoregulation of TDP-43 mRNA levels involves interplay between transcription, splicing, and alternative polyA site selection. *Genes Dev* 26: 1679–1684
- Ayala YM, De Conti L, Avendaño-Vázquez SE, Dhir A, Romano M, D'Ambrogio A, Tollervey J, Ule J, Baralle M, Buratti E et al (2011) TDP-43 regulates its mRNA levels through a negative feedback loop. *EMBO J* 30: 277–288
- Babinchak WM, Haider R, Dumm BK, Sarkar P, Surewicz K, Choi JK, Surewicz WK (2019) The role of liquid-liquid phase separation in aggregation of the TDP-43 low-complexity domain. *J Biol Chem* 294: 6306–6317
- Bah A, Forman-Kay JD (2016) Modulation of intrinsically disordered protein function by post-translational modifications. *J Biol Chem* 291: 6696–6705
- Benayad Z, von Bulow S, Stelzl LS, Hummer G (2021) Simulation of FUS protein condensates with an adapted coarse-grained model. *J Chem Theory Comput* 17: 525–537
- Bolognesi B, Faure AJ, Seuma M, Schmiedel JM, Tartaglia GG, Lehner B (2019) The mutational landscape of a prion-like domain. *Nat Commun* 10: 4162
- Brady OA, Meng P, Zheng Y, Mao Y, Hu F (2011) Regulation of TDP-43 aggregation by phosphorylation and p62/SQSTM1. *J Neurochem* 116: 248–259
- Bremer A, Farag M, Borcherds WM, Peran I, Martin EW, Pappu RV, Mittag T (2021) Deciphering how naturally occurring sequence features impact the phase behaviors of disordered prion-like domains. *bioRxiv* <https://doi.org/10.1101/2021.01.01.425046> [PREPRINT]
- Buratti E (2015) Functional significance of TDP-43 mutations in disease. *Adv Genet* 91: 1–53
- Buratti E (2018) TDP-43 post-translational modifications in health and disease. *Expert Opin Ther Targets* 22: 279–293
- Bussi G, Donadio D, Parrinello M (2007) Canonical sampling through velocity rescaling. *J Chem Phys* 126: 014101
- Ceballos AV, McDonald CJ, Elbaum-Garfinkle S (2018) Methods and strategies to quantify phase separation of disordered proteins. *Methods Enzymol* 611: 31–50
- Choksi DK, Roy B, Chatterjee S, Yusuff T, Bakhoum MF, Sengupta U, Ambegaokar S, Kaye R, Jackson GR (2014) TDP-43 Phosphorylation by casein kinase Iε promotes oligomerization and enhances toxicity *in vivo*. *Hum Mol Genet* 23: 1025–1035
- Conicella AE, Zerze GH, Mittal J, Fawzi NL (2016) ALS mutations disrupt phase separation mediated by alpha-helical structure in the TDP-43 low-complexity C-terminal domain. *Structure* 24: 1537–1549
- Conicella AE, Dignon GL, Zerze GH, Schmidt HB, D'Ordine AM, Kim YC, Rohatgi R, Ayala YM, Mittal J, Fawzi NL (2020) TDP-43 alpha-helical structure tunes liquid-liquid phase separation and function. *Proc Natl Acad Sci USA* 117: 5883–5894
- Crabtree MD, Holland J, Kompella P, Babl L, Turner N, Baldwin AJ (2020) Repulsive electrostatic interactions modulate dense and dilute phase properties of biomolecular condensates. *bioRxiv* <https://doi.org/10.1101/2020.10.29.357863> [PREPRINT]
- Dignon GL, Zheng W, Kim YC, Best RB, Mittal J (2018) Sequence determinants of protein phase behavior from a coarse-grained model. *PLoS Comput Biol* 14: e1005941
- Dormann D, Capell A, Carlson AM, Shankaran SS, Rodde R, Neumann M, Kremmer E, Matsuwaki T, Yamanouchi K, Nishihara M et al (2009) Proteolytic processing of TAR DNA binding protein-43 by caspases produces C-terminal fragments with disease defining properties independent of progranulin. *J Neurochem* 110: 1082–1094
- Durocher D, Henckel J, Fersht AR, Jackson SP (1999) The FHA domain is a modular phosphopeptide recognition motif. *Mol Cell* 4: 387–394
- Ederle H, Funk C, Abou-Ajram C, Hutten S, Funk EBE, Kehlenbach RH, Bailer SM, Dormann D (2018) Nuclear egress of TDP-43 and FUS occurs independently of Exportin-1/CRM1. *Sci Rep* 8: 7084
- Fiesel FC, Weber SS, Supper J, Zell A, Kahle PJ (2012) TDP-43 regulates global translational yield by splicing of exon junction complex component SKAR. *Nucleic Acids Res* 40: 2668–2682
- French RL, Grese ZR, Aligireddy H, Dhavale DD, Reeb AN, Kedia N, Kotzbauer PT, Bieschke J, Ayala YM (2019) Detection of TAR DNA-binding protein 43 (TDP-43) oligomers as initial intermediate species during aggregate formation. *J Biol Chem* 294: 6696–6709
- Gasset-Rosa F, Lu S, Yu H, Chen C, Melamed Z, Guo L, Shorter J, Da Cruz S, Cleveland DW (2019) Cytoplasmic TDP-43 de-mixing independent of stress granules drives inhibition of nuclear import, loss of nuclear TDP-43, and cell death. *Neuron* 102: 339–357.e7
- Gowers RJ, Linke M, Barnoud J, Reddy TJE, Melo MN, Seyler SL, Domański J, Dotson DL, Buchoux S, Kenney IM et al (2016) MDAnalysis: a python package for the rapid analysis of molecular dynamics simulations. In *Proceedings of the 15th Python in Science Conference*, pp 98–105. Austin, TX: SciPy 2016
- Guo Q, Lehmer C, Martínez-Sánchez A, Rudack T, Beck F, Hartmann H, Pérez-Berlanga M, Frottin F, Hipp MS, Hartl FU et al (2018) *In situ* structure of neuronal C9orf72 Poly-GA aggregates reveals proteasome recruitment. *Cell* 172: 696–705.e12
- Haj-Yahya M, Gopinath P, Rajasekhar K, Mirbaha H, Diamond MI, Lashuel HA (2020) Site-specific hyperphosphorylation inhibits, rather than promotes, tau fibrillization, seeding capacity, and its microtubule binding. *Angew Chem Int Ed Engl* 59: 4059–4067
- Halfmann R, Lindquist S (2008) Screening for amyloid aggregation by semi-denaturing detergent-agarose gel electrophoresis. *J Vis Exp* <https://doi.org/10.3791/838>
- Hasegawa M, Arai T, Nonaka T, Kametani F, Yoshida M, Hashizume Y, Beach TG, Buratti E, Baralle F, Morita M et al (2008) Phosphorylated TDP-43 in frontotemporal lobar degeneration and amyotrophic lateral sclerosis. *Ann Neurol* 64: 60–70
- Hofweber M, Dormann D (2019) Friend or foe-Post-translational modifications as regulators of phase separation and RNP granule dynamics. *J Biol Chem* 294: 7137–7150
- Hutten S, Dormann D (2020) A quantitative assay to measure stress granule association of proteins and peptides in semi-permeabilized human cells. *Bio-protocol* 10: e3846
- Hutten S, Usluer S, Bourgeois B, Simonetti F, Odeh HM, Fare CM, Czuppa M, Hruska-Plochan M, Hofweber M, Polymenidou M et al (2020) Nuclear import receptors directly bind to arginine-rich dipeptide repeat proteins and suppress their pathological interactions. *Cell Rep* 33: 108538
- Inukai Y, Nonaka T, Arai T, Yoshida M, Hashizume Y, Beach TG, Buratti E, Baralle FE, Akiyama H, Hisanaga S-I et al (2008) Abnormal

- phosphorylation of Ser409/410 of TDP-43 in FTLD-U and ALS. *FEBS Lett* 582: 2899–2904
- Josephs KA, Whitwell JL, Weigand SD, Murray ME, Tosakulwong N, Liesinger AM, Petrucelli L, Senjem ML, Knopman DS, Boeve BF et al (2014) TDP-43 is a key player in the clinical features associated with Alzheimer's disease. *Acta Neuropathol* 127: 811–824
- Kametani F, Nonaka T, Suzuki T, Arai T, Dohmae N, Akiyama H, Hasegawa M (2009) Identification of casein kinase-1 phosphorylation sites on TDP-43. *Biochem Biophys Res Commun* 382: 405–409
- Kametani F, Obi T, Shishido T, Akatsu H, Murayama S, Saito Y, Yoshida M, Hasegawa M (2016) Mass spectrometric analysis of accumulated TDP-43 in amyotrophic lateral sclerosis brains. *Sci Rep* 6: 23281
- Lancaster AK, Nutter-Upham A, Lindquist S, King OD (2014) PLAAC: a web and command-line application to identify proteins with prion-like amino acid composition. *Bioinformatics* 30: 2501–2502
- Larsen AH, Wang Y, Bottaro S, Grudin S, Arleth L, Lindorff-Larsen K (2020) Combining molecular dynamics simulations with small-angle X-ray and neutron scattering data to study multi-domain proteins in solution. *PLoS Comput Biol* 16: e1007870
- Laurents DV, Stuani C, Pantoja-Uceda D, Buratti E, Mompean M (2021) Aromatic and aliphatic residues of the disordered region of TDP-43 are on a fast track for self-assembly. *Biochem Biophys Res Commun* 578: 110–114
- Li HR, Chiang WC, Chou PC, Wang WJ, Huang JR (2018) TAR DNA-binding protein 43 (TDP-43) liquid-liquid phase separation is mediated by just a few aromatic residues. *J Biol Chem* 293: 6090–6098
- Li HY, Yeh PA, Chiu HC, Tang CY, Tu BP (2011) Hyperphosphorylation as a defense mechanism to reduce TDP-43 aggregation. *PLoS One* 6: e23075
- Li Q, Babinchak WM, Surewicz WK (2021) Cryo-EM structure of amyloid fibrils formed by the entire low complexity domain of TDP-43. *Nat Commun* 12: 1620
- Liachko NF, McMillan PJ, Guthrie CR, Bird TD, Leverenz JB, Kraemer BC (2013) CDC7 inhibition blocks pathological TDP-43 phosphorylation and neurodegeneration. *Ann Neurol* 74: 39–52
- Liachko NF, McMillan PJ, Strovass TJ, Loomis E, Greenup L, Murrell JR, Ghetti B, Raskind MA, Montine TJ, Bird TD et al (2014) The tau tubulin kinases TTBK1/2 promote accumulation of pathological TDP-43. *PLoS Genet* 10: e1004803
- Ling SC, Polymenidou M, Cleveland DW (2013) Converging mechanisms in ALS and FTD: disrupted RNA and protein homeostasis. *Neuron* 79: 416–438
- Mackenzie IR, Rademakers R, Neumann M (2010) TDP-43 and FUS in amyotrophic lateral sclerosis and frontotemporal dementia. *Lancet Neurol* 9: 995–1007
- Marrink SJ, Risselada HJ, Yefimov S, Tieleman DP, de Vries AH (2007) The MARTINI force field: coarse grained model for biomolecular simulations. *J Phys Chem B* 111: 7812–7824
- Martin I, Kim J, Lee B, Kang H, Xu J-C, Jia H, Stankowski J, Kim M-S, Zhong J, Kumar M et al (2014) Ribosomal protein s15 phosphorylation mediates LRRK2 neurodegeneration in Parkinson's disease. *Cell* 157: 472–485
- Martin EW, Holehouse AS, Peran I, Farag M, Incicco JJ, Bremer A, Grace CR, Soranno A, Pappu RV, Mittag T (2020) Valence and patterning of aromatic residues determine the phase behavior of prion-like domains. *Science* 367: 694–699
- Martin EW, Thomasen FE, Milkovic NM, Cuneo MJ, Grace CR, Nourse A, Lindorff-Larsen K, Mittag T (2021) Interplay of folded domains and the disordered low-complexity domain in mediating hnRNP1 phase separation. *Nucleic Acids Res* 49: 2931–2945
- Martinez-Gonzalez L, Rodriguez-Cueto C, Cabezedo D, Bartolome F, Andres-Benito P, Ferrer I, Gil C, Martin-Requero A, Fernandez-Ruiz J, Martinez A et al (2020) Motor neuron preservation and decrease of *in vivo* TDP-43 phosphorylation by protein CK-1delta kinase inhibitor treatment. *Sci Rep* 10: 4449
- May S, Hornburg D, Schludi MH, Arzberger T, Rentzsch K, Schwenk BM, Grässer FA, Mori K, Kremmer E, Banzhaf-Strathmann J et al (2014) C9orf72 FTLD/ALS-associated Gly-Ala dipeptide repeat proteins cause neuronal toxicity and Unc119 sequestration. *Acta Neuropathol* 128: 485–503
- McGibbon RT, Beauchamp KA, Harrigan MP, Klein C, Swails JM, Hernandez CX, Schwantes CR, Wang LP, Lane TJ, Pande VS (2015) MDTraj: a modern open library for the analysis of molecular dynamics trajectories. *Biophys J* 109: 1528–1532
- Michaud-Agrawal N, Denning EJ, Woolf TB, Beckstein O (2011) MDAAnalysis: a toolkit for the analysis of molecular dynamics simulations. *J Comput Chem* 32: 2319–2327
- Molliex A, Temirov J, Lee J, Coughlin M, Kanagaraj AP, Kim HJ, Mittag T, Taylor JP (2015) Phase separation by low complexity domains promotes stress granule assembly and drives pathological fibrillization. *Cell* 163: 123–133
- Monticelli L, Kandasamy SK, Periole X, Larson RG, Tieleman DP, Marrink SJ (2008) The MARTINI coarse-grained force field: extension to proteins. *J Chem Theory Comput* 4: 819–834
- Morris M, Knudsen GM, Maeda S, Trinidad JC, Ioanoviciu A, Burlingame AL, Mucke L (2015) Tau post-translational modifications in wild-type and human amyloid precursor protein transgenic mice. *Nat Neurosci* 18: 1183–1189
- Nedelsky NB, Taylor JP (2019) Bridging biophysics and neurology: aberrant phase transitions in neurodegenerative disease. *Nat Rev Neurol* 15: 272–286
- Neumann M, Sampathu DM, Kwong LK, Truax AC, Micsenyi MC, Chou TT, Bruce J, Schuck T, Grossman M, Clark CM et al (2006) Ubiquitinated TDP-43 in frontotemporal lobar degeneration and amyotrophic lateral sclerosis. *Science* 314: 130–133
- Neumann M, Kwong LK, Lee EB, Kremmer E, Flatley A, Xu Y, Forman MS, Troost D, Kretzschmar HA, Trojanowski JQ et al (2009) Phosphorylation of S409/410 of TDP-43 is a consistent feature in all sporadic and familial forms of TDP-43 proteinopathies. *Acta Neuropathol* 117: 137–149
- Nonaka T, Suzuki G, Tanaka Y, Kametani F, Hirai S, Okado H, Miyashita T, Saito M, Akiyama H, Masai H et al (2016) Phosphorylation of TAR DNA-binding protein of 43 kDa (TDP-43) by truncated casein kinase 1delta triggers mislocalization and accumulation of TDP-43. *J Biol Chem* 291: 5473–5483
- Parrinello M, Rahman A (1981) Polymorphic transitions in single crystals: a new molecular dynamics method. *J Appl Phys* 52: 7182–7190
- Patel A, Lee H, Jawerth L, Maharana S, Jahnel M, Hein M, Stoynov S, Mahamid J, Saha S, Franzmann T et al (2015) A liquid-to-solid phase transition of the ALS protein FUS accelerated by disease mutation. *Cell* 162: 1066–1077
- Perdikari TM, Jovic N, Dignon GL, Kim YC, Fawzi NL, Mittal J (2021) A predictive coarse-grained model for position-specific effects of post-translational modifications. *Biophys J* 120: 1187–1197
- Piana S, Donchev AG, Robustelli P, Shaw DE (2015) Water dispersion interactions strongly influence simulated structural properties of disordered protein states. *J Phys Chem B* 119: 5113–5123
- Pietrek LM, Stelzl LS, Hummer G (2020) Hierarchical ensembles of intrinsically disordered proteins at atomic resolution in molecular dynamics simulations. *J Chem Theory Comput* 16: 725–737
- Ratti A, Buratti E (2016) Physiological functions and pathobiology of TDP-43 and FUS/TLS proteins. *J Neurochem* 138(Suppl 1): 95–111
- Regy RM, Dignon GL, Zheng W, Kim YC, Mittal J (2020) Sequence dependent phase separation of protein-polynucleotide mixtures elucidated using molecular simulations. *Nucleic Acids Res* 48: 12593–12603

- Robustelli P, Piana S, Shaw DE (2018) Developing a molecular dynamics force field for both folded and disordered protein states. *Proc Natl Acad Sci USA* 115: E4758–E4766
- Salado IG, Redondo M, Bello ML, Perez C, Liachko NF, Kraemer BC, Miguel L, Lecourtois M, Gil C, Martinez A et al (2014) Protein kinase CK-1 inhibitors as new potential drugs for amyotrophic lateral sclerosis. *J Med Chem* 57: 2755–2772
- Schmidt HB, Barreau A, Rohatgi R (2019) Phase separation-deficient TDP43 remains functional in splicing. *Nat Commun* 10: 4890
- Serber Z, Ferrell Jr JE (2007) Tuning bulk electrostatics to regulate protein function. *Cell* 128: 441–444
- Strickfaden SC, Winters MJ, Ben-Ari G, Lamson RE, Tyers M, Pryciak PM (2007) A mechanism for cell-cycle regulation of MAP kinase signaling in a yeast differentiation pathway. *Cell* 128: 519–531
- Taylor LM, McMillan PJ, Liachko NF, Strovast TJ, Ghetti B, Bird TD, Keene CD, Kraemer BC (2018) Pathological phosphorylation of tau and TDP-43 by TTBK1 and TTBK2 drives neurodegeneration. *Mol Neurodegener* 13: 7
- Tesei G, Schulze TK, Crehuet R, Lindorff-Larsen K (2021) Accurate model of liquid-liquid phase behaviour of intrinsically-disordered proteins from optimization of single-chain properties. *bioRxiv* <https://doi.org/10.1101/2021.06.23.449550> [PREPRINT]
- Tollervey JR, Curk T, Rogelj B, Briese M, Cereda M, Kayikci M, König J, Hortobágyi T, Nishimura AL, Župunski V et al (2011) Characterizing the RNA targets and position-dependent splicing regulation by TDP-43. *Nat Neurosci* 14: 452–458
- Tziortzouda P, Van Den Bosch L, Hirth F (2021) Triad of TDP43 control in neurodegeneration: autoregulation, localization and aggregation. *Nat Rev Neurosci* 22: 197–208
- Wang A, Conicella AE, Schmidt HB, Martin EW, Rhoads SN, Reeb AN, Nourse A, Ramirez Montero D, Ryan VH, Rohatgi R et al (2018) A single N-terminal phosphomimic disrupts TDP-43 polymerization, phase separation, and RNA splicing. *EMBO J* 37: e97452
- Wang C, Duan Y, Duan G, Wang Q, Zhang K, Deng X, Qian B, Gu J, Ma Z, Zhang S et al (2020) Stress induces dynamic, cytotoxicity-antagonizing TDP-43 nuclear bodies via paraspeckle LncRNA NEAT1-mediated liquid-liquid phase separation. *Mol Cell* 79: 443–458.e7
- Yaffe MB, Rittinger K, Volinia S, Caron PR, Aitken A, Leffers H, Gambin SJ, Smerdon SJ, Cantley LC (1997) The structural basis for 14-3-3: phosphopeptide binding specificity. *Cell* 91: 961–971
- Zhang P, Fan B, Yang P, Temirov J, Messing J, Kim HJ, Taylor JP (2019) Chronic optogenetic induction of stress granules is cytotoxic and reveals the evolution of ALS-FTD pathology. *Elife* 8: e39578



License: This is an open access article under the terms of the Creative Commons Attribution License, which permits use, distribution and reproduction in any medium, provided the original work is properly cited.

4 PUBLICATION II

Targeting the glycine-rich domain of TDP-43 with antibodies prevents its aggregation *in vitro* and reduces neurofilament levels *in vivo*

Published in Acta Neuropathologica Communications, 2023 as

Henrick Riemenschneider, **Francesca Simonetti**, Udit Sheth, Eszter Katona, Stefan Roth, Saskia Hutten, Daniel Farny, Meike Michaelson, Brigitte Nuscher, Michael K. Schmidt, Andrew Flatley, Aloys Schepers, Lara A. Gruijs da Silva, Qihui Zhou, Thomas Klopstock, Arthur Liesz, Thomas Arzberger, Jochen Herms, Regina Feederle, Tania F. Gendron, Dorothee Dormann and Dieter Edbauer

4.1 Aim of the project

The aim of this project is to identify safe and effective epitopes of the RNA-binding protein TDP-43 for the development of active and passive immunotherapy for ALS and FTL. These neurodegenerative diseases are characterized by the cytoplasmic aggregation and nuclear clearance of TDP-43, yet no disease-modifying therapy is currently available. By prescreening peptide antigens across all regions of TDP-43, the project seeks to identify the most immunogenic peptides and raise monoclonal antibodies that can mitigate disease progression *in vivo*, and prevent TDP-43 aggregation *in vitro*. The ultimate goal is to explore therapeutic strategies that inhibit key disease processes and advance potential immunotherapies for TDP-43-related proteinopathies.

RESEARCH

Open Access



Targeting the glycine-rich domain of TDP-43 with antibodies prevents its aggregation in vitro and reduces neurofilament levels in vivo

Henrick Riemenschneider^{1,2}, Francesca Simonetti^{1,3,5†}, Udit Sheth^{6,7†}, Eszter Katona^{1,3†}, Stefan Roth⁴, Saskia Hutten⁵, Daniel Farny¹, Meike Michaelson¹, Brigitte Nuscher⁸, Michael K. Schmidt⁹, Andrew Flatley¹⁰, Aloys Schepers¹⁰, Lara A. Gruijs da Silva^{3,5}, Qihui Zhou¹, Thomas Klopstock^{1,2,11}, Arthur Liesz^{2,4}, Thomas Arzberger^{1,9,12}, Jochen Herms^{1,2,9}, Regina Feederle^{1,2,10}, Tania F. Gendron^{6,7}, Dorothee Dormann^{5,13} and Dieter Edbauer^{1,2,3*} 

Abstract Cytoplasmic aggregation and concomitant nuclear clearance of the RNA-binding protein TDP-43 are found in ~90% of cases of amyotrophic lateral sclerosis and ~45% of patients living with frontotemporal lobar degeneration, but no disease-modifying therapy is available. Antibody therapy targeting other aggregating proteins associated with neurodegenerative disorders has shown beneficial effects in animal models and clinical trials. The most effective epitopes for safe antibody therapy targeting TDP-43 are unknown. Here, we identified safe and effective epitopes in TDP-43 for active and potential future passive immunotherapy. We prescreened 15 peptide antigens covering all regions of TDP-43 to identify the most immunogenic epitopes and to raise novel monoclonal antibodies in wild-type mice. Most peptides induced a considerable antibody response and no antigen triggered obvious side effects. Thus, we immunized mice with rapidly progressing TDP-43 proteinopathy (“rNLS8” model) with the nine most immunogenic peptides in five pools prior to TDP-43ΔNLS transgene induction. Strikingly, combined administration of two N-terminal peptides induced genetic background-specific sudden lethality in several mice and was therefore discontinued. Despite a strong antibody response, no TDP-43 peptide prevented the rapid body weight loss or reduced phospho-TDP-43 levels as well as the profound astrogliosis and microgliosis in rNLS8 mice. However, immunization with a C-terminal peptide containing the disease-associated phospho-serines 409/410 significantly lowered serum neurofilament light chain levels, indicative of reduced neuroaxonal damage. Transcriptomic profiling showed a pronounced neuroinflammatory signature (IL-1β, TNF-α, NfκB) in rNLS8 mice and suggested modest benefits of immunization targeting the glycine-rich region. Several novel monoclonal antibodies targeting the glycine-rich domain potently reduced phase separation and aggregation of TDP-43 in vitro and prevented cellular uptake of preformed aggregates. Our unbiased screen suggests that targeting the RRM2 domain and the C-terminal region of TDP-43 by active or passive immunization may be beneficial in TDP-43 proteinopathies by inhibiting cardinal processes of disease progression.

†Francesca Simonetti, Udit Sheth, and Eszter Katona are equally contributing second authors.

*Correspondence:

Dieter Edbauer

dieter.edbauer@dzne.de

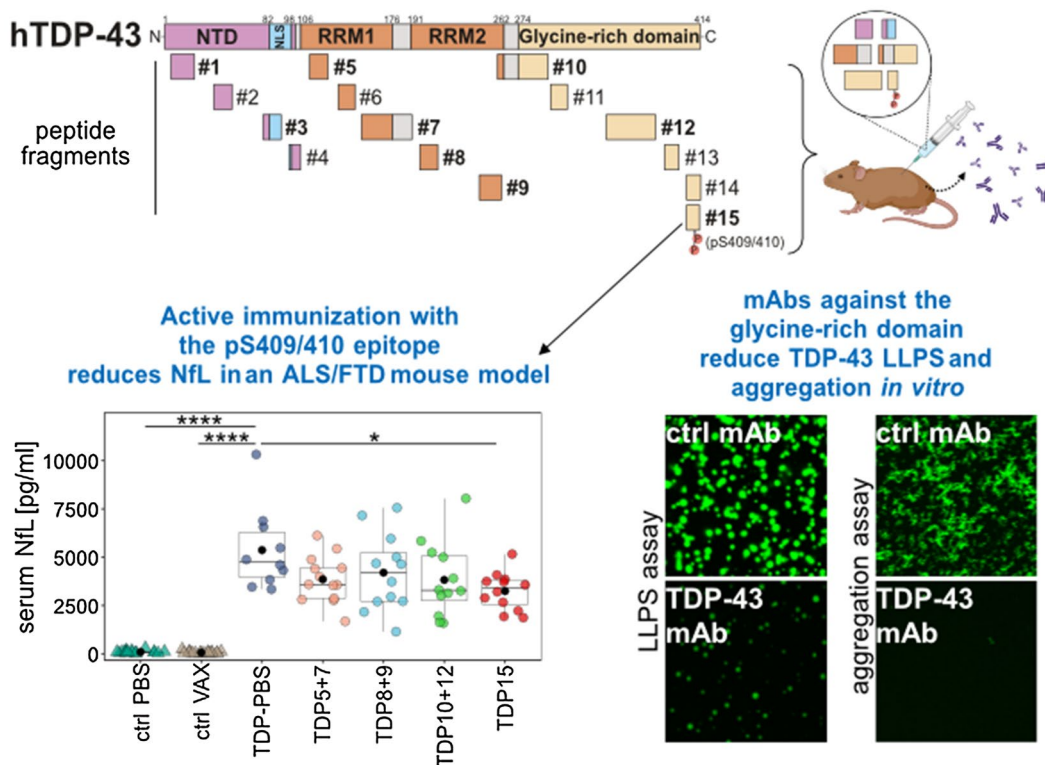
Full list of author information is available at the end of the article



Keywords Neurodegeneration, Amyotrophic lateral sclerosis, Frontotemporal dementia, TDP-43, Immunotherapy, Phase separation, Aggregation

Graphical Abstract

Targeting TDP-43's glycine-rich domain with antibodies ameliorates features of TDP-43 proteinopathy



Introduction

Amyotrophic lateral sclerosis (ALS) and frontotemporal lobar degeneration with TDP-43 inclusions (FTLD-TDP) are related, incurable neurodegenerative disorders with overlapping genetics and neuropathology. Most cases show neuronal and glial cytoplasmic inclusions of the multifunctional RNA-binding protein TDP-43 [30]. Normally, TDP-43 resides mostly in the nucleus where it regulates gene expression at multiple levels with a dominant role in mRNA splicing [46, 55]. TDP-43 inclusions show disease-specific posttranslational modifications, such as proteolytic processing into aggregation-prone 25–35 kDa C-terminal fragments, phosphorylation and ubiquitination [18, 37, 38]. In

contrast to nuclear TDP-43, cytoplasmic inclusions are hyperphosphorylated at serines 409/410 (pS409/410), but the pathophysiological role of C-terminal TDP-43 phosphorylation is still debated [16, 32]. The distribution of TDP-43 pathology strongly correlates with neuron loss in affected central nervous system (CNS) regions of ALS and FTLD-TDP cases, underpinning its key role in the pathophysiology of these diseases [29]. Most aggregate-bearing cells show striking clearance of nuclear TDP-43, suggesting that gain and loss of TDP-43 function pathomechanisms act in concert [27]. In mice, both knockout and overexpression of wild-type TDP-43 are lethal, raising concerns about the safety of TDP-43 targeted therapy [12, 59].

Over the past years, active and passive antibody approaches targeting different extracellular (A β) and intracellular (Tau, α -synuclein, poly-GA) aggregating proteins have emerged as promising options for the treatment of neurodegenerative diseases [34]. Despite limited permeability of the blood brain barrier for antibodies, A β -specific antibodies reduce amyloid load, and two such antibodies are now FDA-approved for the treatment of Alzheimer's disease, though their clinical utility is still debated. Ongoing antibody therapy approaches for intracellular aggregating proteins have been suggested to prevent their unconventional cell-to-cell transmission, thus inhibiting pathogenic spreading and promoting clearance by microglia or preventing toxic neuroinflammation [21, 63]. In addition, low level intracellular antibody uptake may accelerate proteasomal clearance of aggregates through recruitment of the intracellular Fc-receptor TRIM21 [33, 35].

For intracellular Tau aggregates, both passive antibody delivery and active vaccination are currently being tested in clinical trials [40]. We have used active vaccination to target the abundant poly-GA inclusions found in ALS and FTLT cases caused by *C9orf72* repeat expansions [63]. Immunization of presymptomatic mice expressing poly-GA with ovalbumin (OVA)-coupled (GA)₁₀ induced a strong anti-GA response, reduced poly-GA aggregation, prevented microgliosis, and improved motor deficits [63]. For TDP-43, the Julien lab has generated a monoclonal antibody directed against its RNA recognition motif 1 (RRM1) that reduced cytoplasmic TDP-43 levels as well as TDP-43/p65-mediated NF κ B activation in vitro. Intrathecal injection of this antibody ameliorated cytoplasmic TDP-43 mislocalization in the lumbar spinal cord, which was accompanied by microglial activation [44]. Expressing the same antibody in the brain as a single-chain variable fragment (scFv) using AAV also reduced TDP-43 proteinopathy, accompanying neuroinflammation, and behavioral abnormalities in BAC-transgenic TDP-43 mice [45]. Two other scFv antibodies directed against an epitope in the RRM2 domain were genetically engineered to promote TDP-43 aggregate clearance in cell lines and validated in mice using combined in utero electroporation of TDP-43 and scFv [53]. However, active vaccination targeting TDP-43 has not been reported, although this approach would be more convenient and cost-efficient in patients.

Given the importance of TDP-43-associated neurodegeneration in ALS and FTLT-TDP as well as the recent advances in immunotherapies for neurodegenerative disorders, we tested whether active vaccination would ameliorate TDP-43 pathophysiology in vivo. The choice of epitope for active and passive immunotherapy is challenging, because the domains driving gain-of-function

pathomechanisms are unclear and it is still debated whether TDP-43 inclusions are liquid-like, gel-like or amyloid-like [5, 13, 26, 49, 61]. To identify the best target epitopes in vivo, we screened peptide antigens covering all regions of TDP-43 for active immunization, and investigated their effects on TDP-43 phosphorylated at serines 409/410 (pTDP-43), transcriptional alterations, neuroinflammation, and neuroaxonal damage in an aggressive mouse model of TDP-43 proteinopathy. In addition, we raised and characterized a panel of monoclonal antibodies from the immunized mice. Altogether, we found active vaccination targeting the C-terminal low-complexity domain, in particular the C-terminal pS409/410 epitope, to have moderate beneficial effects in vivo, and monoclonal antibodies targeting the C-terminal low-complexity domain to potentially suppress phase separation, aggregation and aggregate uptake of TDP-43 in vitro, commending this region for future antibody-based therapeutic efforts.

Materials and methods

Mice and immunization regimen for active vaccination study

All animal procedures were performed according to institutional guidelines approved by the governmental ethics committee of Upper Bavaria (licenses TV 55.2-2532.Vet_02-17-106 and TV 55.2-2532.Vet_03-17-68). Mice were housed in standard IVC green line cages (Tecniplast, Italy) on a 12-h light/dark cycle in a pathogen-free facility and ad libitum access to food and water. The monogenic lines B6;C3-Tg(NEFH-tTA)8Vle/J (NEFH-tTA line 8, stock #025397) and B6;C3-Tg(tetO-TARDBP*)4Vle/J (tetO-hTDP-43 Δ NLS line 4, stock #014650) were obtained from the Jackson Laboratory (Bar Harbour, USA) and intercrossed to generate bigenic regulatable NLS8 (rNLS8) animals with a mixed C57BL/6J \times C3H/HeJ background. Breeders as well as offspring mice were kept on a doxycycline diet (200 mg/kg, Ssniff, Germany) during hTDP-43 Δ NLS suppression (until aged to 25.5 weeks). To induce hTDP-43 Δ NLS expression, animals were switched to standard chow lacking doxycycline (Ssniff, Germany). For genotyping, DNA was extracted from ear biopsies by the previously described HotSHOT method [54] and transgenes were detected by PCR using the primers recommended by Jackson Laboratory: NEFH-tTA forward 5'-CTCGCG CACCTGCTGAAT-3', NEFH-tTA reverse 5'-CAGTAC AGGGTAGGCTGCTC-3', tetO-TARDBP* forward 5'-TTGCGTGA CTCTTTAGTATTGGTTTGATGA-3', tetO-TARDBP* reverse 5'-CTCATCCATTGCTGCTGC G-3'. Littermates were grouped into indicated immunization cohorts in a randomized and gender-balanced fashion.

Immunization followed our previous protocol for poly-GA vaccination [63]. For the initial immunization of wild-type C57BL/6J mice, a total of 40 µg ovalbumin peptide conjugates (Peptide Specialty Laboratories GmbH, Germany) were mixed with 5 nmol CpG ODN 1668 oligonucleotide (IAX-200-001, Innaxon, UK) in 200 µl PBS and 250 µl Incomplete Freund’s adjuvant (IFA, Sigma, USA) and injected half-half

intraperitoneally (i.p.) and subcutaneously (s.c.) into 8-week-old animals. For the monthly booster immunizations, a total of 40 µg antigen was mixed with 5 nmol CpG ODN 1668 in 500 µl PBS and injected half-half i.p. and s.c. as depicted in Fig. 1B. rNLS8 immunization followed the same regimen (Fig. 1E), but using 250 µl Alhydrogel® adjuvant 2% (Invivogen, USA). The control groups (wild-type C57BL/6J): PBS; rNLS8: ctrl PBS and

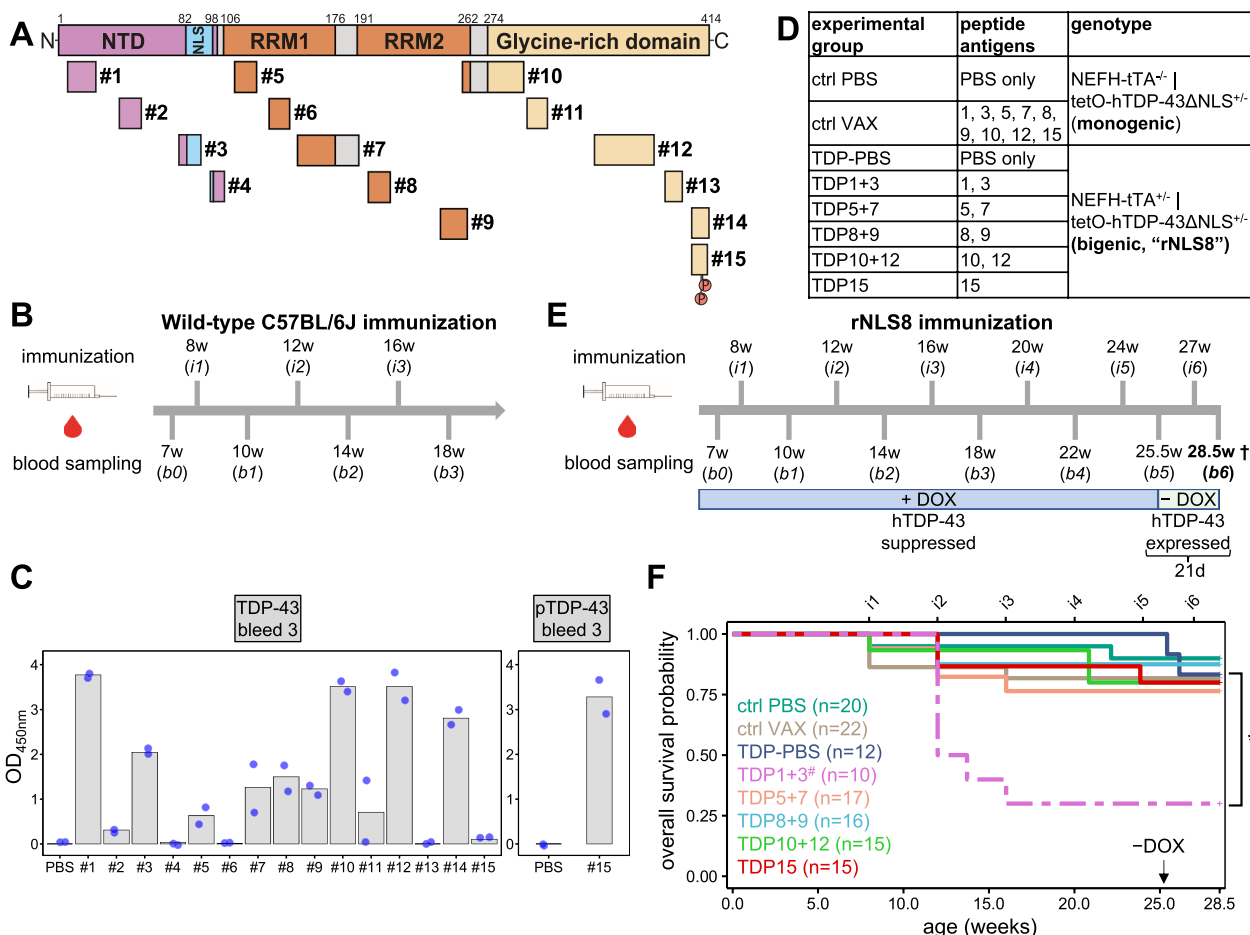


Fig. 1 Epitope scan of TDP-43 reveals differential immunogenicity and safety in mice. Active immunization with 15 different TDP-43 peptides in wild-type C57BL/6J to select the most immunogenic ones for therapeutic vaccination in rNLS8 mice. **A** Localization and relative size of peptides used for active immunization targeting human TDP-43. Peptide 15 contains pS409/410. NTD: N-terminal domain, NLS: Nuclear localization signal, RRM1/2: RNA recognition motif 1/2. **B** Immunization regimen for wild-type C57BL/6J mice (age in weeks). Two mice per peptide antigen were immunized monthly (i1-i3) with serum collected before and in between immunizations (b0-b3). **C** Antibody response towards human recombinant TDP-43 (left panel) or pTDP-43 peptide (pS409/410, right panel) was determined by ELISA after three immunizations. Background-corrected optical density at 450 nm (OD_{450nm}) was measured in duplicates for each animal (dots) with bars representing mean values. All sera were diluted 1:500. Preimmune serum is analyzed in Fig. S1B. **D** Experimental groups for therapeutic vaccination. rNLS8 animals expressing hTDP-43ΔNLS were immunized with either pooled antigens or PBS control. Monogenic littermates received either PBS (ctrl PBS) or a mixture of all peptides used for rNLS8 immunization (ctrl VAX). Peptides 1 and 3 were excluded from the control group after discovering side effects in the TDP1 + 3 group (Fig. 1F). **E** Timeline of immunization and blood sampling in rNLS8 and control mice. After the fifth blood sampling (b5), hTDP-43ΔNLS expression was induced by removing doxycycline (DOX) from the chow. All mice were sacrificed 21 days after transgene induction (28.5 weeks of age). **F** Kaplan–Meier plot showing survival probability of mice during study (humane endpoint). Number of animals at the beginning of the immunization regimen is indicated. Log-rank test and pairwise comparisons with Benjamini–Hochberg correction revealed a statistically significant higher mortality in TDP1 + 3 immunized compared to TDP-PBS control mice (*, $p = 0.039$). Note that immunization of surviving TDP1 + 3 mice was discontinued after 1, 2 or 3 immunizations (#, dashed line)

TDP-PBS) received PBS instead of the peptide conjugates. Immunizations in CD-1 (#022), C3H/HeOuj (#626) and C57BL/6J (#632, all three lines obtained from Charles River Laboratories, Sulzfeld, Germany) were carried out as described for rNLS8 mice (Additional file 1: Fig. S2A).

Serum collection and tissue harvesting

Monthly blood collection was carried out by puncture of the vena facialis using a Goldenrod animal lancet (Bio-Medical Instruments Trading, Germany). Blood clotted during 15 min incubation at room temperature (RT) and serum was obtained as the supernatant after centrifugation (13,000×g for 10 min at 4 °C). Three weeks after transgene induction, an overdosed combination of ketamine (450 mg/kg, Ketabel, belapharm, Germany) with xylazine (30 mg/kg, Xylazin, Serumwerk, Germany) was intraperitoneally injected into rNLS8 and control mice to ensure painless deep anesthesia without recovery, thereby allowing for transcatheter perfusion using ice-cold phosphate-buffered saline (DBPS, Gibco, USA). Collected tissue was either snap-frozen in liquid nitrogen and stored at -80 °C for subsequent biochemical analysis or formalin-fixed (ROTI[®]Histofix 4%, Roth, Germany) for 24 h for immunohistochemistry/immunofluorescence.

TDP-43 antibody ELISA

TDP-43 antibody titers in mouse sera and the binding affinities of purified monoclonal antibodies to TDP-43 were determined by ELISA. To this end, Nunc MaxiSorp[™] flat bottom 96-well plates were incubated with recombinant human TDP-43-MBP-His₆ or a pTDP-43 (pS409/410) peptide (biotinylated version of TDP peptide #15) in PBS overnight at 4 °C. The next day, plates were treated with blocking solution (1% BSA, 0.05% Tween 20 in PBS) for 1 h at RT. Subsequently, serum samples were prediluted in blocking solution as depicted in the figure legends and added for 1 h at RT. Following three washes with 0.05% Tween 20 in PBS, plates were incubated with anti-mouse secondary antibody (Promega, USA) for 1 h at RT. After three more washes, 3,3',5,5'-Tetramethylbenzidine (TMB, Sigma, USA) was used as chromogenic substrate and its reaction was stopped using 2 M H₂SO₄. The optical density at 450 nm (OD450) was measured using a Biotek Cytation 3 plate reader. Background signals were determined by using MBP-His₆ (for TDP-43-MBP-His₆) or PBS (for pTDP-43) as coating agents. Out-of-range signals were manually set to the detection maximum of 4. OD signals of two technical replicates per sample were background-corrected, averaged, and plotted.

Mesoscale discovery immunoassays for pTDP-43 and inflammatory markers

Levels of pTDP-43 and inflammatory markers were measured using the Mesoscale Discovery platform (USA). To generate brain lysates, approximately 50 mg of neocortex tissue from mice was homogenized in cold RIPA buffer (50 mM Tris-HCl pH 8.0, 150 mM NaCl, 5 mM EDTA, 0.5% sodium deoxycholate, 1% Nonidet P-40, 0.1% sodium dodecyl sulfate, and protease and phosphatase inhibitors) and sonicated on ice. Homogenates were centrifuged at 100,000×g for 30 min at 4 °C and the supernatant was collected as RIPA-soluble fraction. The RIPA-insoluble pellet was extracted using 7 M urea buffer (7 M urea, 2 M thiourea, 4% CHAPS, 30 mM Tris-HCl pH 8.5), agitated vigorously at RT for 30 min, and centrifuged at 100,000×g for 30 min at 22 °C. The protein concentrations of the RIPA-soluble and urea-soluble fractions were determined by bicinchoninic acid (BCA) and Bradford assay, respectively.

Levels of pTDP-43 were measured on a homebrew immunoassay performed as previously described [47]. The capture antibody was a mouse monoclonal antibody that detects TDP-43 phosphorylated at serines 409/410 (1:500, TIP-PTD-M01, Cosmo Bio, USA), and the detection antibody was a sulfo-tagged rabbit polyclonal C-terminal TDP-43 antibody (2 µg/ml, 12892-1-AP, Proteintech). Samples were diluted in TBS (Tris-buffered saline) to 35 µg protein per well and tested in duplicate wells. Both RIPA-soluble and RIPA-insoluble fractions were quantified. Response values corresponding to the intensity of emitted light upon electrochemical stimulation of the assay plate using the MSD QUICKPLEX SQ120 were acquired.

Pro-inflammatory markers and cytokine levels were quantified using V-PLEX Plus Mouse Cytokine 19-Plex Kit (K15255G-2, Mesoscale Discovery) according to the manufacturer's protocol using the RIPA-soluble fraction. 650 µg and 250 µg total protein were loaded per well on the pro-inflammatory and cytokine multiplex plate, respectively. Markers for which all measurements were below the detection range determined by the standard curve were neglected. For all other robustly working assays, concentration values below detection range were set to zero. Measurements with a CV of >20% were excluded.

HEK293 CRISPR interference (CRISPRi) *TARDBP* knockdown cells

HEK293 cells were a gift from Martin Dichgans (Institute for Stroke and Dementia Research, University Hospital, LMU Munich) and CRISPRi single cell clones were generated as described before [31]. In detail, HEK293 cells

were cultured in DMEM (Thermo Fisher, USA) supplemented with 10% tetracycline-free fetal bovine serum (Clontech, USA) and 1% Non-Essential Amino Acids (Thermo Fisher). Transgenic lines were generated by co-transfecting cells in a 1:1:2.5 ratio using the following constructs: hAAVS1 1L TALEN (addgene #35431), hAAVS1 1R TALEN (addgene #35432), and pAAVS1-NDi-CRISPRi (Gen1, addgene #73497). This allows integration of the Cas9 cassette under the human safe harbor locus AAVS1 and expression of the fusion protein [Krüppel-associated box (KRAB) repressor domain fused to deactivated Cas9 (dCas9) and a mCherry marker] in a doxycycline-inducible manner. To generate single-cell clones, transfected cells were seeded in serial dilutions under G418 (400 µg/ml) selection and cultured until colonies were visible. After expansion, only single cell clones that showed a uniform and efficient dCas9 induction with tight regulation were used in later experiments. Next, these clones were transfected with a gRNA expression plasmid targeting *TARDBP* (sgRNA sequence: 5'-CAG GGACACCGAAGCAGCGA-3') and clonally selected using Hygromycin (200 µg/ml). Doxycycline-dependent *TARDBP* knockdown was evaluated by immunoblotting and the most efficient clones were used further. For testing mouse antisera in immunoblotting, cells were grown in the absence or presence of 2 µM doxycycline for 72 h, washed with PBS, and lysed on ice in RIPA (137 mM NaCl, 20 mM Tris-HCl pH 7.5, 0.1% SDS, 10% glycerol, 1% Triton X-100, 0.5% deoxycholate, 2 mM EDTA) supplemented with Benzonase Nuclease (67 U/ml), protease inhibitor cocktail, and phosphatase inhibitor cocktail (all from Sigma, USA). Lysates were centrifuged (18,000×g for 30 min at 4 °C) and the protein concentration of the RIPA-soluble supernatant was determined using a BCA assay (Interchim, France). After adding 3×loading buffer (200 mM Tris-HCl pH 6.8, 6% SDS, 20% glycerol, 0.1 g/ml DTT, 0.1 mg Bromophenol Blue), samples were heat denatured at 95 °C for 10 min. Equivalent protein amounts were loaded on 10% SDS-PAGE gels and transferred to Nitrocellulose membranes (GE Healthcare, USA). Membranes were blocked in 5% milk powder and probed with a commercial anti-TDP-43 antibody (1:500, 10782-2-AP, Proteintech) or pooled antisera from five-times immunized mice (bleed 5). An anti-Calnexin antibody (1:7000, ADI-SPA-860, Enzo Life Sciences) was used to detect Calnexin as the loading control protein.

Automated immunohistochemistry (IHC) and immunofluorescence (IF) stainings, image quantification

Immunohistochemistry (chromogenic detection) and immunofluorescence (fluorescent detection) stainings of mouse brain tissue were performed on formalin-fixed,

paraffin-embedded (FFPE) sections of 5 µm thickness using automated staining systems with the following primary antibodies: pTDP-43 (pS409/410) (1:50, clone 1D3, Helmholtz Center Munich), TDP-43 (1:200, 10782-2-AP, Proteintech), Iba1 (1:250, 234308, SYSY), and GFAP (1:500, 173006, SYSY).

Immunohistochemical stainings of pTDP-43 (pS409/410) were performed on a Ventana BenchMark Ultra automated stainer using pretreatment with CC1 buffer and the ultraView Universal DAB Detection Kit (all from Roche). Nuclei were counterstained using hematoxylin. All steps followed standard manufacturer's instructions. Acquisition of bright-field images was performed on a Leica Dmi8 microscope equipped with a HC PL FLUOTAR L 20x/0.40 DRY objective and a DMC4500 camera (Leica Microsystems, Germany). All images were captured using the LAS X software (version 3.7) in tile-scan mode at a 1280×960 pixel resolution.

Immunofluorescence stainings for TDP-43, Iba1, and GFAP were performed on a DCS Delta.36 automated staining system using supplier reagents (DCS-Diagnostics, Germany). All steps were conducted at RT. After deparaffinization, the TR2 (low pH) buffer was used for antigen retrieval. Sections were then blocked and permeabilized using 2% fetal calf serum, 3% goat serum, and 0.2% Triton X-100 in PBS. Next, primary antibodies were added for 1.5 h, followed by an 1 h incubation step with host-specific secondary antibodies (each 1:250, goat anti-rabbit Alexa 488, goat anti-guinea pig Alexa 555, goat anti-chicken Alexa 647; all from Thermo Fisher). Afterwards, nuclei were counterstained using DAPI (1:5000 in PBS, 15 min) and sections were mounted with Vectashield Vibrance (VEC-H-1700, Biozol, Germany). Stained sections were imaged on a PANNORAMIC "MIDI II" Digital Slide Scanner (3DHitech, Hungary) equipped with a 20×objective and the Panoramic Slide Scanner software (version 2.0.5). To quantify Iba1 and GFAP signals automatically, a customized ImageJ/Fiji (version 1.53t) script to detect cell soma was used. In brief, images were background-subtracted (rolling ball method, radius 50 pixels) and despeckled (median filter) first. Next, Morphological Filters and Gray Scale Attribute Filtering (both from the MorphoLibJ plugin, version 1.6.0) were applied, followed by auto thresholding (Iba1: IJ_IsoData; GFAP: auto local threshold, Phansalkar method). Cell soma were then counted using the "Analyze Particles" function (size Iba1: 15–150 pixels²; size GFAP: 50–200 pixels²). Afterwards, cell counts were normalized to the hippocampal area analyzed.

Images of TDP-43 (human+mouse) stained sections were acquired on an inverted LSM710 Axio Observer. Z1 confocal laser scanning microscope equipped with a Plan-Apochromat 40x/1.40 Oil DIC M27 objective and

a PMT detector. Images were taken at 2048×2048 pixel resolution in z-stack mode (step size 0.42 μm) using the ZEN 2011 software (black edition, Carl Zeiss, Germany). For each animal investigated, three fields of view in the frontal cortex area were acquired. Using CellPose (version 2.2) [41, 52], nuclear (based on DAPI staining) and pan-TDP-43 (based on TDP-43 staining) signals were segmented (cyto2 model, cell diameter=100 pixels, flow threshold=0.4). Z-series were projected into two dimensions using Image J's sum slices method. Based on the outlines obtained from CellPose segmentation, nuclear and cytoplasmic (non-nuclear) TDP-43 intensities were measured, and their ratio was calculated. Ratios of the three fields of view were averaged and plotted as depicted in Fig. 4C.

Patient tissue, immunofluorescence

Patient brain sections for immunofluorescence stainings were provided by the Neurobiobank Munich and Ludwig-Maximilians-University (LMU) Munich. Their usage was reviewed and approved by the ethical committee at LMU Munich. For immunofluorescence staining, 5 μm-thick formalin-fixed and paraffin-embedded sections from the Gyrus frontalis medius region were deparaffinized and rehydrated using a standard xylene/ethanol gradient. Heat-mediated antigen retrieval was performed for 30 min in citrate buffer pH 6.0 using a boiling steamer. Next, sections were treated with blocking buffer (2% fetal calf serum, 3% goat serum, 0.2% Triton X-100 in PBS) and incubated for 1 h at RT with either a commercially available primary antibody (pTDP-43 (pS409/410), 80007-1-RR, 1:500 or TDP-43, 10782-2-AP, 1:350, both from Proteintech), pooled blood sera from five-times immunized mice (bleed 5) or the purified TDP-43 monoclonal antibodies, each diluted in blocking solution (0.2% fetal calf serum, 0.2% bovine serum albumin, 0.02% fish gelatine in PBS). Subsequently, tissues were incubated with goat anti-mouse Alexa 488- and goat anti-rabbit Alexa 555-coupled secondary antibodies (each 1:400, both from Thermo Fisher) for 1 h at RT. After each incubation step, three washes with 0.05% Tween 20 in PBS were performed. DAPI was used to counterstain nuclei (1:5000 in PBS, 10 min, RT) and sections were briefly incubated with Sudan black solution to reduce autofluorescence. Lastly, tissue sections were mounted using Vectashield Vibrance (VEC-H-1700, Biozol, Germany) and imaged with an inverted LSM710 Axio Observer. Z1 confocal laser scanning microscope equipped with a Plan-Apochromat 63x/1.40 Oil DIC M27 objective and a PMT detector. Images were acquired at 2048×2048 pixel resolution with unidirectional scanning using two-fold frame averaging and the ZEN 2011 software (black edition, Carl Zeiss, Germany).

Neurofilament light chain (NfL) measurement

Neurofilament light chain (NfL) levels in blood sera were quantified using the Simoa NF-light Advantage Kit (103186, Quanterix, USA). Sera were diluted 1:40 (v/v) in sample dilution buffer and measured on a Simoa HD-1 Analyzer (Quanterix) following manufacturer's instructions. NfL serum concentration was interpolated from standard curves and mean values from duplicate measurements were plotted.

Transcriptomics

RNA from approximately 30 mg of mouse neocortical tissue was isolated using Direct-zol RNA Microprep (R2062, Zymo Research, Germany) according to manufacturer's instructions. Transcriptome analysis was performed at BGI (China). After cDNA library preparation, 100 bp pair-ended sequencing was performed on a DNBSEQ platform with a depth of ~20 million read pairs per sample. Data were aligned to the mouse genome (GRCm38.p6) and differential gene expression was analyzed using DESeq2 [28]. Gene ontology analysis was performed using clusterProfiler [60]. Meaningful and highly significantly enriched GO categories were manually selected and depicted in Fig. 6C. The full expression data is presented in Additional file 2: Table S1.

Monoclonal antibody generation from immunized Balb/c and C57BL/6J mice

Balb/c mice were immunized with 40 μg of OVA-coupled TDP-43 peptide #7 (aa. 153–191) together with 5 nmol CpG (TIB MOLBIOL, Germany) in 200 μl PBS and an equal volume of Incomplete Freund's adjuvant (IFA; Sigma, USA). Booster injections without IFA were given 8 and 13 weeks later. C57BL/6J mice from the pilot immunization cohort (Fig. 1B/C) were treated as described before but received an additional booster injection before splenectomy. Immune spleen cells from immunized Balb/c and C57BL/6J mice vaccinated with other epitopes (see Additional file 1: Fig. S1A) were collected three days (Balb/c mice) or seven days (C57BL/6J) after the final boost for fusion with P3X63Ag8.653 myeloma cells using standard procedures. Hybridoma supernatants were screened 10 days later in a flow cytometry assay (iQue, Intellicyt, Sartorius, Germany). Briefly, recombinant TDP-43-MBP-His₆ fusion protein was captured to 3D-Aldehyde beads (PolyAN, Germany) and incubated for 90 min with hybridoma supernatant and Atto 488-coupled isotype-specific monoclonal rat anti-mouse IgG secondary antibodies. Antibody binding was analyzed using ForeCyt software (Sartorius, Germany). Clones were further validated and selected for up-scaling by sandwich ELISA. Briefly, Nunc MaxiSorp™ flat bottom 96-well plates were coated with either N-terminal

(10782-2-AP, Proteintech) or C-terminal (12892-1-AP, Proteintech) binding TDP-43 antibody overnight at 4 °C. The next day, recombinant TDP-43-MBP-His₆ was added in serial dilution for 2 h at RT, followed by a 2 h incubation with the hybridoma supernatants at RT. As a secondary antibody, the respective HRP-conjugated isotype-specific mouse IgG antibody (Helmholtz Center Munich) was added for 1 h at RT. Between each step, plates were washed three times with PBS supplemented with 0.05% Tween 20. Plates were measured as described before (see TDP-43 antibody ELISA) and supernatants with the best signal-to-noise ratio with both N-terminal and C-terminal TDP-43 capture antibodies were selected. Hybridoma cells from selected supernatants were sub-cloned at least twice by limiting dilution to obtain stable monoclonal cell lines (see Additional file 1: Fig. S1A).

Recombinant protein expression and purification

TDP-43-MBP-His6

Human TDP-43-MBP-His₆ was purified as described before [16] from plasmid pJ4M TDP-43-TEV-MBP-His₆ (addgene #104480) [57]. Briefly, protein expression was performed in *E. coli* BL21-DE3 Rosetta 2 induced with 0.5 mM IPTG and grown overnight at 16 °C. Bacteria were resuspended in lysis buffer (20 mM Tris pH 8.0, 1 M NaCl, 10 mM imidazole, 10% glycerol, 4 mM β-mercaptoethanol and 1 μg/ml each of aprotinin, leupeptin hemisulfate, and pepstatin A) supplemented with 0.1 mg/ml RNase A and lysed using lysozyme and sonication. Next, the protein was purified by Ni-NTA agarose (Qiagen) and eluted with lysis buffer containing 300 mM imidazole. To separate monomeric TDP-43-MBP-His₆ from protein aggregates and contaminants, a final size exclusion chromatography (SEC) (Hiload 16/600 Superdex 200 pg, GE Healthcare) purification step was performed in purification buffer (20 mM Tris pH 8.0, 300 mM NaCl, 5% glycerol supplemented with 2 mM TCEP). The purified protein was concentrated using Amicon ultra centrifugal filters, then flash frozen, and stored at -80 °C. To determine protein concentration, absorbance at 280 nm was measured using the respective extinction coefficient (ε) predicted by the ProtParam tool. Moreover, the A₂₆₀/280 ratio was determined and found to be between 0.5–0.7. Prior to use in any downstream assays assessing phase separation, TDP-43-MBP-His₆ aliquots were centrifuged (21,000 × g for 10 min at 4 °C) to remove preexisting protein precipitates.

His6-TEV protease

His₆-TEV protease expression and purification was performed as described in [20].

Fluorescent labeling of purified TDP-43 and monoclonal antibodies

TDP-43-MBP-His₆ was labeled with Alexa Fluor 488 C5 maleimide (Thermo Fisher) and monoclonal TDP-43 antibodies were conjugated with DyLight™ 650 NHS Ester (Thermo Fisher), both at a low (~0.01–0.05) labelling efficiency to not interfere with condensate formation. Following manufacturer's instructions, TDP-43-MBP-His₆ was mixed with the Alexa Fluor reagent in a 100:1 or 20:1 protein:fluorescent dye molar ratio and kept in the dark for 2 h at RT. Monoclonal antibodies and DyLight dye were used in a 50:1 protein:fluorescent dye molar ratio and incubated for 1 h at RT protected from light. Excess dye was removed by consecutive washes with TDP-43 purification buffer (TDP-43-MBP-His₆) or PBS (monoclonal antibodies) using Amicon ultra centrifugal filters (Merck, Germany) and protein concentrations were determined. Labeled proteins were used for confocal microscopy, aggregation, and phase separation assays, respectively. For flow-cytometry based uptake assays, TDP-43-MBP-His₆ was labeled with pHrodo™ iFL Green STP Ester (Thermo Fisher) at a labeling efficiency of ~0.7–1.0. The labeling procedure was carried out as described above with a protein:fluorescent dye molar ratio of 1:1 and an incubation step of 1 h.

In vitro aggregation and phase separation assays

Aggregation assay

In 1.5 ml low binding tubes (Eppendorf), 8 μM Alexa 488-labeled TDP-43-MBP-His₆ was mixed with 4 μM unlabeled monoclonal antibody (isotype controls or TDP-43 antibodies, respectively) in aggregation buffer (50 mM Tris pH 8.0, 150 mM NaCl, 5% glycerol, 5% sucrose, 150 mM imidazole pH 8.0) supplemented with 1 × protease inhibitor (Sigma) and incubated with 100 μg/ml His₆-TEV protease. Samples were constantly agitated at 1000 rpm for 30 min at RT and subsequently transferred into a 384-well imaging plate (781900, Greiner Bio-One, Germany), which was tightly sealed to avoid any evaporation. Samples were incubated for 48 h at RT and imaged using a LSM710 confocal microscope with a Plan-Apochromat 10x/0.45 M27 objective. Image acquisition was performed with a two-line averaging and at a pixel resolution of 1024 × 1024 (Carl Zeiss).

Sedimentation assay

1 μM TDP-43-MBP-His₆ was mixed with 0.5 μM unlabeled monoclonal antibody (isotype controls or TDP-43 antibodies, respectively) in Hepes buffer (20 mM Hepes pH 7.5, 150 mM NaCl, 1 mM DTT). To remove the MBP-His₆ solubilization tag and trigger liquid–liquid phase separation (LLPS), 20 μg/ml His₆-TEV protease

was added. The resulting condensates were pelleted by centrifugation ($21,000\times g$ for 15 min at 4 °C) after 2 h of incubation at 30 °C. Afterwards, equal amounts of supernatant (S) and condensate (C) fractions were loaded onto 10% SDS-PAGE gels, transferred to Nitrocellulose membranes and TDP-43 was detected by immunoblotting using an extreme C-terminal anti-TDP-43 antibody (epitope aa. 405–414, TIP-TD-P09, Cosmo Bio, USA). Quantification of the chemiluminescence signals in each lane was performed using an Amersham ImageQuant™ 800 imaging system (Cytiva, USA) and GelAnalyzer software (version 19.1). Ratios of the supernatant (S) and the total [supernatant (S) + condensate (C)] signals are represented and statistically analyzed.

Microscopic condensate assay

10% Pluronic F-127 solution was used to treat uncoated μ -Slide 18 Well—Flat chambers (81821, Ibidi, Germany) for 1 h at RT. Afterwards, wells were washed five times with MilliQ water. Prior to setting up the condensate formation reaction, the buffer of the purified Alexa 488-labeled TDP-43-MBP-His₆ preparation was exchanged to Hepes buffer (20 mM Hepes pH 7.5, 150 mM NaCl, 1 mM DTT). 7 μ M Alexa 488-coupled TDP-43-MBP-His₆ was mixed with 3.5 μ M DyLight 650-labeled monoclonal antibody (isotype controls or TDP-43 antibodies, respectively) in low binding tubes and 100 μ g/ml His₆-TEV protease was added to the reaction. Samples were transferred to μ -Slide 18 Well—Flat chambers and imaged using a Zeiss LSM710 confocal microscope after 30–60 min. For confocal microscopy, a Plan-Apochromat 63x/1.40 Oil DIC M27 objective was used and images were captured with two-line averaging at 2048 \times 2048 pixel resolution.

To analyze fusion events of antibody-treated and TEV protease-cleaved TDP-43, condensates were formed in 18-well ibiTreat slides (81826, Ibidi) using 20 μ M of Alexa 488-labeled TDP-43-MBP-His₆, 10 μ M of unlabeled monoclonal antibodies (isotype control IgG2c, 36C5 or 36C10, respectively) and 100 μ g/ml His₆-TEV protease in Hepes buffer. After an incubation step of 10 min at RT, condensates were imaged in 5 s intervals within a time window of up to 45 min after cleavage. An inverted spinning disc microscope (Visiscope 5 Elements, Visitron Systems GmbH, Germany), built on a Nikon Ti2 stand equipped with a confocal spinning disc (CSU-W1; Yokogawa, Japan) with 50 μ m pinhole diameter and a 60x/1.2 NA water immersion objective was used for acquisition. Imaging was performed using the 488 nm laser line for excitation and 525/50 bandpass filter (Chroma) for collecting the fluorescence emission. Images were captured using sCMOS camera (Prime BSI,

Photometrics) and a frame of 1033 \times 1033 pixels in 12-bit acquisition mode.

TDP-43 uptake assay

SH-SY5Y cells were cultured in DMEM/F12 (1:1) medium + L-Glutamine + 15 mM Hepes (Gibco) supplemented with 10% fetal bovine serum, until they reached a confluency of ~80%. Cells were then harvested and seeded in a 24-well plate (5×10^4 cells/well). The following day, recombinant pHrodo Green-labeled TDP-43-MBP-His₆ was used to prepare 10 μ M of aggregates during an incubation step of 2 h (see *Aggregation assay*). Subsequently, 10 μ M of single mAbs (isotype controls IgG1, IgG2c, 30D3, 31E9, 36C5 or 36C10) or equivalent amounts of PBS were added individually to the TDP-43 aggregates and incubated for 30 min at RT. Afterwards, media of SH-SY5Y cells were aspirated completely and 500 μ l of fresh media containing 500 nM TDP-43 aggregate/mAb mix or 500 nM monomeric TDP-43-MBP-His₆ were added on cells for ~20–24 h at 37 °C and 5% CO₂. The day after, cells were washed twice and harvested for flow cytometry analysis. Flow cytometry experiments were performed on a BD FACSVerser™ instrument (BD Biosciences, USA) and analyzed using FlowJo software (version 10.6.2, Treestar). In brief, singlets were detected using FSC-A versus FSC-H parameters. Live cells were identified as SYTOX™ Blue⁻ (negative) (Thermo Fisher) cells out of the single cell population. Lastly, the relative fluorescence of FITC in live single cells was analyzed. For each condition tested, at least 1800 live cells were recorded.

Data visualization and statistical analysis

Experimenters were blinded to genotype during immunization study and all subsequent immunoassays in which samples were distributed randomly. Animal experiments (immunizations and blood collection) were carried out in random order. Data were visualized and statistically analyzed using R (version 3.6.1) with RStudio. Assumptions for parametric tests were assessed by Shapiro–Wilk test/Q-Q plots and Levene's test. Longitudinal changes of body weights were analyzed by two- or three-way repeated measures ANOVA. One-way ANOVA followed by pairwise t-test with Benjamini–Hochberg correction was used as parametric test to statistically compare more than two groups. Kruskal–Wallis test and subsequent pairwise Wilcoxon Rank Sum Tests with Benjamini–Hochberg correction were used as non-parametric tests. Individual datapoints are generally displayed as scatterplots plus bar graphs [mean + standard deviation (SD)] or box plots (box indicates lower quartile, median and upper quartile, whiskers extend to the most extreme data point within 1.5 \times the interquartile range of the box).

P-values within graphs are reported as follows: * denotes $p \leq 0.05$, ** $p \leq 0.01$, *** $p \leq 0.001$, **** $p \leq 0.0001$.

Results

Immunogenicity and safety greatly vary between TDP-43 peptide epitopes

To determine which epitopes of TDP-43 induce sufficient antibody titers to slow disease progression in a TDP-43 mouse model, we selected 14 peptide antigens, collectively covering all domains and 2/3 of sequence of human TDP-43 (Fig. 1A and Additional file 1: S1A), based on predicted antigenicity. Within long, continuous, predicted antigenic stretches, we chose peptides of up to ~40 amino acids in length (peptide 7, 10 and 12). Apart from peptides 5, 7, 8, 11 and 12, all epitopes are fully conserved between human and mouse TDP-43. In addition, we designed peptide 15 to include phosphorylated serines 409/410 because phosphorylation at these sites is highly disease-specific [18]. To increase immunogenicity, we conjugated all peptides to ovalbumin (OVA). After three immunizations of wild-type C57BL/6J mice with the OVA conjugates, antibody responses were measured in an indirect ELISA using recombinant full-length human TDP-43. Peptides 1, 3, 10, 12, and 14 elicited the strongest antibody response, while peptides 4, 6, and 13 induced the lowest antibody titers (Fig. 1C). As expected, preimmune sera did not detect TDP-43 (Additional file 1: Fig. S1B). Notably, sera from mice immunized with the C-terminal phospho-peptide did not bind to non-phosphorylated recombinant TDP-43, but strongly reacted with the cognate phospho-peptide by indirect ELISA (Fig. 1C, right panel). Immunization with all peptides was well tolerated without apparent side effects in wild-type C57BL/6J mice.

To identify therapeutically relevant epitopes, we vaccinated rNLS8 mice that develop key features of human ALS/FTD pathology, such as cytoplasmic aggregation and nuclear clearance of TDP-43 as well as prodromal motor deficits upon induction of the hTDP-43ΔNLS transgene following doxycycline withdrawal [56]. Due to the large number of highly immunogenic antigens, bigenic mice (hereafter called rNLS8) were immunized with five pools of antigens (Fig. 1D): we used the two peptides with the highest antigenicity (Fig. 1C) from either the N-terminus (peptides 1 and 3), RRM1 (peptides 5 and 7), RRM2 (peptides 8 and 9) or the glycine-rich low-complexity domain (peptides 10 and 12) as well as the antigen harboring the disease-specific phosphorylation site (peptide 15). Mock-immunized bigenic animals (TDP-PBS) served as controls to evaluate therapeutic benefits. Potential side effects mediated by active immunization in a non-diseased context were monitored by treatment of monogenic control animals (not expressing

the TDP-43ΔNLS transgene upon doxycycline withdrawal) with a mixture of all peptide antigens (peptides 1, 3, 5, 7, 8, 9, 10, 12, 15). Based on previous results [63], all animals were vaccinated five times prior to, and once after, transgene induction to trigger high antibody titers (Fig. 1E). All rNLS8 mice developed progressive weight loss and muscle weakness and were sacrificed 21 days after doxycycline withdrawal to facilitate direct comparison of treatment effects on pathology (see below).

In contrast to the immunization in wild-type C57BL/6J mice, combined peptides 1 + 3 caused acute lethality in rNLS8 mice with a mixed C57BL/6J × C3H/HeJ background even prior to transgene expression. Seven of the ten mice immunized with the pooled peptides 1 and 3 unexpectedly died or had to be sacrificed shortly after the second or third immunization and we thus stopped further boosting the remaining three animals (Fig. 1F, dashed line). All other peptides were equally well tolerated in the rNLS8 and control mice. To address the role of the different genetic backgrounds for the unexpected toxicity, we conducted two immunizations with the antigen pools from Fig. 1D in C57BL/6J, C3H/HeOuJ, and CD-1 mice (Additional file 1: Fig. S2A-D). The antibody titers were comparable between the three lines (Additional file 1: Fig. S2B). Surprisingly, only one of six CD-1 and none of the C3H/HeOuJ or C57BL/6J mice receiving peptides 1 + 3 developed symptoms requiring euthanasia. Hence, immunization with TDP-43 peptides shows strikingly different side effects in different mouse strains, which may be attributed to a loss-of-function mutation in the Tlr4 receptor found in C3H/HeJ mice but not the otherwise genetically very similar C3H/HeOuJ line [8]. Nevertheless, our data establish several highly antigenic and potentially safe epitopes for active TDP-43 immunotherapy.

Epitopes in the glycine-rich domain of TDP-43 induce a strong antibody response

Next, we analyzed the antibody response in immunized rNLS8 mice by ELISA, immunofluorescence and immunoblots. Using an ELISA against recombinant full-length TDP-43, dilution series of pooled sera from five-times immunized animals revealed the strongest immune response in mice vaccinated with peptides 10 + 12. The three surviving mice from the TDP1+3 group had a similarly strong response, although they only received one, two or three immunizations (Fig. 2A, left panel). Peptide pools 5 + 7 and 8 + 9, which targeted RRM1 and RRM2, respectively, induced weaker antibody responses. Antisera from animals immunized with the phospho-peptide (TDP15) did not detect unphosphorylated TDP-43 expressed in *E. coli* (Fig. 2A, left panel), but strongly reacted with the cognate phospho-peptide (Fig. 2A, right

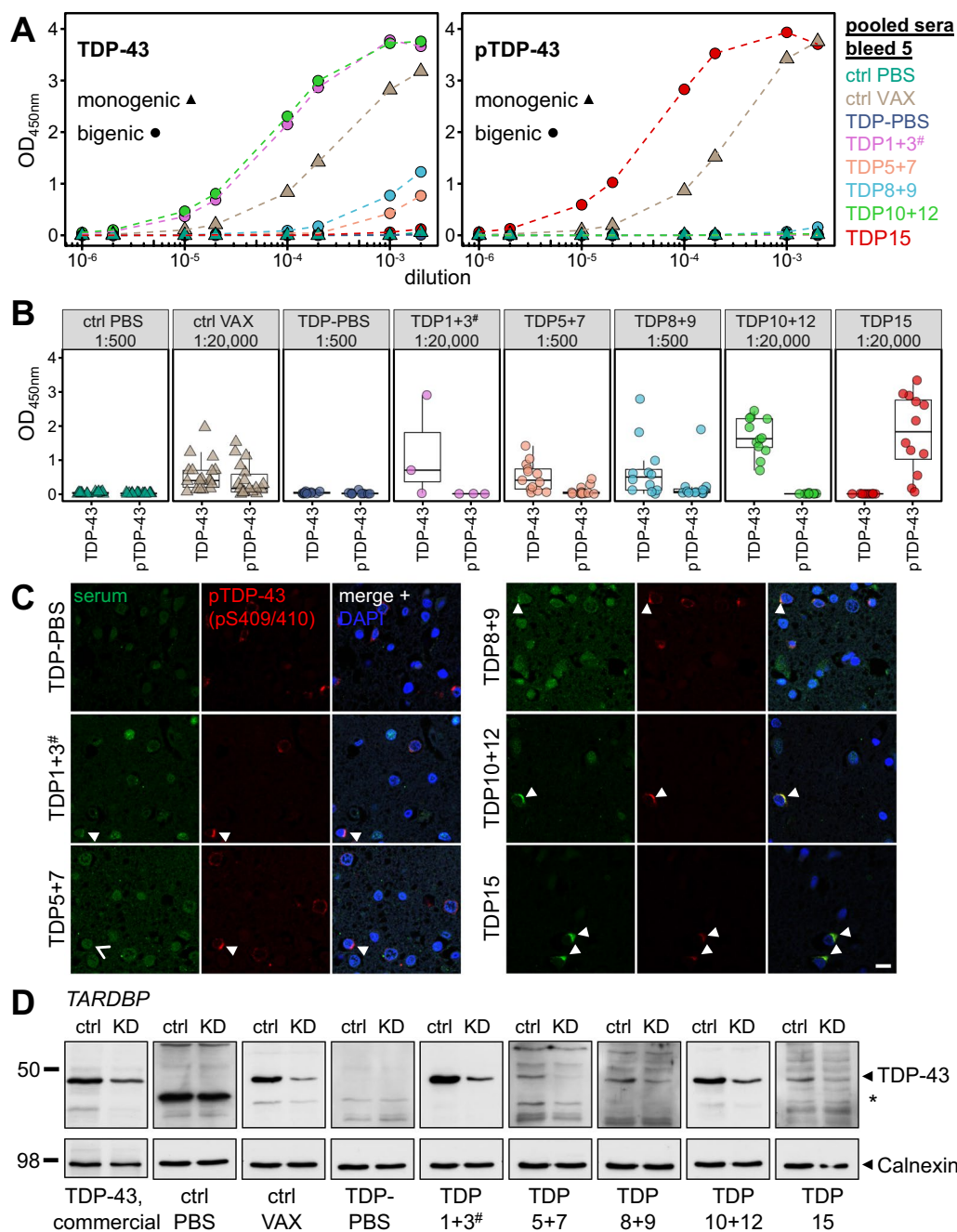


Fig. 2 C-terminal TDP-43 peptides elicit high-titer antibodies detecting patient TDP-43 aggregates. TDP-43-specific antibody responses in sera from mice receiving five immunizations (except TDP1 + 3 with 1–3 immunizations) were analyzed by ELISA, immunofluorescence stainings, and immunoblot. **A** A dilution series of pooled sera was analyzed by ELISA against recombinant full-length TDP-43 (left panel) or pTDP-43 peptide (pS409/410, right panel). Background-corrected mean OD₄₅₀ was measured in duplicates. Triangular shapes indicate monogenic animals, circles represent rNLS8 mice (labeling consistent throughout the following figures). **B** Antibody response in antisera from individual mice was measured as in **(A)** in single dilutions (1:500 or 1:20,000) to analyze inter-animal variability. Control (ctrl) PBS n = 17, ctrl VAX n = 18, TDP-PBS n = 10, TDP1 + 3 n = 3, TDP5 + 7 n = 13, TDP8 + 9 n = 13, TDP10 + 12 n = 12, and TDP15 n = 12. Note that the number of immunizations in TDP1 + 3 animals (1, 2 or 3) correlates with the resulting titer. **C** Double immunofluorescence stainings of pooled antisera and phosphorylated TDP-43 (pS409/410) were performed on frontal cortex sections of a sporadic FTLD case. Representative images are shown. Arrowheads indicate strong (TDP10 + 12, TDP15) or weak (TDP1 + 3, TDP8 + 9) labeling of pTDP-43 inclusions with antisera. TDP5 + 7 antiserum failed to detect pTDP-43-positive inclusions (open arrowhead). Images from a healthy control are shown in Fig. S3A. Scale bar = 10 μm. **D** Immunoblotting of HEK293 cell lysates of doxycycline-inducible *TARDBP* knockdown (KD) and control (ctrl) using a commercial TDP-43 antibody (left lane) or pooled antisera. Asterisk denotes a prominent non-specific band detected with the ctrl PBS serum. Calnexin was used as a loading control

panel). Antisera from monogenic control mice receiving the antigen mix including the phospho-peptide (#15) also detected the phospho-peptide by ELISA, albeit at a lower level.

Due to the lack of dilutional linearity in the ELISA, we compared the antibody response of individual animals within each group using a fixed dilution of the antisera. As in the pooled analysis (Fig. 2A), the antibody response was most robust in the TDP10+12 and TDP15 animals (Fig. 2B). Of note, the three doses of peptides 1+3 were highly immunogenic in the surviving animal consistent with results in three inbred mouse strains (Additional file 1: Fig. S2B). To analyze the kinetics of the antibody response, we compared the antibody response for pooled sera from all groups over time (Additional file 1: Fig. S2E). In contrast to our anti-GA immunization [63], anti-TDP-43 titers plateaued already two weeks after the second immunization, suggesting that preselecting highly immunogenic epitopes within TDP-43 strongly accelerated the response.

We next asked whether the antisera could detect disease-associated TDP-43 inclusions in human patient sections. Indeed, antisera of TDP10+12 and TDP15 mice strongly stained the characteristic cytoplasmic pTDP-43-positive inclusions in brain sections of an FTLD patient which are absent in a healthy control, with TDP15 antisera showing almost no affinity for nuclear TDP-43 compared to TDP10+12 (Fig. 2C, Additional file 1: S3A). TDP1+3 and, to a lesser extent, TDP8+9 antisera still detected some pTDP-43 inclusions as well as nuclear TDP-43. At the same dilution, antisera from TDP5+7 immunized animals failed to stain cytoplasmic aggregates. Co-staining of human tissue with commercial pan-TDP-43 antibody further confirmed specificity of the antisera (Additional file 1: Fig. S3B).

To test whether the strong ELISA and immunofluorescence signal depend on the native TDP-43 conformation and to rule out poor accessibility of the certain epitopes in native TDP-43, we validated the specificity of antisera using denatured TDP-43 in cellular lysates of a CRISPR interference (CRISPRi) mediated inducible

TARDBP knockdown in stably transfected HEK293 cells. Pooled antisera specifically detected a ~43 kDa band of endogenous human TDP-43 that was reduced upon doxycycline-induced knockdown of *TARDBP* transcription (Fig. 2D). As expected, the TDP15 antisera showed a very low signal in the absence of pathological TDP-43 phosphorylation in HEK293 cells. Consistent with the ELISA data, TDP1+3 and TDP10+12 antisera showed the strongest signals and were highly TDP-43-specific.

Taken together, antigens derived from the glycine-rich domain (peptides 10+12 and 15) reliably induced high-titer antibodies and detected disease-associated cytoplasmic TDP-43 inclusions.

Immunization with the C-terminal pS409/410 epitope reduces NfL levels in rNLS8 mice without slowing the rapid body weight loss

Since disease-relevant phenotypes progress rapidly in aged rNLS8 mice [51], we sacrificed all mice 21 days after transgene induction, when the first animals reached humane endpoint criteria (mostly weight loss), allowing us to compare the pathology and progression at a fixed time point (Fig. 1E). As body weight loss is a cardinal symptom of ALS patients and the rNLS8 mouse model [56], we monitored body weight of all immunized mice to assess the efficacy and potential adverse effects of the immunization (Fig. 3A). While there was no significant effect of vaccination on body weight prior to transgene expression, all rNLS8 mice lost weight ~14 days after transgene induction regardless of the immunization regimen (Fig. 3A/B).

Neurofilament levels in blood and CSF are emerging as a powerful biomarker for detecting neuroaxonal damage in mouse models and patients affected by ALS [22]. Thus, we measured neurofilament light chain (NfL) levels in serum collected from mice at the time of sacrifice (bleed 6). We found that serum NfL was strongly elevated in rNLS8 mice compared to the monogenic controls (Fig. 3C). Interestingly, immunization with the highly immunogenic peptide 15 significantly reduced serum NfL in rNLS8 mice compared to the TDP-PBS control,

(See figure on next page.)

Fig. 3 TDP-43 active immunization does not prevent weight loss, but the pTDP-43 antigen moderately lowers NfL. Body weight and NfL levels were analyzed in immunized control and rNLS8 mice. **A** Development of body weight in control and rNLS8 mice before and after transgene induction using doxycycline withdrawal. Mean values are plotted group-wise, *n* as indicated. The longitudinal effects of treatment (peptide immunization vs. no immunization), genotype (control vs. rNLS8), age as well as their interactions were analyzed using a three-way repeated measures ANOVA. On doxycycline chow, only age had a statistically significant effect on the body weight ($p = 1.99 \times 10^{-102}$), but not the treatment ($p = 0.74$). After transgene induction, genotype ($p = 0.018$), age ($p = 2.34 \times 10^{-26}$), and their interaction ($p = 2.20 \times 10^{-26}$), but not treatment ($p = 0.901$), had a statistically significant effect on the body weight. **B** Comparison of the percentage body weight (BW) loss from transgene induction (25.5 weeks of age) to end-stage (28.5 weeks of age) against the TDP-PBS group using pairwise t-test with Benjamini–Hochberg correction revealed a statistically significant difference for both monogenic groups (ctrl PBS vs. TDP-PBS: $p = 1.47 \times 10^{-11}$, ctrl VAX vs. TDP-PBS: $p = 6.38 \times 10^{-10}$) only. Group means are indicated as black dots. **C** Neurofilament light chain (NfL) levels in the serum of end-stage mice were quantified using the Simoa® platform. Comparisons against TDP-PBS mice using pairwise Wilcoxon test with Benjamini–Hochberg correction revealed a statistically significant difference in NfL levels for ctrl PBS ($p = 8.3 \times 10^{-7}$), ctrl VAX ($p = 8.3 \times 10^{-7}$), and TDP15 immunized mice ($p = 0.013$). Mean values are indicated as black dots

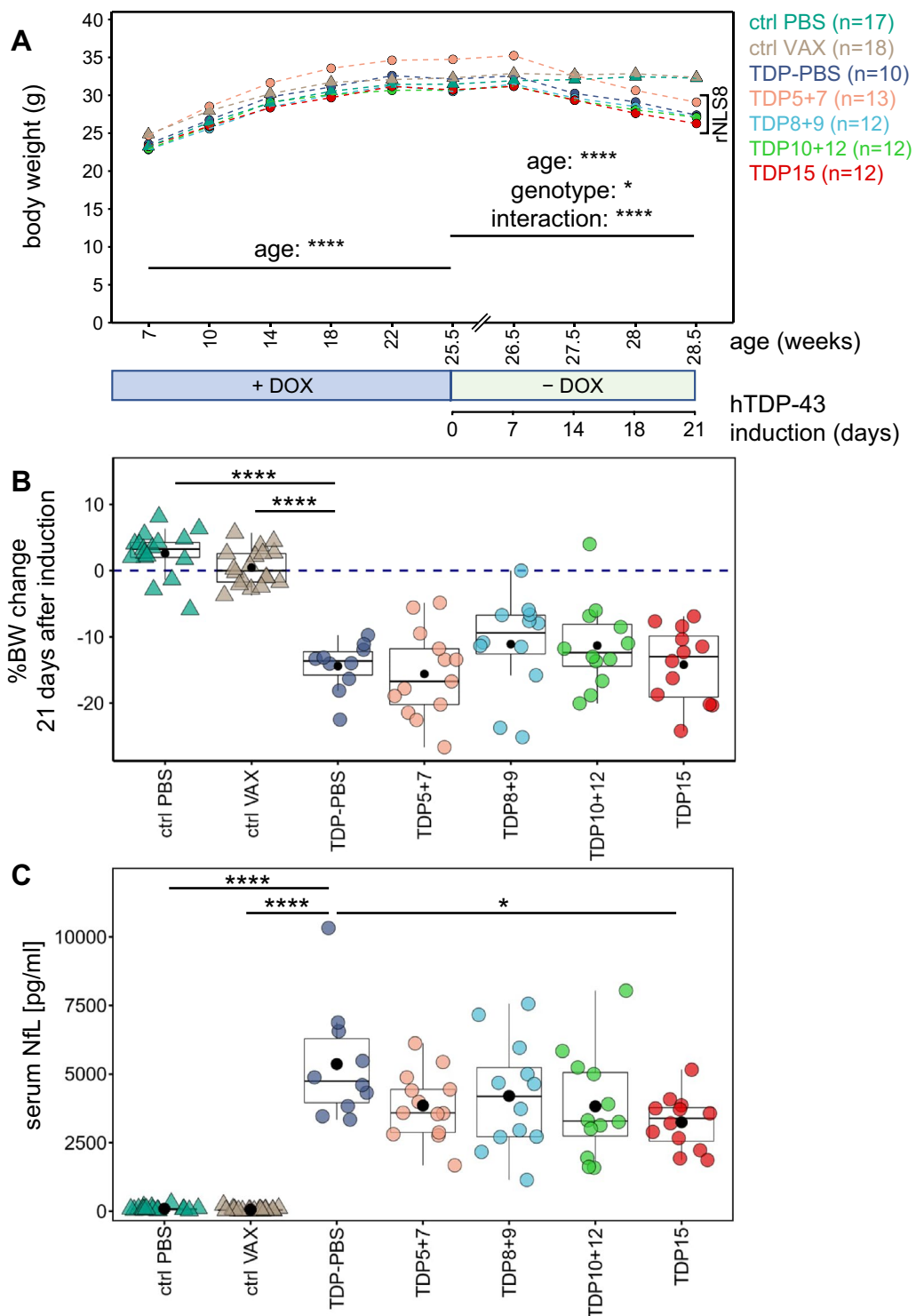


Fig. 3 (See legend on previous page.)

suggesting that targeting the disease-specific phospho-epitope by active immunization might have beneficial effects on TDP-43-mediated disease progression.

None of the peptide antigens reduces pTDP-43 pathology or gliosis in immunized mice

To further investigate the potential benefits of TDP-43 peptide vaccination in rNLS8 mice, we analyzed disease-associated pS409/410 TDP-43 levels and neuroinflammation in treated animals. Using a previously established immunoassay, we quantified pTDP-43 in the cerebral cortex (Fig. 4A). This assay showed a significant accumulation of pTDP-43 in the rNLS8 mice compared to controls. As expected, pTDP-43 was strongly enriched in the urea-soluble fraction compared to the RIPA-soluble fraction. However, pTDP-43 levels did not differ between the rNLS8 groups, indicating that even high antibody titers in serum cannot prevent brain pTDP-43 accumulation in rNLS8 mice.

These findings were confirmed by pTDP-43 immunohistochemistry, which visualized characteristic pTDP-43 inclusions in the CA3 area of the hippocampus, which is like the neocortex considerably affected by TDP-43 pathology three weeks after transgene induction (Fig. 4B, arrows). In addition, we analyzed subcellular TDP-43 distribution to complement the pTDP-43 data. Immunofluorescence stainings using a pan-TDP-43 antibody (detecting both human and mouse TDP-43) revealed pronounced cytoplasmic TDP-43 signal in bigenic animals compared to a predominant nuclear localization of endogenous TDP-43 in monogenic mice (Fig. 4C). The ratio of cytoplasmic-to-nuclear TDP-43 was not affected in any of the treatment groups.

Moreover, GFAP and Iba1 immunofluorescence revealed widespread early microgliosis (Fig. 5A) and astrogliosis in rNLS8 mice compared to controls (Fig. 5B). However, immunization with neither of the antigens markedly affected astrocyte or microglia activation as indicated by their comparable abundance and cellular morphology.

Immunization against C-terminal epitopes slightly rescues the gene expression changes in rNLS8 mice

To identify functional correlates of reduced NfL levels in TDP15 mice, we investigated neocortical gene expression profiles using RNAseq. To this end, we analyzed all PBS-treated controls (ctrl PBS) and rNLS8 mice (TDP-PBS) as well as all rNLS8 animals vaccinated with promising peptides from the C-terminal domain (TDP10+12 and TDP15). Transgene induction in rNLS8 mice dramatically altered the transcriptome, dominated by a strong inflammatory signature, which

is in line with our immunofluorescence stainings of GFAP and Iba1 (Fig. 5). The data correspond well to the previously reported signature of isolated early- and late-stage rNLS8 microglia (Additional file 1: Fig. S4A) [19]. Vaccinated and PBS-treated rNLS8 mice showed an overall similar gene expression pattern when compared to control littermates (Fig. 6A). Top upregulated genes in rNLS8 mice included *Cxcl10*, *Ccl4*, *Ccl5*, and *Cst7*. Principal component analysis clearly separated controls from all rNLS8 groups but showed no clustering among the rNLS8 treatment groups (Fig. 6B). Comparison to the TargetALS RNAseq dataset from ALS spinal cord and motor cortex revealed shared differentially expressed genes, although the overlap is modest (Fig. 6A/C, Additional file 1: Fig. S4B). Gene ontology analysis indicated that many pathways induced in ALS spinal cords are also upregulated in rNLS8 mice, including IL-1 β , TNF- α and NF κ B signaling (Fig. 6C). The rNLS8 model displayed a stronger enrichment of interferon-related genes (Fig. 6C). The top concordant hits between rNLS8 neocortex and ALS spinal cord are inflammation-related (Fig. 6C and Additional file 1: S4B). No individual gene was differentially expressed in TDP10+12 or TDP15 immunized rNLS8 animals compared to the PBS-treated rNLS8 animals after multiple testing correction. However, comparing the log-fold changes between vaccinated and control rNLS8 animals (TDP10+12 vs. TDP-PBS and TDP15 vs. TDP-PBS) to transgene induced changes (TDP-PBS vs. ctrl PBS) (Fig. 6D) revealed a significant inverse correlation, which was more pronounced for the animals immunized with peptides 10+12. This indicates a trend for a slight overall rescue of transcriptional alterations in immunized rNLS8 mice.

To confirm inflammatory phenotypes identified by the transcriptomics and to assess potential therapeutic benefits of the immunization at the protein level, we measured the levels of 19 pro-inflammatory markers and cytokines in cortical brain lysates using a multiplexed immunoassay. While some of the analytes fell below detection levels at the tested concentrations (IFN- γ , IL-10, IL-12p70, IL-2, IL-4), we identified IL-1 β , IP-10 (CXCL10), KC/GRO (CXCL1), MCP-1 (CCL2), MIP-1 α (CCL3), and TNF- α to be significantly upregulated in rNLS8 mice compared to monogenic control animals (Fig. 6E). KC/GRO (CXCL1) and CCL2 are known to be activated by IL-1 β and TNF- α via NF κ B signaling and activate monocytes/microglia, while IP10 (CXCL10) is a well-known target of interferons consistent with the transcriptome data (Fig. 6C). In contrast, several interleukins measured in the panel were not altered in rNLS8 mice (Fig. S4C/D). No immunization regimen significantly affected levels of any cytokine

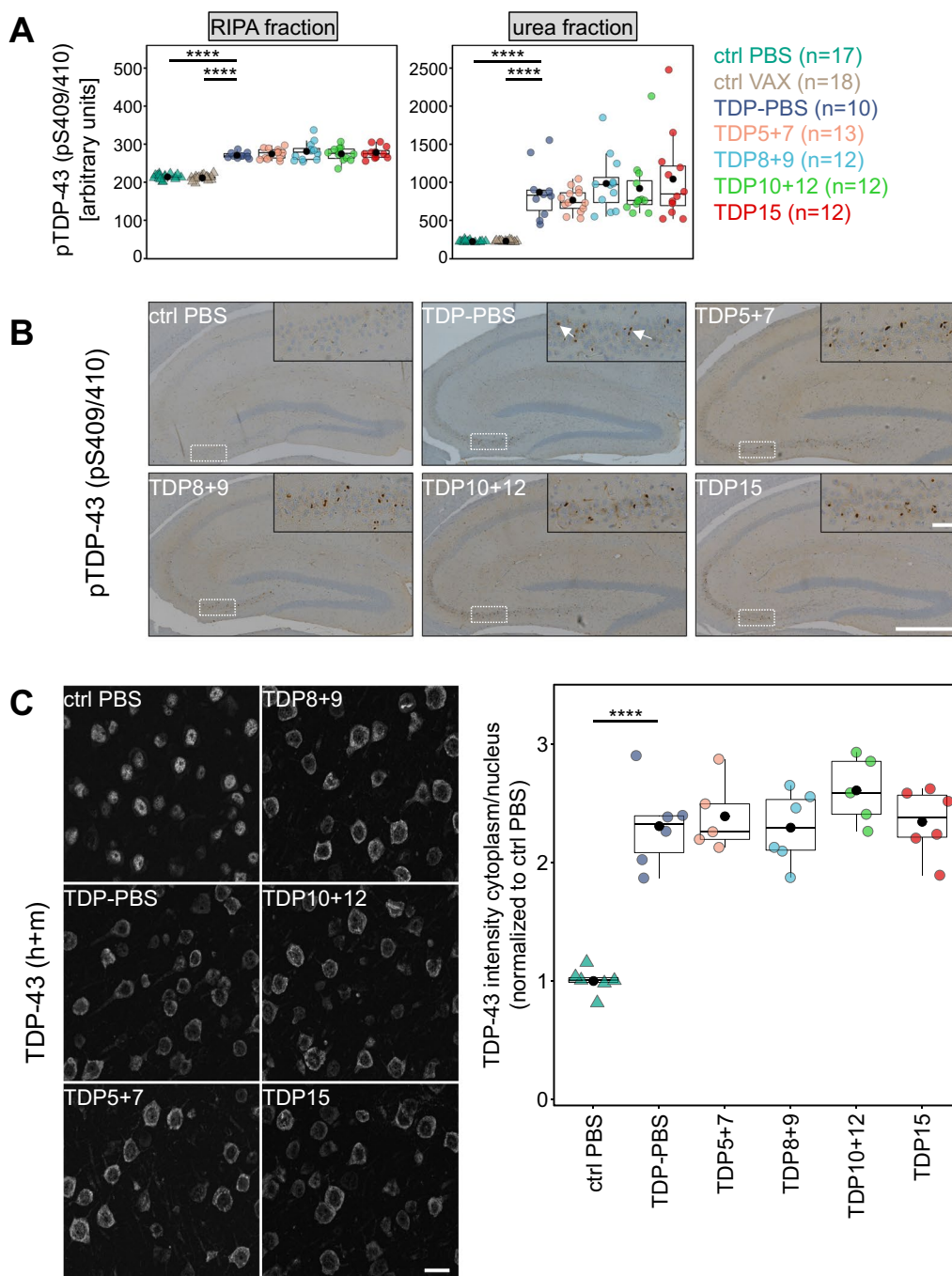


Fig. 4 Active immunization does not affect pTDP-43 levels and TDP-43 cytoplasmic-to-nuclear distribution in rNLS8 mice. Cerebral TDP-43 pathology was analyzed by ELISA, immunohistochemistry, and immunofluorescence stainings in vaccinated rNLS8 mice. **A** Phospho-TDP-43 (pS409/410) levels were measured in RIPA and urea fractions from neocortex. Only monogenic animals showed statistically significant differences in RIPA lysates (ctrl PBS: $p = 7.63 \times 10^{-5}$, ctrl VAX: $p = 7.63 \times 10^{-5}$) and urea lysates (ctrl PBS: $p = 7.70 \times 10^{-5}$, ctrl VAX: $p = 7.70 \times 10^{-5}$) when compared to TDP-PBS group by pairwise Wilcoxon test with Benjamini–Hochberg correction. Mean values are plotted as black dots. **B** Immunohistochemical staining in the hippocampal region using an antibody against pS409/410 TDP-43. Representative images for each group are shown. Magnified insets are displayed on the top right corner and their position in the overview is depicted by dashed rectangles. Arrows in the inset denote characteristic pTDP-43 inclusions in the CA3 region. Scale bar overview = 500 μm , scale bar inset = 50 μm . **C**: Immunofluorescence staining of total TDP-43 (human + mouse) in the frontal neocortex. Representative images for each group are depicted in the left panel (Scale bar = 20 μm). Note that control PBS images were taken at a higher gain to compensate for the lower levels of endogenous TDP-43. Right panel shows quantification of the ratios of the cytoplasmic-to-nuclear TDP-43 intensities (after normalization to the ctrl PBS group). Mean values are plotted as black dots. Pairwise t-test with Benjamini–Hochberg correction indicated a statistically significant difference between monogenic ctrl PBS and bigenic TDP-PBS animals ($p = 3.32 \times 10^{-5}$). Control (ctrl) PBS n=6, TDP-PBS n=6, TDP5+7 n=5, TDP8+9 n=6, TDP10+12 n=5, and TDP15 n=6

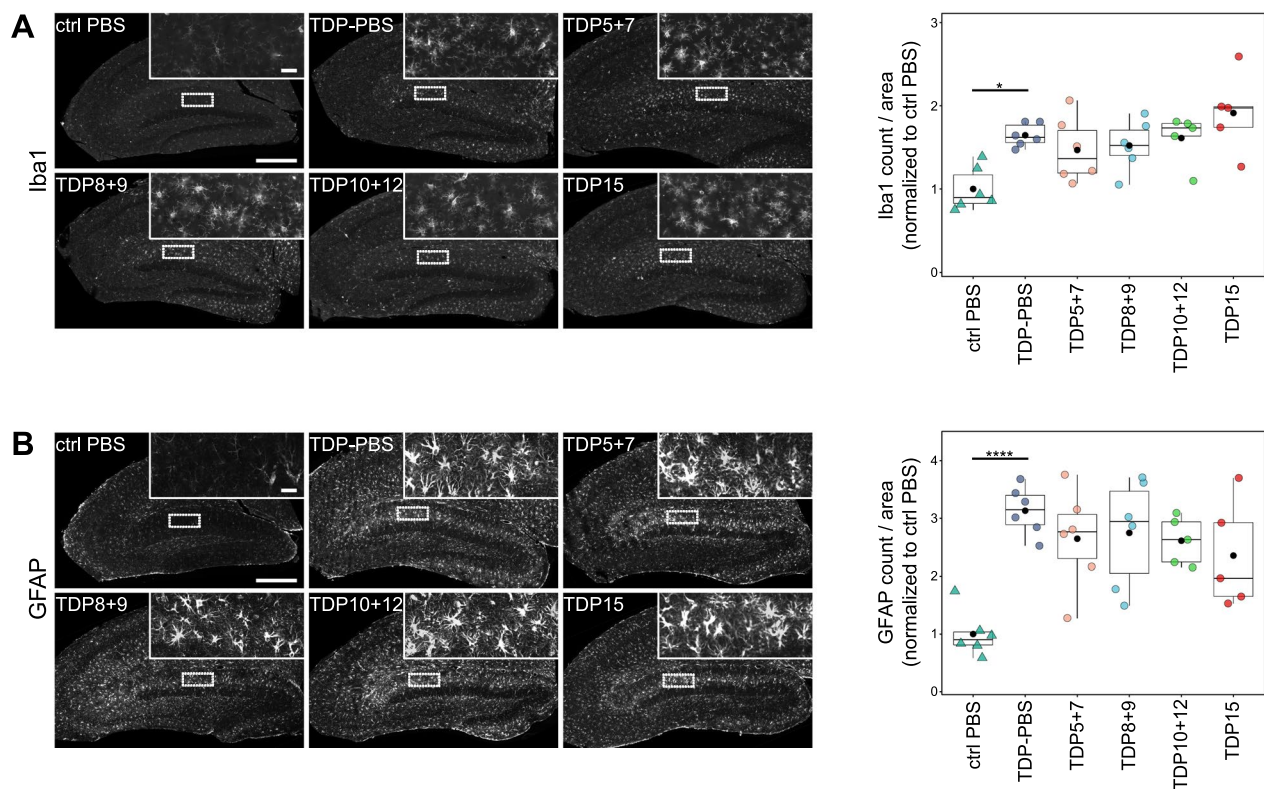


Fig. 5 Profound micro- and astrogliosis in the rNLS8 model are unchanged upon vaccination with TDP-43 peptides. Using an automated staining and analysis pipeline, microglia (Iba1) and astrocyte (GFAP) signals were quantified in hippocampal regions. Representative immunofluorescence images of Iba1 (**A**) or GFAP (**B**)-stained hippocampal regions. Magnified insets are shown on the top right corner and their position in the overview is indicated by dashed rectangles. Scale bar overview = 500 μm , scale bar inset = 50 μm . Right panels show automated quantification of the Iba1 (**A**) and GFAP (**B**) cell count per area, followed by normalization to the ctrl PBS group. Mean values are plotted as black dots. Pairwise Wilcoxon test with Benjamini–Hochberg correction revealed an increased Iba1 count in the TDP-PBS group when compared to ctrl PBS animals ($p=0.011$). GFAP counts were analyzed using pairwise t-test with Benjamini–Hochberg correction and were statistically different between TDP-PBS and ctrl PBS mice ($p=2.04 \times 10^{-5}$). None of the vaccinated groups are significantly different from TDP-PBS. Control (ctrl) PBS $n=6$, TDP-PBS $n=6$, TDP5+7 $n=6$, TDP8+9 $n=6$, TDP10+12 $n=5$, and TDP15 $n=5$

(See figure on next page.)

Fig. 6 Widespread transcriptional changes in rNLS8 mice are modestly rescued by immunization targeting the glycine-rich region. **A** Differentially expressed genes from rNLS8 mice (TDP-PBS, TDP10+12, TDP15) compared to controls (ctrl PBS) and motor cortex (MCtx) and spinal cord (SC) of sporadic ALS patients compared to no-disease controls (dataset from [25]). From each group the 25 genes with largest absolute log2 fold change (LFC) also reaching statistical significance (indicated by asterisk) are depicted. Color code denotes LFC. **B** Principal component analysis (PCA) of transcriptomes separates animals based on genotype (control vs. rNLS8), but not on therapeutic intervention or gender. **C** Gene ontology analysis of differentially expressed genes (cutoff $|\text{LFC}| > 1$) in ALS spinal cord and TDP-PBS mice, each both compared to non-diseased controls. Manual selection of categories with > 4 genes. Full list is shown in Additional file 3: Table S2. **D** Fold-change of genes differentially expressed in TDP-PBS vs. control mice plotted against the fold-change between vaccinated and PBS-treated rNLS8 animals. Blue line shows linear regression. Pearson's product-moment correlation shows partial rescue of gene expression ($p < 2 \times 10^{-16}$ for both, correlation coefficient -0.49 and -0.12 as indicated). **E** Cytokine levels determined by multiplex assay from cortical tissue show inflammatory response in rNLS8 animals. Pairwise t-test with Benjamini–Hochberg correction revealed statistically significant differences between ctrl (monogenic) and bigenic TDP-PBS animals: IL-1 β : ctrl PBS $p=2.57 \times 10^{-5}$, ctrl VAX $p=0.004$; IP-10: ctrl PBS $p=6.26 \times 10^{-5}$, ctrl VAX $p=6.26 \times 10^{-5}$; KC/GRO: ctrl PBS $p=9.17 \times 10^{-4}$, ctrl VAX $p=2.13 \times 10^{-4}$; MCP-1: ctrl PBS $p=7.98 \times 10^{-6}$, ctrl VAX $p=7.98 \times 10^{-6}$; MIP-1a: ctrl PBS $p=3.44 \times 10^{-5}$, ctrl VAX $p=3.44 \times 10^{-5}$; TNF- α : ctrl PBS $p=5.64 \times 10^{-4}$, ctrl VAX $p=5.64 \times 10^{-4}$. TNF- α and IL-1 β : Control (ctrl) PBS $n=6$, ctrl VAX $n=6$, TDP-PBS $n=10$, TDP5+7 $n=6$, TDP8+9 $n=9$, TDP10+12 $n=9$, and TDP15 $n=7$; IP-10, KC/GRO, MCP-1 and MIP-1a: Control (ctrl) PBS $n=10$, ctrl VAX $n=10$, TDP-PBS $n=10$, TDP5+7 $n=13$, TDP8+9 $n=12$, TDP10+12 $n=12$, and TDP15 $n=12$. Non-affected cytokines are shown in Supplemental Fig. S4C

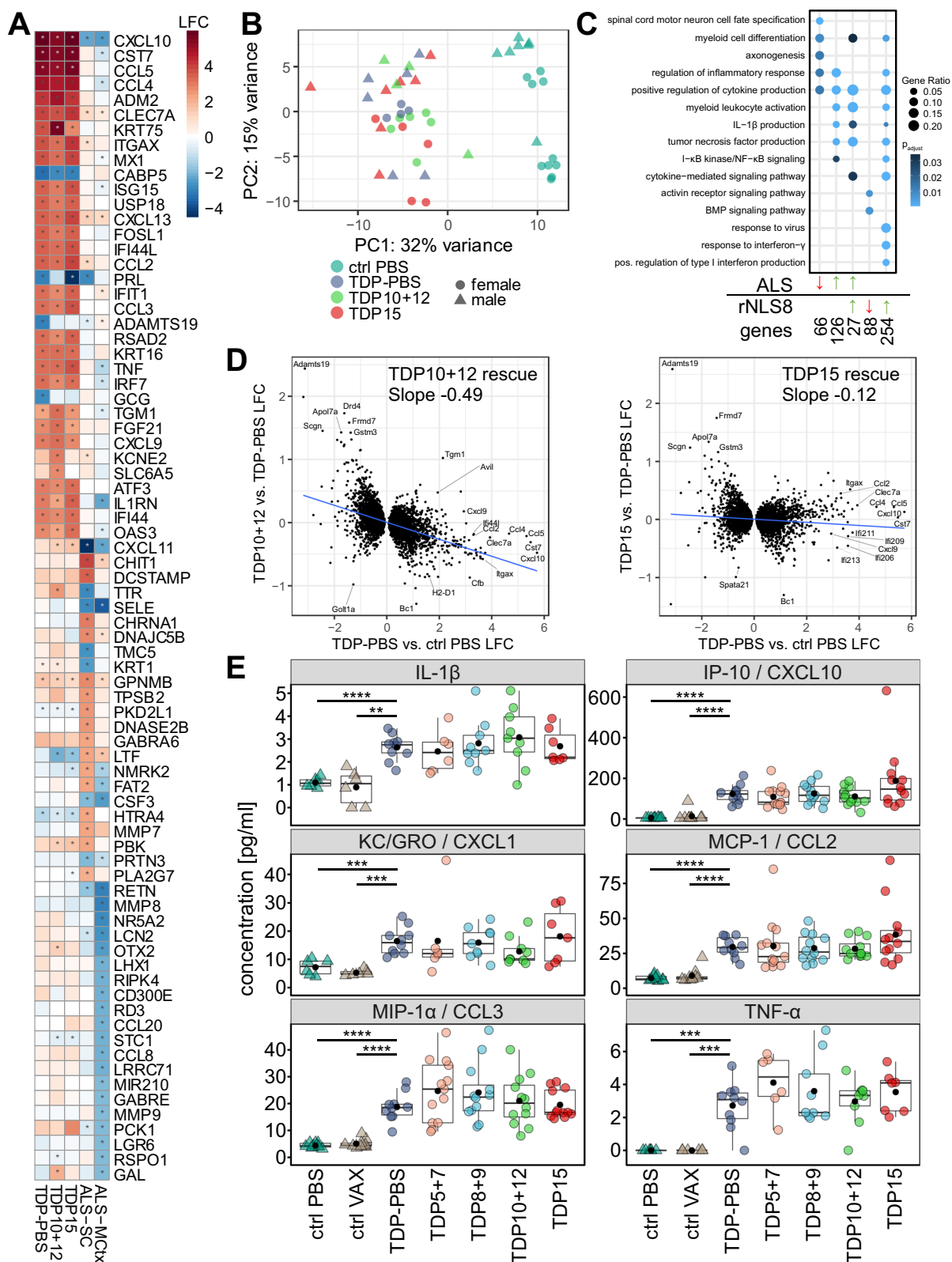


Fig. 6 (See legend on previous page.)

quantified. Interestingly, among the markers measured by immunoassay, only *Cxcl10*, *Ccl2*, *Ccl3* and *Tnf* were strongly upregulated at the transcriptomic level as well (Fig. S4D). The chemokine profile in rNLS8 mice is likely driven by IL-1 β and TNF- α and is consistent with strong monocyte/microglia activation (Fig. 5A).

Novel monoclonal antibodies targeting the RRM2 or the C-terminal glycine-rich region inhibit TDP-43 aggregation in vitro

To investigate the effects of antibodies induced by active vaccination in vitro, we generated a panel of monoclonal antibodies (mAbs) recognizing specific domains of TDP-43 by hybridoma generation using the spleens from immunized C57BL/6J mice (see Fig. 1B/C). Since we failed to generate mAbs from the spleens of C57BL/6J mice immunized with peptide 7, we generated mAbs by immunization of Balb/c mice with this peptide antigen. Using ELISA against recombinant TDP-43, we pre-screened our 47 mAb clones and selected promising mAbs for the peptide epitopes 3, 7, 8, 10, and 12 (not shown) to characterize their effects on TDP-43 aggregation (Fig. 7A and Additional file 1: S1A).

To monitor TDP-43 aggregation in vitro, we used a recently established aggregate formation assay that relies on the cleavage of the solubilization tag MBP (maltose-binding protein) from a TDP-43-MBP-His₆ fusion protein, followed by agitation in an aggregation-promoting buffer (Fig. 7B) [14, 16]. In the presence of isotype control mAbs (molar ratio antibody:TDP-43-MBP-His₆ = 1:2), fluorescently-labeled TDP-43 readily formed aggregates that we visualized after 48 h (Fig. 6C, top panel). While clones 25C1, 27A3 (targeting peptide 3), 26A2, 26F12 (targeting peptide 7), and 31D9 (targeting peptide 10) had only moderate effects in suppressing TDP-43 aggregate formation, clones 30D3 (targeting peptide 8), 31E9 (targeting peptide 10), 36C5, and 36C10 (targeting peptide 12) strongly inhibited TDP-43 aggregate formation in this assay (Fig. 7C).

(See figure on next page.)

Fig. 7 Antibodies targeting RRM2 and the glycine-rich region of TDP-43 suppress aggregation and LLPS in vitro. **A** Schematic overview of a panel of novel TDP-43 monoclonal antibodies (mAbs) raised from immunization in Fig. 1 as indicated. The most potent mAbs are highlighted in bold. **B** Aggregation and condensation assays using recombinant TDP-43-MBP-His₆. Upon cleavage of the solubilization tag maltose-binding protein (MBP) using TEV protease, soluble TDP-43 forms aggregates (**C**) or condensates (**D/E**), depending on the buffer conditions. Condensates were either analyzed by pelleting (**D**) or by confocal microscopy (**E**). mAbs were added to soluble TDP-43-MBP-His₆ together with TEV protease. **C** Representative images of Alexa 488-labeled and in vitro aggregated TDP-43, treated with the indicated mAb (molar ratio TDP-43-MBP-His₆: mAb = 1:2). Images were taken 48 h after TEV cleavage. Clones 30D3 and 31E9 nearly completely prevented aggregation. Overview and magnified insets on the right bottom corner are shown. Scale bar overview = 100 μ m, scale bar inset = 50 μ m. **D** Sedimentation assay to analyze condensation of cleaved TDP-43-MBP-His₆ in the presence of mAbs. Supernatant (S) and condensates (C) were separated by centrifugation 2 h after TEV cleavage. Representative immunoblots and quantification of S/(C+S) ratios (bar graphs indicate mean + SD) from four replicates are shown. An asterisk indicates the residual uncleaved TDP-43-MBP-His₆, the arrowhead marks the cleaved TDP-43 band. mAbs were compared to their respective isotype controls using pairwise t-test with Benjamini–Hochberg correction for multiple testing: IgG2c vs. 30D3: $p=0.017$; IgG2c vs. 36C5: $p=3.24*10^{-4}$; IgG2c vs. 36C10: $p=0.016$; IgG1 vs. 27A3: $p=0.021$; IgG1 vs. 31E9: $p=3.87*10^{-4}$. **E** Confocal images of Alexa 488-coupled TDP-43-MBP-His₆ and DyLight 650-labeled mAbs show liquid–liquid phase separation of TDP-43 and co-partitioning of mAbs with TDP-43 condensates after TEV protease cleavage. Scale bar = 10 μ m

As TDP-43 aggregates are believed to arise from TDP-43 condensates that are formed by liquid–liquid phase separation (LLPS) and then undergo a liquid-to-solid state transition [3, 36, 57], we also assessed the capacity of the monoclonal antibodies to suppress TDP-43 condensate formation. Using a buffer containing physiological salt concentrations and no aggregation-promoting ingredients, TDP-43 rapidly undergoes LLPS after proteolytic removal of the MBP solubility tag [57]. To assess TDP-43 condensation in the presence of mAbs, we first used a sedimentation assay in which we separated the soluble fraction (S) and the condensate fraction (C) by centrifugation, followed by densitometric quantification of the TDP-43 signals in each fraction [16]. In line with the aggregation assay, clones 30D3, 31E9, 36C5, and 36C10 also significantly reduced TDP-43 condensate formation (Fig. 7D).

Next, we visualized TDP-43 condensates and assessed co-partitioning of mAbs into these condensates, by performing the condensation assay with fluorescently labeled TDP-43 and mAbs, and imaged condensates by confocal microscopy (Fig. 7E). As expected, isotype control mAbs did not co-localize with TDP-43 condensates, whereas 30D3 and 31E9 reduced condensate formation and co-partitioned into the remaining condensates. However, the 30D3-treated condensates appeared to have an amorphous, less liquid-like phenotype. In contrast, 36C5 and 36C10 increased the TDP-43 condensate size with prominent co-partitioning of both antibodies, suggesting that TDP-43 condensates become more fluid in the presence of these mAbs that both target an internal epitope of the glycine-rich domain. Fusion events observed by live imaging indeed indicated that condensates are larger and have more fluid-like character in the presence of antibodies 36C5 and 36C10 (Additional file 1: Fig. S5A). However, condensates fused relatively slowly and did not fully relax into perfectly round spheres, suggesting they are not ideal liquid-like droplets. Of interest, these four antibodies also showed the highest affinity among our

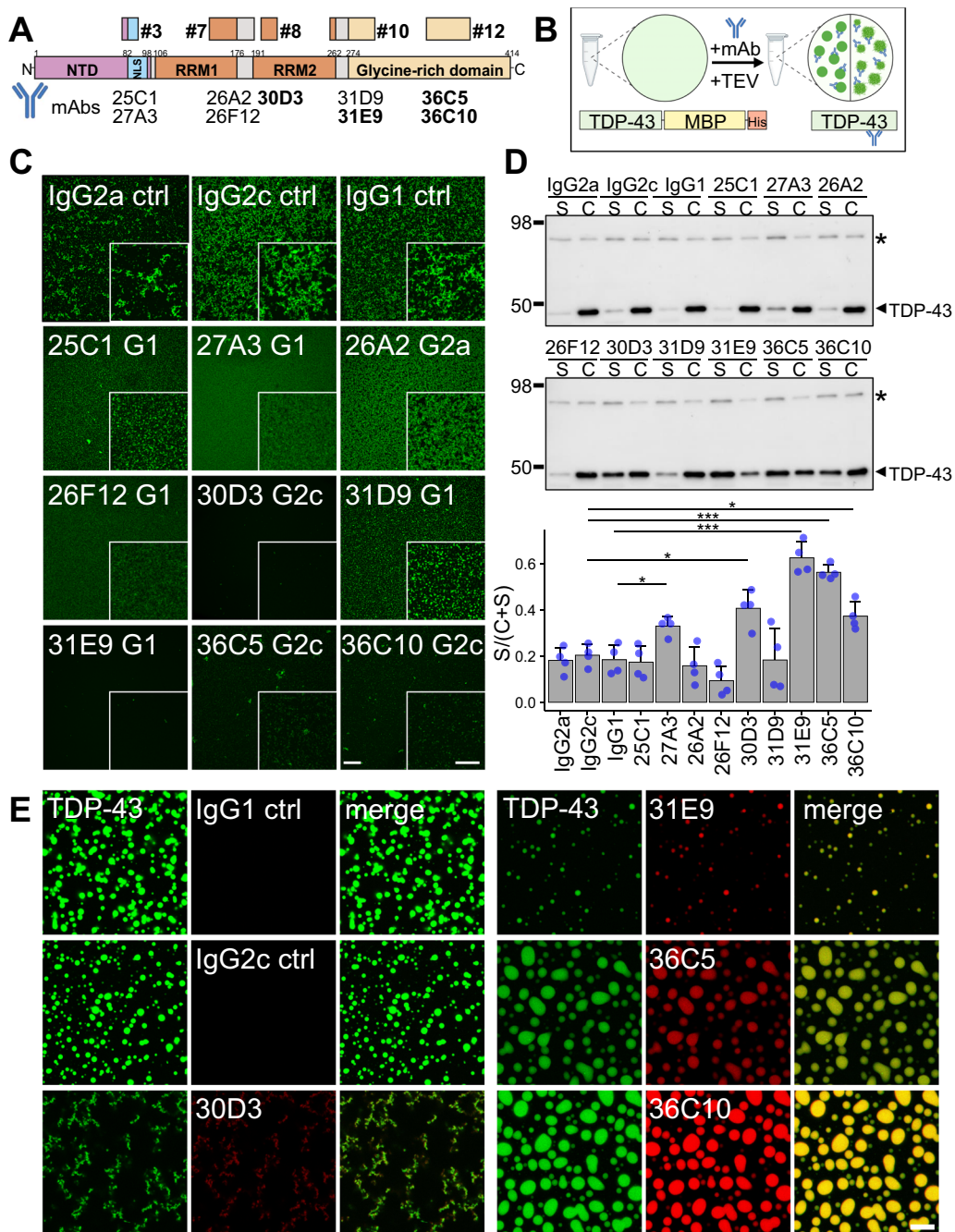


Fig. 7 (See legend on previous page.)

pool of TDP-43 mAbs (Additional file 1: Fig. S5B). The comparable affinity among these four antibodies suggests that the exact epitopes drive the differential effect on condensate morphology in Fig. 7E. As expected, these four mAbs stained nuclear TDP-43 and cytoplasmic aggregates in FTLN brains (Additional file 1: Fig. S5C). Together, our data suggest that TDP-43 peptides 8, 10, and 12 can induce potent antibodies capable of inhibiting

TDP-43 phase separation and aggregation in multiple *in vitro* assays.

mAbs targeting the C-terminal glycine-rich region inhibit cellular uptake of TDP-43 aggregates

Since inhibition of cell-to-cell transmission could slow the progression in TDP-43 proteinopathies, we

tested how the mAbs affect cellular uptake of TDP-43 aggregates.

Therefore, we established a flow-cytometry based assay using pHrodo-conjugated recombinant TDP-43, which shows increased fluorescence upon uptake in the endolysosomal compartment. To avoid interference of antibodies with aggregate formation, we induced aggregate formation of pHrodo-conjugated TDP-43-MBP-His₆ using TEV cleavage (for 30 min) and then incubated the samples with individual mAbs at equimolar ratios for additional 30 min before adding them to SH-SY5Y cells (Fig. 8A). Unlabeled TDP-43 and incubation at 22 °C to inhibit endocytosis served as negative controls. Importantly, we noticed significant uptake of preaggregated pHrodo-TDP-43 compared to the background defined by unlabeled TDP-43. Moreover, incubation at 22 °C reduced the signal nearly to the background level determined using unlabeled TDP-43 (Fig. 8B/C). To confirm the effects of mAbs on TDP-43 uptake we preincubated monomeric and aggregated TDP-43 with mAbs as described above. 31E9 and to a lesser extent 36C10 reduced the number of pHrodo-TDP-43-positive cells, while the moderate effect of 36C5 did not reach statistical significance. We did not observe substantial uptake of monomeric pHrodo-conjugated TDP-43-MBP-His₆, suggesting aggregation promotes cellular uptake.

Taken together, high-affinity antibodies targeting the RRM2 or the C-terminal low complexity domain potently suppress TDP-43 phase separation, aggregation, and cellular aggregate uptake, all processes implicated in TDP-43 proteinopathies.

Discussion

We used an active immunization approach in a fast-progressing murine model of ALS/FTD to target TDP-43 proteinopathy with antibodies *in vivo*. To this end, we systematically analyzed the immunogenicity, safety, and efficacy of predicted immunogenic regions covering all major domains of TDP-43. Only vaccinating with a C-terminal epitope containing the Ser409/410 phosphorylation sites significantly reduced serum NfL *in vivo*. By generating a panel of monoclonal antibodies, we identified several clones directed against the RRM2 and the glycine-rich domain that potently inhibited TDP-43 aggregation and phase separation *in vitro*, events tightly linked to neurodegeneration in ALS/FTD [3, 36].

TDP-43 mouse model

The inducible rNLS8 model mimics gain- and loss-of-function components of TDP-43 proteinopathies, reflected by prominent cytoplasmic aggregation and accompanying nuclear clearance of TDP-43 [56]. Although aged rNLS8 mice become symptomatic at a

similar time point after transgene induction as young rNLS8 mice, their disease progression is accelerated compared to young animals, resulting in a ~30% shorter lifespan [51]. In line with these findings, the lifetime of many proteins increases in the brains of old mice and aggregation-prone and low-complexity domain-harboring proteins, including TDP-43, are one of the most stabilized groups [23]. Based on our experience with anti-GA immunization [63], we had chosen a four-month immunization regimen to achieve high antibody titers, which required inducing the transgene in aged, fast-progressing rNLS8 mice. However, the anti-TDP-43 immune response already plateaued after two immunizations and future studies could be done in younger animals.

Moreover, immunofluorescence and transcriptomics revealed pronounced microgliosis by three weeks after transgene induction. In young animals, profound microgliosis has only been reported in the recovery stage, *i.e.*, after switching off transgene induction [50], while transcriptomic profiling suggested microglial activation in older animals already after inducing transgene expression, as seen in our hands [19]. Thus, aging may influence the microglial response to TDP-43 aggregation, which should be taken into account for future mouse studies of ALS/FTD. Therefore, analyzing the effects of TDP-43 immunotherapy in younger animals using passive immunization might reveal effects of the therapy masked by the aggressive progression of disease in aged rNLS8 mice.

As in previous reports, we used the rNLS8 model in a mixed genetic background resulting from crossing F1 C57BL/6J×C3H/HeJ hybrid parents [56], which may explain the large variance observed in transcriptome analysis even in the control groups. While principal component analysis could clearly separate rNLS8 mice from monogenic control mice, the remaining variance could not be explained by the antigen groups or gender. This high variability may explain why we could not detect a single gene that was significantly changed upon immunization after FDR correction, although transcriptome-wide expression differences show a subtle but significant rescue of transgene-induced changes. Backcrossing the rNLS8 line to an inbred genetic background may reduce variability and thus increase statistical power in future therapeutic studies. Indeed, rNLS8 mice on a pure C57Bl/6Jausb background were used in a recent study and found to be phenotypically consistent with the originally described mixed background mice [56, 62].

Safety and immunogenicity of TDP-43 peptide antigens

TDP-43 is a potentially risky drug target because its nuclear levels need to be maintained in a narrow range and it is required for regular cellular function in all cell types [6, 42]. In our immunization regimen, only the

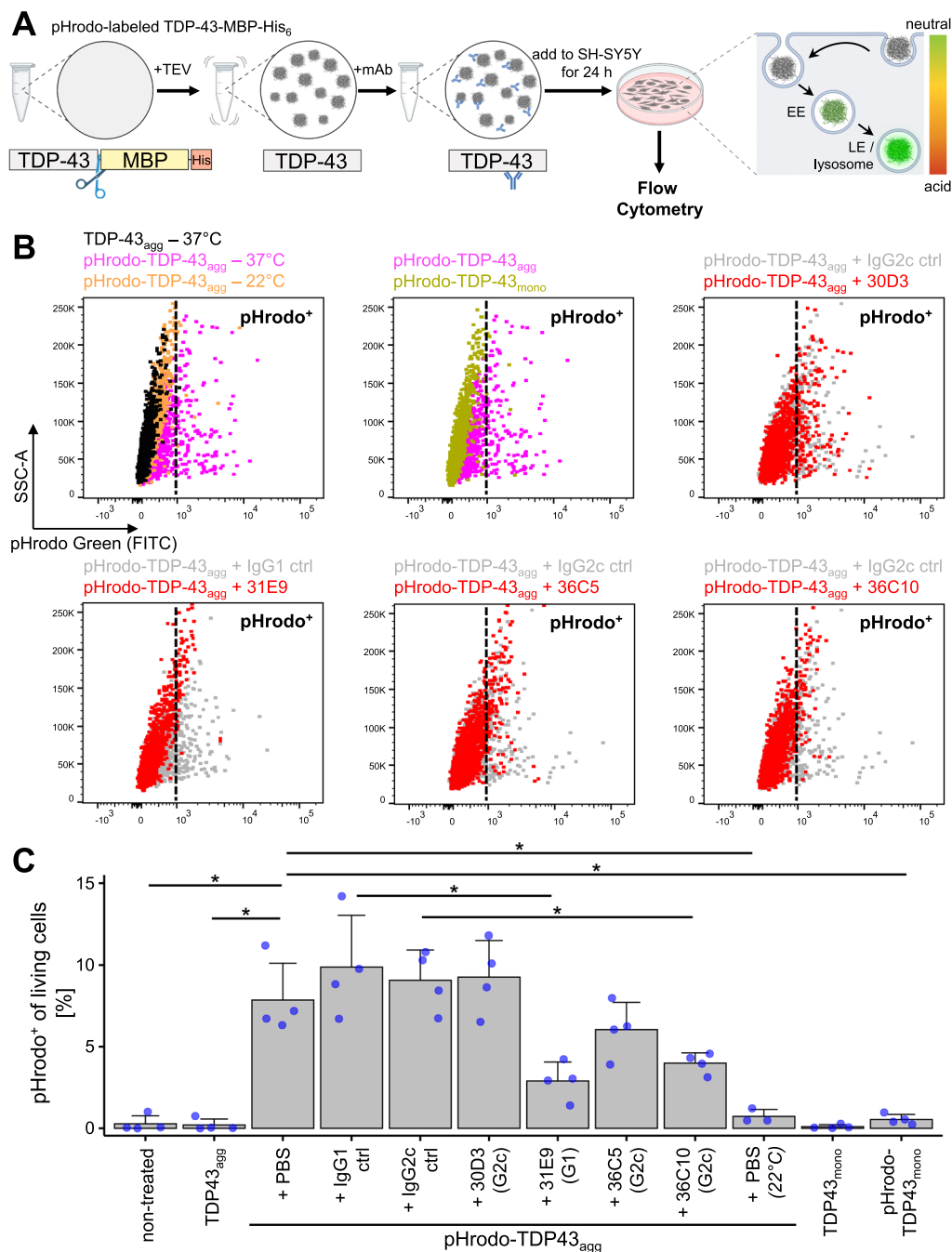


Fig. 8 TDP-43 mAbs suppress cellular uptake of recombinant TDP-43 aggregates. **A** Overview of TDP-43 uptake assay. Aggregation of pHrodo Green-labeled TDP-43-MBP-His₆ was induced by TEV protease cleavage and thorough shaking for 30 min, followed by a 2 h incubation step at room temperature. Preformed aggregates were then incubated with mAbs for 30 min before addition to SH-SY5Y cells. Upon cellular uptake via endocytosis, the pHrodo-tagged aggregates show increased fluorescence in acidic compartments, such as early endosomes (EE), and, even more so, in late endosomes (LE) or lysosomes. After 24 h of incubation, pHrodo fluorescence was analyzed by flow cytometry in the FITC channel. **B** Representative flow cytometry dot plots showing uptake of pHrodo-TDP-43_{agg} in combination with different control or TDP-43 specific mAbs in SH-SY5Y cells. Data are shown as relative fluorescence in the FITC channel (x-axis) and side scatter (SSC-A, y-axis). Relevant comparisons are overlaid. Cells were pregated to identify live singlets (not shown). Vertical dotted lines indicate gating for pHrodo⁺ live singlets. **C** Quantification of TDP-43 aggregate uptake in SH-SY5Y cells, measured as percentage of pHrodo-positive cells of total live single cells. Bar graphs represent mean + SD from n = 3–4 independent experiments. The following comparisons revealed statistically significant differences after pairwise t-test with Benjamini–Hochberg correction: pHrodo-TDP-43_{agg} + IgG1 ctrl vs. pHrodo-TDP-43_{agg} + 31E9 (G1): $p = 0.037$; pHrodo-TDP-43_{agg} + IgG2c ctrl vs. pHrodo-TDP-43_{agg} + 36C10 (G2c): $p = 0.023$; non-treated vs. pHrodo-TDP-43_{agg}: $p = 0.023$; pHrodo-TDP-43_{mono} vs. pHrodo-TDP-43_{agg}: $p = 0.023$; TDP-43_{agg} vs. pHrodo-TDP-43_{agg}: $p = 0.023$; pHrodo-TDP-43_{agg} vs. pHrodo-TDP-43_{agg} (22 °C): $p = 0.023$

phospho-peptide (#15) induced disease-specific antibodies, while even the aggregated peptide antigens (peptides 7, 8, 10) induced antibodies detecting physiological TDP-43 in the nucleus. Moreover, five peptide antigens (5, 7, 8, 11, and 12) are not fully conserved between human and mouse TDP-43 and may have induced antibodies preferentially targeting human TDP-43 but sparing mouse TDP-43, as it has been observed for mAbs [24]. Thus, the residual expression of endogenous mouse TDP-43 together with the human transgene in rNLS8 mice may occlude potential loss-of-function toxicity induced by these antibodies in cells expressing only human TDP-43.

While most screened peptide antigens induced detectable antibody response in C57BL/6J mice, we noticed striking differences in the antibody titer unrelated to the peptide length. Thus, we used only the most immunogenic peptides from our pilot study for therapeutic studies in rNLS8 mice. To our surprise, we noticed unexpected toxicity for the highly immunogenic N-terminal TDP-43 peptides 1 and 3 in the mixed C57BL/6J×C3H/HeJ background in contrast to the pilot study in C57BL/6J mice. As most of the TDP1+3 animals unexpectedly died or had to be sacrificed shortly after the second or third immunization, we suspect that an anaphylactic reaction or local intraperitoneal toxicity occurred, rather than on-target toxicity due to gradually accumulating TDP-43 antibodies interfering with endogenous TDP-43 function. Interestingly, C3H/HeJ mice (but not the otherwise genetically similar C3H/HeOuJ strain) carry a loss-of-function mutation in *Tlr4*, the receptor for bacterial lipopolysaccharide. Loss of *Tlr4* has been discussed as a cause for stronger anaphylactic response to peanut antigen in C3H/HeJ mice compared to C3H/HeOuJ and Balb/c mice [8], but other genetic differences in the mixed C57BL/6J×C3H/HeJ background may also promote anaphylaxis towards peptides 1+3 in this model. Although we cannot fully explain the different safety profiles in these lines, our findings highlight the importance of considering genetic background-specific variations for preclinical trials in rodent models.

Efficacy of TDP-43 active vaccination

To investigate the efficacy of anti-TDP-43 vaccination, we analyzed body weight, pTDP-43 levels, and serum NfL levels, a widely used clinical biomarker for neuroaxonal damage. While we did not observe beneficial effects on weight loss and pTDP-43 levels, immunization with the disease-associated C-terminal phospho-TDP-43 epitope significantly reduced NfL levels. These findings support the disease-promoting role of TDP-43 phosphorylation at serines 409/410, although the effects of C-terminal phosphorylation on TDP-43's biophysical properties are controversially debated based on in vitro data [2, 16, 43].

We also investigated altered neuroinflammation upon vaccination, because microglia are emerging as key modulators in multiple neurodegenerative diseases, including TDP-43 proteinopathies [58], and active vaccination targeting poly-GA in our *C9orf72* ALS model affected microglia activation more than poly-GA levels [63]. While anti-TDP-43 immunized mice still showed pronounced microgliosis and astrogliosis as well as elevated chemokine levels, transcriptomics revealed a small overall reduction of the disease signature.

One postulated mode of action for antibody-based therapy is the prevention of cell-to-cell propagation of transmissible species of aggregation-prone proteins. Transmission has been extensively shown for proteins implicated in various neurodegenerative diseases, including Tau, α -synuclein, and for TDP-43 [9, 15, 39, 43]. Interestingly, two mAbs targeting the C-terminal domain efficiently prevented cellular uptake of preformed TDP-43 aggregates in neuron-like cells. A possible explanation for the modest effect of TDP-43 vaccination in rNLS8 mice may be the high and widespread deposition of TDP-43 aggregates in this model, which clearly exceeds the pathology in human ALS/FTD and cannot recapitulate focal onset and spreading of TDP-43 pathology across different brain regions over time [9, 48]. Since 95% of neurons in cortical layer 5 are found to be hTDP-43-positive already one week after transgene induction [56], it seems unlikely that spreading of TDP-43 species plays a dominant role in pathogenesis in the rNLS8 mouse model and therefore therapeutic antibodies cannot counteract this process. Very recently, systemic administration of a mAb targeting the C-terminal domain of TDP-43 was shown to reduce pTDP-43 levels and microgliosis in rNLS8 mice and neuron loss using the slower-progressing Camk2a-tTA model [1]. Previously, AAV-based expression or intrathecal injection of TDP-43 antibodies could ameliorate phenotypes in a BAC-transgenic TDP-43 mouse model but this model has a far slower progression with less abundant TDP-43 pathology than the rNLS8 mice [44, 45].

mAbs can inhibit key disease features of TDP-43 in vitro

As passive antibody therapy may overcome weak immunogenicity of crucial epitopes and avoid acute toxicity, we generated a large panel of monoclonal TDP-43 antibodies targeting several of our selected epitopes. Four out of nine novel high-affinity antibodies targeting RRM2 (peptide 8, amino acids 198–211), the C-terminal glycine-rich region (peptide 12, aa. 342–379) or the linking region (peptide 10, aa. 258–296) strongly inhibited aggregation and altered phase separation of recombinant TDP-43 in different assays, while antibodies binding TDP-43 further N-terminal were less effective. These findings are consistent with the dominant role of the C-terminal glycine-rich domain

in driving phase separation and aggregation of TDP-43 [7, 11, 13, 17]. A recent cryo-electron microscopy structure of TDP-43 aggregates extracted from ALS/FTD cortices revealed an ordered filament core comprised of aa. 282–360 [4], highlighting the importance of this glycine (G), glutamine (Q), and asparagine (N)-rich region for pathological TDP-43 aggregation. The significance of the Q/N-rich region (within the glycine-rich domain) for TDP-43 aggregation is further emphasized by the finding that tandem repeats of residues 331–369 trigger the formation of phosphorylated and ubiquitinated TDP-43 aggregates in cultured cells [10]. The overlap of our peptides 10 (aa. 258–296) and 12 (aa. 342–379) with these regions possibly explains the extraordinary aggregation-suppressing effect of the monoclonal antibodies raised against these regions.

Interestingly, antibodies targeting the glycine-rich region either resulted in the formation of much smaller and fewer TDP-43 condensates (31E9) or caused the formation of larger liquid-like droplets enriched in anti-TDP-43 antibodies (36C5 and 36C10), reminiscent of the phase separation behavior of a TDP-43 mutant containing multiple phospho-mimetic substitutions in the C-terminal domain [16]. Collectively, these findings suggest that disturbing the self-self-interaction of the C-terminal low complexity domain, either by hyperphosphorylation or high-affinity antibodies, suppresses both TDP-43 phase separation and aggregation, thereby supporting the fundamental role of TDP-43 C-terminal region for these processes.

Moreover, we show that aggregated TDP-43 is preferentially taken up by neuron-like cells compared to monomeric TDP-43, which can be blocked efficiently by two mAbs targeting the C-terminal domain (31E9 and 36C10), but not by 30D3 targeting the RRM2 domain. Interestingly, Afroz et al. show that a mAb targeting the C-terminal domain can inhibit seeding from patient material, promote phagocytic clearance by microglia and inhibit aggregate formation *in vitro* [1], but they have not analyzed effects on phase separation or neurofilament levels. Together with our findings, these data highlight the importance of the C-terminal region in the process of cell-to-cell transmission of aggregates.

Conclusions

Taken together, we addressed efficacy and safety risks of TDP-43 immunotherapy for ALS/FTD by unbiased epitope screening *in vitro* and *in vivo*. We identified several highly immunogenic peptides in TDP-43 and raised a panel of novel mAbs potentially useful for therapy. Despite concerns about on-target toxicity of anti-TDP-43 antibodies due to the essential role of TDP-43 for cellular survival, we only detected unexpected safety risks of highly immunogenic N-terminal peptides, presumably due to anaphylaxis in one of four genetic backgrounds

tested. In a fast-progressing TDP-43 mouse model, targeting the glycine-rich domain was most beneficial and partially rescued the disease signature detected by transcriptomics. While none of the antigens reduced the effect on neuropathology and the characteristic body weight loss, vaccination with a peptide including the disease-associated pS409/410 site significantly reduced NfL levels, the gold standard biomarker for ALS progression. Moreover, we identified mAbs targeting the glycine-rich domain that efficiently block disease-related phase separation and aggregation of TDP-43 *in vitro*, and suppress aggregate uptake in cells. Spreading and seeding of TDP-43 are crucial for the clinical progression of ALS after focal onset, but we assume it may be less relevant in the fast-progressing rNLS8 mice with widespread neuronal protein expression. Our finding that mAbs can alter the phase separation properties of a disease-linked protein, establishes a new mode of action for antibody therapy. Our study suggests that targeting the glycine-rich domain with antibodies ameliorates key pathomechanisms of TDP-43 proteinopathies.

Abbreviations

ALS	Amyotrophic lateral sclerosis
FTD	Frontotemporal dementia
FTLD-TDP	Frontotemporal lobar degeneration with TDP-43 inclusions
rNLS8 mice	'Regulatable' or NEFH-tTA/tetO-hTDP-43ΔNLS bigenic mice
mAb	Monoclonal antibody
CNS	Central nervous system
Aβ	Amyloid beta
RRM1/2	RNA recognition motif 1/2
NLS	Nuclear localization sequence
NTD	N-terminal domain
LLPS	Liquid–liquid phase separation
scFv	Single-chain variable fragment
pTDP-43	TDP-43 phosphorylated at serines 409/410
i.p.	Intraperitoneally
s.c.	Subcutaneously
NfL	Neurofilament light chain
OVA	Ovalbumin
CSF	Cerebrospinal fluid
MBP	Maltose-binding protein
LPS	Lipopolysaccharide
RT	Room temperature
OD	Optical density
DOX	Doxycycline
ctrl	Control
Mctx	Motor cortex
SC	Spinal cord

Supplementary Information

The online version contains supplementary material available at <https://doi.org/10.1186/s40478-023-01592-z>.

Additional file 1: Figure S1. TDP-43 epitopes and preimmune control serum. A: Overview of peptide antigens conjugated with ovalbumin through the N-terminal cysteine residue. Note that OVA conjugates of peptides 7, 8, 10, and 11 showed some aggregation *in vitro*. Peptides in bold were highly immunogenic in C57BL/6J wild-type mice and were thus used for the treatment study in rNLS8 mice. Novel monoclonal antibodies were raised in C57BL/6J mice, except of 26A2 and 26F12,

which were generated from immunized Balb/c mice. B: Preimmune serum contains no detectable antibodies against human recombinant TDP-43 or pTDP-43 peptide as determined by ELISA. Background-corrected mean optical density at 450 nm was measured in duplicates per animal. All sera were diluted 1:100. **Figure S2.** Combined TDP-43 peptides are equally immunogenic and safe in three inbred mouse strains. Antibody response plateaus already after two immunizations. A: Timeline of immunization with pooled TDP-43 peptides, blood sampling, and body weight measurement of C57BL/6J, C3H/HeOJ, and CD-1 mice. For each strain, six animals per treatment group were used. B: A dilution series of pooled sera was analyzed by ELISA against recombinant full-length TDP-43 or pTDP-43 peptide. Background-corrected mean OD450 was measured in duplicates. Triangular shapes indicate CD-1, circles represent C57BL/6J, and squares depict C3H/HeOJ animals. Open shapes correspond to first blood sampling, while b2 is illustrated by filled shapes. C: Kaplan–Meier plot indicating survival probability of mice from different strains. No antigen combination caused statistically significant lethality in any of the strains investigated. D: Development of body weight over 14-week study period. Mean values are plotted group-wise. Only age, but not treatment or the interaction between treatment and age, had a statistically significant effect on the body weight as revealed by a two-way repeated measures ANOVA. C57BL/6J: $p = 1.74 \times 10^{-24}$; C3H/HeOJ: $p = 2.56 \times 10^{-33}$; CD-1: $p = 1.37 \times 10^{-29}$. E: Dilution series of pooled rNLS8 sera from different time points were analyzed by ELISA against recombinant full-length TDP-43 or pTDP-43 peptide. Background-corrected mean OD450 was measured in duplicates. Note that the antibody response plateaued after two immunizations. Age of animals is annotated for each timepoint. **Figure S3.** Additional immunofluorescence stainings of pooled antisera confirm specificity towards nuclear and mislocalized TDP-43. Double immunofluorescence stainings of pooled antisera and with either phosphorylated TDP-43 or pan-TDP-43 were performed on frontal cortex sections of an FTLD case and a healthy control. A: Antisera from TDP1 + 3# and TDP10 + 12 animals reliably stained nuclear TDP-43 but no cytoplasmic inclusions in a control case negative for pTDP-43. B: Double immunofluorescence with a commercial TDP-43 antibody validates specificity of pooled antisera in patients. Antisera from TDP1 + 3# and TDP10 + 12 mice detected both nuclear and cytoplasmic TDP-43, while TDP15 sera showed strong preference for cytoplasmic TDP-43 with little affinity to nuclear TDP-43. Representative images are shown. All scale bars = 10 μ m. **Figure S4.** Additional comparisons of gene expression profiles and cytokine assays in rNLS8 mice. A: Expression patterns of genes characterizing early, late, and recovery stage in isolated microglia [19] in rNLS8 mice/ALS patients. Asterisks denote significant changes. LFC: log₂-fold change. B: Concordant gene expression changes between rNLS8 mice and ALS patients. Only statistically significant genes with a LFC value ≥ 1 are shown. The 27 genes upregulated in both conditions cluster into different GO categories as depicted in Fig. 6C. C: Cytokine levels determined by multiplex assay from cortical tissue of vaccinated rNLS8 mice and controls as in Fig. 6E. Non-affected analytes are shown. From the panel INF- γ , IL-2, IL-4, IL-10, IL-12p70 could not be detected at all. IL-5 and IL-6: Control PBS n = 6, ctrl VAX n = 6, TDP-PBS n = 10, TDP5 + 7 n = 6, TDP8 + 9 n = 9, TDP10 + 12 n = 9, and TDP15 n = 7; IL-9, IL-15, IL-17A/F, IL-27p28/IL-30, IL-33, and MIP-2: Control PBS n = 10, ctrl VAX n = 10, TDP-PBS n = 10, TDP5 + 7 n = 13, TDP8 + 9 n = 12, TDP10 + 12 n = 12, and TDP15 n = 12. MIP-2 levels were only statistically significantly elevated in TDP-PBS compared to ctrl PBS mice ($p = 0.004$), but not ctrl VAX mice as indicated by pairwise t-test with Benjamini–Hochberg correction. D: RNAseq-based gene expression of all detected cytokines from the cytokine/chemokine panel in rNLS8 mice and ALS patients compared to controls as in Fig. 6A. Asterisks denote significant changes. **Figure S5.** Characterization of TDP-43 mAbs on droplet formation, affinity, and patient inclusions. A: Representative time-lapse images of Alexa 488-labeled TDP-43 condensates obtained by spinning disc confocal microscopy. TDP-43 treated with isotype control antibody does not fuse, while mAbs targeting the C-terminal glycine-rich region increase droplet mobility, leading to slow fusion events and enlarged TDP-43 droplets. Scale bar = 2.5 μ m. B: Novel TDP-43 mAbs were analyzed by ELISA against recombinant TDP-43 in dilution series. Background-corrected OD450 are shown. C: mAbs which most potently inhibited TDP-43 aggregation and LLPS detected pTDP-43-positive inclusions in a FTLD patient and additionally stained nuclear TDP-43 by immunofluorescence.

Additional file 2: Table S1. Differential expression analysis of control PBS, TDP-PBS, TDP10+12, and TDP15 neocortex using DESeq2 as described in the methods. Samples are compared to either ctrl PBS or TDP-PBS. In column D “-1” and “+1” indicate significant genes and the direction of change.

Additional file 3: Table S2. Full Gene Ontology enrichment analysis for differentially expressed genes from TargetALS patients in spinal cord and genes expressed in rNLS8 mice, each both compared to non-diseased controls. Selected data are shown in Fig. 6C.

Acknowledgements

We thank Jürgen Bernhagen and Bettina Schmid for critical comments to the manuscript. Christian Haass provided the Simoa™ platform for serum NFL measurements. We thank the Mikael Simons laboratory, Sarah Jäkel, and Charlene Hurler for providing and assisting with the PANNORAMIC digital slide scanner. We acknowledge support from the Microscopy Core Facility of IMB Mainz. BioRender (<https://app.biorender.com/>) was used to create Figures 7B and 8A.

Author contributions

HR performed, analyzed and interpreted animal and most in vitro experiments with help from FS, SH, DF, MM, BN, LAGS and QZ. EK prescreened novel monoclonal TDP-43 antibodies and acquired the cytokine data. US conducted and analyzed the pTDP-43 immunoassay. SR and AL helped acquiring and analyzing flow cytometry data. MKS performed automated IHC stainings. AF, AS and RF generated novel monoclonal TDP-43 antibodies. TK contributed to the conception of the study. TA and JH provided human tissue and supervised neuropathological analysis. TFG supervised and interpreted pTDP-43 immunoassays. DD supervised and interpreted in vitro experiments. DE designed, supervised and interpreted the study and helped with data analysis. DE wrote the manuscript with input from all other authors. All authors read and approved the final manuscript.

Funding

Open Access funding enabled and organized by Projekt DEAL. This work was supported by NOMIS foundation (DE). We acknowledge funding from the Deutsche Forschungsgemeinschaft (DFG, German Research Foundation) SyNergy EXC 2145 – 390857198 (JH, DD, RF and DE), Emmy Noether and Heisenberg programmes (DO1804/1-2; DO1804/5-1 to DD), priority programme SPP2191 (project ID 402723784 to DD) and the Hans and Ilse Breuer Foundation Alzheimer Research Award (DD).

Availability of data and materials

All data supporting the conclusions of this article are included within the article and its supplementary materials. The raw data for the transcriptomics analysis are available under the GEO accession code GSE233669.

Declarations

Ethics approval and consent to participate

All animal procedures were performed according to institutional guidelines approved by the governmental ethics committee of Upper Bavaria (licenses TV 55.2–2532.Vet_02-17–106 and TV 55.2–2532.Vet_03-17–68). Use of human tissue was approved by the LMU ethics committee (#18–899).

Consent for publication

Not applicable.

Competing interests

The authors declare that they have no competing interests.

Author details

¹German Center for Neurodegenerative Diseases (DZNE), Munich, Feodor-Lynen-Str. 17, 81377 Munich, Germany. ²Munich Cluster of Systems Neurology (SyNergy), Feodor-Lynen-Str. 17, 81377 Munich, Germany. ³Ludwig-Maximilians-Universität (LMU) Munich, Graduate School of Systemic Neurosciences (GSN), 81377 Munich, Germany. ⁴Institute for Stroke and Dementia Research (ISD), University Hospital, LMU Munich, Feodor-Lynen-Str. 17,

81377 Munich, Germany. ⁵Institute of Molecular Physiology, Faculty of Biology, Johannes Gutenberg-Universität (JGU), Hanns-Dieter-Hüsch-Weg 17, 55128 Mainz, Germany. ⁶Department of Neuroscience, Mayo Clinic, 4500 San Pablo Road, Jacksonville, FL 32224, USA. ⁷Mayo Clinic Graduate School of Biomedical Sciences, Mayo Clinic, Jacksonville, FL 32224, USA. ⁸Chair of Metabolic Biochemistry, Biomedical Center (BMC), Faculty of Medicine, Ludwig-Maximilians-Universität (LMU) Munich, Feodor-Lynen-Str. 17, 81377 Munich, Germany. ⁹Center for Neuropathology and Prion Research, University Hospital, LMU Munich, Feodor-Lynen-Str. 23, 81377 Munich, Germany. ¹⁰Monoclonal Antibody Core Facility, Helmholtz Zentrum München, German Research Center for Environmental Health (GmbH), Ingolstädter Landstr. 1, 85764 Neuherberg, Germany. ¹¹Friedrich Baur Institute at the Department of Neurology, University Hospital, LMU Munich, Ziemssenstr. 1a, 80336 Munich, Germany. ¹²Department of Psychiatry and Psychotherapy, University Hospital, LMU Munich, Nußbaumstr. 7, 80336 Munich, Germany. ¹³Institute of Molecular Biology (IMB), Ackermannweg 4, 55128 Mainz, Germany.

Received: 11 March 2023 Accepted: 31 May 2023

Published online: 11 July 2023

References

- Afroz T, Chevalier E, Audrain M, Dumayne C, Ziehm T, Moser R, Egesipe AL, Mottier L, Ratnam M, Neumann M et al (2023) Immunotherapy targeting the C-terminal domain of TDP-43 decreases neuropathology and confers neuroprotection in mouse models of ALS/FTD. *Neurobiol Dis* 179:106050. <https://doi.org/10.1016/j.nbd.2023.106050>
- Aikio M, Wobst HJ, Odeh HM, Lee BL, Class B, Ollerhead TA, Mack KL, Ford AF, Barbieri EM, Cupo R et al (2021) Opposing roles of p38 α -mediated phosphorylation and arginine methylation in driving TDP-43 proteinopathy. *bioRxiv*: 2021.2008.2004.455154. <https://doi.org/10.1101/2021.08.04.455154>
- Alberti S, Dormann D (2019) Liquid-liquid phase separation in disease. *Annu Rev Genet* 53:171–194. <https://doi.org/10.1146/annurev-genet-112618-043527>
- Arseni D, Hasegawa M, Murzin AG, Kametani F, Arai M, Yoshida M, Ryskeldi-Falcon B (2021) Structure of pathological TDP-43 filaments from ALS with FTL. *Nature*. <https://doi.org/10.1038/s41586-021-04199-3>
- Arseni D, Hasegawa M, Murzin AG, Kametani F, Arai M, Yoshida M, Ryskeldi-Falcon B (2022) Structure of pathological TDP-43 filaments from ALS with FTL. *Nature* 601:139–143. <https://doi.org/10.1038/s41586-021-04199-3>
- Ayala YM, De Conti L, Avendano-Vazquez SE, Dhir A, Romano M, D'Ambrogio A, Tollervy J, Ule J, Baralle M, Buratti E et al (2011) TDP-43 regulates its mRNA levels through a negative feedback loop. *EMBO J* 30:277–288. <https://doi.org/10.1038/emboj.2010.310>
- Babinchak WM, Haider R, Dumm BK, Sarkar P, Surewicz K, Choi JK, Surewicz WK (2019) The role of liquid-liquid phase separation in aggregation of the TDP-43 low-complexity domain. *J Biol Chem* 294:6306–6317. <https://doi.org/10.1074/jbc.RA118.007222>
- Berin MC, Zheng Y, Domaradzki M, Li XM, Sampson HA (2006) Role of TLR4 in allergic sensitization to food proteins in mice. *Allergy* 61:64–71. <https://doi.org/10.1111/j.1398-9995.2006.01012.x>
- Bretschneider J, Del Tredici K, Lee VM, Trojanowski JQ (2015) Spreading of pathology in neurodegenerative diseases: a focus on human studies. *Nat Rev Neurosci* 16:109–120. <https://doi.org/10.1038/nrn3887>
- Budini M, Buratti E, Stuani C, Guarnaccia C, Romano V, De Conti L, Baralle FE (2012) Cellular model of TAR DNA-binding protein 43 (TDP-43) aggregation based on its C-terminal Gln/Asn-rich region. *J Biol Chem* 287:7512–7525. <https://doi.org/10.1074/jbc.M111.288720>
- Cao Q, Boyer DR, Sawaya MR, Ge P, Eisenberg DS (2019) Cryo-EM structures of four polymorphic TDP-43 amyloid cores. *Nat Struct Mol Biol* 26:619–627. <https://doi.org/10.1038/s41594-019-0248-4>
- Chiang PM, Ling J, Jeong YH, Price DL, Aja SM, Wong PC (2010) Deletion of TDP-43 down-regulates Tbc1d1, a gene linked to obesity, and alters body fat metabolism. *Proc Natl Acad Sci USA* 107:16320–16324. <https://doi.org/10.1073/pnas.1002176107>
- Conicella AE, Dignon GL, Zerze GH, Schmidt HB, D'Ordine AM, Kim YC, Rohatgi R, Ayala YM, Mittal J, Fawzi NL (2020) TDP-43 alpha-helical structure tunes liquid-liquid phase separation and function. *Proc Natl Acad Sci USA*. <https://doi.org/10.1073/pnas.1912055117>
- French RL, Grese ZR, Aligredy H, Dhavale DD, Reeb AN, Kedia N, Kotzbauer PT, Bieschke J, Ayala YM (2019) Detection of TAR DNA-binding protein 43 (TDP-43) oligomers as initial intermediate species during aggregate formation. *J Biol Chem* 294:6696–6709. <https://doi.org/10.1074/jbc.RA118.005889>
- Furukawa Y, Kaneko K, Watanabe S, Yamanaka K, Nukina N (2011) A seeding reaction recapitulates intracellular formation of Sarkosyl-insoluble transactivation response element (TAR) DNA-binding protein-43 inclusions. *J Biol Chem* 286:18664–18672. <https://doi.org/10.1074/jbc.M111.231209>
- Grujic da Silva LA, Simonetti F, Hutten S, Riemenschneider H, Sternburg EL, Pietrek LM, Gebel J, Dotsch V, Edbauer D, Hummer G et al (2022) Disease-linked TDP-43 hyperphosphorylation suppresses TDP-43 condensation and aggregation. *EMBO J* 41:e108443. <https://doi.org/10.15252/embj.2021108443>
- Guenther EL, Cao Q, Trinh H, Lu J, Sawaya MR, Cascio D, Boyer DR, Rodriguez JA, Hughes MP, Eisenberg DS (2018) Atomic structures of TDP-43 LCD segments and insights into reversible or pathogenic aggregation. *Nat Struct Mol Biol* 25:463–471. <https://doi.org/10.1038/s41594-018-0064-2>
- Hasegawa M, Arai T, Nonaka T, Kametani F, Yoshida M, Hashizume Y, Beach TG, Buratti E, Baralle M, Morita M et al (2008) Phosphorylated TDP-43 in frontotemporal lobar degeneration and amyotrophic lateral sclerosis. *Ann Neurol* 64:60–70. <https://doi.org/10.1002/ana.21425>
- Hunter M, Spiller KJ, Dominique MA, Xu H, Hunter FW, Fang TC, Canter RG, Roberts CJ, Ransohoff RM, Trojanowski JQ et al (2021) Microglial transcriptome analysis in the rNLS8 mouse model of TDP-43 proteinopathy reveals discrete expression profiles associated with neurodegenerative progression and recovery. *Acta Neuropathol Commun* 9:140. <https://doi.org/10.1186/s40478-021-01239-x>
- Hutten S, Usluer S, Bourgeois B, Simonetti F, Odeh HM, Fare CM, Czuppa M, Hruska-Plochan M, Hofweber M, Polyimenidou M et al (2020) Nuclear import receptors directly bind to arginine-rich dipeptide repeat proteins and suppress their pathological interactions. *Cell Rep* 33:108538. <https://doi.org/10.1016/j.celrep.2020.108538>
- Joly-Amado A, Davtyan H, Serraneau K, Jules P, Zitnyar A, Pressman E, Zagorski K, Antonyan T, Hovakimyan A, Paek HJ et al (2020) Active immunization with tau epitope in a mouse model of tauopathy induced strong antibody response together with improvement in short memory and pSer396-tau pathology. *Neurobiol Dis* 134:104636. <https://doi.org/10.1016/j.nbd.2019.104636>
- Khalil M, Teunissen CE, Otto M, Piehl F, Sormani MP, Gatteringer T, Barro C, Kappos L, Comabella M, Fazekas F et al (2018) Neurofilaments as biomarkers in neurological disorders. *Nat Rev Neurol* 14:577–589. <https://doi.org/10.1038/s41582-018-0058-z>
- Cluever V, Russo B, Mandad S, Kumar NH, Alevra M, Ori A, Rizzoli SO, Urlaub H, Schneider A, Fornasiero EF (2022) Protein lifetimes in aged brains reveal a proteostatic adaptation linking physiological aging to neurodegeneration. *Sci Adv* 8:eabn4437. <https://doi.org/10.1126/sciadv.abn4437>
- Kwong LK, Irwin DJ, Walker AK, Xu Y, Riddle DM, Trojanowski JQ, Lee VM (2014) Novel monoclonal antibodies to normal and pathologically altered human TDP-43 proteins. *Acta Neuropathol Commun* 2:33. <https://doi.org/10.1186/2051-5960-2-33>
- LaClair KD, Zhou Q, Michaelsen M, Wefers B, Brill MS, Janjic A, Rathkolb B, Farny D, Cygan M, de Angelis MH et al (2020) Congenic expression of poly-GA but not poly-PR in mice triggers selective neuron loss and interferon responses found in C9orf72 ALS. *Acta Neuropathol* 140:121–142. <https://doi.org/10.1007/s00401-020-02176-0>
- Li Q, Babinchak WM, Surewicz WK (2021) Cryo-EM structure of amyloid fibrils formed by the entire low complexity domain of TDP-43. *Nat Commun* 12:1620. <https://doi.org/10.1038/s41467-021-21912-y>
- Ling SC, Polyimenidou M, Cleveland DW (2013) Converging mechanisms in ALS and FTD: disrupted RNA and protein homeostasis. *Neuron* 79:416–438. <https://doi.org/10.1016/j.neuron.2013.07.033>
- Love MI, Huber W, Anders S (2014) Moderated estimation of fold change and dispersion for RNA-seq data with DESeq2. *Genome Biol* 15:550. <https://doi.org/10.1186/s13059-014-0550-8>

29. Mackenzie IR, Arzberger T, Kremmer E, Troost D, Lorenzl S, Mori K, Weng SM, Haass C, Kretzschmar HA, Edbauer D et al (2013) Dipeptide repeat protein pathology in C9orf72 mutation cases: clinico-pathological correlations. *Acta Neuropathol* 126:859–879. <https://doi.org/10.1007/s00401-013-1181-y>
30. Mackenzie IR, Rademakers R, Neumann M (2010) TDP-43 and FUS in amyotrophic lateral sclerosis and frontotemporal dementia. *Lancet Neurol* 9:995–1007. [https://doi.org/10.1016/S1474-4422\(10\)70195-2](https://doi.org/10.1016/S1474-4422(10)70195-2)
31. Mandegar MA, Huebsch N, Frolov EB, Shin E, Truong A, Olvera MP, Chan AH, Miyaoka Y, Holmes K, Spencer CI et al (2016) CRISPR interference efficiently induces specific and reversible gene silencing in human iPSCs. *Cell Stem Cell* 18:541–553. <https://doi.org/10.1016/j.stem.2016.01.022>
32. Martinez-Gonzalez L, Rodriguez-Cueto C, Cabezudo D, Bartolome F, Andres-Benito P, Ferrer I, Gil C, Martin-Requero A, Fernandez-Ruiz J, Martinez A et al (2020) Motor neuron preservation and decrease of in vivo TDP-43 phosphorylation by protein CK-1 delta kinase inhibitor treatment. *Sci Rep* 10:4449. <https://doi.org/10.1038/s41598-020-61265-y>
33. McEwan WA, Falcon B, Vaysburd M, Clift D, Oblak AL, Ghetti B, Goedert M, James LC (2017) Cytosolic Fc receptor TRIM21 inhibits seeded tau aggregation. *Proc Natl Acad Sci USA* 114:574–579. <https://doi.org/10.1073/pnas.1607215114>
34. Mortada I, Farah R, Nabha S, Ojcius DM, Fares Y, Almawi WY, Sadier NS (2021) Immunotherapies for neurodegenerative diseases. *Front Neurol* 12:6539. <https://doi.org/10.3389/fneur.2021.654739>
35. Mukadam AS, Miller LVC, Smith AE, Vaysburd M, Sakya SA, Sanford S, Keeling S, Tuck BJ, Katsinelos T, Green C et al (2023) Cytosolic antibody receptor TRIM21 is required for effective tau immunotherapy in mouse models. *Science* 379:1336–1341. <https://doi.org/10.1126/science.abn1366>
36. Nedelsky NB, Taylor JP (2019) Bridging biophysics and neurology: aberrant phase transitions in neurodegenerative disease. *Nat Rev Neurol* 15:272–286. <https://doi.org/10.1038/s41582-019-0157-5>
37. Neumann M, Kwong LK, Lee EB, Kremmer E, Flatley A, Xu Y, Forman MS, Troost D, Kretzschmar HA, Trojanowski JQ et al (2009) Phosphorylation of S409/410 of TDP-43 is a consistent feature in all sporadic and familial forms of TDP-43 proteinopathies. *Acta Neuropathol* 117:137–149. <https://doi.org/10.1007/s00401-008-0477-9>
38. Neumann M, Sampathu DM, Kwong LK, Truax AC, Micsenyi MC, Chou TT, Bruce J, Schuck T, Grossman M, Clark CM et al (2006) Ubiquitinated TDP-43 in frontotemporal lobar degeneration and amyotrophic lateral sclerosis. *Science* 314:130–133. <https://doi.org/10.1126/science.1134108>
39. Nonaka T, Masuda-Suzukake M, Arai T, Hasegawa Y, Akatsu H, Ohi T, Yoshida M, Murayama S, Mann DM, Akiyama H et al (2013) Prion-like properties of pathological TDP-43 aggregates from diseased brains. *Cell Rep* 4:124–134. <https://doi.org/10.1016/j.celrep.2013.06.007>
40. Novak P, Kovacech B, Katina S, Schmidt R, Scheltens P, Kontsejkova E, Ropele S, Fialova L, Kramberger M, Paulenka-Ivanovova N et al (2021) ADAMANT: a placebo-controlled randomized phase 2 study of AADvac1, an active immunotherapy against pathological tau in Alzheimer's disease. *Nature Aging* 1:521–534. <https://doi.org/10.1038/s43587-021-00070-2>
41. Pachitariu M, Stringer C (2022) Cellpose 2.0: how to train your own model. *Nat Methods* 19:1634–1641. <https://doi.org/10.1038/s41592-022-01663-4>
42. Polymenidou M, Lagier-Tourenne C, Hutt KR, Huelga SC, Moran J, Liang TY, Ling SC, Sun E, Wanczewicz E, Mazur C et al (2011) Long pre-mRNA depletion and RNA missplicing contribute to neuronal vulnerability from loss of TDP-43. *Nat Neurosci* 14:459–468. <https://doi.org/10.1038/nn.2779>
43. Porta S, Xu Y, Restrepo CR, Kwong LK, Zhang B, Brown HJ, Lee EB, Trojanowski JQ, Lee VM (2018) Patient-derived frontotemporal lobar degeneration brain extracts induce formation and spreading of TDP-43 pathology in vivo. *Nat Commun* 9:4220. <https://doi.org/10.1038/s41467-018-06548-9>
44. Pozzi S, Codron P, Soucy G, Renaud L, Cordeau PJ, Dutta K, Bareil C, Julien JP (2020) Monoclonal full-length antibody against TAR DNA binding protein 43 reduces related proteinopathy in neurons. *JCI Insight* 5:1. <https://doi.org/10.1172/jci.insight.140420>
45. Pozzi S, Thammisetty SS, Codron P, Rahimian R, Plourde KV, Soucy G, Bareil C, Phaneuf D, Kriz J, Gravel C et al (2019) Virus-mediated delivery of antibody targeting TAR DNA-binding protein-43 mitigates associated neuropathology. *J Clin Invest* 130:1. <https://doi.org/10.1172/JCI123931>
46. Prasad A, Bharathi V, Sivalingam V, Girdhar A, Patel BK (2019) Molecular mechanisms of TDP-43 misfolding and pathology in amyotrophic lateral sclerosis. *Front Mol Neurosci* 12:25. <https://doi.org/10.3389/fnmol.2019.00025>
47. Prudencio M, Gonzales PK, Cook CN, Gendron TF, Daugherty LM, Song Y, Ebbert MTW, van Blitterswijk M, Zhang YJ, Jansen-West K et al (2017) Repetitive element transcripts are elevated in the brain of C9orf72 ALS/FTLD patients. *Hum Mol Genet* 26:3421–3431. <https://doi.org/10.1093/hmg/ddx233>
48. Ravits JM, La Spada AR (2009) ALS motor phenotype heterogeneity, focality, and spread: deconstructing motor neuron degeneration. *Neurology* 73:805–811. <https://doi.org/10.1212/WNL.0b013e3181b6bbbd>
49. Riemenschneider H, Guo Q, Bader J, Frottin F, Farny D, Kleinberger G, Haass C, Mann M, Hartl FU, Baumeister W et al (2022) Gel-like inclusions of C-terminal fragments of TDP-43 sequester stalled proteasomes in neurons. *EMBO Rep* 1:e53890. <https://doi.org/10.15252/embr.202153890>
50. Spiller KJ, Restrepo CR, Khan T, Dominique MA, Fang TC, Canter RG, Roberts CJ, Miller KR, Ransohoff RM, Trojanowski JQ et al (2018) Microglia-mediated recovery from ALS-relevant motor neuron degeneration in a mouse model of TDP-43 proteinopathy. *Nat Neurosci* 21:329–340. <https://doi.org/10.1038/s41593-018-0083-7>
51. Spiller KJ, Restrepo CR, Khan T, Stieber AM, Kwong LK, Trojanowski JQ, Lee VM (2016) Progression of motor neuron disease is accelerated and the ability to recover is compromised with advanced age in rNLS8 mice. *Acta Neuropathol Commun* 4:105. <https://doi.org/10.1186/s40478-016-0377-5>
52. Stringer C, Wang T, Michaelos M, Pachitariu M (2021) Cellpose: a generalist algorithm for cellular segmentation. *Nat Methods* 18:100–106. <https://doi.org/10.1038/s41592-020-01018-x>
53. Tamaki Y, Shodai A, Morimura T, Hikami R, Minamiyama S, Ayaki T, Tooyama I, Furukawa Y, Takahashi R, Urushitani M (2018) Elimination of TDP-43 inclusions linked to amyotrophic lateral sclerosis by a misfolding-specific intrabody with dual proteolytic signals. *Sci Rep* 8:6030. <https://doi.org/10.1038/s41598-018-24463-3>
54. Truett GE, Heeger P, Mynatt RL, Truett AA, Walker JA, Warman ML (2000) Preparation of PCR-quality mouse genomic DNA with hot sodium hydroxide and tris (HotSHOT). *Biotechniques* 29(5):54. <https://doi.org/10.2144/00291bm09>
55. Tziortzouda P, Van Den Bosch L, Hirth F (2021) Triad of TDP43 control in neurodegeneration: autoregulation, localization and aggregation. *Nat Rev Neurosci*. <https://doi.org/10.1038/s41583-021-00431-1>
56. Walker AK, Spiller KJ, Ge G, Zheng A, Xu Y, Zhou M, Tripathy K, Kwong LK, Trojanowski JQ, Lee VM (2015) Functional recovery in new mouse models of ALS/FTLD after clearance of pathological cytoplasmic TDP-43. *Acta Neuropathol* 130:643–660. <https://doi.org/10.1007/s00401-015-1460-x>
57. Wang A, Conicella AE, Schmidt HB, Martin EW, Rhoads SN, Reeb AN, Nourse A, Ramirez Montero D, Ryan VH, Rohatgi R et al (2018) A single N-terminal phosphomimic disrupts TDP-43 polymerization, phase separation, and RNA splicing. *EMBO J* 37:1. <https://doi.org/10.15252/emboj.201797452>
58. Xie M, Liu YU, Zhao S, Zhang L, Bosco DB, Pang YP, Zhong J, Sheth U, Martens YA, Zhao N et al (2022) TREM2 interacts with TDP-43 and mediates microglial neuroprotection against TDP-43-related neurodegeneration. *Nat Neurosci* 25:26–38. <https://doi.org/10.1038/s41593-021-00975-6>
59. Xu YF, Gendron TF, Zhang YJ, Lin WL, D'Alton S, Sheng H, Casey MC, Tong J, Knight J, Yu X et al (2010) Wild-type human TDP-43 expression causes TDP-43 phosphorylation, mitochondrial aggregation, motor deficits, and early mortality in transgenic mice. *J Neurosci* 30:10851–10859. <https://doi.org/10.1523/JNEUROSCI.1630-10.2010>
60. Yu G, Wang LG, Han Y, He QY (2012) clusterProfiler: an R package for comparing biological themes among gene clusters. *OMICS* 16:284–287. <https://doi.org/10.1089/omi.2011.0118>
61. Yu H, Lu S, Gasior K, Singh D, Vazquez-Sanchez S, Tapia O, Toprani D, Beccari MS, Yates JR 3rd, Da Cruz S et al (2021) HSP70 chaperones RNA-free TDP-43 into anisotropic intranuclear liquid spherical shells. *Science* 371:1. <https://doi.org/10.1126/science.abb4309>
62. Zamani A, Walker AK, Rollo B, Ayers KL, Farah R, O'Brien TJ, Wright DK (2022) Impaired glymphatic function in the early stages of disease in a TDP-43 mouse model of amyotrophic lateral sclerosis. *Transl Neurodegener* 11:17. <https://doi.org/10.1186/s40035-022-00291-4>
63. Zhou Q, Mareljic N, Michaelsen M, Parhizkar S, Heindl S, Nuscher B, Farny D, Czuppa M, Schludi C, Graf A et al (2020) Active poly-GA vaccination prevents microglia activation and motor deficits in a C9orf72 mouse model. *EMBO Mol Med* 12:e10919. <https://doi.org/10.15252/emmm.201910919>

Publisher's Note

Springer Nature remains neutral with regard to jurisdictional claims in published maps and institutional affiliations.

5 PUBLICATION III

Direct binding of TDP-43 and Tau drives their co-condensation
and suppresses Tau fibril formation

Submitted as

Francesca Simonetti, Saskia Hutten, Lisa Marie Ramirez, Henrick Riemenschneider, Janine Hochmair, Martina Schifferer, Ali Rezaei, Ivan Urosevic, Weijia Zhong, Viktoria Ruf, Tammarn Lashley, Mikael Simons, Markus Zweckstetter, Magdalini Polymenidou, Susanne Wegmann, Dieter Edbauer, Dormann Dormann

5.1 Aim of the project

The aim of this project is to investigate the molecular mechanisms underlying the co-pathology of Tau and TDP-43 in AD. While Tau aggregates are a hallmark of AD, over half of patients also exhibit TDP-43 inclusions, which are associated with increased disease severity. The project aims to explore how Tau and TDP-43 mutually influence each other's aggregation, condensation, and seeding, both with recombinant proteins and diseased brain samples. By shedding light on the potential direct interaction between Tau and TDP-43, the project aims to elucidate the pathogenic mechanisms behind their co-occurrence in AD.

Direct binding of TDP-43 and Tau drives their co-condensation and suppresses Tau fibril formation

Francesca Simonetti^{1,2,3}, Saskia Hutten³, Lisa Marie Ramirez^{4,5}, Henrick Riemenschneider¹, Janine Hochmair⁶, Martina Schifferer¹, Ali Rezaei^{1,2}, Ivan Urosev⁷, Weijia Zhong⁷, Viktoria Ruf⁸, Tammarn Lashley⁹, Mikael Simons^{1,2,10}, Markus Zweckstetter^{4,5}, Magdalini Polymenidou⁷, Susanne Wegmann⁶, Dieter Edbauer^{*1,2,10}, Dorothee Dormann^{*3,10,11}

¹ Deutsches Zentrum für Neurodegenerative Erkrankungen (DZNE), Munich 81377, Germany

² Graduate School of Systemic Neurosciences (GSN), Planegg 82152, Germany

³ Johannes Gutenberg University (JGU), Institute of Molecular Physiology, Mainz 55128, Germany

⁴ Deutsches Zentrum für Neurodegenerative Erkrankungen (DZNE), Göttingen 37075, Germany

⁵ Max Planck Institute for Multidisciplinary Sciences, Göttingen 37075, Germany

⁶ Deutsches Zentrum für Neurodegenerative Erkrankungen (DZNE), Berlin 10117, Germany

⁷ University of Zurich, Zurich 8006, Switzerland

⁸ Center for Neuropathology and Prion disease, Faculty of Medicine LMU, Munich 81377, Germany

⁹ UCL Queen Square Institute of Neurology, London WC1N 3BG, UK

¹⁰ Munich Cluster of Systems Neurology (SyNergy), Munich 81377, Germany

¹¹ Institute of Molecular Biology (IMB), Mainz 55128, Germany

*Correspondence: ddormann@uni-mainz.de or dieter.edbauer@dzne.de

Abstract

Neuronal Tau aggregates are a hallmark of Alzheimer's disease (AD), but more than half of the patients exhibit additional TDP-43 inclusions and frequent co-aggregates of both proteins. TDP-43 co-pathology is associated with increased disease severity, although causality remains unclear. Here we demonstrate that Tau and TDP-43 mutually promote each other's condensation *in vitro*, forming irregular, multiphasic co-condensates. Moreover, we show that Tau promotes TDP-43 aggregation, while TDP-43 suppresses the formation of Tau fibrils *in vitro*. Specifically, the N- but not the C-terminal domain of TDP-43 hinders formation of Tau fibrils while increasing Tau seeding in a biosensor assay specific for proteopathic Tau seeds. Furthermore, using reporter cell lines for Tau and TDP-43 seeding, we show that FTLD-TDP type A and AD brains contain both seeding-competent Tau and TDP-43, suggesting reciprocal induction of seeding-competent species. Our results reveal a direct Tau/TDP-43 interaction and shed light on the molecular mechanisms that may underlie Tau/TDP-43 co-pathology in AD.

Keywords

Alzheimer's disease; phase separation; protein aggregation; Tau; TDP-43.

Introduction

Intracellular protein aggregates are a common feature of all neurodegenerative diseases. Protein inclusions occur in neurons and/or glial cells and are intimately linked to the process of neurodegeneration (Taylor et al., 2002). In Alzheimer's disease (AD), the microtubule-associated protein Tau, which regulates axonal transport and synapse function, mislocalizes from axons into insoluble cytosolic inclusions called neurofibrillary tangles (NFTs) (Guo et al., 2017). Since Tau deposits in AD correlates with neurodegeneration and disease severity, the stereotypic spreading of Tau pathology from the transentorhinal regions to the neocortex is used for disease staging (Braak and Braak, 1995), although Tau oligomers may be more neurotoxic than solid aggregates (Berger et al., 2007; Lasagna-Reeves et al., 2011; Takeda et al., 2015; Usenovic et al., 2015). Over 60% of AD patients additionally feature cytosolic deposits of the nuclear DNA/RNA-binding protein TDP-43 (TAR DNA binding protein of 43 kDa) (Amador-Ortiz et al., 2007; Josephs et al., 2014a, 2014b; Kadokura et al., 2009; Tomé et al., 2021, 2020; Tremblay et al., 2011), first discovered in the affected brain regions of amyotrophic lateral sclerosis (ALS) and frontotemporal dementia (FTD) patients (Neumann et al., 2006). TDP-43 is involved in many steps of RNA processing (Ratti and Buratti, 2016), and its nuclear loss and cytoplasmic aggregation causes subtle yet detrimental dysregulation of mRNA processing, for example incorporation of cryptic exons into mRNA (Ling et al., 2013; Melamed et al., 2019; Polymenidou et al., 2011; Tziortzouda et al., 2021).

In AD, TDP-43 deposits are mainly found in the limbic regions and frontal cortex (Amador-Ortiz et al., 2007; Arai et al., 2009; Josephs et al., 2015; Latimer and Liachko, 2021; Meneses et al., 2021; Tomé et al., 2020). TDP-43 deposition is associated with greater hippocampal volume loss and more severe cognitive impairment (Josephs et al., 2014b, 2017; Thomas et al., 2020), suggesting an important contribution of TDP-43 to neurodegeneration in AD. TDP-43 aggregates often colocalize with Tau NFTs in the amygdala and hippocampus of AD patients (Davis et al., 2017; Higashi et al., 2007; Smith et al., 2018; Tomé et al., 2021), and proximity ligation and co-immunoprecipitation experiments have suggested that TDP-43 interacts with Tau in the AD brain (Tomé et al., 2021). Moreover, studies in animal models further support the idea that the presence of TDP-43 exacerbates Tau pathology. A study in *C. elegans* demonstrated that TDP-43 enhances Tau neurotoxicity, resulting in neuronal dysfunction and pathological Tau accumulation

(Latimer et al., 2022). Moreover, TDP-43 overexpression in APP/PSEN1 mice decreased A β plaque deposition but increased Tau aggregation (Davis et al., 2017). Lastly, cytoplasmic accumulation of endogenous phosphorylated TDP-43 was reported in two different Tau transgenic mouse models, but not in mouse models of A β deposition, α -synucleinopathy or Huntington's disease (Clippinger et al., 2013). However, whether Tau and TDP-43 directly interact and influence each other's condensation, aggregation or seeding behavior remains unknown.

Notably, both Tau and TDP-43 contain extended intrinsically disordered regions (IDRs) that drive various self-assembly forms, including oligomers and droplet-like condensates that form through phase separation (PS) (Ambadipudi et al., 2017; Wang et al., 2018; Wegmann et al., 2018). While PS is essential for the formation of membraneless organelles and various cellular functions (Alberti et al., 2019), it can give rise to amyloid-like aggregates through aberrant liquid-to-solid phase transitions (Alberti and Dormann, 2019; Alberti and Hyman, 2016; Nedelsky and Taylor, 2019; Patel et al., 2015). Both TDP-43 and Tau have been shown to form liquid- or gel-like condensates *in vitro*, and it has been postulated that condensates may facilitate pathological aggregation (Ambadipudi et al., 2017; Kanaan et al., 2020; Wang et al., 2018; Wegmann et al., 2018; Yan et al., 2024; Zhang et al., 2017). Thus, direct interaction of TDP-43 and Tau may affect their phase transition and aggregation behavior.

Moreover, oligomeric or aggregated TDP-43 and Tau can be released and taken up by neighboring cells and thereby spread from cell to cell (Brettschneider et al., 2015; De Rossi et al., 2021; Dujardin and Hyman, 2019; Feiler et al., 2015), providing additional possibilities for intra- or extracellular encounters. These mechanisms give rise to the stereotypical spreading of protein aggregates throughout the brain, which has been observed for the prion protein (PrP), A β , Tau, α -synuclein and TDP-43 (Dujardin and Hyman, 2019; Jucker and Walker, 2011; Polymeridou and Cleveland, 2011; Uemura et al., 2020). To what extent TDP-43 and Tau influence each other's seeding behavior when Tau seeds encounter TDP-43 and vice versa is still poorly understood.

Here we show that TDP-43 and Tau significantly influence each other's condensation and aggregation behavior *in vitro*, leading to the formation of amorphous, multiphasic Tau/TDP-43 co-condensates. We also find that TDP-43 prevents Tau fibril formation *in vitro*; specifically, the N-terminal domain (NTD), but not the C-terminal domain (CTD) of TDP-43 suppresses Tau fibrillization and significantly enhances seeding in biosensor cells specific for Tau aggregation. Moreover, seeding experiments in reporter cell lines with SarkoSpin brain extracts from AD and FTLD-TDP patients (with a primary Tau and TDP-43 pathology, respectively) show that these extracts contain seeding-competent species of the other protein. This suggests that even in the absence of visible Tau or TDP-43 inclusions, pathological conformations of Tau or TDP-43 can be present, possibly triggered by interaction with the other protein, aggravating disease pathogenesis. Based on our data, we propose that low levels of cytosolic full-length TDP-43 could initially have a protective role against Tau aggregation. However, the Tau/TDP-43 interaction may lead to the formation of seeding competent oligomers as well as co-condensates that may eventually transition into the Tau/TDP-43 co-aggregates observed in AD patients.

Results

Tau induces formation of large, irregular TDP-43 condensates *in vitro*

To gain a molecular understanding of how Tau and TDP-43 influence each other's assembly and aggregation behavior, we performed several *in vitro* assays with fluorescently labeled recombinant proteins. Full-length wild-type Tau (2N4R isoform) was labeled with DyLight 650, and TDP-43, tagged with a maltose-binding protein (MBP) tag for solubilization (Wang et al., 2018), was labeled with Alexa Fluor 488.

We induced TDP-43 condensation by cleaving the MBP-His₆ tag from TDP-43-MBP-His₆ using TEV protease in a physiological buffer, and visualized the resulting condensates by spinning disk confocal microscopy (Fig. 1A). In the absence of Tau, TDP-43 formed distinct round condensates, but the addition of Tau at equimolar concentration induced the formation of larger, irregularly shaped TDP-43 structures that also contained Tau (Fig. 1B, Fig. EV1B and Movie EV1A, B). Moreover, unlabeled Tau induced similar large, irregularly shaped TDP-43 condensates as DyLight650-Tau, excluding effects of dye conjugation on TDP-43 condensates (Fig. 1C). Titration of unlabeled Tau (0.2-10 μ M) showed that the formation of these irregular TDP-43 condensates already occurred at a Tau:TDP-43 ratio of 1:10 (Fig. EV1A). In addition, neither recombinant MBP, nor α -synuclein, another neurodegeneration protein prone to aggregation and phase-separation (Ray et al., 2020), affected the number or morphology of TDP-43 condensates when added at different concentrations (Fig. 1C). We also observed that fluorescently labeled LD650- α -synuclein was excluded from Alexa488-TDP-43 condensates, contrary to DyLight650-Tau (Fig. EV1B, C). Finally, quantitative analysis of condensate images confirmed that only the addition of Tau, but not MBP or α -synuclein, reduced the number and roundness but increased the size of TDP-43 condensates (Fig. 1D).

Collectively, our data show that even at low concentrations, Tau alters the phase separation behavior of TDP-43. Additionally, Tau co-partitions into TDP-43 condensates and causes the formation of large, irregular TDP-43 structures.

Tau promotes TDP-43 aggregation *in vitro*

To test whether Tau affects TDP-43 aggregation *in vitro*, we first performed semi-denaturing detergent agarose gel electrophoresis (SDD-AGE). In this previously established TDP-43 aggregation assay (French et al., 2019; Gruijs da Silva et al., 2022) the protein is agitated for 30 min in an aggregation-promoting buffer and then incubated for several days (Fig. 2A). For the SDD-AGE assay, TDP-43-MBP was incubated in the presence or absence of Tau, MBP and α -synuclein, omitting the TEV cleavage to slow aggregation and allow formation of high molecular weight (HMW) species of TDP-43-MBP to be monitored over time (Gruijs da Silva et al., 2022). We observed that the addition of Tau, but not MBP or α -synuclein, significantly accelerated the formation of HMW species of TDP-43-MBP (Fig. 2B, C).

To visualize these aggregates by confocal microscopy, we performed the same aggregation assay with Alexa488-labelled TDP-43, cleaving off the MBP solubility tag to accelerate aggregation (Fig. 2D). The presence of recombinant Tau, but not MBP, promoted TDP-43 aggregation in a dose-dependent manner, as quantified by the aggregate area (Fig. 2E, F). α -synuclein increased TDP-43 aggregation only at the highest concentration, but to a lesser extent than Tau. Moreover, by labeling Tau and α -synuclein with Dylight-650 and LD-650, respectively, we observed that Tau was more enriched in TDP-43 aggregates than α -synuclein (Fig. EV1D, E). Taken together, our results demonstrate that Tau can promote TDP-43 aggregation *in vitro*, suggesting that the two proteins interact directly.

Under molecular crowding conditions, TDP-43 and Tau co-condense into multiphasic structures with intra-Tau condensates

After having shown an influence of Tau on TDP-43 phase separation and aggregation, we sought to determine the influence of TDP-43 on Tau condensation. Tau is known to phase separate through complex coacervation in presence of polyanions, such as heparin or RNA, or upon addition of molecular crowding agents, such as polyethylene glycol (PEG) (Ambadipudi et al., 2017; Hochmair et al., 2022; Ukmar-Godec et al., 2019; Wegmann et al., 2018; Zhang et al., 2017). To examine how TDP-43 (at 0.5 to 2-fold molar ratio) affects Tau condensation, we induced Tau phase separation at physiological salt concentration (150 mM NaCl) with 5% (w/v) PEG, and measured the turbidity of the protein solutions to quantify Tau phase separation. Addition of TDP-

43-MBP, caused a dose-dependent increase in turbidity compared to the MBP or α -synuclein controls (Fig. 3A), suggesting that TDP-43 can promote Tau condensation.

To further confirm this hypothesis, we analyzed phase separation of DyLight488-Tau with Alexa633-TDP-43-MBP (molar ratio of proteins 1:1) and 10% PEG, and visualized the condensates after 24 hours by confocal microscopy. We observed that TDP-43 and Tau co-phase separated into large condensates that exhibited pronounced wetting of the supporting dish surface, reminiscent of previously reported Tau:RNA co-condensate wetting of charged surfaces (Hochmair et al., 2022). In addition, we also observed numerous small, internal Tau condensates within the Tau/TDP-43-MBP co-phase (Fig. 3B, high-resolution images). These small Tau condensates may form either by excess Tau in solution attaching to pre-existing Tau/TDP-43 co-condensates, or by de-mixing within the Tau/TDP-43 co-condensates,

By investigating earlier time points, we observed that Tau alone only gradually formed small condensates over time, but mixing both proteins strongly increased their phase separation already after 1 hour of incubation, and the pronounced wetting and intra-Tau droplet phenotype was already observed at this timepoint (Fig. 3C). Contrarily, MBP and α -synuclein did not alter the Tau condensation behavior (Fig. 3C).

To investigate the effect of TDP-43 on Tau condensation in the absence of crowding agent, we induced Tau condensate formation by coacervation with heparin in low salt. Similar to what we observed in the presence of PEG, addition of TDP-43-MBP to Tau caused the formation of irregularly shaped Tau condensates, showing some intra-Tau condensates and wetting-behavior (Fig. EV2). This was not the case for TDP-43-MBP alone, Tau+MBP or Tau+ α -synuclein, confirming that the wetting and intra-Tau condensate formation depend on the interaction of Tau and TDP-43.

TDP-43 suppresses Tau fibril formation via the TDP-43 N-terminal domain

Next, we investigated whether TDP-43 also affects Tau fibrillization *in vitro*. Using a classical heparin-induced polymerization assay, we examined aggregation of Tau into paired helical filaments (PHFs) over 5 days (Barghorn et al., 2005), in the presence or absence of equimolar concentrations (50 μ M) of TDP-43-MBP, MBP or α -synuclein (Fig. 4A). Consistent with previous reports, negative staining electron microscopy (EM) showed that Tau alone formed long fibrillar aggregates under these conditions (Fig. 4B, C). Similar fibrils were observed in the presence of MBP or α -synuclein, but the addition of TDP-43-MBP resulted in the formation of much smaller structures with an average length <100 nm. Similar small assemblies were also observed for TDP-43-MBP alone, suggesting that the small, non-fibrillar structures observed for Tau+TDP-43-MBP are either small TDP-43 assemblies, or Tau/TDP-43 co-assemblies.

To determine whether TDP-43 suppresses Tau fibril formation or leads to the disassembly of already formed Tau PHFs, we examined earlier time points. In the absence of TDP-43-MBP, Tau fibrils were readily detectable after 1 day (Fig. EV3) and increased in number and length over time. In contrast, in the presence of TDP-43-MBP, no fibers were observed at any time point, instead small (<100 nm) structures emerged on day 2, which increased in number over time. These data suggest that full-length TDP-43 prevents the formation of Tau fibrils, rather than disassembling preformed Tau fibrils.

To investigate which region of TDP-43 is responsible for suppressing Tau fibril formation, we purified the recombinant TDP-43 N-terminal domain (TDP-43-NTD-MBP, aa. 1-266), lacking the IDR, and the C-terminal domain (TDP-43-CTD-MBP, aa. 267-414) comprising the IDR only, and performed *in vitro* Tau fibrillization experiments as described above.

As shown before, Tau incubated with full-length TDP-43-MBP did not form any fibrillar structures. When mixed with TDP-43-NTD-MBP, Tau not only formed fewer long fibrils, but also abundant smaller structures with an average size below 100 nm, similar to the assemblies formed by TDP-43-NTD-MBP alone or Tau in the presence of full-length TDP-43 (Fig. 4D, E). In contrast, when Tau was mixed with TDP-43-CTD-MBP, long Tau fibers were observed, as for Tau alone.

Together, our data show that full-length TDP-43 and, to a lesser extent, the NTD, but not the CTD, inhibit Tau fibrillization.

The NTD of TDP-43 promotes the formation of seeding-competent Tau species

One way to assess the pathogenicity of the small non-fibrillar assemblies observed in Tau+TDP-43-MBP and Tau+TDP-43-NTD-MBP mixtures is to test their seeding potency in so-called Tau biosensor cells, a reporter cell line stably co-expressing two variants of the Tau repeat domain (RD) with the pathogenic P301S mutation fused to either CFP or YFP (HEK293 CFP/YFP-TauRD^{P301S}; (Holmes et al., 2014). In this assay, the lipotransfection of material containing aggregated or oligomeric Tau (=Tau seeds) causes CFP/YFP-TauRD^{P301S} aggregation in the cytoplasm of the reporter cells, detectable as a CFP-YFP FRET signal and visible as bright accumulations by microscopy in the green channel ($\lambda=488$ nm excitation; Fig. 5A). Notably, the seeding of Tau aggregation in Tau biosensor cells is known to be highly specific for Tau and is not triggered by other protein seeds in the inoculum (Holmes et al., 2014). We therefore transfected the different Tau fibril preparation shown in Fig. 4 into Tau biosensor cells and analyzed their effect on TauRD^{P301S} aggregation. Consistent with published results, we observed several Tau-RD aggregates in the cytoplasm upon transfection of Tau-only fibrils, and similar Tau-RD aggregate numbers were observed upon transfection of Tau+MBP, Tau+ α -synuclein and Tau+TDP-43-CTD-MBP samples (Fig. 5B, C). Interestingly, the Tau+TDP-43-MBP structures exhibited a lower seeding potency, although the difference did not reach statistical significance, suggesting that the small non-fibrillar assemblies observed for this condition by negative-stain EM may be mostly small TDP-43 assemblies (Fig. 4B, C). Strikingly, the Tau+TDP-43-NTD-MBP sample caused a significant increase in seeding compared to Tau alone, indicating that the small structures observed for Tau+TDP-43-NTD-MBP co-incubation could be Tau oligomers (Fig. 4D, E), the most seeding-competent Tau species (Berger et al., 2007; Lasagna-Reeves et al., 2011; Takeda et al., 2015; Usenovic et al., 2015).

Together, these results suggest that the NTD of TDP-43 may promote Tau oligomerization, giving rise to highly seeding competent Tau species.

FTLD-TDP and AD brains contain seeding competent species of Tau and TDP-43, respectively

To test whether TDP-43 may indeed trigger the formation of Tau seeds in human brains, we examined the seeding capacity of patient brain extracts in the Tau biosensor cells (Fig. 6A). We extracted sarkosyl-insoluble material from the frontal cortex of AD, FTLD-Tau, FTLD-TDP type A patients or non-demented controls (Non-ND) (Table 1) according to the established SarkoSpin procedure (Laferrière et al., 2019) and transfected Tau biosensor cells with these SarkoSpin extracts to assess the presence of Tau seeds in the different samples. Western blot analysis detected mainly TDP-43 but not Tau in the FTLD-TDP extracts, in contrast, mainly Tau but not TDP-43 was observed in the FTLD-Tau and AD extracts (Fig. EV4A). Analysis of Tau-RD aggregation by live cell confocal microscopy showed that not only the AD and FTLD-Tau extracts, but also the FTLD-TDP extracts induced pronounced Tau-RD aggregation after 3 days compared to the Non-ND controls (Fig. 6B, C and Fig. EV4B). Transfecting the cells with recombinant TDP-43 aggregates did not induce Tau seeding, confirming the specificity of the cell line for Tau seeds and excluding cross-seeding between the two proteins (Fig. EV4C). Thus, our data suggest that despite the absence of visible histological Tau pathology (Fig. EV4A), FTLD-TDP type A brains can contain seeding-competent Tau species, possibly triggered by the presence of mislocalized TDP-43.

Additionally, we used a cellular TDP-43 seeding assay described in (De Rossi et al., 2021) to test whether FTLD-Tau and AD extracts contain seeding competent TDP-43 species. In this assay, HEK293 cells with doxycycline-inducible TDP-43-HA expression are transfected with SarkoSpin extracts and subsequent immunostaining for the HA-tag and phospho-TDP-43 can be used to

detect *de novo* formed TDP-43 “neoaggregates”, which result from cytoplasmic mislocalization of TDP-43-HA and its subsequent aggregation and phosphorylation (De Rossi et al., 2021) (Fig. 6D). Indeed, SarkoSpin extracts from AD patients induced the formation of cytosolic TDP-43 neoaggregates as potently as the FTLD-TDP type A positive controls, while the FTLD-Tau extracts did not significantly seed TDP-43 (Fig. 6E, F and Fig. EV4D). This indicates that AD brains can contain TDP-43 seeding competent species, despite the lack of detection of TDP-43 in these SarkoSpin extracts (Fig. EV4A).

Thus, we surprisingly found that even though FTLD-TDP type A and AD patients display distinct predominant protein pathology on the histopathological and biochemical level, they contain both seeding-competent Tau and TDP-43 species.

Discussion

Recent post mortem studies highlight the frequent co-occurrence of Tau and TDP-43 inclusion pathology in Alzheimer's Disease (AD), with significant implications for disease progression. Since ~60% of AD cases show Tau/TDP-43 co-pathology, targeting this interaction may be an attractive therapeutic approach for this population. Thus, understanding the molecular interplay between Tau and TDP-43, and the development of their co-pathology is crucial. Our study reveals a direct interaction between Tau and TDP-43 and that the two proteins significantly affect each other's condensation and aggregation behavior *in vitro*, as well as the formation of proteopathic seeds in human brain, supporting the view that the two pathologies are interlinked and do not develop completely independently.

Specifically, we observed that Tau and TDP-43 co-condense into irregularly shaped or multiphasic co-condensates. In particular the presence of TDP-43 strongly promotes Tau phase separation into large co-condensates with intra-Tau droplets (Fig. 7). It remains to be determined whether the two proteins initially are completely mixed and then de-mix, or whether new Tau droplets are nucleated on the surface of the TDP-43 condensates or Tau/TDP-43 co-phases. Similar multiphasic co-condensates have been described for Tau and the prion protein (PrP) or Tau and TIA-1 in presence of RNA (Ash et al., 2021; Rai et al., 2023), as well as for α -synuclein and the TDP-43-CTD, where α -synuclein forms clusters on the surface of TDP-43-CTD-RNA condensates and nucleates the formation of heterotypic amyloid fibrils (Dhakal et al., 2023). Moreover, it has been proposed that the co-condensation of Tau and α -synuclein into highly crowded yet dynamic condensates creates an ideal reservoir for amyloid nucleation (Gracia et al., 2022). Based on these studies, it can be speculated that Tau/TDP-43 co-condensates may further develop into heterotypic Tau/TDP-43 co-aggregates, similar to those observed in AD patients (Tomé et al., 2021), or may nucleate amyloid fibrils of one or both proteins.

Experiments in cultured cells support the notion that condensation and demixing processes of Tau also occur in cells, and Tau condensation was proposed to have a physiological role in regulating microtubule dynamics (Hernández-Vega et al., 2017; Zhang et al., 2020). However, Tau droplets can quickly transition into gel-like structures that over time turn into amyloid-like aggregates with seeding capacities (Kanaan et al., 2020; Wegmann et al., 2018). The extent to which condensation processes contribute to aggregate formation in patient tissue remains a crucial question in the neurodegeneration field. Numerous studies have shown that droplet-like condensates can convert into solid and fibrillar structures by liquid-to-solid phase transitions (Hofweber et al., 2018; Molliex et al., 2015; Patel et al., 2015), and that amyloids can emerge at the surface of condensates (Emmanouilidis et al., 2024; Linsenmeier et al., 2023; Shen et al., 2023). Hence, a common view is that condensates could serve as precursors of amyloid-like aggregates in neurodegenerative diseases (Alberti and Dormann, 2019; Alberti and Hyman, 2016;

Nedelsky and Taylor, 2019; Zbinden et al., 2020). However, a recent study indicates that condensates may alternatively act as protein sinks and suppress formation of amyloid fibrils (Das et al., 2024). Thus, further research is required to clarify the role of condensation processes in protein aggregation.

Additionally, our negative stain EM experiments showed that Tau and TDP-43, when mixed together, form oligomeric species <100 nm in size (Fig. 4). This method does not allow us to determine whether these oligomers contain predominantly Tau or TDP-43 molecules, or a mixture of both proteins, hence further biophysical investigations are needed to determine the composition of these oligomeric species. However, our experiments in Tau biosensor cells, which are highly specific for detecting Tau seeds (fibrils or oligomers), but not other protein assemblies (Holmes et al., 2014), suggest that the oligomers seen for mixtures of Tau and full-length TDP-43 or the TDP-43 CTD may be predominantly TDP-43 assemblies, whereas the oligomers seen for mixtures of Tau and the TDP-43 NTD may be Tau oligomers, the most seeding-competent form of Tau (Berger et al., 2007; Lasagna-Reeves et al., 2011; Takeda et al., 2015; Usenovic et al., 2015). Further research will be required to elucidate the molecular interaction of the TDP-43 NTD with Tau and the oligomeric species that form upon TDP-43/Tau interaction.

At the same time, we observed that full-length TDP-43 and its NTD, but not its CTD, suppress heparin-induced Tau fibril formation (Fig. 4). These data suggest that cytosolically mislocalized full-length TDP-43 might be able to initially inhibit Tau aggregation in the brain, whereas C-terminal fragments of TDP-43, frequently found in cytoplasmic aggregates in post-mortem AD brains (Tomé et al., 2020), may not be able to do so. Given our results that TDP-43 suppresses Tau fibril formation, we speculate that TDP-43 bind to the protofilament core on Tau (~306-378aa) (Fitzpatrick et al., 2017; Oakley et al., 2020) or part of this region (Fig. 7). Which region(s) in the TDP-43 NTD are engaged in the Tau interaction remains to be determined. The protofilament core region of Tau contains numerous positively and negatively charged residues, as do the folded N-terminus, the NLS region and both RRM regions in TDP-43's NTD, hence all of these subregions are good candidates for engaging in an electrostatic interaction with Tau.

Our finding that TDP-43 suppresses Tau fibril formation echoes reports that TDP-43 inhibits the early stages of amyloid-beta (A β) fibrillization (Shih et al., 2020). This activity also depends on the NTD (amino acids 1-256) and not the CTD of TDP-43, as does the suppression of Tau fibril formation. Strikingly, TDP-43 injection in AD mice not only inhibits A β fibrillization and increases A β oligomers, but also elicits memory deficits and inflammation (Shih et al., 2020). Our data suggest that TDP-43 might act similarly on Tau, inhibiting its fibrillization, while enhancing the formation of seeding-competent Tau oligomers that are thought to be highly toxic (Gerson and Kaye, 2013; Tai et al., 2012; Ward et al., 2012).

Another interesting question is where and under which conditions TDP-43 and Tau (in different assembly forms) may encounter each other in the neuronal cytoplasm, potentially influencing each other's condensation, aggregation and seeding behavior. Normally, TDP-43 is predominantly located in the nucleus, but small amounts are also found in the cytoplasm, especially under cellular stress conditions (Dewey et al., 2011; Gruijs da Silva et al., 2022) or after nucleocytoplasmic transport defects associated with neurodegenerative diseases and/or aging (Chou et al., 2018; D'Angelo et al., 2009; Hutten et al., 2020). Vice versa, somatodendritic Tau aggregates may trigger cytoplasmic mislocalization of TDP-43 through direct interaction, especially if the interaction site involves the NLS. Elevated cytosolic TDP-43 might trigger condensation or somatodendritic mislocalization of Tau. Upon cellular stress, cytosolic TDP-43 is recruited into stress granules (SGs) (Bentmann et al., 2012; Dewey et al., 2011), membraneless RNP granules that recruit many RNA-binding proteins, including the aggregation-prone, disease-linked proteins FUS, hnRNP-A1/A2, TIA-1, but also Tau (Ash et al., 2021; Vanderweyde et al., 2012; Wolozin

and Ivanov, 2019). Hence, under conditions of cellular stress, TDP-43 and Tau might encounter each other in SGs and might undergo co-condensation, and subsequent aggregation there.

Using two HEK293 reporter cell lines previously established to investigate TDP-43 and Tau seeding (Holmes et al., 2014; De Rossi et al., 2021), we found that seeding-competent Tau and TDP-43 can be present in FTLD-TDP and AD patient brain, respectively, even without visible inclusion pathology. Specifically, FTLD-TDP type A SarkoSpin extracts elicited intracellular Tau-RD aggregation (Fig. 6), indicating that they contain seeding-competent Tau species; *vice versa*, AD Sarkospin extracts promoted cytosolic TDP-43 aggregation, although no insoluble TDP-43 was detected by immunoblotting (Fig. 6 and Fig. EV4). This data could be explained by the fact that prion-like spreading of protein pathology may occur before the deposition of aggregates. For example, extracts derived from different brain regions of AD patients can have seeding capacity despite no detectable pTau or visible NFTs in the tissues (DeVos et al., 2018; Furman et al., 2017). A similar mechanism may occur for TDP-43, in which the loss of nuclear TDP-43 and accumulation of small TDP-43 assemblies in the cytoplasm may occur before deposition of cytosolic TDP-43 aggregates. Our results are in line with a recent study by Tomé and colleagues who showed that sarkosyl-insoluble homogenates derived from AD brains with TDP-43 co-pathology exhibit enhanced intracellular Tau seeding compared to AD brains without TDP-43 co-pathology, both in the HEK293 Tau-RD reporter cell line and the hippocampus of a TDP-43 transgenic mouse model (Tomé et al., 2023). Even though the nature of the patient brain-derived “seeds” (oligomers vs. aggregates) remains to be determined, the observed phenomena further support a pathological interaction between TDP-43 and Tau, enhancing spread of pathology and thereby potentially aggravating neurodegeneration.

In summary, our data provide molecular insights into the interaction of Tau and TDP-43 to support co-pathology observed in animal models and AD patients (Chornenkyy et al., 2019; Latimer and Liachko, 2021; Montalbano et al., 2020; Spires-Jones et al., 2017; Tomé et al., 2023). We propose that full-length TDP-43, once in the cytoplasm, interacts with Tau and suppresses Tau fibril formation (Fig. 7). At the same time, this interaction promotes Tau/TDP-43 co-condensation, which may initially be protective by sequestering Tau and TDP-43 molecules and thereby reducing their availability for oligomer or fibril formation. However, over time Tau/TDP-43 co-condensates may undergo structural transitions into solid aggregates, or their surface might nucleate amyloid fibers, as shown for other condensate systems (Hofweber et al., 2018; Molliex et al., 2015; Patel et al., 2015)(Emmanouilidis et al., 2024; Linsenmeier et al., 2023; Shen et al., 2023), providing a possible mechanistic explanation for how Tau/TDP-43 co-aggregates in AD patients may form.

Materials & Methods

cDNA constructs

Bacterial expressing constructs

The plasmid pJ4M TDP-43-TEV-MBP-His₆ (addgene #104480) was used to generate human TDP-43 tagged with TEV-MBP-His₆ (TDP-43-MBP) as described in (Wang et al., 2018); from the same backbone, we cloned TEV-MBP-His₆ (MBP), TDP-43-NTD(aa 1-266)-TEV-MBP- His₆ (TDP-43-NTD-MBP) and TDP-43-CTD(aa 267-414)-TEV-MBP- His₆ (TDP-43-CTD-MBP) as described in (Conicella et al., 2016).

Similarly, full-length wildtype Tau (2N4R, hTau40) was introduced into a pNG2 vector, as previously described in (Barghorn et al., 2005).

Finally, the plasmid pET5a/aSynuclein (136 TAT), originally developed by Philipp Kahle at LMU Munich and modified with a 136TAC/TAT mutation by Matthias Habeck, was used to purify

recombinant α -synuclein (used unlabeled in the experiments). The pT7-7 α -synuclein N122C plasmid (original wild-type plasmid by Hilal Lashuel, Addgene #36046) was used to purify recombinant α -synuclein (used labeled in the experiments).

Recombinant protein expression and purification

TDP-43-MBP

TDP-43-MBP and TDP-43-NTD-MBP were purified as previously described in (Grujics da Silva et al., 2022). In brief, the expression of proteins was performed in *E. coli* BL21-DE3 Rosetta 2 using 0.5 mM isopropyl-beta-thiogalactoside (IPTG) overnight (o/n) at 16°C. Cells were resuspended in lysis buffer (50 mM Tris pH 8.0, 1 M NaCl, 10mM imidazole, 10% (v/v) glycerol, 4 mM β -mercaptoethanol and 1 μ g/ml of aprotinin, leupeptin hemisulfate and pepstatin A) supplemented with 100 μ g/ml RNase A and 100 μ g/ml lysozyme followed by sonication. The protein was then purified by Ni-NTA agarose beads (Qiagen, #30210) and eluted with lysis buffer containing 300 mM imidazole. Next, a purification step with size exclusion chromatography (SEC; Hiload 16/600 Superdex 200 pg, GE Healthcare) was carried out in storage buffer (50 mM Tris pH 8, 300 mM NaCl, 5% (v/v) glycerol supplemented with 2 mM TCEP), in order to separate soluble TDP-43-MBP-His₆ and TDP-43-NTD-MBP from protein aggregates and contaminants. The purified dimeric TDP-43-MBP-His₆ and TDP-43-NTD-MBP fractions were pooled together and protein was concentrated using MWCO 30 Amicon ultra centrifugal filters (Merck, #UFC503024) and then flash frozen and stored at -80°C. To determine protein concentration, absorbance at 280 nm was measured using the respective molecular weight (kDa) and extinction coefficient (ϵ) predicted by the ProtParam tool and the A260/280 nm ratio for recombinant TDP-43-MBP was consistently ≤ 0.6 .

TDP-43-CTD-MBP was expressed as His-FKBP-3C-TDP43(267-414)-TEV-MBP in *E. coli* BL21-DE3 codon plus using 0.5 mM IPTG overnight at 16°C. Cell pellet were lysed in IMAC buffer (30 mM Tris pH 8.0, 300 mM NaCl, 15 mM imidazole), supplemented with 2 mM MgCl₂, 0.5 mM TCEP, Sm nuclease and protease inhibitors, using a cell homogenizer. Subsequently, TX-100 (final 0.1%) was added to the lysate and the protein was purified using Ni-NTA agarose and TDP-43-CTD-MBP protein eluted by 1 mg/ ml of His-3C protease in IMAC buffer containing 1 mM DTT. Finally, a purification step with Superdex200 16/600 was performed in storage buffer (20 mM HEPES pH 7.4, 150 mM NaCl, 10 % Glycerol, 1 mM DTT). Protein containing fractions were pooled, concentrated using MWCO 10 Amicon ultra centrifugal filters (Merck, #UFC5010) and then flash frozen and stored at -80°C.

TEV-MBP-His₆

The TEV-MBP-His₆ protein expression was performed in *E. coli* BL21 Star* and induced with 0.5 mM IPTG o/n at 20°C. Next, cells were lysed in 1X PBS with 4 mM β -mercaptoethanol supplemented with 100 μ g/ml lysozyme and sonicated. The protein was then purified by Ni-NTA agarose beads and eluted in 1X PBS, 4 mM β -mercaptoethanol, 1 M NaCl containing 300 mM imidazole. Finally, protein concentration was measured after dialysis into TDP-43-MBP-His₆ storage buffer (20 mM Tris pH 8.0, 300 mM NaCl, 10% (v/v) glycerol supplemented with 2 mM TCEP).

His₆-TEV protease

His₆-TEV expression was performed similarly as the above proteins. The protein expression was induced in *E. coli* BL21-DE3 Rosetta-LysS with 1 mM IPTG overnight at 20°C. Cells were lysed in 50 mM Tris pH8, 200 mM NaCl, 20 mM imidazole, 10% (v/v) glycerol, 4 mM β -mercaptoethanol, supplemented with 0.1 mg/ml RNase A and 100 μ g/ml lysozyme, followed by sonication. His₆-TEV was then purified using Ni-NTA agarose beads, and eluted with lysis buffer at pH 8.5 containing 1 M NaCl and 800 mM imidazole. Finally, His₆-TEV protein concentration was

measured and the protein was dialyzed into storage buffer (50 mM Tris, 150 mM NaCl, 20% glycerol, 2 mM Dithiothreitol (DTT)).

hTau441-WT

hTau441-WT expression was carried out in *E. coli* BL21 (DE3) with a 2 h induction using 0.5 mM IPTG at 37°C. Cells were then resuspended in lysis buffer (20 mM Na-MES pH 6.8, 1 mM EDTA, proteinase inhibitors, 5 mM DTT) followed by lysis with the high-pressure homogenizer. Then, 500 mM NaCl were added and the lysate was boiled at 95°C for 20 min, followed by o/n dialysis at 4°C first in 20 mM Na-MES pH 6.8, 50 mM NaCl, 1 mM EDTA (buffer A) and after 2 h in 20 mM Na-MES pH 6.8, 1 M NaCl, 1 mM EDTA (buffer B). Protein was then purified into a cation-exchange chromatography column (HisTrap, HP) and eluted with buffer B.

Next, a purification step with SEC was carried out in gel filtration buffer (1X PBS, 1 mM DTT). The purified monomeric *hTau441-WT* was concentrated and its concentration was measured as described for the other proteins above.

α-synuclein

Purification of α -synuclein (used unlabeled in the experiments) - The procedure for the expression and purification of α -synuclein was carried out as previously described (Nuscher et al., 2004; Ruf et al., 2019, 2020). In brief, the plasmid pET-5acontaining human wildtype alpha-Synuclein with a codon 136 TAC > TAT nucleotide exchange for improved bacterial expression was introduced into BL21(DE3) *E. coli* (New England Biolabs, Ipswich, MA, USA). Bacterial cultures were grown at 37 °C until an optical density (OD) of approximately 0.5. Protein expression was subsequently induced by adding 1 M IPTG (PepLab, Erlangen, Germany) and maintained over 4 hours at 37 °C. After heat inactivation of proteases and cell lysis, the protein was extracted from the filtrated lysate via an anion exchange column (HiTrap Q HP, 5 ml; GE Healthcare, Chicago, IL, USA) and further purified via gel filtration chromatography (Superdex 75 10/300 GL; GE Healthcare, Chicago, IL, USA).

The concentration of the protein was adjusted to 1 mg/mL, after which the aliquots were snap-frozen in liquid nitrogen and stored at -80 °C.

Purification of α -synuclein (afterwards labeled for the experiments) - The preparation of α -synuclein was conducted as previously described (Hoyer et al., 2002). Briefly, the pT7-7 α -synuclein N122C plasmid (original wild-type plasmid by Hilal Lashuel, Addgene #36046) was transformed into BL21 Ai cells. The cells were grown in LB medium at 37°C to an OD600 of 0.7, and expression was induced with IPTG and arabinose, followed by shaking overnight at 28°C. After harvesting, the cells were lysed in lysis buffer (50 mM Tris, 10 mM EDTA, 1 mM PMSF) using three cycles through a continuous flow cell disruptor (Constant Systems Ltd.). The cell lysate was centrifuged at 20,000 x g for 1 h. The supernatant was transferred to a new tube and incubated in boiling water for 25 min. The solution was centrifuged again at 20,000 x g for 45 min. The resulting supernatant was supplemented with 10 mg/ml streptomycin sulfate and incubated for 15 minutes at 4°C, followed by centrifugation at 20,000 x g for 45 minutes. The supernatant was then treated with 361 mg/ml ammonium sulfate and incubated for 30 min at 4°C. After centrifugation at 20,000 x g for 45 min, the pellet was resuspended in 25 mM Tris, pH 7.7, and dialyzed against the same buffer twice overnight at 4°C.

Labeling of recombinant proteins with fluorescent dyes

TDP-43-MBP was labeled with AlexaFluor-488 or AlexaFluor-633 C₅ maleimide (Thermo Fisher) following the manufacturer's instructions at low labeling efficiency (0.05-0.1) to minimize the effect of the dye on the protein condensation and aggregation behavior. In brief, dye was added to the

protein in storage buffer (20 mM Tris pH 8.0, 300 mM NaCl, 10% glycerol, 2 mM TCEP) with a protein:dye ratio of ~50:1, for 2 h at Room Temperature (RT) and protected from light.

Similarly, Tau and MBP were labelled with DyLight-488 or DyLight-650 NHS Ester (Thermo Fisher) at low labeling efficiency (0.05-0.1) with a protein:dye ratio of ~50:1. The storage buffer for Tau is 1X PBS, 1 mM DTT, instead for MBP the same storage buffer of TDP-43-MBP is used. Following the manufacturer protocol, the proteins were incubated with the dye in the dark for 1 h at RT.

α -synuclein was labelled as described for the above proteins using AlexaFluor-488 C₅ maleimide (Thermo Fisher) or LD650-MAL (Lumidyne) in PBS storage buffer.

In all cases, free dye was removed by repeated washes in protein-specific storage buffer using an Amicon ultra centrifugal columns (Merck Millipore).

***In vitro* phase separation and aggregation assays**

Formation of Alexa488-TDP-43 condensates formation

Each time before starting any *in vitro* assay, TDP-43-MBP and MBP were centrifuged at 21,000 g for 10 min at 4°C to discard any preformed protein precipitates.

Alexa488-TDP-43 phase separation was performed by cleavage of 5 μ M Alexa488-TDP-43-TEV-MBP-His₆ with 100 μ g/mL His₆-TEV protease at RT in PS buffer (20 mM HEPES pH 7.5, 150 mM NaCl, 1 mM DTT). Alexa488-TDP-43 condensates were formed in absence or presence of unlabeled or 650-labeled Tau, MBP and α -synuclein, respectively, at 0.5 to 2-fold concentration; proteins mixtures were added to μ -Slide 18 Well-Flat ibiTreat chambers (Ibidi, #81826). Images were taken either after ~30 min of TEV addition with the confocal microscope to visualize the condensates formation, or after 15 min TEV addition with the spinning disc confocal microscope to generate a time lapse over the time course of 45 min.

Alexa488-TDP-43 aggregates formation

Using low binding tubes (Eppendorf), 10 μ M Alexa488-TDP-43 was cleaved with 100 μ g/mL TEV protease at RT in aggregation buffer (50 mM Tris pH 8.0, 250 mM NaCl, 5% glycerol, 5% sucrose, 150 mM imidazole pH 8.0), in absence or presence of unlabeled or 650-labeled Tau, MBP and α -synuclein, respectively, at 0.5 to 2-fold concentration. Consequently, proteins mixtures were shaken on a thermomixer at 1,000 rpm at 22°C for 30min and then transferred to a μ -Slide 18 Well-Flat ibiTreat chamber. Images of aggregates were taken after ~2 h with the confocal microscope.

To display the dual colors images in Fig. EV1D, a linear enhancement for brightness and contrast was applied.

Semi-denaturing detergent agarose gel electrophoresis (SDD-AGE)

SDD-AGE experiments were performed following the protocols of (French et al., 2019) and (Halfmann and Lindquist, 2008). 2 μ M TDP-43-TEV-MBP-His₆ was incubated alone or in presence of unlabeled Tau, MBP and α -synuclein at equimolar concentration in aggregation buffer supplemented with 1X protease inhibitors (Sigma). Proteins samples were collected at different time points (0, 1 h, 2 h, 8 h, 1 day (d), 2 d, 6 d) after 30 min shaking at 1,000 rpm at 22°C on the thermomixer. Later, 5 μ L of each sample was diluted in SDD-AGE buffer (40 mM Tris-HCl pH 6.8, 5% glycerol, 0.5% SDS, 0.1% bromphenol-blue) and analysed by horizontal 1.5% agarose gel electrophoresis (1.5% agarose in 20 mM Tris, 200 mM glycine and 0.1% SDS) in running buffer (60 mM Tris, 20 mM acetate, 20 mM glycine 1 mM EDTA, 0.1% SDS) for ~6h at 60 V. Afterwards, proteins were transferred from the gel to a nitrocellulose membrane (see protocol Halfmann and Lindquist, 2008 for details) and detected by standard Western Blot (WB) procedure. Rabbit anti TDP-43 N-term antibody (Proteintech, #10782-2-AP) was used to visualize the monomers, oligomers and high-molecular-weight species bands.

Turbidity assay

For the turbidity assay, Tau (5 μM) condensates in the presence or absence of TDP-43-MBP, MBP and α -synuclein in three different concentrations (2, 4 and 8 μM) were prepared in condensation buffer (20 mM HEPES pH 7.5, 150 mM NaCl, 0.1 mM EDTA, 2 mM DTT) with the addition of 5% (w/vol) polyethelene glycol 8000 (PEG) (Roth, #0263.1). Samples were then transferred into a 384-well μClear plates (Greiner) and the absorbance was measured at 600 nm in a plate reader (Cytation 3, Biotek). Measurements were collected every 5 minutes over the course of 1 hour, followed by measurements every 15 minutes for additional 2 hours. Prior to each measurement, the plate was shaken for 5 sec to prevent sedimentation of the dense phase.

DyLight488-Tau condensates formation

Tau phase separation was performed by adding 4 μM DyLight488-Tau in condensation buffer (20 mM HEPES pH 7.5, 150 mM NaCl, 0.1 mM EDTA, 2 mM DTT) with 10% (w/vol) PEG, or 5 μM DyLight488-Tau in a low salt buffer (25 mM HEPES pH 7.5, 10 mM NaCl, 1 mM DTT) with 2.2 $\mu\text{g}/\text{mL}$ Heparin (Appllichem, #A3004,0001). DyLight488-Tau condensates were formed in absence or presence of unlabeled TDP-43-MBP, MBP, α -synuclein, TDP-43-NTD-MBP and TDP-43-CTD-MBP or Alexa633-TDP-43-MBP, DyLight650-MBP and LD650- α -synuclein at 0.5 to 2-fold concentration; proteins mixtures were then added to μ -Slide 18 Well-Flat ibiTreat chambers, and, images were taken after 1 h, 4 h and 24 h of PEG addition, or after \sim 20 min of Heparin addition.

Tau fibrils formation

In order to prepare *in vitro* Tau fibrils, 50 μM of unlabeled Tau in absence and presence of equimolar concentration of unlabeled TDP-43-MBP, MBP, α -synuclein, TDP-43-NTD-MBP and TDP-43-CTD-MBP were added in 1X PBS, 0.3% NaN_3 , 2 mM DTT buffer with 12.5 μM Heparin for 1, 2 and 5 days at 37°C.

Fibrils were then imaged by Transmission Electron Microscopy (TEM), and analysed by ImageJ/Fiji software measuring the length of the structure in μm .

Cell Culture assays

Cellular Tau seeding assay

HEK293 CFP/YFP-TauRD^{P301S} cells used for the Tau seeding experiments co-express two Tau-repeat domains (TauRD) carrying the frontotemporal dementia (FTD)-mutation P301S and fused to either the cyan or the yellow fluorescent proteins (CFP and YFP, respectively) (Holmes et al., 2014) provided by Marc Diamond. μ -Slide 8 Well ibiTreat chambers (Ibidi, #80826) were coated with 50 $\mu\text{g}/\text{mL}$ poly-D-lysine for at least 1h, and subsequently 2×10^4 cells/well were seeded on these plates and grown in Opti-MEM GlutaMAX Supplement (Thermo Fisher, #51985026), supplemented with 5% Fetal Bovine Serum (FBS) and 1% penicillin/streptomycin (Pen/Strep) medium. The next day, 5 μg of either 5 days old recombinant Tau aggregates formed in presence and absence of TDP-43-MBP, MBP, α -synuclein, TDP-43-NTD-MBP and TDP-43-CTD-mBP, or SarkoSpin extracts obtained from FTLD-TDP, FTLD-Tau, AD-Tau or Non-ND patients, respectively, were added in OPTI-MEM and transfected into the cells with 0.8% lipofectamine 2000 (Invitrogen, #52887); after 2h, cell medium was completely exchanged with fresh grow medium. For live cell confocal microscopy, intracellular aggregates were visualized after 1 or 3 days after cell transfection as bright accumulations by FRET signal (green channel, $\lambda=488$ nm excitation), and nuclei were stained using Hoechst 33342 (1:2000, Invitrogen, #H3570).

Cellular TDP-43 seeding assay

TDP-43 seeding assay was performed using HEK293T Flp-In-T-REx cells (provided by Magdalini Polymenidou, University of Zurich) that express nuclear TDP-43-HA under a doxycycline inducible promoter (Laferrère et al., 2019). Cells were grown in DMEM high glucose GlutaMAX Supplement (Thermo Fisher, #61965026), 5% FBS Tet system approved (Thermo Fisher, #A47364-01) and 1% Pen/Strep. After coating plates with 50 µg/mL poly-D-lysine for at least 1h, 5×10^4 cells/well were seeded and induced ~5/6 h using 1 µg/mL of doxycycline (Sigma, D9891). On the next day, 14.2 µg of FTLD-TDP, FTLD-Tau, AD-Tau, and Non-ND patient extracts were incubated with OptiMEM and Lipofectamine2000 for 30 min and subsequently added to the cells. Medium was replaced with fresh medium supplemented with 7 µM Palbociclib (Sigma, #PZ0383) and 1 µg/mL of doxycycline 3 h after transfection and once more on the following day, again with 7 µM Palbociclib and 1 µg/mL of doxycycline. Finally, cells were fixed and stained 6 days after transfection.

Immunostaining

After fixation of HEK-TDP-43-HA cells with 4% PFA for 10 min, cells were washed with 1X PBS supplemented with 2 mM MgCl₂ and 1mM CaCl₂ (PBS+). Subsequently, cells were permeabilized for 5 min using 0.2 % Triton X-100 in PBS. After several washes in PBS+ to remove detergent, cells were blocked with 2% BSA in PBS+ for 30min at RT. Incubation with primary antibodies mouse anti HA antibody (#9658, Sigma) and rabbit phospho TDP-43 antibody (#80007-1-RR, Proteintech) diluted in blocking buffer was carried out for 2-3 hours at RT, or o/n at 4 °C. After three washes with PBS+, cells were incubated with secondary antibodies diluted in blocking buffer for 1h at RT. Finally, nuclei were counterstained using DAPI at 0.5 µg/mL in PBS+ for 5 min, before coverslips were mounted with ProLong™ Diamond Antifade reagent (#36961, Invitrogen) on microscopy slides.

To display the images in Fig. 6E and Fig. EV4D, a linear enhancement for brightness and contrast was applied.

Patient samples

Postmortem brain tissue

Patient samples were kindly provided by Tammarny Lashley (Queen Square Brain Bank (QSBB) for Neurological Disorders at University of College of London (UCL)), and the Netherland Brain Bank (NBB) at the Netherlands Institute for Neuroscience, Amsterdam (Table 1).

Homogenization of brain tissue

Homogenization of patient brain tissue was performed as described in (De Rossi et al., 2021; Laferrère et al., 2019).

SarkoSpin preparation on brain homogenates

After homogenisation with Precellys Evolution Touch Homogenizer (#P002511-PEVT0-a.0) of patient brain tissue, 150 µL of brain homogenate (approximately 30 mg of tissue per aliquot) were prepared in high salt (HS) buffer 10 mM Tris-HCl, pH 7.4, 150 mM NaCl, 0.5 mM EDTA, 1 mM DTT, complete EDTA-free protease inhibitors (Roche, #04693132001), PhosphoSTOP phosphatase inhibitors (Roche, #4906845001), and stored at -80°C. Subsequently, 50 µL of HS buffer with 1 µL benzonase HC (Merck Millipore, #71205-3) and 14 mM MgCl₂ was added to each aliquot to digest nucleic acids for 5 min at RT; then, 200 µL of 2X HS buffer containing 4% w/v N-lauroyl-sarcosine (Sigma, #61739) was added, and samples were incubated on a thermoblock for 45 min at 38°C with 600 rpm shaking to solubilise non-aggregated proteins. Furthermore, 200 µL of ice-cold HS buffer with 0.5% sarkosyl was added and the samples were centrifuged at 21200 x g for 30 min at RT to pellet the sarkosyl-insoluble protein fraction. The supernatant was removed, and pellets were washed twice with 200 µL of 1X PBS to remove as much of the surrounding

lipids as possible. Pellets for immediate use were resuspended in 100 μ L of PBS by sonication (Branson Sonifier W-250 D, amplitude = 60%, pulse = 2s on/ 2s off, time = 3 minutes), or dry pellets were snap frozen on dry ice and stored at -80°C prior to use.

Fluorescent and chemiluminescent western blot of patient samples

The concentration of protein in resuspended sarkosyl-insoluble fractions was determined using a BCA assay, according to the manufacturer's instructions (Interchim, #UP40840A). 3X Loading buffer (200 mM Tris-HCl pH 6.8, 6% SDS, 20% Glycerol, 0.1 g/mL DTT, 0.1 mg Bromophenol Blue) was added to a final concentration of 1X in each sample, and these were then denatured for 10 minutes at 80°C . 2 μ g of sarkosyl-insoluble protein were loaded per lane on 10% Tris-Glycine gel, and the samples were run at 180 V for 1h; then, proteins were transferred to a PVDF membrane (Invitrogen, #IB24002) using the iBlot2 dry transfer system (7 minute transfer time at 20 V). Membranes were subsequently washed with 1X Tris-buffered saline with 0.1% Tween-20 (TBST), and blocked for 30 minutes at RT in iBlock blocking buffer (Invitrogen, #T2015). Primary antibodies for TDP-43 (Proteintech 10782-2-AP, 1:2500) and Tau (BioLegend 835204, 1:1000) were added to membranes in iBlock blocking buffer, and these were then incubated for 2.5 h at RT. Membranes were then washed in TBST, and secondary staining was carried out in iBlock blocking buffer, for 1 h in the dark at RT. The fluorescent secondary antibodies used were goat anti-mouse Alexa-fluor 647 (Thermo Scientific, #A-21235) and goat anti-rabbit Alexa-fluor 568 (Thermo Scientific, #A-11011); for chemiluminescent WB, the Horseradish peroxidase (HRP)-conjugated anti-mouse (Promega, #W402B) and HRP anti-rabbit (Promega, #W401B) secondary antibodies were used with a final dilution of 1:10000. Membranes were subsequently washed 3x in TBST and developed using a Fusion FX imager Vilber (fluorescent WB) or AMERSHAM ImageQuant 800 (chemiluminescent WB).

Microscopy

Confocal microscopies

- a. Images of fluorescently labeled proteins were acquired on an inverted Zeiss LSM800 Axio Observer.Z1/7 and a LSM710 Axio Observer confocal laser scanning microscopes (Carl Zeiss) using a Plan-Apochromat 63x/1.40 Oil DIC M27 objective and two-line averaging at $101.41\ \mu\text{m} \times 101.41\ \mu\text{m}$ scaled resolution.
To display the dual colors images in Fig. EV1B and D, a linear enhancement for brightness and contrast was applied.
- b. For the HEK cells experiments, the same LSM800 microscope was used, with a Plan-Apochromat 20x/0.8 M27 objective and two-line averaging at $319.45\ \mu\text{m} \times 319.45\ \mu\text{m}$ scaled resolution.
To display the dual colors images in Fig 6E and Fig. EV4D, a linear enhancement for brightness and contrast was applied.

The following excitation and emission wavelength fluorescence settings were used for detection: DAPI 353-465 nm, GFP 493-517 nm, Alexa555 553-568 nm, Alexa633 631-647 nm and Dy650 654-675 nm.

- c. For high resolution imaging of Tau/TDP-43 condensates, an inverted Zeiss Axio Observer 7 confocal microscope was used, with a LSM 900 laser module equipped with lasers for 488 and 640 nm. Images were taken using sequential, bidirectional scanning and two-fold frame averaging with a 63x/1.4 oil objective. 20 Z-stacks with 0.17 μm intervals were acquired with an image pixel size of 40 nm using the Airyscan 2 detector (490-700 nm). Subsequently, images were processed using the built-in Airyscan 3D imaging processing plugin in the Zen software.

Spinning disc confocal microscopy

The TDP-43 PS time lapse experiments were performed using an inverted spinning disc microscope (Visiscope 5 Elements, Visitron Systems GmbH, Germany - IMB Microscopy Core Facility), built on a Nikon Ti2 stand equipped with a confocal spinning disc (CSU-W1; Yokogawa, Japan) and a 60x/1.2 NA water objective was used for acquisition.

Negative staining and transmission electron microscopy (TEM)

Tau fibrils were diluted in distilled water to a final concentration of 1 μ M. For transmission electron microscopic (TEM) observation, carbon coated copper grids (Science Services) were glow discharged for 30 sec in a Harrick plasma cleaner (PDC-32G-2) to facilitate adsorption. After fixing the grid by anti-capillary inverse tweezers (Dumont) a sample volume of 1.5 μ l was pipetted onto the grid for 2 min and blotted shortly using filter paper (Whatman). Negative staining was performed by addition of 1.5 μ L 1% uranyl acetate in water for 30 s. After blotting, the grid was air dried for at least 30 min. Transmission Electron Microscopy micrographs were acquired on a JEM 1400plus (JEOL) equipped with a XF416 camera (TVIPS) and the EM-Menu software (TVIPS).

Quantification and analysis

All the statistical analyses were performed with GraphPad Prism 10.2, and details are provided in each figure legend.

In vitro experiments quantification

In the experiments depicting the formation of Alexa488-TDP-43 condensates and aggregates in the presence or absence of unlabeled Tau, MBP or α -synuclein, structures were quantified using an in-house script made with python 3.8 through the AICSImageIO library (Maxfield Brown et al., 2021), a tool designed for reading multidimensional bioimaging formats. To mitigate background noise, the intensity of pixels with an intensity below a threshold of 10 or 50 (for the phase separation and aggregation assay, respectively) was set to 0, while preserving the other pixel values. Then, the images were thresholded using Li thresholding algorithm and labeled through scikit-image package. The images were then assessed for object quantity and area through scikit-image to analyse condensates and aggregates, respectively.

For the other TDP-43 and Tau *in vitro* experiments, the quantification was always carried out with the ImageJ/Fiji software, analysing the area or the mean fluorescence intensity of particles bigger than 0.3 μ m, with a circularity of 0.00-1.00.

SDD-AGE analysis

The SDD-AGE analysis was performed in ImageJ/Fiji by creating a ROI for each different band size (monomers, oligomers, high molecular species as indicated) for all the time points. ROIs were then measured as area of the bands and values were normalized to the sum of the area of the bands at time 0.

Cellular images analysis

Analysis of the Tau cellular seeding assay was performed in ImageJ/Fiji software. Briefly, Tau cytoplasmic aggregates, as a result of FRET signal visualized in the green channel, were counted using the Find Maxima command with prominence > 150 or 180; the values were then plotted as number of aggregates per number of cells

For the TDP-43 seeding assay, images were read using python 3.8 through the AICSImageIO library (Maxfield Brown et al., 2021). To mitigate background noise, the background level was set to 0 for each channel, while preserving the other pixel values. Cellpose (Stringer et al., 2021) was used to create an AI-assisted mask of nuclei from the DAPI channel (with the parameters: flow threshold=1, diameter=150, cell probability threshold=0, model type="cyto"), enabling the separation of cytoplasmic and nuclear signal for each channel. Colocalization of cytoplasmic HA

(green channel) and cytoplasmic pS409/410-TDP-43 (red channel) were performed using numpy arrays. Objects were labeled with a threshold intensity of 35 using the scikit-image library. Objects with a pixel size smaller than 10 pixels were identified through the scikit-image library and discarded from the analysis. The quantity and area of objects in the colocalized signal was calculated using the scikit-image library and divided per the number of nuclei as determined from Cellpose output.

Acknowledgements

We thank Cornelia Niemann and Georg Kislinger for technical support and Eszter Katona for valuable discussions and comments on the manuscript. We thank Tom Scheidt for the generous gift of labelled alpha-synuclein. We are grateful to the imaging core facilities of the Institute for Molecular Biology (IMB) Mainz for access to microscopes and technical support, and to the Protein Production Core Facility of IMB Mainz, especially Sabine Heinen and Martin Möckel, for production of recombinant hTau441-WT.

This work was supported by the Alzheimer Research Award by the Hans and Ilse Breuer Foundation (to D.D.), an anonymous foundation, and the German Research Foundation (DFG) within the Heisenberg Programme (project number 442698351, to DD).

The ZEISS LSM 900 was funded by the Ministry of Science and Health of Rhineland-Palatinate and the European Regional Development Fund (ERDF/REACT-EU, Grant No. 84012490). The Spinning Disk Confocal System (IMB Microscopy Core Facility) was supported by the Deutsche Forschungsgemeinschaft (INST 247/912-1FUGG), and the Stellaris spinning disc confocal microscope (IMB Microscopy Core Facility) is funded by the DFG (project number 497669232). The transmission electron microscopy was supported by the DFG under Germany's Excellence Strategy within the framework of the Munich Cluster for Systems Neurology (EXC 2145 SyNergy, ID 390857198, to DD, DE and MS) and SFB TRR 274/2 2024 – 408885537 project Z01 (to MS). MP gratefully acknowledges the support of the Swiss National Science Foundation (310030_192650) and the Association for Frontotemporal Dementia (AFTD Biomarker Initiative grant).

Authors contribution

Conceptualization: F.S., D.E., D.D. Methodology: F.S., S.H., J.H., H.R., L.M.R., M.S., I.U., W.Z., T.L., M.Z., M.P., S.W., D.E., D.D.; I.U. performed part of the SarkoSpin preparation of brain homogenates and part of the extracts WB analysis; W.Z. performed part of the SarkoSpin preparation of brain homogenates; M.S. took some of the final images (Fig. 4B) using the EM microscope. Software: A.R. Validation: F.S., D.E., D.D. Formal Analysis: F.S., S.H., A.R., I.U., W.Z., L.M.R. Investigation: F.S., S.H., I.U., W.Z., L.M.R. Resources: M.S., V.R., T.L., M.Z., M.P., S.W., D.E., D.D. Data Curation: F.S., S.H., A.R. Writing – original draft: F.S., D.E., D.D. Writing – review & editing: all. Visualization: F.S., S.H., S.W., D.E., D.D. Supervision: D.E., D.D. Project Administration: D.E., D.D. Funding Acquisition: D.E., D.D.

Disclosure and competing interest statement

The authors declare that they have no competing interests.

References

- Alberti, S., Dormann, D., 2019. Liquid-Liquid Phase Separation in Disease. *Annu. Rev. Genet.* 53, 171–194. <https://doi.org/10.1146/annurev-genet-112618-043527>
- Alberti, S., Gladfelter, A., Mittag, T., 2019. Considerations and Challenges in Studying Liquid-Liquid Phase Separation and Biomolecular Condensates. *Cell* 176, 419–434. <https://doi.org/10.1016/j.cell.2018.12.035>
- Alberti, S., Hyman, A.A., 2016. Are aberrant phase transitions a driver of cellular aging? *BioEssays News Rev. Mol. Cell. Dev. Biol.* 38, 959–968. <https://doi.org/10.1002/bies.201600042>
- Amador-Ortiz, C., Lin, W.-L., Ahmed, Z., Personett, D., Davies, P., Duara, R., Graff-Radford, N.R., Hutton, M.L., Dickson, D.W., 2007. TDP-43 immunoreactivity in hippocampal sclerosis and Alzheimer's disease. *Ann. Neurol.* 61, 435–445. <https://doi.org/10.1002/ana.21154>
- Ambadipudi, S., Biernat, J., Riedel, D., Mandelkow, E., Zweckstetter, M., 2017. Liquid-liquid phase separation of the microtubule-binding repeats of the Alzheimer-related protein Tau. *Nat. Commun.* 8, 275. <https://doi.org/10.1038/s41467-017-00480-0>
- Arai, T., Mackenzie, I.R.A., Hasegawa, M., Nonaka, T., Niizato, K., Tsuchiya, K., Iritani, S., Onaya, M., Akiyama, H., 2009. Phosphorylated TDP-43 in Alzheimer's disease and dementia with Lewy bodies. *Acta Neuropathol. (Berl.)* 117, 125–136. <https://doi.org/10.1007/s00401-008-0480-1>
- Ash, P.E.A., Lei, S., Shattuck, J., Boudeau, S., Carlomagno, Y., Medalla, M., Mashimo, B.L., Socorro, G., Al-Mohanna, L.F.A., Jiang, L., Öztürk, M.M., Knobel, M., Ivanov, P., Petrucelli, L., Wegmann, S., Kanaan, N.M., Wolozin, B., 2021. TIA1 potentiates tau phase separation and promotes generation of toxic oligomeric tau. *Proc. Natl. Acad. Sci. U. S. A.* 118, e2014188118. <https://doi.org/10.1073/pnas.2014188118>
- Barghorn, S., Biernat, J., Mandelkow, E., 2005. Purification of recombinant tau protein and preparation of Alzheimer-paired helical filaments in vitro. *Methods Mol. Biol. Clifton NJ* 299, 35–51. <https://doi.org/10.1385/1-59259-874-9:035>
- Bentmann, E., Neumann, M., Tahirovic, S., Rodde, R., Dormann, D., Haass, C., 2012. Requirements for Stress Granule Recruitment of Fused in Sarcoma (FUS) and TAR DNA-binding Protein of 43 kDa (TDP-43). *J. Biol. Chem.* 287, 23079–23094. <https://doi.org/10.1074/jbc.M111.328757>
- Berger, Z., Roder, H., Hanna, A., Carlson, A., Rangachari, V., Yue, M., Wszolek, Z., Ashe, K., Knight, J., Dickson, D., Andorfer, C., Rosenberry, T.L., Lewis, J., Hutton, M., Janus, C., 2007. Accumulation of Pathological Tau Species and Memory Loss in a Conditional Model of Tauopathy. *J. Neurosci.* 27, 3650–3662. <https://doi.org/10.1523/JNEUROSCI.0587-07.2007>
- Braak, H., Braak, E., 1995. Staging of Alzheimer's disease-related neurofibrillary changes. *Neurobiol. Aging* 16, 271–278; discussion 278-284. [https://doi.org/10.1016/0197-4580\(95\)00021-6](https://doi.org/10.1016/0197-4580(95)00021-6)
- Braak, H., Braak, E., 1991. Neuropathological stageing of Alzheimer-related changes. *Acta Neuropathol. (Berl.)* 82, 239–259. <https://doi.org/10.1007/BF00308809>
- Brettschneider, J., Del Tredici, K., Lee, V.M.-Y., Trojanowski, J.Q., 2015. Spreading of pathology in neurodegenerative diseases: a focus on human studies. *Nat. Rev. Neurosci.* 16, 109–120. <https://doi.org/10.1038/nrn3887>

- Choronenkyy, Y., Fardo, D.W., Nelson, P.T., 2019. Tau and TDP-43 proteinopathies: kindred pathologic cascades and genetic pleiotropy. *Lab. Investig. J. Tech. Methods Pathol.* 99, 993–1007. <https://doi.org/10.1038/s41374-019-0196-y>
- Chou, C.-C., Zhang, Y., Umoh, M.E., Vaughan, S.W., Lorenzini, I., Liu, F., Sayegh, M., Donlin-Asp, P.G., Chen, Y.H., Duong, D.M., Seyfried, N.T., Powers, M.A., Kukar, T., Hales, C.M., Gearing, M., Cairns, N.J., Boylan, K.B., Dickson, D.W., Rademakers, R., Zhang, Y.-J., Petrucelli, L., Sattler, R., Zarnescu, D.C., Glass, J.D., Rossoll, W., 2018. TDP-43 pathology disrupts nuclear pore complexes and nucleocytoplasmic transport in ALS/FTD. *Nat. Neurosci.* 21, 228–239. <https://doi.org/10.1038/s41593-017-0047-3>
- Clippinger, A.K., D’Alton, S., Lin, W.-L., Gendron, T.F., Howard, J., Borchelt, D.R., Cannon, A., Carlomagno, Y., Chakrabarty, P., Cook, C., Golde, T.E., Levites, Y., Ranum, L., Schultheis, P.J., Xu, G., Petrucelli, L., Sahara, N., Dickson, D.W., Giasson, B., Lewis, J., 2013. Robust cytoplasmic accumulation of phosphorylated TDP-43 in transgenic models of tauopathy. *Acta Neuropathol. (Berl.)* 126, 39–50. <https://doi.org/10.1007/s00401-013-1123-8>
- Conicella, A.E., Zerze, G.H., Mittal, J., Fawzi, N.L., 2016. ALS Mutations Disrupt Phase Separation Mediated by α -Helical Structure in the TDP-43 Low-Complexity C-Terminal Domain. *Struct. Lond. Engl.* 1993 24, 1537–1549. <https://doi.org/10.1016/j.str.2016.07.007>
- D’Angelo, M.A., Raices, M., Panowski, S.H., Hetzer, M.W., 2009. Age-dependent deterioration of nuclear pore complexes causes a loss of nuclear integrity in postmitotic cells. *Cell* 136, 284–295. <https://doi.org/10.1016/j.cell.2008.11.037>
- Das, T., Zaidi, F., Farag, M., Ruff, K.M., Messing, J., Taylor, J.P., Pappu, R.V., Mittag, T., 2024. Metastable condensates suppress conversion to amyloid fibrils. *BioRxiv Prepr. Serv. Biol.* 2024.02.28.582569. <https://doi.org/10.1101/2024.02.28.582569>
- Davis, S.A., Gan, K.A., Dowell, J.A., Cairns, N.J., Gitcho, M.A., 2017. TDP-43 expression influences amyloid β plaque deposition and tau aggregation. *Neurobiol. Dis.* 103, 154–162. <https://doi.org/10.1016/j.nbd.2017.04.012>
- De Rossi, P., Lewis, A.J., Furrer, J., De Vos, L., Demeter, T., Zbinden, A., Zhong, W., Wiersma, V.I., Scialo, C., Weber, J., Guo, Z., Scaramuzza, S., Di Fabrizio, M., Böing, C., Castaño-Díez, D., Al-Amoudi, A., Pérez-Berlanga, M., Lashley, T., Stahlberg, H., Polymenidou, M., 2021. FTLTD-TDP assemblies seed neoaggregates with subtype-specific features via a prion-like cascade. *EMBO Rep.* 22, e53877. <https://doi.org/10.15252/embr.202153877>
- DeVos, S.L., Corjuc, B.T., Oakley, D.H., Nobuhara, C.K., Bannan, R.N., Chase, A., Commins, C., Gonzalez, J.A., Dooley, P.M., Frosch, M.P., Hyman, B.T., 2018. Synaptic Tau Seeding Precedes Tau Pathology in Human Alzheimer’s Disease Brain. *Front. Neurosci.* 12, 267. <https://doi.org/10.3389/fnins.2018.00267>
- Dewey, C.M., Cenik, B., Sephton, C.F., Dries, D.R., Mayer, P., Good, S.K., Johnson, B.A., Herz, J., Yu, G., 2011. TDP-43 is directed to stress granules by sorbitol, a novel physiological osmotic and oxidative stressor. *Mol. Cell. Biol.* 31, 1098–1108. <https://doi.org/10.1128/MCB.01279-10>
- Dhakal, S., Mondal, M., Mirzazadeh, A., Banerjee, S., Ghosh, A., Rangachari, V., 2023. α -Synuclein emulsifies TDP-43 prion-like domain—RNA liquid droplets to promote heterotypic amyloid fibrils. *Commun. Biol.* 6, 1227. <https://doi.org/10.1038/s42003-023-05608-1>
- Dujardin, S., Hyman, B.T., 2019. Tau Prion-Like Propagation: State of the Art and Current Challenges. *Adv. Exp. Med. Biol.* 1184, 305–325. https://doi.org/10.1007/978-981-32-9358-8_23
- Emmanouilidis, L., Bartalucci, E., Kan, Y., Ijavi, M., Pérez, M.E., Afanasyev, P., Boehringer, D., Zehnder, J., Parekh, S.H., Bonn, M., Michaels, T.C.T., Wiegand, T., Allain, F.H.-T., 2024. A solid

beta-sheet structure is formed at the surface of FUS droplets during aging. *Nat. Chem. Biol.* 1–9. <https://doi.org/10.1038/s41589-024-01573-w>

Feiler, M.S., Strobel, B., Freischmidt, A., Helferich, A.M., Kappel, J., Brewer, B.M., Li, D., Thal, D.R., Walther, P., Ludolph, A.C., Danzer, K.M., Weishaupt, J.H., 2015. TDP-43 is intercellularly transmitted across axon terminals. *J. Cell Biol.* 211, 897–911. <https://doi.org/10.1083/jcb.201504057>

Fitzpatrick, A.W.P., Falcon, B., He, S., Murzin, A.G., Murshudov, G., Garringer, H.J., Crowther, R.A., Ghetti, B., Goedert, M., Scheres, S.H.W., 2017. Cryo-EM structures of tau filaments from Alzheimer's disease. *Nature* 547, 185–190. <https://doi.org/10.1038/nature23002>

French, R.L., Grese, Z.R., Aligireddy, H., Dhavale, D.D., Reeb, A.N., Kedia, N., Kotzbauer, P.T., Bieschke, J., Ayala, Y.M., 2019. Detection of TAR DNA-binding protein 43 (TDP-43) oligomers as initial intermediate species during aggregate formation. *J. Biol. Chem.* 294, 6696–6709. <https://doi.org/10.1074/jbc.RA118.005889>

Furman, J.L., Vaquer-Alicea, J., White, C.L., Cairns, N.J., Nelson, P.T., Diamond, M.I., 2017. Widespread tau seeding activity at early Braak stages. *Acta Neuropathol. (Berl.)* 133, 91–100. <https://doi.org/10.1007/s00401-016-1644-z>

Gerson, J.E., Kaye, R., 2013. Formation and propagation of tau oligomeric seeds. *Front. Neurol.* 4, 93. <https://doi.org/10.3389/fneur.2013.00093>

Gracia, P., Polanco, D., Tarancón-Díez, J., Serra, I., Bracci, M., Oroz, J., Laurents, D.V., García, I., Cremades, N., 2022. Molecular mechanism for the synchronized electrostatic coacervation and co-aggregation of alpha-synuclein and tau. *Nat. Commun.* 13, 4586. <https://doi.org/10.1038/s41467-022-32350-9>

Grujic da Silva, L.A., Simonetti, F., Hutten, S., Riemenschneider, H., Sternburg, E.L., Pietrek, L.M., Gebel, J., Dötsch, V., Edbauer, D., Hummer, G., Stelzl, L.S., Dormann, D., 2022. Disease-linked TDP-43 hyperphosphorylation suppresses TDP-43 condensation and aggregation. *EMBO J.* 41, e108443. <https://doi.org/10.15252/embj.2021108443>

Guo, T., Noble, W., Hanger, D.P., 2017. Roles of tau protein in health and disease. *Acta Neuropathol. (Berl.)* 133, 665–704. <https://doi.org/10.1007/s00401-017-1707-9>

Halfmann, R., Lindquist, S., 2008. Screening for Amyloid Aggregation by Semi-Denaturing Detergent-Agarose Gel Electrophoresis. *J. Vis. Exp.* 838. <https://doi.org/10.3791/838>

Hernández-Vega, A., Braun, M., Scharrel, L., Jahnel, M., Wegmann, S., Hyman, B.T., Alberti, S., Diez, S., Hyman, A.A., 2017. Local Nucleation of Microtubule Bundles through Tubulin Concentration into a Condensed Tau Phase. *Cell Rep.* 20, 2304–2312. <https://doi.org/10.1016/j.celrep.2017.08.042>

Higashi, S., Iseki, E., Yamamoto, R., Minegishi, M., Hino, H., Fujisawa, K., Togo, T., Katsuse, O., Uchikado, H., Furukawa, Y., Kosaka, K., Arai, H., 2007. Concurrence of TDP-43, tau and alpha-synuclein pathology in brains of Alzheimer's disease and dementia with Lewy bodies. *Brain Res.* 1184, 284–294. <https://doi.org/10.1016/j.brainres.2007.09.048>

Hochmair, J., Exner, C., Franck, M., Dominguez-Baquero, A., Diez, L., Brognaro, H., Kraushar, M.L., Mielke, T., Radbruch, H., Kaniyappan, S., Falke, S., Mandelkow, E., Betzel, C., Wegmann, S., 2022. Molecular crowding and RNA synergize to promote phase separation, microtubule interaction, and seeding of Tau condensates. *EMBO J.* 41, e108882. <https://doi.org/10.15252/embj.2021108882>

Hofweber, M., Hutten, S., Bourgeois, B., Spreitzer, E., Niedner-Boblenz, A., Schifferer, M., Ruepp, M.-D., Simons, M., Niessing, D., Madl, T., Dormann, D., 2018. Phase Separation of FUS Is

Suppressed by Its Nuclear Import Receptor and Arginine Methylation. *Cell* 173, 706-719.e13. <https://doi.org/10.1016/j.cell.2018.03.004>

Holmes, B.B., Furman, J.L., Mahan, T.E., Yamasaki, T.R., Mirbaha, H., Eades, W.C., Belaygorod, L., Cairns, N.J., Holtzman, D.M., Diamond, M.I., 2014. Proteopathic tau seeding predicts tauopathy in vivo. *Proc. Natl. Acad. Sci.* 111. <https://doi.org/10.1073/pnas.1411649111>

Hoyer, W., Antony, T., Cherny, D., Heim, G., Jovin, T.M., Subramaniam, V., 2002. Dependence of alpha-synuclein aggregate morphology on solution conditions. *J. Mol. Biol.* 322, 383–393. [https://doi.org/10.1016/s0022-2836\(02\)00775-1](https://doi.org/10.1016/s0022-2836(02)00775-1)

Hutten, S., Usluer, S., Bourgeois, B., Simonetti, F., Odeh, H.M., Fare, C.M., Czuppa, M., Hruska-Plochan, M., Hofweber, M., Polymenidou, M., Shorter, J., Edbauer, D., Madl, T., Dormann, D., 2020. Nuclear Import Receptors Directly Bind to Arginine-Rich Dipeptide Repeat Proteins and Suppress Their Pathological Interactions. *Cell Rep.* 33, 108538. <https://doi.org/10.1016/j.celrep.2020.108538>

Josephs, K.A., Dickson, D.W., Tosakulwong, N., Weigand, S.D., Murray, M.E., Petrucelli, L., Liesinger, A.M., Senjem, M.L., Spychalla, A.J., Knopman, D.S., Parisi, J.E., Petersen, R.C., Jack, C.R., Whitwell, J.L., 2017. Rates of hippocampal atrophy and presence of post-mortem TDP-43 in patients with Alzheimer's disease: a longitudinal retrospective study. *Lancet Neurol.* 16, 917–924. [https://doi.org/10.1016/S1474-4422\(17\)30284-3](https://doi.org/10.1016/S1474-4422(17)30284-3)

Josephs, K.A., Murray, M.E., Whitwell, J.L., Parisi, J.E., Petrucelli, L., Jack, C.R., Petersen, R.C., Dickson, D.W., 2014a. Staging TDP-43 pathology in Alzheimer's disease. *Acta Neuropathol. (Berl.)* 127, 441–450. <https://doi.org/10.1007/s00401-013-1211-9>

Josephs, K.A., Whitwell, J.L., Tosakulwong, N., Weigand, S.D., Murray, M.E., Liesinger, A.M., Petrucelli, L., Senjem, M.L., Ivnik, R.J., Parisi, J.E., Petersen, R.C., Dickson, D.W., 2015. TAR DNA-binding protein 43 and pathological subtype of Alzheimer's disease impact clinical features. *Ann. Neurol.* 78, 697–709. <https://doi.org/10.1002/ana.24493>

Josephs, K.A., Whitwell, J.L., Weigand, S.D., Murray, M.E., Tosakulwong, N., Liesinger, A.M., Petrucelli, L., Senjem, M.L., Knopman, D.S., Boeve, B.F., Ivnik, R.J., Smith, G.E., Jack, C.R., Parisi, J.E., Petersen, R.C., Dickson, D.W., 2014b. TDP-43 is a key player in the clinical features associated with Alzheimer's disease. *Acta Neuropathol. (Berl.)* 127, 811–824. <https://doi.org/10.1007/s00401-014-1269-z>

Jucker, M., Walker, L.C., 2011. Pathogenic protein seeding in Alzheimer disease and other neurodegenerative disorders. *Ann. Neurol.* 70, 532–540. <https://doi.org/10.1002/ana.22615>

Kadokura, A., Yamazaki, T., Lemere, C.A., Takatama, M., Okamoto, K., 2009. Regional distribution of TDP-43 inclusions in Alzheimer disease (AD) brains: their relation to AD common pathology. *Neuropathol. Off. J. Jpn. Soc. Neuropathol.* 29, 566–573. <https://doi.org/10.1111/j.1440-1789.2009.01017.x>

Kanaan, N.M., Hamel, C., Grabinski, T., Combs, B., 2020. Liquid-liquid phase separation induces pathogenic tau conformations in vitro. *Nat. Commun.* 11, 2809. <https://doi.org/10.1038/s41467-020-16580-3>

Laferrière, F., Maniecka, Z., Pérez-Berlanga, M., Hruska-Plochan, M., Gilhespy, L., Hock, E.-M., Wagner, U., Afroz, T., Boersema, P.J., Barmettler, G., Foti, S.C., Asi, Y.T., Isaacs, A.M., Al-Amoudi, A., Lewis, A., Stahlberg, H., Ravits, J., De Giorgi, F., Ichas, F., Bezard, E., Picotti, P., Lashley, T., Polymenidou, M., 2019. TDP-43 extracted from frontotemporal lobar degeneration subject brains displays distinct aggregate assemblies and neurotoxic effects reflecting disease progression rates. *Nat. Neurosci.* 22, 65–77. <https://doi.org/10.1038/s41593-018-0294-y>

Lasagna-Reeves, C.A., Castillo-Carranza, D.L., Sengupta, U., Clos, A.L., Jackson, G.R., Kaye, R., 2011. Tau oligomers impair memory and induce synaptic and mitochondrial dysfunction in wild-type mice. *Mol. Neurodegener.* 6, 39. <https://doi.org/10.1186/1750-1326-6-39>

Latimer, C.S., Liachko, N.F., 2021. Tau and TDP-43 synergy: a novel therapeutic target for sporadic late-onset Alzheimer's disease. *GeroScience* 43, 1627–1634. <https://doi.org/10.1007/s11357-021-00407-0>

Latimer, C.S., Stair, J.G., Hincks, J.C., Currey, H.N., Bird, T.D., Keene, C.D., Kraemer, B.C., Liachko, N.F., 2022. TDP-43 promotes tau accumulation and selective neurotoxicity in bigenic *Caenorhabditis elegans*. *Dis. Model. Mech.* 15, dmm049323. <https://doi.org/10.1242/dmm.049323>

Ling, S.-C., Polymenidou, M., Cleveland, D.W., 2013. Converging mechanisms in ALS and FTD: disrupted RNA and protein homeostasis. *Neuron* 79, 416–438. <https://doi.org/10.1016/j.neuron.2013.07.033>

Linsenmeier, M., Faltova, L., Morelli, C., Capasso Palmiero, U., Seiffert, C., Küffner, A.M., Pinotsi, D., Zhou, J., Mezzenga, R., Arosio, P., 2023. The interface of condensates of the hnRNPA1 low-complexity domain promotes formation of amyloid fibrils. *Nat. Chem.* 15, 1340–1349. <https://doi.org/10.1038/s41557-023-01289-9>

Maxfield Brown, E., Toloudis, D., Sherman, J., Swain-Browden, M., Lambert, T., 2021. AICSImageIO: Image Reading, Metadata Conversion, and Image Writing for Microscopy Images in Pure Python.

Melamed, Z., López-Erauskin, J., Baughn, M.W., Zhang, O., Drenner, K., Sun, Y., Freyermuth, F., McMahon, M.A., Beccari, M.S., Artates, J.W., Ohkubo, T., Rodriguez, M., Lin, N., Wu, D., Bennett, C.F., Rigo, F., Da Cruz, S., Ravits, J., Lagier-Tourenne, C., Cleveland, D.W., 2019. Premature polyadenylation-mediated loss of stathmin-2 is a hallmark of TDP-43-dependent neurodegeneration. *Nat. Neurosci.* 22, 180–190. <https://doi.org/10.1038/s41593-018-0293-z>

Meneses, A., Koga, S., O'Leary, J., Dickson, D.W., Bu, G., Zhao, N., 2021. TDP-43 Pathology in Alzheimer's Disease. *Mol. Neurodegener.* 16, 84. <https://doi.org/10.1186/s13024-021-00503-x>

Molliex, A., Temirov, J., Lee, J., Coughlin, M., Kanagaraj, A.P., Kim, H.J., Mittag, T., Taylor, J.P., 2015. Phase separation by low complexity domains promotes stress granule assembly and drives pathological fibrillization. *Cell* 163, 123–133. <https://doi.org/10.1016/j.cell.2015.09.015>

Montalbano, M., McAllen, S., Cascio, F.L., Sengupta, U., Garcia, S., Bhatt, N., Ellsworth, A., Heidelman, E.A., Johnson, O.D., Doskocil, S., Kaye, R., 2020. TDP-43 and Tau Oligomers in Alzheimer's Disease, Amyotrophic Lateral Sclerosis, and Frontotemporal Dementia. *Neurobiol. Dis.* 146, 105130. <https://doi.org/10.1016/j.nbd.2020.105130>

Montine, T.J., Phelps, C.H., Beach, T.G., Bigio, E.H., Cairns, N.J., Dickson, D.W., Duyckaerts, C., Frosch, M.P., Masliah, E., Mirra, S.S., Nelson, P.T., Schneider, J.A., Thal, D.R., Trojanowski, J.Q., Vinters, H.V., Hyman, B.T., 2012. National Institute on Aging–Alzheimer's Association guidelines for the neuropathologic assessment of Alzheimer's disease: a practical approach. *Acta Neuropathol. (Berl.)* 123, 1–11. <https://doi.org/10.1007/s00401-011-0910-3>

Nedelsky, N.B., Taylor, J.P., 2019. Bridging biophysics and neurology: aberrant phase transitions in neurodegenerative disease. *Nat. Rev. Neurol.* 15, 272–286. <https://doi.org/10.1038/s41582-019-0157-5>

Neumann, M., Sampathu, D.M., Kwong, L.K., Truax, A.C., Micsenyi, M.C., Chou, T.T., Bruce, J., Schuck, T., Grossman, M., Clark, C.M., McCluskey, L.F., Miller, B.L., Masliah, E., Mackenzie, I.R., Feldman, H., Feiden, W., Kretzschmar, H.A., Trojanowski, J.Q., Lee, V.M.-Y., 2006. Ubiquitinated

TDP-43 in frontotemporal lobar degeneration and amyotrophic lateral sclerosis. *Science* 314, 130–133. <https://doi.org/10.1126/science.1134108>

Nuscher, B., Kamp, F., Mehnert, T., Odoj, S., Haass, C., Kahle, P.J., Beyer, K., 2004. Alpha-synuclein has a high affinity for packing defects in a bilayer membrane: a thermodynamics study. *J. Biol. Chem.* 279, 21966–21975. <https://doi.org/10.1074/jbc.M401076200>

Oakley, S.S., Maina, M.B., Marshall, K.E., Al-Hilaly, Y.K., Harrington, C.R., Wischik, C.M., Serpell, L.C., 2020. Tau Filament Self-Assembly and Structure: Tau as a Therapeutic Target. *Front. Neurol.* 11, 590754. <https://doi.org/10.3389/fneur.2020.590754>

Patel, A., Lee, H.O., Jawerth, L., Maharana, S., Jahnel, M., Hein, M.Y., Stoyanov, S., Mahamid, J., Saha, S., Franzmann, T.M., Pozniakovski, A., Poser, I., Maghelli, N., Royer, L.A., Weigert, M., Myers, E.W., Grill, S., Drechsel, D., Hyman, A.A., Alberti, S., 2015. A Liquid-to-Solid Phase Transition of the ALS Protein FUS Accelerated by Disease Mutation. *Cell* 162, 1066–1077. <https://doi.org/10.1016/j.cell.2015.07.047>

Polymenidou, M., Cleveland, D.W., 2011. The seeds of neurodegeneration: prion-like spreading in ALS. *Cell* 147, 498–508. <https://doi.org/10.1016/j.cell.2011.10.011>

Polymenidou, M., Lagier-Tourenne, C., Hutt, K.R., Huelga, S.C., Moran, J., Liang, T.Y., Ling, S.-C., Sun, E., Wancewicz, E., Mazur, C., Kordasiewicz, H., Sedaghat, Y., Donohue, J.P., Shiue, L., Bennett, C.F., Yeo, G.W., Cleveland, D.W., 2011. Long pre-mRNA depletion and RNA missplicing contribute to neuronal vulnerability from loss of TDP-43. *Nat. Neurosci.* 14, 459–468. <https://doi.org/10.1038/nn.2779>

Rai, S.K., Khanna, R., Avni, A., Mukhopadhyay, S., 2023. Heterotypic electrostatic interactions control complex phase separation of tau and prion into multiphasic condensates and co-aggregates. *Proc. Natl. Acad. Sci. U. S. A.* 120, e2216338120. <https://doi.org/10.1073/pnas.2216338120>

Ratti, A., Buratti, E., 2016. Physiological functions and pathobiology of TDP-43 and FUS/TLS proteins. *J. Neurochem.* 138 Suppl 1, 95–111. <https://doi.org/10.1111/jnc.13625>

Ray, S., Singh, N., Kumar, R., Patel, K., Pandey, S., Datta, D., Mahato, J., Panigrahi, R., Navalkar, A., Mehra, S., Gadhe, L., Chatterjee, D., Sawner, A.S., Maiti, S., Bhatia, S., Gerez, J.A., Chowdhury, A., Kumar, A., Padinhateeri, R., Riek, R., Krishnamoorthy, G., Maji, S.K., 2020. α -Synuclein aggregation nucleates through liquid-liquid phase separation. *Nat. Chem.* 12, 705–716. <https://doi.org/10.1038/s41557-020-0465-9>

Ruf, V.C., Nübling, G.S., Willikens, S., Shi, S., Schmidt, F., Levin, J., Bötzel, K., Kamp, F., Giese, A., 2019. Different Effects of α -Synuclein Mutants on Lipid Binding and Aggregation Detected by Single Molecule Fluorescence Spectroscopy and ThT Fluorescence-Based Measurements. *ACS Chem. Neurosci.* 10, 1649–1659. <https://doi.org/10.1021/acscchemneuro.8b00579>

Ruf, V.C., Shi, S., Schmidt, F., Weckbecker, D., Nübling, G.S., Ködel, U., Mollenhauer, B., Giese, A., 2020. Potential sources of interference with the highly sensitive detection and quantification of alpha-synuclein seeds by qRT-QuIC. *FEBS Open Bio* 10, 883–893. <https://doi.org/10.1002/2211-5463.12844>

Shen, Yi, Chen, A., Wang, W., Shen, Yinan, Ruggeri, F.S., Aime, S., Wang, Z., Qamar, S., Espinosa, J.R., Garaizar, A., St George-Hyslop, P., Colleparado-Guevara, R., Weitz, D.A., Vigolo, D., Knowles, T.P.J., 2023. The liquid-to-solid transition of FUS is promoted by the condensate surface. *Proc. Natl. Acad. Sci.* 120, e2301366120. <https://doi.org/10.1073/pnas.2301366120>

Shih, Y.-H., Tu, L.-H., Chang, T.-Y., Ganesan, K., Chang, W.-W., Chang, P.-S., Fang, Y.-S., Lin, Y.-T., Jin, L.-W., Chen, Y.-R., 2020. TDP-43 interacts with amyloid- β , inhibits fibrillization, and

worsens pathology in a model of Alzheimer's disease. *Nat. Commun.* 11, 5950. <https://doi.org/10.1038/s41467-020-19786-7>

Smith, V.D., Bachstetter, A.D., Ighodaro, E., Roberts, K., Abner, E.L., Fardo, D.W., Nelson, P.T., 2018. Overlapping but distinct TDP-43 and tau pathologic patterns in aged hippocampi. *Brain Pathol. Zurich Switz.* 28, 264–273. <https://doi.org/10.1111/bpa.12505>

Spires-Jones, T.L., Attems, J., Thal, D.R., 2017. Interactions of pathological proteins in neurodegenerative diseases. *Acta Neuropathol. (Berl.)* 134, 187–205. <https://doi.org/10.1007/s00401-017-1709-7>

Stringer, C., Wang, T., Michaelos, M., Pachitariu, M., 2021. Cellpose: a generalist algorithm for cellular segmentation. *Nat. Methods* 18, 100–106. <https://doi.org/10.1038/s41592-020-01018-x>

Tai, H.-C., Serrano-Pozo, A., Hashimoto, T., Frosch, M.P., Spires-Jones, T.L., Hyman, B.T., 2012. The Synaptic Accumulation of Hyperphosphorylated Tau Oligomers in Alzheimer Disease Is Associated With Dysfunction of the Ubiquitin-Proteasome System. *Am. J. Pathol.* 181, 1426–1435. <https://doi.org/10.1016/j.ajpath.2012.06.033>

Takeda, S., Wegmann, S., Cho, H., DeVos, S.L., Commins, C., Roe, A.D., Nicholls, S.B., Carlson, G.A., Pitstick, R., Nobuhara, C.K., Costantino, I., Frosch, M.P., Müller, D.J., Irimia, D., Hyman, B.T., 2015. Neuronal uptake and propagation of a rare phosphorylated high-molecular-weight tau derived from Alzheimer's disease brain. *Nat. Commun.* 6, 8490. <https://doi.org/10.1038/ncomms9490>

Taylor, J.P., Hardy, J., Fischbeck, K.H., 2002. Toxic proteins in neurodegenerative disease. *Science* 296, 1991–1995. <https://doi.org/10.1126/science.1067122>

Thal, D.R., Rüb, U., Orantes, M., Braak, H., 2002. Phases of A beta-deposition in the human brain and its relevance for the development of AD. *Neurology* 58, 1791–1800. <https://doi.org/10.1212/wnl.58.12.1791>

Thomas, D.X., Bajaj, S., McRae-McKee, K., Hadjichrysanthou, C., Anderson, R.M., Collinge, J., 2020. Association of TDP-43 proteinopathy, cerebral amyloid angiopathy, and Lewy bodies with cognitive impairment in individuals with or without Alzheimer's disease neuropathology. *Sci. Rep.* 10, 14579. <https://doi.org/10.1038/s41598-020-71305-2>

Tomé, S.O., Gomes, L.A., Li, X., Vandenberghe, R., Tousseyn, T., Thal, D.R., 2021. TDP-43 interacts with pathological τ protein in Alzheimer's disease. *Acta Neuropathol. (Berl.)*. <https://doi.org/10.1007/s00401-021-02295-2>

Tomé, S.O., Tsaka, G., Ronisz, A., Ospitalieri, S., Gawor, K., Gomes, L.A., Otto, M., Von Arnim, C.A.F., Van Damme, P., Van Den Bosch, L., Ghebremedhin, E., Laureyssen, C., Slegers, K., Vandenberghe, R., Rousseau, F., Schymkowitz, J., Thal, D.R., 2023. TDP-43 pathology is associated with increased tau burdens and seeding. *Mol. Neurodegener.* 18, 71. <https://doi.org/10.1186/s13024-023-00653-0>

Tomé, S.O., Vandenberghe, R., Ospitalieri, S., Van Schoor, E., Tousseyn, T., Otto, M., von Arnim, C.A.F., Thal, D.R., 2020. Distinct molecular patterns of TDP-43 pathology in Alzheimer's disease: relationship with clinical phenotypes. *Acta Neuropathol. Commun.* 8, 61. <https://doi.org/10.1186/s40478-020-00934-5>

Tremblay, C., St-Amour, I., Schneider, J., Bennett, D.A., Calon, F., 2011. Accumulation of TAR DNA Binding Protein-43 (TDP-43) in Mild Cognitive Impairment and Alzheimer Disease. *J. Neuropathol. Exp. Neurol.* 70, 788–798. <https://doi.org/10.1097/NEN.0b013e31822c62cf>

- Tziortzouda, P., Van Den Bosch, L., Hirth, F., 2021. Triad of TDP43 control in neurodegeneration: autoregulation, localization and aggregation. *Nat. Rev. Neurosci.* 22, 197–208. <https://doi.org/10.1038/s41583-021-00431-1>
- Uemura, N., Uemura, M.T., Luk, K.C., Lee, V.M.-Y., Trojanowski, J.Q., 2020. Cell-to-Cell Transmission of Tau and α -Synuclein. *Trends Mol. Med.* 26, 936–952. <https://doi.org/10.1016/j.molmed.2020.03.012>
- Ukmar-Godec, T., Hutten, S., Grieshop, M.P., Rezaei-Ghaleh, N., Cima-Omori, M.-S., Biernat, J., Mandelkow, E., Söding, J., Dormann, D., Zweckstetter, M., 2019. Lysine/RNA-interactions drive and regulate biomolecular condensation. *Nat. Commun.* 10, 2909. <https://doi.org/10.1038/s41467-019-10792-y>
- Usenovic, M., Niroomand, S., Drolet, R.E., Yao, L., Gaspar, R.C., Hatcher, N.G., Schachter, J., Renger, J.J., Parmentier-Batteur, S., 2015. Internalized Tau Oligomers Cause Neurodegeneration by Inducing Accumulation of Pathogenic Tau in Human Neurons Derived from Induced Pluripotent Stem Cells. *J. Neurosci.* 35, 14234–14250. <https://doi.org/10.1523/JNEUROSCI.1523-15.2015>
- Vanderweyde, T., Yu, H., Varnum, M., Liu-Yesucevitz, L., Citro, A., Ikezu, T., Duff, K., Wolozin, B., 2012. Contrasting Pathology of the Stress Granule Proteins TIA-1 and G3BP in Tauopathies. *J. Neurosci.* 32, 8270–8283. <https://doi.org/10.1523/JNEUROSCI.1592-12.2012>
- Wang, A., Conicella, A.E., Schmidt, H.B., Martin, E.W., Rhoads, S.N., Reeb, A.N., Nourse, A., Ramirez Montero, D., Ryan, V.H., Rohatgi, R., Shewmaker, F., Naik, M.T., Mittag, T., Ayala, Y.M., Fawzi, N.L., 2018. A single N-terminal phosphomimic disrupts TDP-43 polymerization, phase separation, and RNA splicing. *EMBO J.* 37, e97452. <https://doi.org/10.15252/embj.201797452>
- Ward, S.M., Himmelstein, D.S., Lancia, J.K., Binder, L.I., 2012. Tau oligomers and tau toxicity in neurodegenerative disease. *Biochem. Soc. Trans.* 40, 667–671. <https://doi.org/10.1042/BST20120134>
- Wegmann, S., Eftekhazadeh, B., Tepper, K., Zoltowska, K.M., Bennett, R.E., Dujardin, S., Laskowski, P.R., MacKenzie, D., Kamath, T., Commins, C., Vanderburg, C., Roe, A.D., Fan, Z., Mollieux, A.M., Hernandez-Vega, A., Muller, D., Hyman, A.A., Mandelkow, E., Taylor, J.P., Hyman, B.T., 2018. Tau protein liquid-liquid phase separation can initiate tau aggregation. *EMBO J.* 37, e98049. <https://doi.org/10.15252/embj.201798049>
- Wolozin, B., Ivanov, P., 2019. Stress granules and neurodegeneration. *Nat. Rev. Neurosci.* 20, 649–666. <https://doi.org/10.1038/s41583-019-0222-5>
- Yan, X., Kuster, D., Mohanty, P., Nijssen, J., Pombo-García, K., Rizuan, A., Franzmann, T.M., Sergeeva, A., Passos, P.M., George, L., Wang, S.-H., Shenoy, J., Danielson, H.L., Honigmann, A., Ayala, Y.M., Fawzi, N.L., Mittal, J., Alberti, S., Hyman, A.A., 2024. Intra-condensate demixing of TDP-43 inside stress granules generates pathological aggregates. *BioRxiv Prepr. Serv. Biol.* 2024.01.23.576837. <https://doi.org/10.1101/2024.01.23.576837>
- Zbinden, A., Pérez-Berlangua, M., De Rossi, P., Polymenidou, M., 2020. Phase Separation and Neurodegenerative Diseases: A Disturbance in the Force. *Dev. Cell* 55, 45–68. <https://doi.org/10.1016/j.devcel.2020.09.014>
- Zhang, X., Lin, Y., Eschmann, N.A., Zhou, H., Rauch, J.N., Hernandez, I., Guzman, E., Kosik, K.S., Han, S., 2017. RNA stores tau reversibly in complex coacervates. *PLoS Biol.* 15, e2002183. <https://doi.org/10.1371/journal.pbio.2002183>
- Zhang, X., Vigers, M., McCarty, J., Rauch, J.N., Fredrickson, G.H., Wilson, M.Z., Shea, J.-E., Han, S., Kosik, K.S., 2020. The proline-rich domain promotes Tau liquid-liquid phase separation in cells. *J. Cell Biol.* 219, e202006054. <https://doi.org/10.1083/jcb.202006054>

Figure legends

Figure 1: Tau, but not MBP or α -synuclein, causes formation of large irregular TDP-43 condensates

- A. Scheme of Alexa488-TDP-43 phase separation assay upon TEV-cleavage of the MBP-solubility tag; created with BioRender.com.
- B. Time series of Alexa488-TDP-43 condensates formation (8 μ M) in presence or absence of DyLight650-Tau (8 μ M), from 20 to 45 min after cleavage with TEV protease; images represent frames of movie EV1A, B; scale bar: 10 μ m.
- C. Confocal images of Alexa488-TDP-43 condensates (5 μ M) in presence of unlabeled Tau, MBP or α -synuclein (2, 5 or 10 μ M), 30 min after TEV-cleavage. Scale bar: 15 μ m in overview and 8 μ m in inset.
- D. Quantification of number of particles, circularity, and size of the TDP-43 condensates. Bar graphs show the mean of (n=2) experimental replicates \pm SD. ****P < 0.0001 by one-way ANOVA with Dunnett's multiple comparison test to TDP-43 alone.

Figure 2: Tau, but not MBP or α -synuclein, promotes TDP-43 aggregation

- A. Scheme of TDP-43 aggregation assay for SDD-AGE experiment; created with BioRender.com.
- B. SDD-AGE of TDP-43-MBP (2 μ M) in the presence of the indicated protein (2 μ M) after agitation and incubation for the presented time period (h = hours, d = days); TDP-43 was visualized by immunoblotting and the middle vertical black line divides two blots which derive from the same experiment and were processed in parallel. $^{\circ\circ\circ}$ = high molecular weight (HMW) species, $^{\circ\circ}$ = oligomers and $^{\circ}$ = monomers.
- C. Quantification of band intensities of the high molecular weight species from (n=3) experimental replicates, normalized to the timepoint 0; values show the mean \pm SEM; **P = 0.0039 and *P = 0.0273 by two-way ANOVA with Dunnett's multiple comparison test to TDP-43-MBP alone at the respective time points (0, 1h, 2h, 8h, 1d, 2d, 6d).
- D. Scheme of Alexa488-TDP-43 aggregation for confocal imaging; created with BioRender.com.
- E. Confocal images of Alexa488-TDP-43 aggregates (10 μ M) in presence of unlabeled Tau, MBP or α -synuclein (5, 10 or 20 μ M) 2h after the agitation step. Scale bar: 20 μ m in overview and 15 μ m in inset.
- F. Quantification of the total area covered by the TDP-43 aggregates (Aggr. area). Bar graph shows the mean of (n=4) experimental replicates \pm SD. ***P = 0.0008 and *P = 0.0255 by one-way ANOVA with Dunnett's multiple comparison test to TDP-43 alone.

Figure 3: TDP-43 causes the formation of large, amorphous Tau condensates *in vitro*

- A. Turbidity measurements (optical density [OD] at 600 nm) 1h after PEG addition to Tau (4 μ M) in absence or presence of MBP, α -synuclein or TDP-43-MBP (2, 4, 8 μ M). Values show mean of (n=3) replicates \pm SEM. ***P = 0.0006 by one-way ANOVA with Dunnett's multiple comparison test to Tau alone.
- B. High resolution images of 1:1 DyLight488-Tau with Alexa633-TDP-43-MBP mixed condensates after 24 h incubation. Scale bar: 10 μ m.
- C. Confocal microscopy images of 4 μ M DyLight488-Tau, Alexa633-TDP-43-MBP alone, or DyLight488-Tau in equimolar presence of Alexa633-TDP-43-MBP, DyLight650-MBP or LD650- α -synuclein at the indicated timepoints (1, 4, 24 h). Scale bar: 20 μ m in overview and 5 μ m in inset.

Figure 4: TDP-43 inhibits Tau fibrillization via the TDP-43 N-terminal domain (NTD).

A. Scheme of Tau fibrillization assay; created with BioRender.com.
 B. EM images of Tau, TDP-43-MBP, MBP or α -synuclein only (50 μ M), and Tau in presence of TDP-43-MBP, MBP or α -synuclein, respectively, at equimolar ratio after 5 days incubation. Scale bars: 0.1 μ m for Tau+TDP-43-MBP and TDP-43-MBP only, and 0.5 μ m for Tau only, Tau+MBP, MBP only, Tau+ α -synuclein and α -synuclein only.
 C. Quantification of fibril length (μ m) from (n \geq 2) independent replicates; values show the length of protein structures in μ m and the bar graphs represent the mean \pm SEM; ****P < 0.0001 by one-way ANOVA with Dunnett's multiple comparison test to Tau only.
 D. EM images of Tau, TDP-43-MBP, TDP-43-NTD-MBP and TDP-43-CTD-MBP only (50 μ M), and Tau in presence of TDP-43-MBP, TDP-43-NTD-MBP and TDP-43-CTD-MBP, respectively, at equimolar ratio after 5 days incubation. Scale bars: 0.1 μ m for TDP-43-MBP only, 0.2 μ m for Tau only, Tau+TDP-43-MBP, TDP-43-NTD-MBP only, and Tau+TDP-43-CTD-MBP and 0.5 μ m for Tau+TDP-43-NTD-MBP and TDP-43-CTD-MBP only.
 E. Quantification of fibril length (μ m) from (n \geq 2) independent replicates; values show the length of protein structures in μ m and the bar graphs represent the mean \pm SEM; ****P < 0.0001 by one-way ANOVA with Dunnett's multiple comparison test to Tau only.

Figure 5: The TDP-43 NTD causes the formation of highly seeding-competent Tau species

A. Scheme of Tau seeding assay in HEK293 GFP/YFP-TauRD^{P301S} using 5 days old recombinant Tau aggregates as seeds, in the presence or absence of the indicated proteins; created with BioRender.com.
 B. Representative confocal images of cytosolic Tau aggregates (green) formed after seeding the cells with 5 days old recombinant Tau aggregates +/- TDP-43-MBP, TDP-43-NTD-MBP, TDP-43-CTD-MBP, MBP and α -synuclein, respectively. No seeds condition corresponds to the addition to the cells of lipofectamine only. Scale bar: 70 μ m in overview and 15 μ m in inset.
 C. Quantification of number of aggregates per cell. Bar graphs show the number of biological replicates \pm SEM in (n \geq 3) independent experiments. ****P < 0.0001 by one-way ANOVA with Dunnett's multiple comparison test to Tau only.

Figure 6: FTLD-TDP type A and AD brains contain seeding-competent species of Tau and TDP-43, respectively

A. Scheme of Tau seeding assay in HEK293 GFP/YFP-TauRD^{P301S} using SarkoSpin patient extracts as seeds; created with BioRender.com.
 B. Representative confocal images of cytosolic Tau aggregates (green) formed after seeding the cells with Non-ND 1, AD-Tau 1, FTLD-Tau 1, or FTLD-TDP 1 SarkoSpin extracts, respectively. Scale bar: 100 μ m in overview and 20 μ m in inset.
 C. Quantification of number of aggregates per cell. Bar graphs show the number of biological replicates \pm SEM in (n=3) independent experiments. ****P < 0.0001 and ***P = 0.0006 by one-way ANOVA with Dunnett's multiple comparison test to Non-ND 1.
 D. Scheme of TDP-43 seeding assay using doxycycline-inducible TDP-43-HA HEK293 cells; created with BioRender.com.
 E. Representative confocal images of cytosolic pS409/410-positive TDP-43 neoaggregates in HEK293 cells, after transfection with Non-ND 1, FTLD-TDP 4, FTLD-Tau 2 and AD-Tau 1 SarkoSpin patient extracts. DAPI is depicted in blue, HA staining in green, and pS409/410 in red. Scale bar: 100 μ m in overview and 20 μ m in inset.
 F. Quantification of HA and pS409/410-TDP-43 colocalization as number of neoaggregates per number of cells and area of neoaggregates per number of neoaggregates. Bar graphs show the number of biological replicates \pm SEM in (n=3) independent experiments. ****P < 0.0001 by one-way ANOVA with Dunnett's multiple comparison test to Non-ND 1.

Figure 7: Consequences of the TDP-43/Tau interaction on molecular assembly and seeding behavior.

Upper part: Model illustrating that Tau (green) and TDP-43 (red) directly interact, possibly via TDP-43's N-terminal domain and Tau's fibrillization core region. This interaction leads to the formation of irregular and multiphasic Tau/TDP-43 co-condensates, promotes TDP-43 aggregation and suppresses formation of Tau fibrils.

Lower part: Extracts of AD brains with predominant Tau pathology seed intracellular TDP-43 aggregation in a HEK293 TDP-43 reporter cell line. Similarly, extracts of FTLD-TDP type A with predominant TDP-43 pathology seed intracellular Tau aggregation in HEK293 Tau biosensor cells. Figure created with BioRender.com.

Table 1: List of post mortem brain tissue used to extract SarkoSpin fractions.

For the α -synuclein and TDP-43 columns, 1 = additional pathology is present, 0 = additional pathology is absent, na = additional pathology non-investigated. Braak Tau – refers to the spread of the Tau pathology (Braak and Braak, 1991); Thal Phase – refers to the spread of the A β pathology (Thal et al., 2002); CERAD – refers to the frequency of the A β plaques in the cortical areas; ABC – is the National Institute on Aging-Alzheimer's Association (NIA-AA) staging for Alzheimer's disease (Montine et al., 2012).

Abbreviations: Non-ND: non-neurodegenerative disease; FTLD: frontotemporal lobar degeneration; AD: Alzheimer's disease; na: non-investigated; HD: Huntington's disease; PNFA: progressive non-fluent aphasia; CBD: corticobasal degeneration; bvFTD: behavioural variant frontotemporal dementia; PSP: progressive supranuclear palsy; FTD-PPA: frontotemporal dementia-primary progressive aphasia; PART: primary age related tauopathy; CAA: cerebral amyloid angiopathy; AGD: argyrophilic grain disease; α -syn: α -synuclein.

Expanded View figure legends

Figure EV1

A. Confocal microscopy images of Alexa488-TDP-43 (5 μ M) in presence of unlabeled Tau at the indicated concentrations (0.2, 0.5, 1, 2, 5, 10 μ M) after ~30min of TEV addition. Scale bar: 15 μ m in overview and 5 μ m in inset.

B. Condensates images of Alexa488-TDP-43 (10 μ M) with equimolar DyLight650-Tau and LD650- α -synuclein ~1h after TEV-cleavage. Scale bar: 20 μ m in overview and 3 μ m in inset.

C. Quantification of DyLight650-Tau and LD650- α -synuclein proteins colocalization within the Alexa488-TDP-43 condensates in (n=4) independent replicates; values show the mean fluorescence intensity, and the bar graphs represents the mean \pm SD; ****P < 0.0001 by unpaired t-test with Welch's correction.

D. Aggregates images of Alexa488-TDP-43 aggregates (10 μ M) in presence of DyLight650-Tau or LD650- α -synuclein (10 μ M). Scale bar: 20 μ m in overview and 3 μ m in inset.

E. Quantification of the colocalization of Tau-DyLight650 and α -synuclein-LD650 within Alexa488-TDP-43 aggregates in (n=3) independent replicates; values show the mean fluorescence intensity, and the bar graphs represents the mean \pm SD; ****P < 0.0001 by unpaired t-test with Welch's correction.

Figure EV2

Confocal images of DyLight488-Tau (5 μ M) only, Alexa633-TDP-43-MBP only and DyLight488-Tau in presence of unlabeled TDP-43-MBP, MBP or α -synuclein (2, 5 or 10 μ M) after ~30 min of Heparin addition. Scale bar: 25 μ m in overview and 10 μ m in inset.

Figure EV3

EM images of Tau or Tau + TDP-43-MBP (both 50 μ M) at the indicated time points (day 1, 2, 5). Scale bar: 0.2 μ m.

Figure EV4

A. Western blot (WB) of SarkoSpin patient extracts from frontal cortex of FTLD-TDP, FTLD-Tau, AD and Non-ND patients; band below 55 kDa represents TDP-43, bands between 55 and 70 kDa represents Tau. White spaces between the blots correspond to removal of samples not used for the final experiments; the dash line separates two different blots performed in two separate experiments.

B. Representative confocal images of intracellular Tau aggregates (green) after 3 day of seeding with the indicated patient aggregates. Scale bar: 100 μ m in overview and 20 μ m in inset.

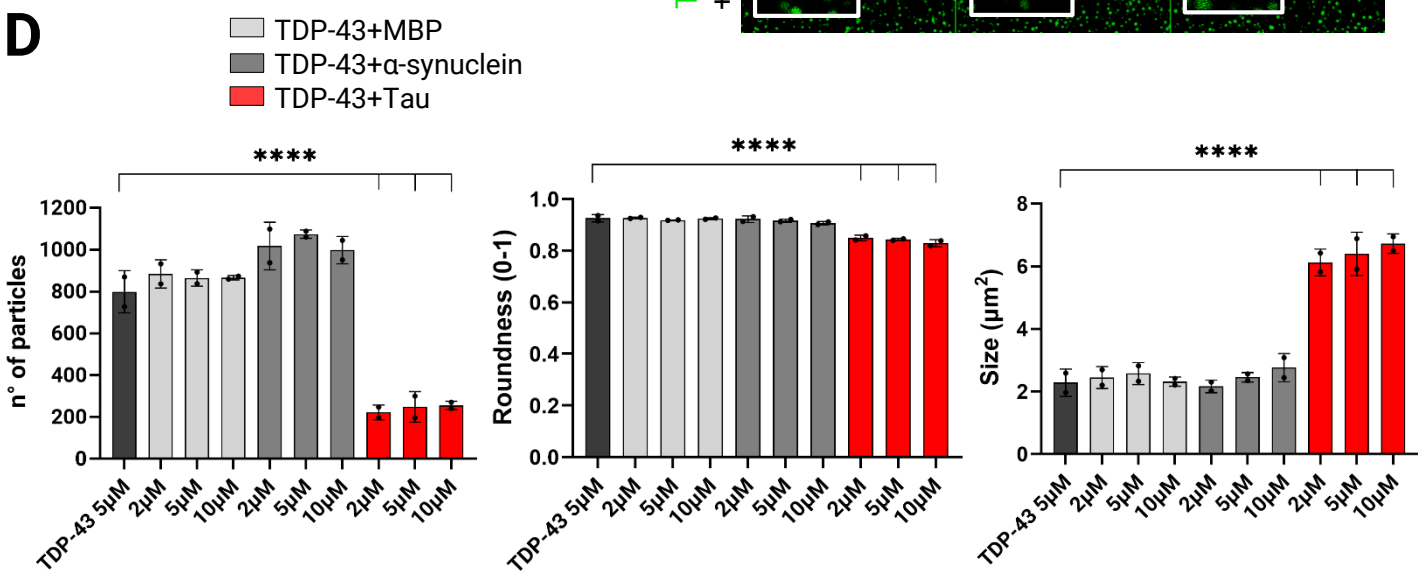
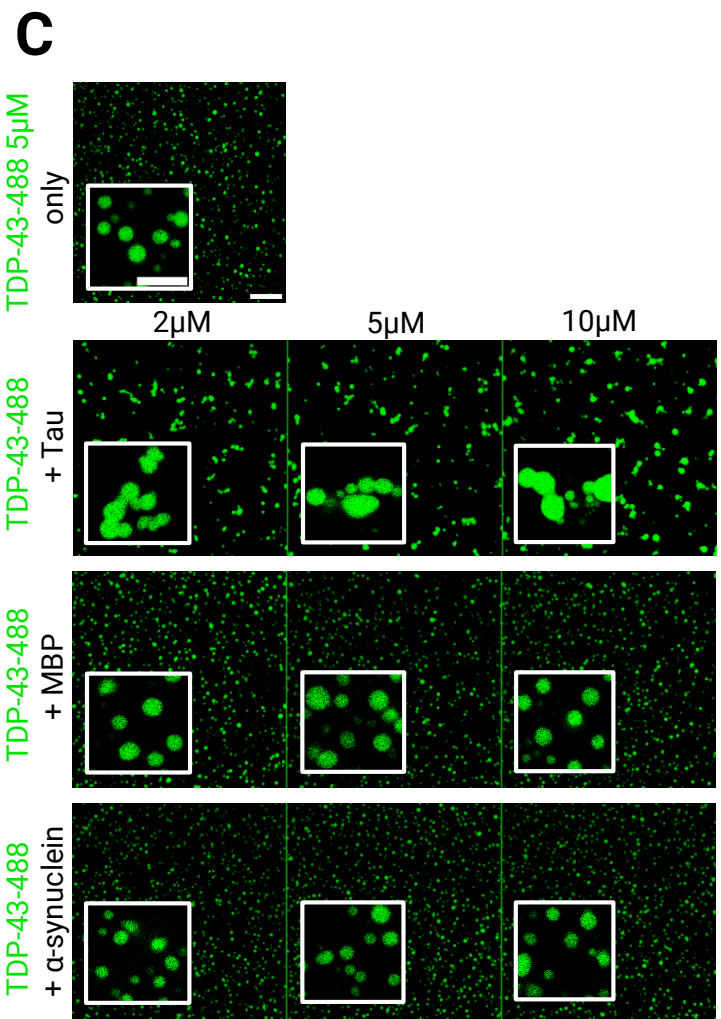
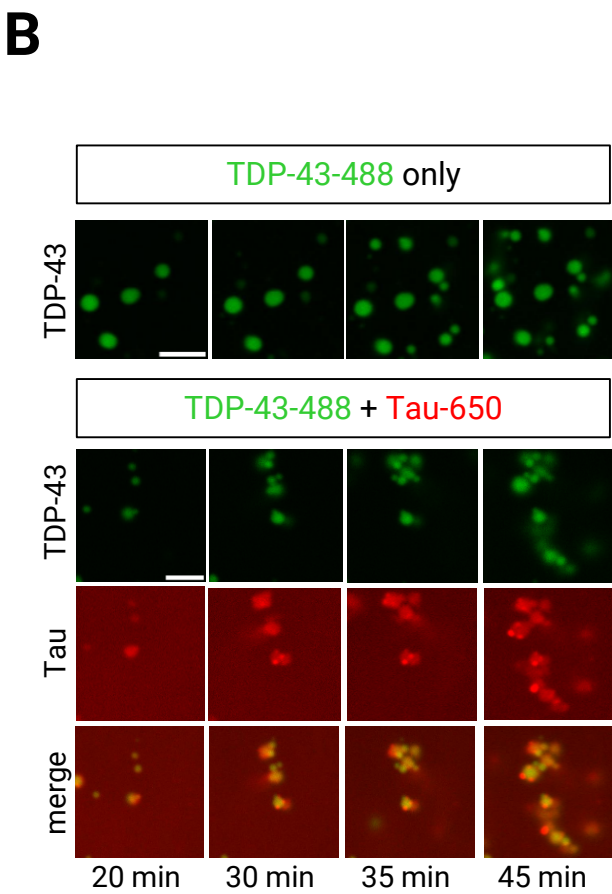
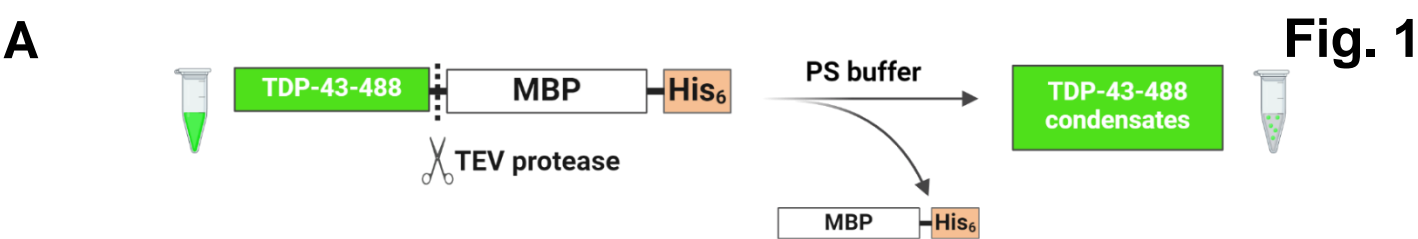
C. Images of intracellular Tau aggregates (in green) after transfecting the cells with recombinant Tau (rTau) aggregates and recombinant TDP-43 (rTDP-43) aggregates; scale bar: 50 μ m in overview and 15 μ m in inset.

D. Representative confocal images of cytosolic pS409/410-positive TDP-43 neoaggregates in HEK293 cells, after transfection with the indicated SarkoSpin extracts. DAPI is depicted in blue, HA staining in green, and pS409/410 in red. Scale bar: 100 μ m in overview and 20 μ m in inset.

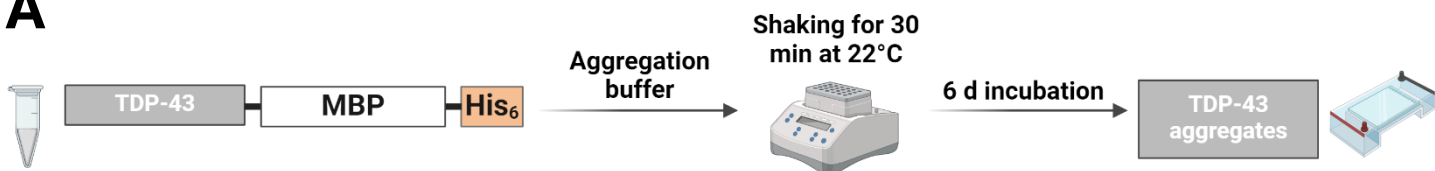
Movie EV1

A. Movie of Alexa488-TDP-43 condensate formation (8 μ M) from 20 to 45 min after cleavage with TEV protease.

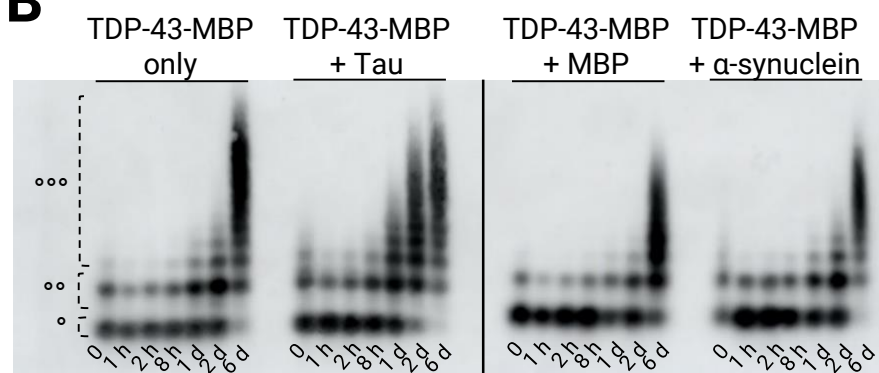
B. Movie of Alexa488-TDP-43 (8 μ M) + DyLight650-Tau (8 μ M) condensate formation from 20 to 45 min after cleavage with TEV protease.



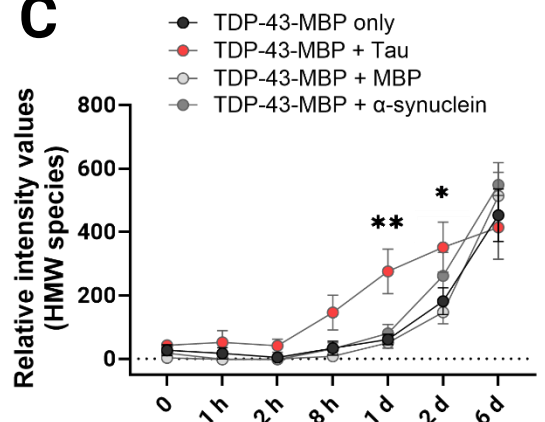
A



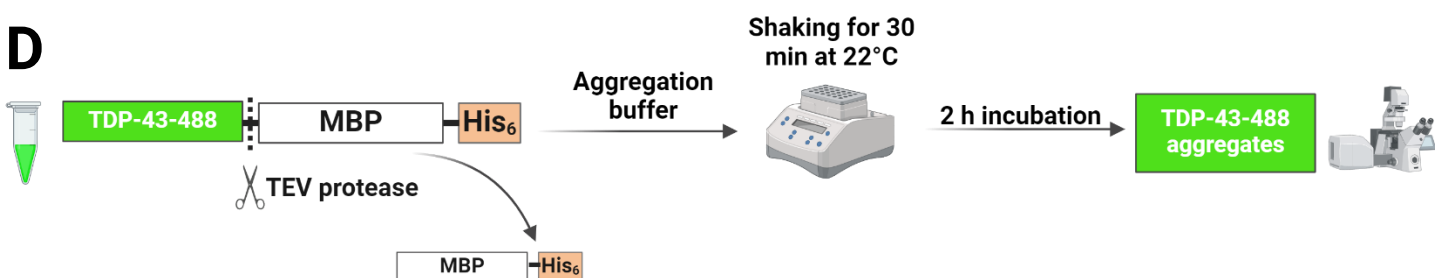
B



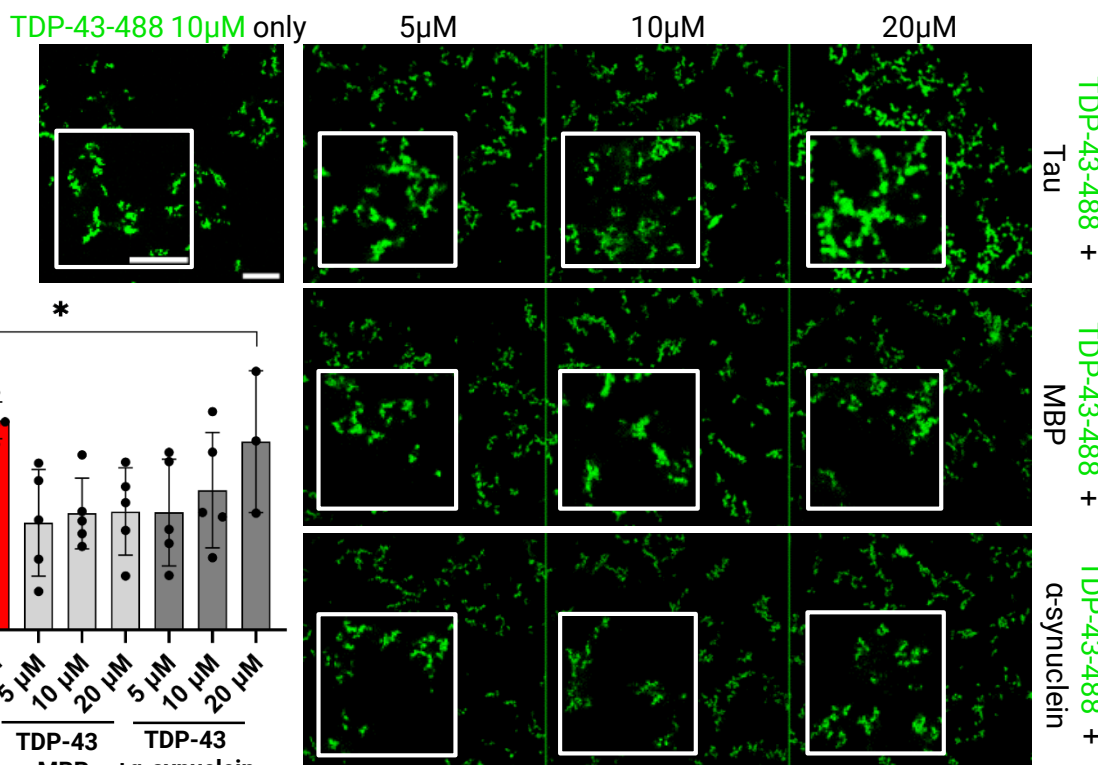
C



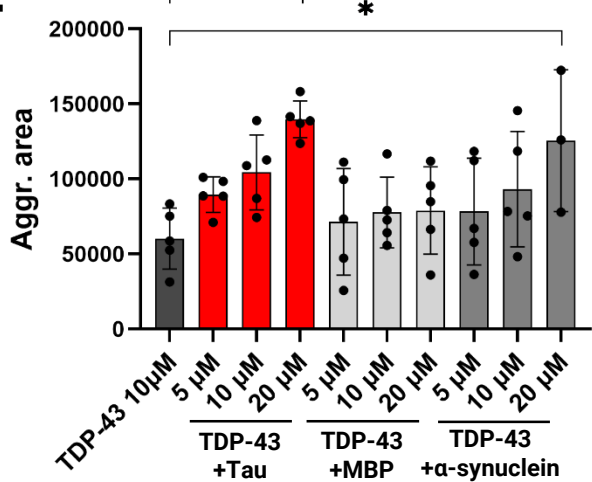
D

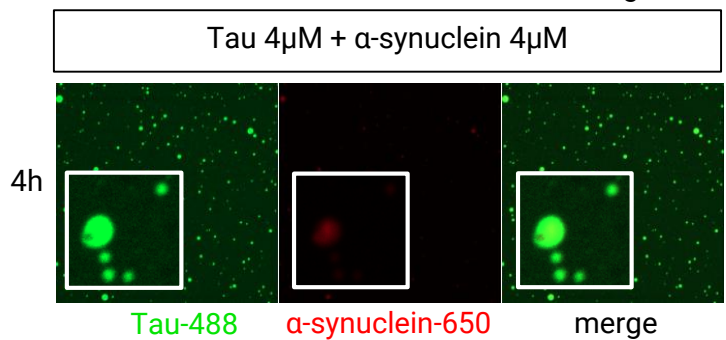
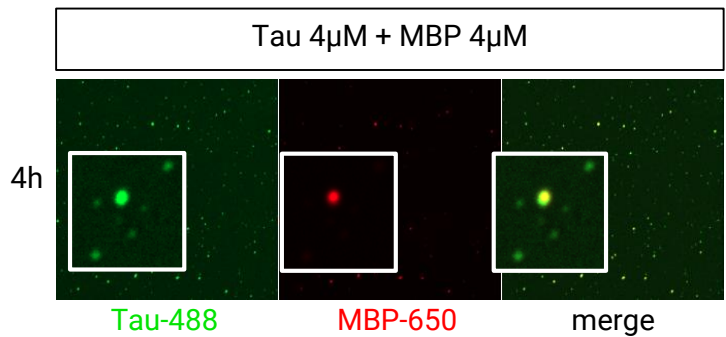
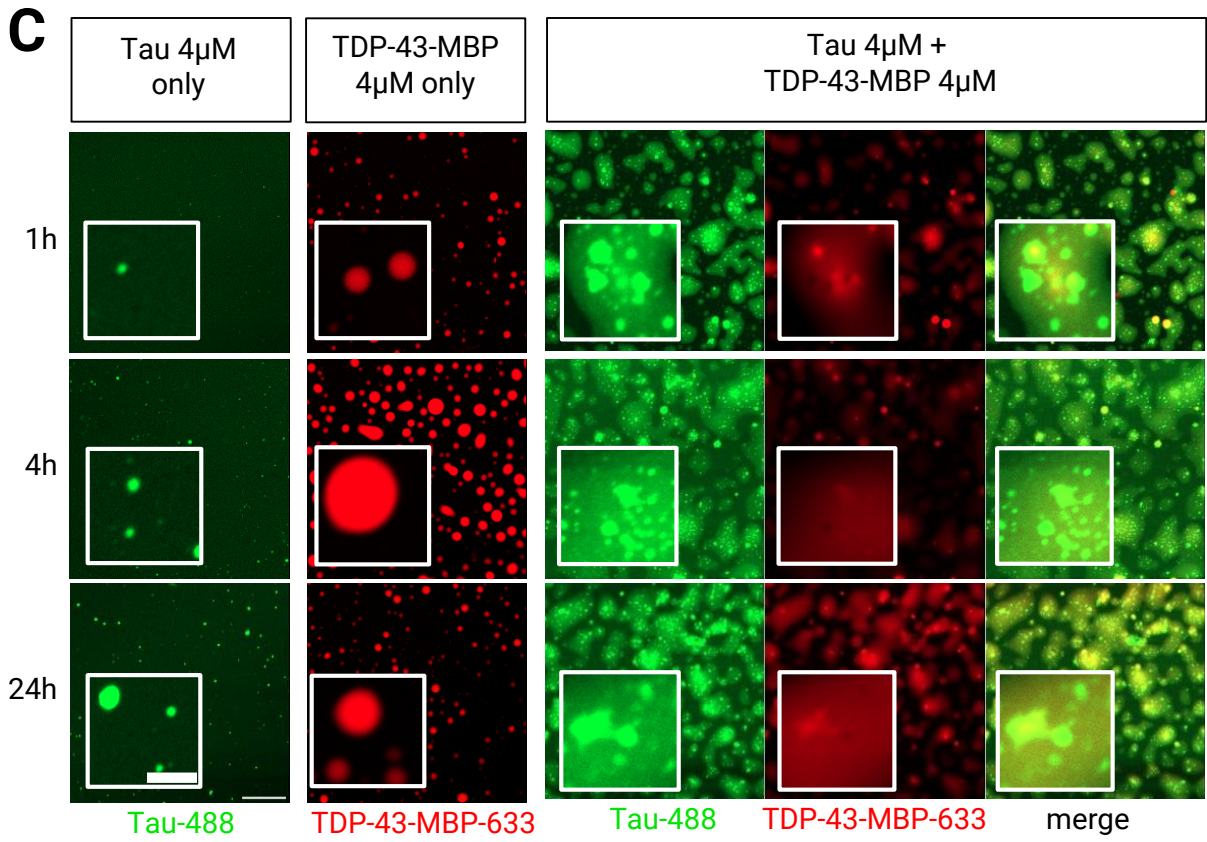
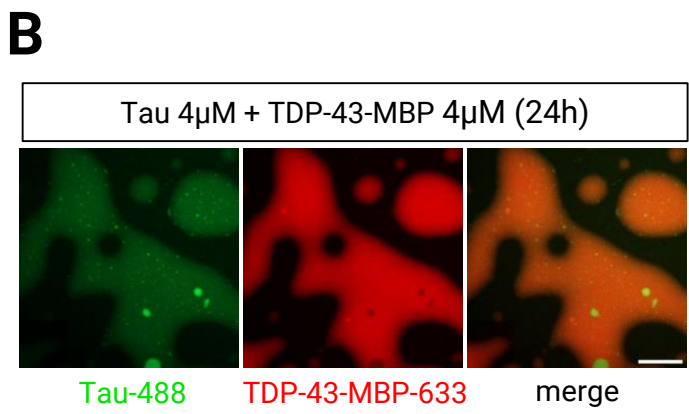
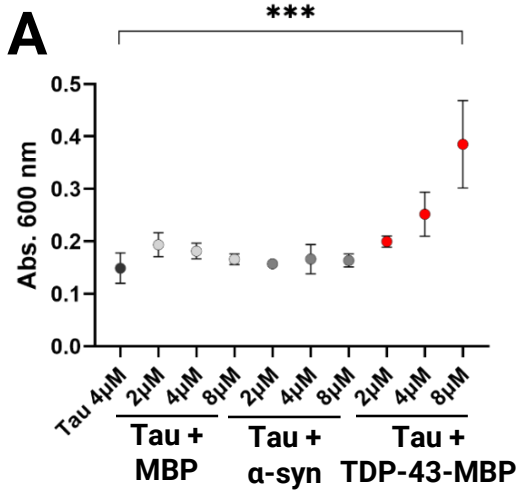


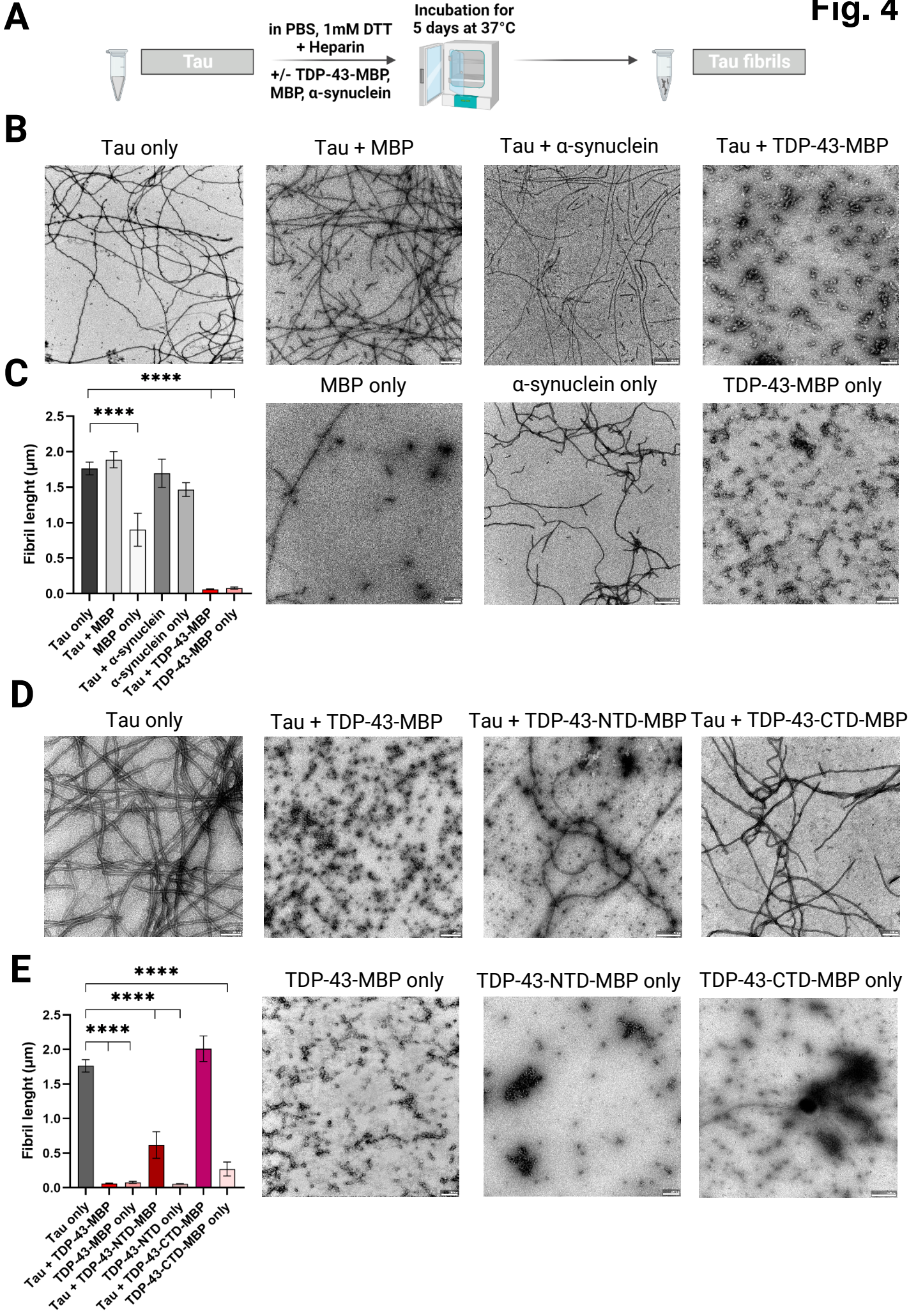
E

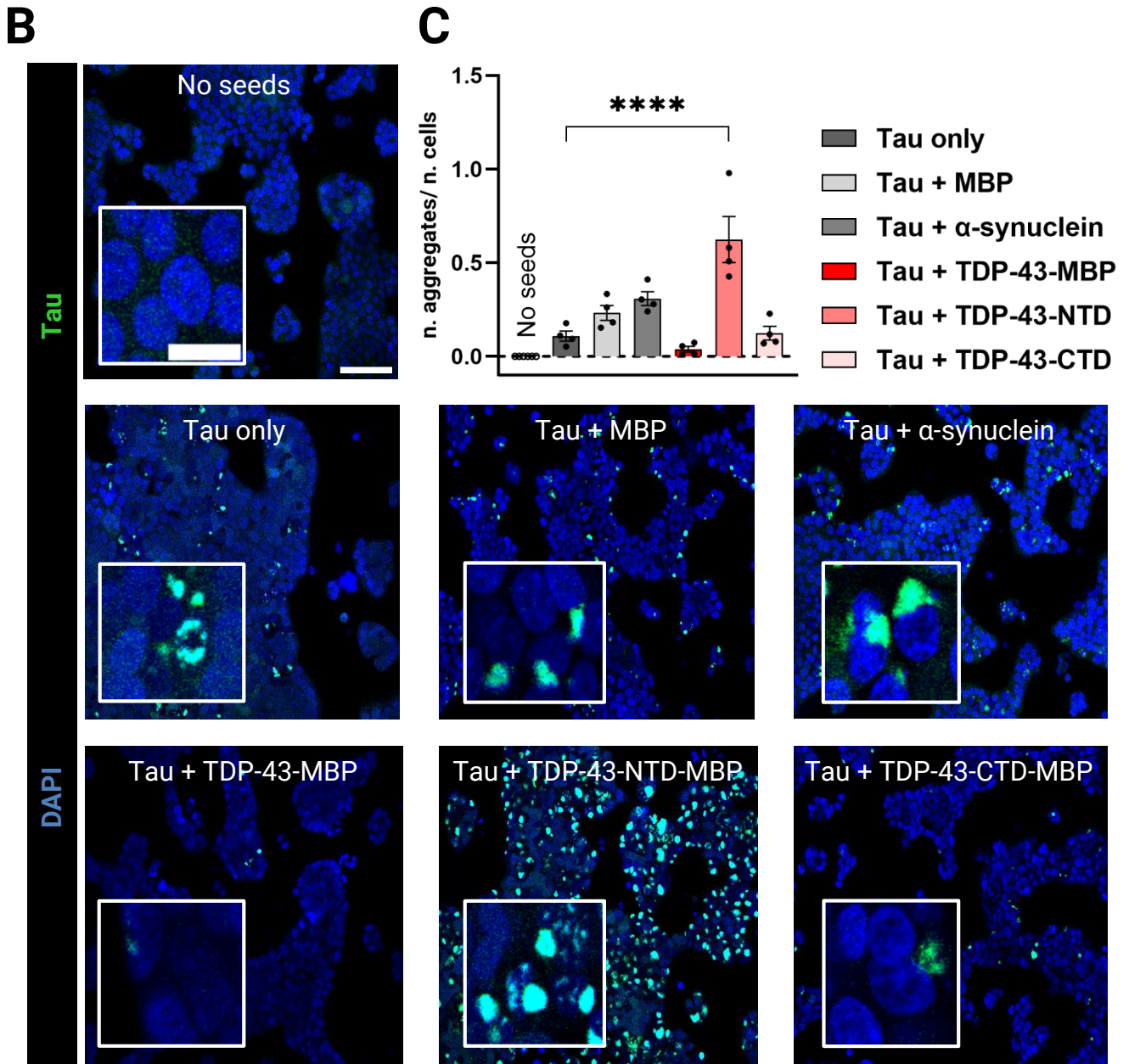
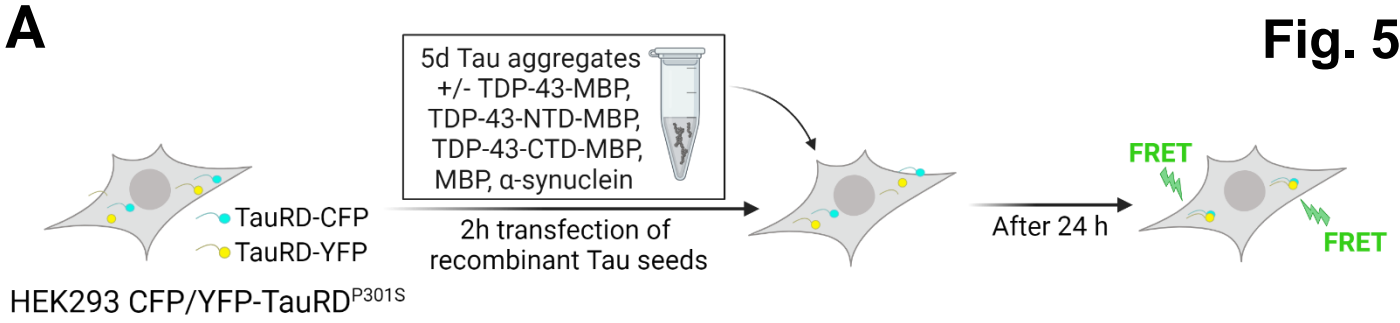


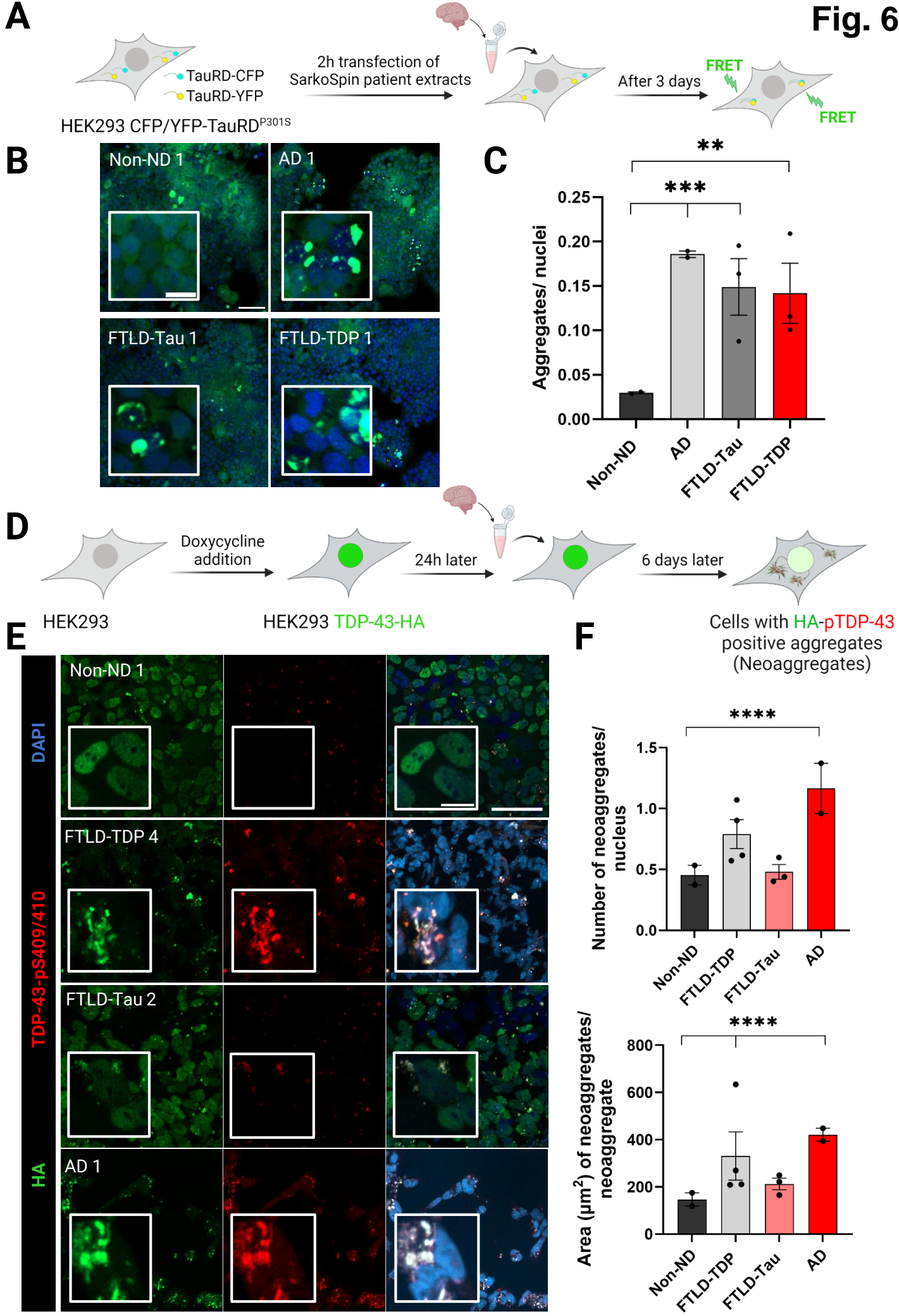
F

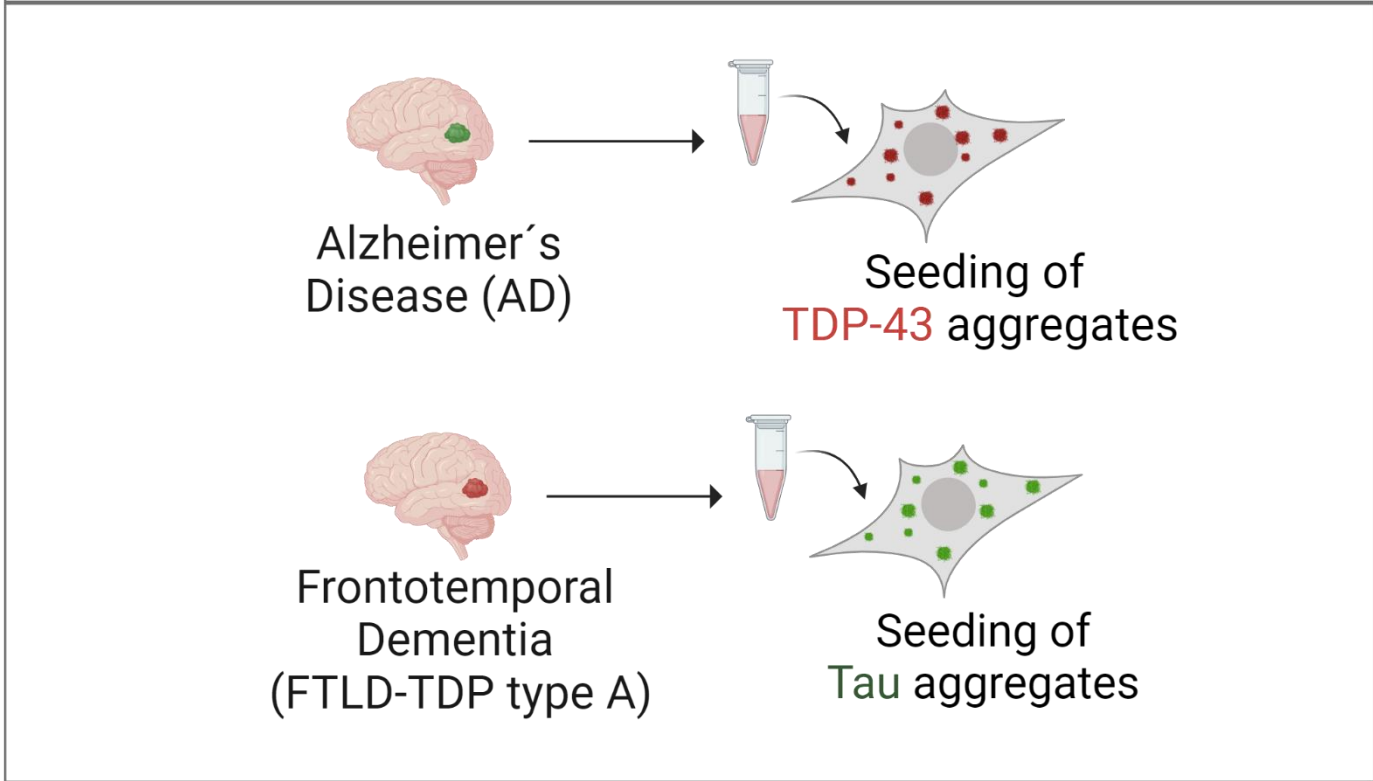
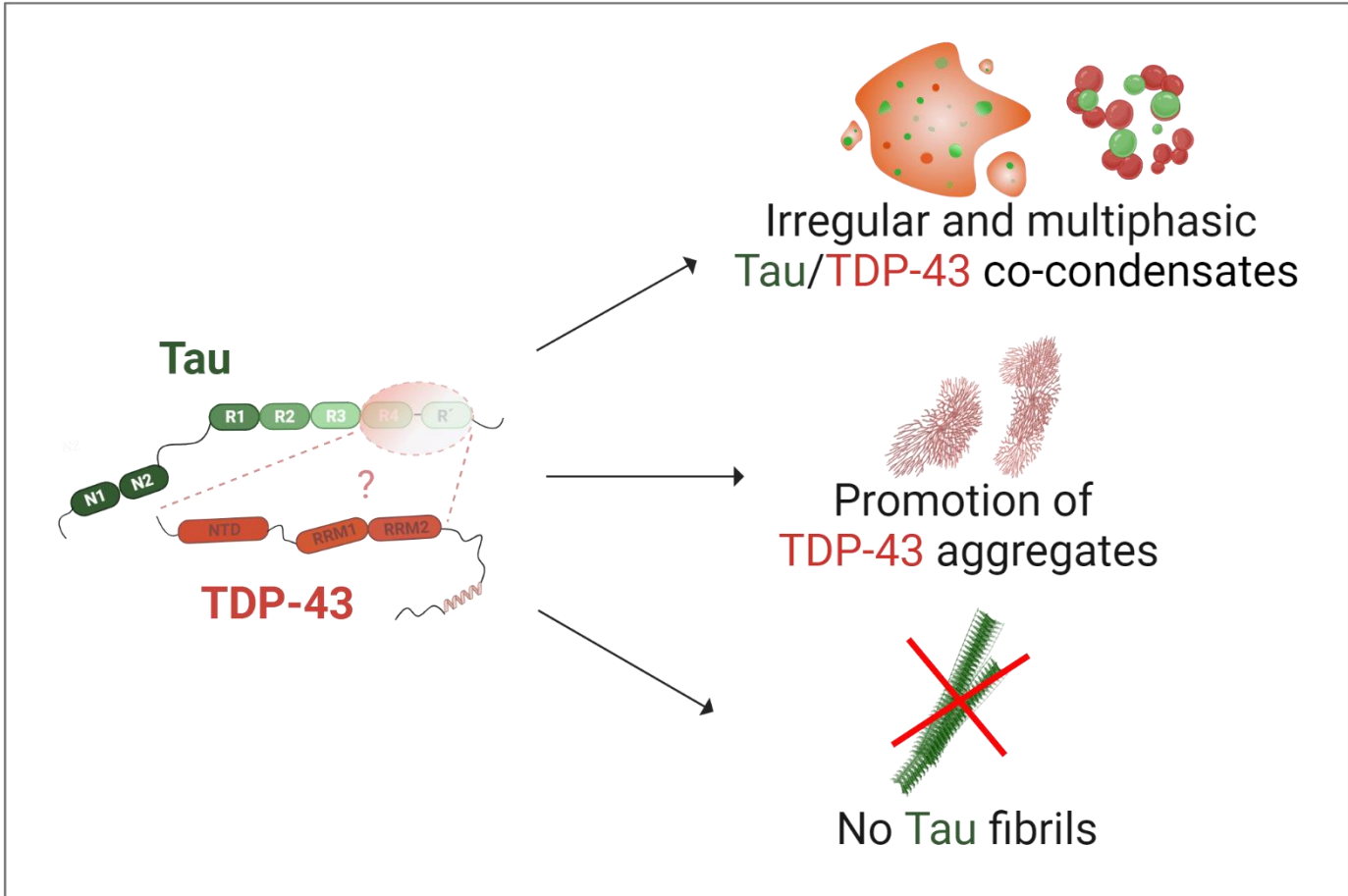












Pathology Diagnosis	Gender	Age at onset	Age at death	Duration	PM delay (hours)	Brain weight	Clinical	Mutations	Braak Tau	Thal Phase	CERAD	ABC	CAA	α -synuclein	TDP-43	notes	Region	Sender
Non-ND 1	M	na	68	na	7:00										0		Motor cortex	UCSD
Non-ND 2	F	na	90	na	6:05	1255			3							PART; small infarctions; slight CAA	Left Superior Frontal Gyrus	Netherlands Brain Bank
FTLD-TDP 1 (Type A)	F	56	67	11	85:35	789	PNFA	C9ORF72	2	0	0	A0B1C0	0	0	1		Frontal Cortex	QSBB, UCL, London
FTLD-TDP 2 (Type A)	M	51	61	10	35:15	1065	CBD		1	1	0	A1B1C0	1	0	1		Frontal Cortex	QSBB, UCL, London
FTLD-TDP 3 (Type A)	M	53	63	10	77:20	955	Pick's disease	C9ORF72	0	0	0	A0B0C0	0	1	1	incidental Lewy body disease	Frontal Cortex	QSBB, UCL, London
FTD-TDP 4 (Type A)	M	59			4:45	1060										single wires and diffuse neuronal	Superior Frontal Gyrus	Netherlands Brain Bank
FTLD-Tau 1	F	36	69	33	82:52	1079	bvFTD	MAPT Q351R (exon 12 c.1052A >G)	4	1	0	A1B2C0	0	0	0		Frontal Cortex	QSBB, UCL, London
FTDP-Tau 2	M	59	66	7	58:10	1399	FTLD-17T	MAPT 10+16	na	na	na	na	na	na	na		Frontal Cortex	QSBB, UCL, London
FTLD-Tau 3	M	41	45	4	27:55	1224	PSP	MAPT L284R	0	0	0	A0B0C0	0	0	0	AGD	Frontal Cortex	QSBB, UCL, London
AD 1	M	76	82	6	24:00	1208	FTD-PPA		6	5	2	A3B3C2	3	1	1	Limbic α -syn and TDP-43	Frontal Cortex	QSBB, UCL, London
AD 2	F	59	79	20	30:25	961	AD		6	5	3	A3B3C3	3	1	1	Neocortical α -syn and limbic TDP-43	Frontal Cortex	QSBB, UCL, London

6 DISCUSSION

The following discussion concerns Publication III.

Our study suggests a direct interaction between Tau and TDP-43, which significantly affects the *in vitro* phase separation and aggregation behavior of both proteins (Fig. 19, upper part). Specifically, Tau partitions into TDP-43 condensates, causing them to cluster and promoting the formation of high molecular weight species. Similarly, TDP-43 favors phase separation of Tau, inducing large Tau/TDP-43 multiphasic co-assemblies with amorphous morphology and intra-Tau condensates. Moreover, we show that TDP-43 suppresses the formation of Tau fibrils, while its N-terminal domain (TDP-43-NTD) might promote the formation of oligomeric Tau species, as suggested by the increased seeding capacity of the “Tau+TDP-43-NTD” structures detected in HEK biosensor cells.

Additionally, our data shows that seeding-competent species of TDP-43 and Tau are present in brain extracts derived from AD and FTLN-TDP type A patients, respectively, even in the absence of detectable histopathological aggregates (Fig. 19, lower part).

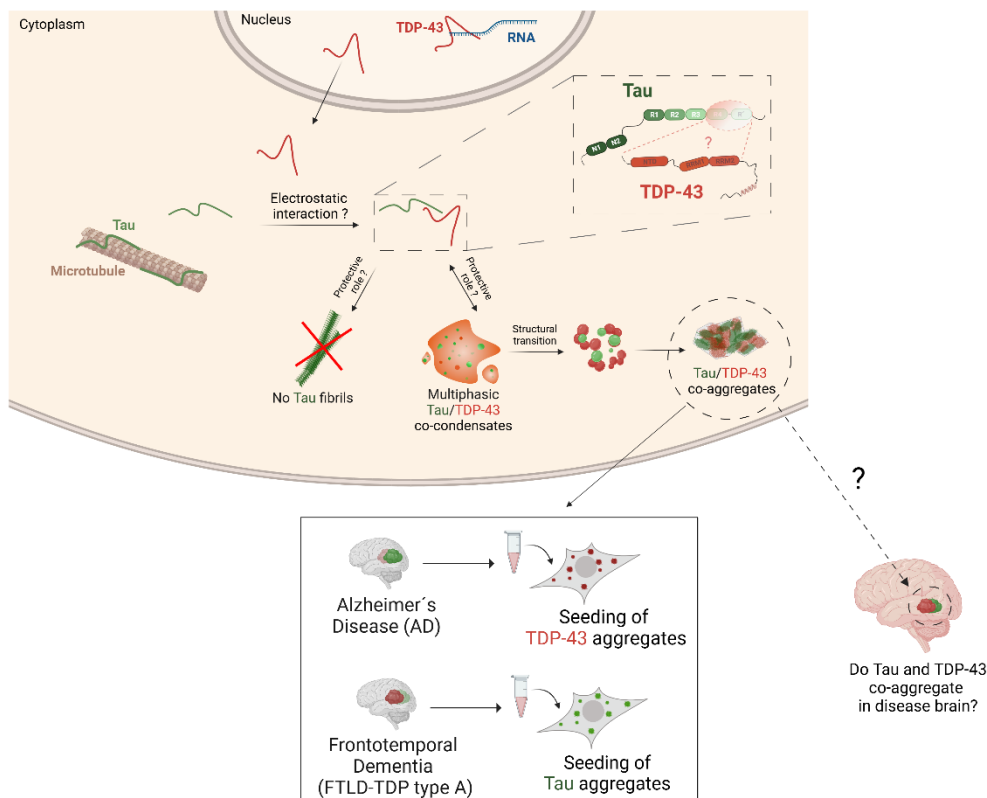


Figure 19 – Illustration of key findings from Publications III

Tau and TDP-43 may encounter in the cell cytoplasm under stress conditions, such as within SGs. These proteins can directly interact via electrostatic interactions, preventing Tau fibril formation in favor of Tau/TDP-43 multiphasic co-condensates. If the stress persists, Tau/TDP-43 co-condensates could undergo structural changes, becoming more solid-like aggregates, which could eventually co-deposit in the brain. While it remains uncertain whether Tau and TDP-43 co-aggregate in the same brain inclusions, our findings suggest that even if they are not detectable in the same aggregates, they could still have an effect on each other and increase their seeding activity – figure created with BioRender.

In the following paragraphs, I will discuss our findings in more detail and present our hypotheses, supported by arguments that integrate previously published data and some more speculative thoughts.

6.1 Potential implications of the Tau and TDP-43 interaction

In recent decades, extensive research has elucidated that neurodegenerative diseases do not result solely from the deposition of a single hallmark protein, but rather from the synergistic effect of different pathological protein aggregates, leading to the emergence of co-pathologies (Nonaka et al., 2018; Robinson et al., 2018; Spires-Jones et al., 2017).

The most studied example is the Tau/TDP-43 co-pathology found in over 60% of AD patients (Amador-Ortiz et al., 2007; Josephs et al., 2014b, 2014a; Kadokura et al., 2009; Tomé et al., 2021, 2020; Tremblay et al., 2011).

AD patients with TDP-43 pathology are generally associated with more severe neurodegeneration; in particular, they show greater brain atrophy in the temporal lobe, where increased TDP-43 inclusions have been observed, mainly in the amygdala and hippocampus. These patients also exhibit a more pronounced functional impairment, severe memory loss and an overall acceleration in cognitive decline (Josephs et al., 2008, 2014b, 2019).

Despite extensive clinical evidence of TDP-43 pathology in a substantial fraction of AD patients, and several descriptions of Tau and TDP-43 inclusions partially occurring in the same brain regions, it is still under debate whether the two proteins interact and get deposited in the same cells or even in the same aggregates.

Earlier studies using double immunostaining for TDP-43 and phospho-Tau (pTau) have shown that partial intracellular colocalization of TDP-43 and Tau in AD cases occurs in some neurons, although at an infrequent rate (Amador-Ortiz et al., 2007; Kadokura et al., 2009). Contrarily, more recent publications have revealed that colocalization of TDP-43 and Tau inclusions in the same cells occur at a high rate. For instance, it has been reported that ~25% of hippocampal cells of both advanced AD and cerebral age-related TDP-43 with sclerosis (CARTS) patients exhibit a colocalization of TDP-43 and pTau (Smith et al., 2018). In addition, another study showed that over 40% of cells in the amygdala and entorhinal cortex of AD and Dementia with Lewy bodies (DLB) patients present TDP-43 neuronal cytoplasmic inclusions (NCIs) colocalized with Tau NFTs (Higashi et al., 2007). Finally, it was shown that in the CA1 region of the hippocampus more than 70% of neurons displayed colocalized phospho-TDP-43 (pTDP-43) and pTau, relative to total pTDP-43 (Tomé et al., 2021). In this study a proximity ligation assay (PLA) furthermore detected a close physical proximity of Tau and TDP-43, suggesting that these two proteins likely interact with each other in the hippocampus of AD patients (Tomé et al., 2021).

Therefore, it appears that deposited Tau and TDP-43 can be found in the same aggregates of AD brains, supporting the notion of a possible direct interaction between the two proteins. However, the exact mechanism by which this Tau/TDP-43 co-pathology arises remains uncertain.

To investigate this, we conducted a study to determine whether these two proteins directly interact at the molecular level, using *in vitro* and cellular models, to gain initial insights into how the pathological pathway towards Tau/TDP-43 co-deposition might develop.

Based on our results, we speculate about the possibility that full-length TDP-43, once in the cytoplasm, may initially prevent the formation of Tau fibrillar structures, as observed in our *in vitro* fibrillization experiments. At the same time, TDP-43 might influence Tau oligomer formation, and Tau and TDP-43 form co-condensates that may acquire pathological properties and ultimately contribute to the Tau/TDP-43 aggregation and pathogenesis of AD.

In a very recent study, Tomè and colleagues injected a mouse model, which had ubiquitin-positive but TDP-43-negative inclusions, with TDP-43 seeds derived from AD patient brains with and without TDP-43 pathology; they observed increased pTau seeding and pronounced nuclear clearance of physiological TDP-43, only in the mice treated with seeds derived from AD patients with TDP-43 pathology. They could also recapitulate the same result in the HEK biosensor cells, where they observed increased Tau aggregate formation in cells treated with seeds from AD patients with TDP-43 pathology (Tomé et al., 2023).

These results support the findings from our seeding experiments. First, we found by Western Blot (WB) analysis that SarkoSpin patient extracts from AD and FTL-D-TDP type A brains predominantly contained visible Tau and TDP-43 aggregates, respectively. Nevertheless, using two cellular models to measure Tau and TDP-43 seeding, we observed that AD extracts could seed not only intracellular Tau but also TDP-43 aggregation, and similarly, FTL-D-TDP type A extracts could seed not only TDP-43 but also Tau aggregation. These findings suggest that seeding competent species of both proteins are present in these brain extracts, despite the lack of neuropathological evidence of Tau and TDP-43 aggregates or insoluble protein in the WB analysis.

This phenomenon might be explained by the prion-like transcellular spread of protein pathology, which likely occurs before the deposition of large aggregates. This concept has previously been described for Tau. Using the HEK biosensor cells, seeding potential of AD brain samples from different brain regions was analyzed by flow cytometry and Tau seeding was observed even in tissues without detectable pTau or NFTs, suggesting that the spreading of Tau is an early event in disease pathogenesis and can be detected already before tangle deposition (DeVos et al., 2018; Furman et al., 2017).

Therefore, a similar mechanism may underlie Tau/TDP-43 pathological spreading which may precede deposition of TDP-43/Tau co-aggregates, explaining the discrepant findings on the frequency of Tau/TDP-43 aggregate co-occurrence in the same cells (Amador-Ortiz et al., 2007; Kadokura et al., 2009; Tomé et al., 2021), and further supporting the notion that the presence of TDP-43 exacerbates neurodegeneration in AD patients (Josephs et al., 2017, 2014b).

These interpretations suggest that the loss of nuclear TDP-43 and its subsequent pathological effects may arise after interacting with Tau in the cytoplasm. TDP-43 and Tau co-deposition in aggregates may be the final event of this pathological cascade.

6.2 The presence of TDP-43 exacerbates Tau pathology

As mentioned before, TDP-43 pathology in AD patients is linked to increased neurodegeneration and overall worsened pathology (Josephs et al., 2014b, 2017). Recently, Tomé and colleagues supported this notion by demonstrating that the presence of TDP-43 significantly impacts Tau pathogenesis and aggravates the condition of AD patients (Tomé et al., 2023).

Several studies in animal models further reinforce the concept that Tau/TDP-43 co-pathology exacerbates neurodegeneration (Clippinger et al., 2013; Latimer et al., 2022).

In two different Tau transgenic mouse models, Clippinger and colleagues showed an increase in cytoplasmic pTDP-43 in neurons of mice with high level of Tau pathological aggregates (Clippinger et al., 2013). Additionally, they observed colocalization of pTDP-43 and pTau, which supports studies reporting a high rate of co-pathology in the same cells in patients (Higashi et al., 2007; Smith et al., 2018; Tomé et al., 2021). However, they also found aggregates containing only pTau, speculating that the abnormal microtubule organization and aberrant transport caused by Tau accumulation might contribute to the mislocalization and subsequent aggregation of TDP-43, suggesting that Tau pathology precedes the deposition of TDP-43 inclusions (Clippinger et al., 2013).

Another *in vivo* study also shows that the presence of TDP-43 aggravates Tau pathology (Latimer et al., 2022). In this work, a novel *C. elegans* model of Tau and TDP-43 co-morbidity was developed, expressing wild-type human Tau and low pan-neuronal expression of human TDP-43 (Tau+TDP-43-low Tg animals); these animals, in comparison to those with no co-morbidity, manifested increased sensory and behavioral impairments and worsened motility. They revealed that TDP-43 increases Tau neurotoxicity, likely promoting its pathological accumulation. Additionally, they observed that the presence of both proteins caused selective vulnerability of different neurotransmitter classes of neurons, suggesting that neuronal loss correlates with increased sensitivity due to the co-pathology (Latimer et al., 2022).

Interestingly, Latimer and colleagues also highlighted an important aspect of the potential interplay between Tau and TDP-43. They observed in the Tau+TDP-43-low Tg animals that neither the total nor the phosphorylated levels of TDP-43 were elevated; in contrast, there was an increase in both total and phosphorylated Tau; thus, they proposed that Tau's influence on pathological TDP-43 is not as evident as the impact that TDP-43 has on Tau (Latimer et al., 2022).

This finding is reminiscent of our *in vitro* data, in which we observed that both proteins influence each other's phase separation and aggregation behavior, but TDP-43 has a more striking effect on Tau condensation and fibrillization than the other way around.

This could also reinforce the idea that Tau aggregation in AD might occur before TDP-43 pathology arises. However, further investigation is needed to elucidate and confirm this hypothesis.

6.3 Protein condensation: Protective mechanism or precursor to aggregate formation?

Our study also examines how Tau and TDP-43 influence each other's phase separation behavior *in vitro*. We reported that Tau co-partitions into TDP-43 condensates, causing them to cluster, and favoring their aggregation. Additionally, TDP-43 strongly influences Tau phase separation, promoting the formation of multiphasic amorphous Tau/TDP-43 co-condensates with intra-Tau droplets.

Similar multicomponent co-assemblies have already been described in previous studies on phase separation behavior of other proteins involved in neurodegenerative diseases.

Rai and colleagues showed that Tau and PrP undergo spontaneous complex phase separation through heterotypic interactions; they form mixed droplets containing both proteins, which, upon aging, acquire a solid-like structure and become aggregates. Conversely, by adding increased RNA concentration in the buffer mix, Tau and PrP form condensates with multiphasic morphologies: core-shell droplets with internal PrP and peripheral Tau, or nested droplets with intra-PrP droplets and Tau at the edges (Rai et al., 2023). These immiscible assemblies are reminiscent of those we observe in Tau/TDP-43 co-phase separation experiments.

One more example of a similar multiphasic phenotype of protein condensates is shown in a study examining the *in vitro* interplay between Tau and the RNA-binding protein TIA1, a stress granules (SGs) marker. Ash and colleagues observed that in the presence of RNA, Tau concentrates into small microdomains within large TIA1 droplets (Ash et al., 2021), structures resembling the Tau/TDP-43 multiphasic co-condensates with intra Tau droplets we observed in our experiments.

Furthermore, a study demonstrated that α -synuclein can act as a Pickering agent on TDP-43-CTD, when they encounter each other in the cytoplasm of cells under stress conditions associated with the formation of SGs. A small fraction of cytoplasmic α -synuclein was found to interact with TDP-43-CTD within SGs, localizing at their periphery and encapsulating these organelles. Over time, this interaction may trigger the formation of aggregates (Dhakal et al., 2023).

Finally, another example of multiphasic condensate formation involving two proteins associated with neurodegenerative diseases is the *in vitro* interaction of Tau and α -synuclein. Tau and α -synuclein were reported to form spontaneous co-droplets, which interestingly grow in size while maintaining a more internal liquid-like structure. These latter serve as ideal reservoir for protein aggregate nucleation, favored by a highly crowded yet dynamic environment. Remarkably, in Tau/ α -synuclein condensates with a more gel-like structure, internal amyloid formation was not observed, suggesting that an initial less rigid protein network might be crucial for specific interactions necessary for amyloid nucleation (Gracia et al., 2022).

In our study, we included α -synuclein as negative control and monitored its condensation with Tau over 4 hours (h), observing that the two proteins form droplets of different sizes, and round in shape. This result is consistent with the findings of Gracia and colleagues, who, however, further monitor the condensation of Tau and α -synuclein over the period of 24 h; with this longer time course, they revealed the formation of Tau/ α -synuclein co-droplets with internal amyloid formation, which were characterized using Thioflavin T (ThT), a fluorescent dye which stain for amyloids (Gracia et al., 2022).

These examples illustrate how phase separation events may lead to protein aggregation. In fact, it has been widely described that condensation can precede protein aggregation processes in the pathogenesis of various neurodegenerative disease (Alberti and Dormann, 2019).

It is known that protein condensates, formed as a physiological response to cellular needs, can transition from a liquid to a solid state, a process that may generate protein aggregates under pathological conditions.

In this regard, previous experiments in neurons have shown that Tau condensates can revert to amyloid-like structures, capable of seeding cellular Tau aggregation (Wegmann et al., 2018; Zhang et al., 2020); similarly, TDP-43 condensation in stress granules (SGs) is considered the initiation event for TDP-43 aggregation and subsequent seeding in cells (Polymenidou and Cleveland, 2011; Zhang et al., 2019).

A common view is that SGs form in the cellular cytoplasm as a result of phase separation of different RNA-binding proteins and RNAs to protect cells during stress. However, under pathological conditions, these SGs fail to dissolve and instead may become reservoirs for aggregation of proteins, which change from a liquid state to a solid-like structure.

In contrast, a very recent research presents a new perspective on SGs. Das and colleagues describe SGs as metastable condensates which protect against fibril formation. The metastability is the energetic state in a dynamic environment that precedes the lowest state of energy; higher metastability defines condensates as sinks for proteins, thereby slowing down the conversion to fibrils. Thus, the interactions which drive SGs formation can facilitate the stabilization of disordered condensates rather than ordered fibrillar structures, concluding that condensation and fibril formation are two separate processes driven by different interactions (Das et al., 2024).

Taken together, protein condensation is still a controversially discussed phenomenon in neurodegenerative diseases. On the one hand, it could be protective by reducing the amount of protein available for aggregation, and maintaining them in a liquid state; on the other hand, it could be pathological because the condensation of proteins in droplets increases the local protein concentration, which may favor aggregate formation. In addition, recent studies have described a novel mechanism by which condensates can promote protein aggregation. In fact, it has been demonstrated that the surface of protein droplets can contain β -sheet structures that act as a solid shell and can eventually induce mature droplets to transition into fibrils (Emmanouilidis et al., 2024; Linsenmeier et al., 2023; Shen et al., 2023).

Interestingly, this debate recapitulates our findings. TDP-43 and Tau promote their phase separation *in vitro*, leading to the formation of multiphasic co-assemblies with low internal dynamics (FRAP data not shown in the manuscript). Based on the findings of Tau/ α -synuclein co-condensation, it has been proposed that low internal dynamism within co-condensates reduces the propensity to form amyloids (Gracia et al., 2022). This could indicate that the Tau and TDP-43 interaction makes these proteins less likely to form amyloids. Consistent with this, we found that TDP-43 inhibits Tau fibril formation.

Together these results support the idea that initially the Tau/TDP-43 interaction seems not to favor aggregate formation and that Tau/TDP-43 co-condensation might be protective and may even prevent the two proteins from aggregating. However, over time, as the concentration of

Tau and TDP-43 increases in the cytoplasm or as the condensates persist, this protective role may be lost; eventually, the co-assemblies may nucleate aggregates at the surface, or they may form seeding-competent species that lead to propagation of pathology throughout the brain and ultimately exacerbate neurodegeneration in AD.

6.4 Cellular events that potentially favor Tau and TDP-43 interaction

An interesting matter is certainly understanding where and under which conditions Tau and TDP-43 may encounter each other in the cell.

As described previously, TDP-43 is physiologically located in the nucleus, but it relocates to the cytoplasm mainly under stress conditions, during which it is recruited into SGs (Dewey et al., 2011). The composition of SGs has been extensively studied, and in addition to numerous RNA-binding proteins, Tau is another SG-associated protein (Vanderweyde et al., 2012, 2016; Wolozin and Ivanov, 2019).

Tau is known to interact with SGs proteins, such as TIA1 and this interaction has been shown to promote neurodegeneration (Apicco et al., 2018; Ash et al., 2021; Jiang et al., 2019; Vanderweyde et al., 2016); additionally, phase separation of Tau is favored by RNA presence (Hochmair et al., 2022; Zhang et al., 2017), and the high content of RNA in SGs makes these organelles ideal recruiters of Tau protein in the somatodendritic region, where RNA is more abundant than in axons (Wolozin and Ivanov, 2019).

Therefore, a hypothesis is that under stress, TDP-43 is recruited to cytoplasmic SGs, where it may encounter Tau. Possibly in this environment, the two proteins could directly interact and undergo phase separation together, forming multiphasic co-condensates. This would be in line with the hypothesis that SGs become pathological reservoirs for protein aggregation (Bentmann et al., 2013; Wolozin and Ivanov, 2019). Such mechanism could plausibly explain how Tau/TDP-43 convert into pathological aggregates under stress conditions.

A recent finding that potentially strengthens this pathological route is the demixing event described for TDP-43/G3BP1 in SGs (Yan et al., 2024). This study highlights that the high concentration of TDP-43 in SGs, coupled with oxidative stress condition which favors homotypic interactions, are two critical events that cause TDP-43 to demix from other SGs components, like G3BP1/RNA. Such demixing process inside SGs may facilitate the transition from a liquid-like RNP granule to a solid pathological aggregate (Yan et al., 2024).

Hence, SGs seem to provide an environment that favors protein demixing and subsequent aggregation, suggesting a similar mechanism could occur for Tau and TDP-43 if they interact and form multiphasic condensates inside SGs.

Nevertheless, demixing has also been recently described as a default process by which the different biological condensates form in cells; thus, this process can also be associated with physiological events (Zhu et al., 2024).

Membraneless organelles formed via phase separation arise and persist through percolated molecular interactions, which are strong and difficult to break. Consequently, demixing

describes the high-valent interactions and low mobility of these molecular condensates, defining their ability to ultimately form segregated organelles within cells (Zhu et al., 2024).

Therefore, as mentioned before, further studies are needed to elucidate when and how condensation becomes pathological. However, the new study which proposes that SGs protect proteins from fibril formation (Das et al., 2024), reinforce the hypothesis that the interplay between Tau and TDP-43, whether occurring within SGs or somewhere else, could be the result of an initially physiological mechanism. Tau and TDP-43 interaction and co-condensation could at first act as a protective mechanism, which, however, becomes pathological over time as the SGs transform into solid inclusions during prolonged stress.

Another cellular event that could facilitate interactions between Tau and TDP-43 molecules is the pathological protein seeding observed in neurodegenerative diseases, which provides additional potential mechanisms for intra- and extracellular encounters (Jucker and Walker, 2011).

During pathological spreading, proteins are released and taken up by neighboring cells; given that both Tau and TDP-43 undergo this mechanism, it may be possible that these two proteins interact during this event. In fact, recent findings showed that the presence of TDP-43 increases Tau seeding (Tomé et al., 2023), and even though the nature of these seeds is still under debate, these results support the notion of a pathological interaction between Tau and TDP-43.

In line with this idea, our results in two seeding reporter cell lines show that TDP-43 and Tau with seeding potency are present in brain extracts from patients with AD and FTLD-TDP type A, respectively, even in the absence of histopathological signs. Therefore, we speculate that the interaction between Tau and TDP-43 enhances their seeding capability, ultimately aggravating and/or accelerating the disease progression.

Lastly, Tau and TDP-43 could potentially also interact within the autophagy-lysosomal pathway. In disease conditions, both proteins form pathological aggregates that are initially targeted by the autophagy-lysosomal pathway for clearance (Budini et al., 2017; Jiang and Bhaskar, 2020).

This mechanism is a primary system used by the cells to maintain homeostasis and regulate the degradation of protein aggregates, organelles, lipid droplets and other molecules (Budini et al., 2017). The autophagy-lysosomal pathway begins intracellularly with the formation of a double-membrane structure, termed autophagosome, that engulfs cytosolic cargoes; this subsequently fuses with the lysosome, generating an autophagolysosome where the cargoes are finally degraded by lysosomal enzymes (Budini et al., 2017).

It has been widely demonstrated that autophagy inhibition is associated with the accumulation of Tau aggregates, and *vice versa*, autophagy promotion results in Tau degradation both *in vitro* and *in vivo* (Jiang and Bhaskar, 2020). Additionally, it has been shown that Tau fibrils evade autophagy clearance by hiding potential ubiquitination sites within their fibrillar structure, despite being targeted by p62. This finding also explains the presence of ubiquitinated Tau fibrils found in AD brains (Ferrari et al., 2024).

Comparably, autophagy vacuole proteins have been found to colocalize with TDP-43 aggregates, initially counteracting their accumulation and later being associated with ALS and other TDP-43 proteinopathies (Hiji et al., 2008; Mizuno et al., 2006). Furthermore, cellular experiments showed that inhibition of autophagy increases the cytoplasmic accumulation of C-terminal fragments of TDP-43 (Caccamo et al., 2009); on the contrary, disrupting a complex of TDP-43 with heat shock protein Hsp90 and cell division cycle 37 (Cdc37) can promote TDP-43 degradation via the autophagy-lysosomal pathway (Jinwal et al., 2012). Interestingly, this study also showed that after transfecting cells overexpressing TDP-43 with increasing amounts of Tau, the disassembly of the TDP-43/Hsp90/Cdc37 complex is impaired, leading to reduced TDP-43 clearance (Jinwal et al., 2012). In conclusion, the authors of this work propose that cytosolic accumulation of Tau influences the degradation of TDP-43, supporting the hypothesis of a possible interaction between the two proteins along the autophagy-lysosomal pathway.

6.5 Potential domains of Tau and TDP-43 involved in their interaction

To better understand how to target the Tau/TDP-43 interaction, it is crucial to identify the specific regions of Tau and TDP-43 involved in their binding.

Nuclear magnetic resonance (NMR) is an excellent method for revealing interaction sites between two proteins. For instance, NMR experiments can be conducted using either the full-length versions of Tau and TDP-43, or mutants lacking specific protein sequences, or containing certain amino acids mutations; in this way, it is possible to identify the exact motifs in Tau and TDP-43 that are responsible for their interaction.

Furthermore, dynamic light scattering (DLS) is a valuable technique to get more insights in protein interactions, as it can determine the size of proteins and detect the formation of high weight molecular species in solution. Therefore, to further validate our observation of Tau/TDP-43 *in vitro* interaction, conducting DLS analysis of Tau and TDP-43 mixed in solution would be crucial; ideally, this should be performed in physiological buffer conditions to closely mimic the cellular environment and to better understand how Tau and TDP-43 interact under natural conditions.

Nevertheless, based on our results, we can make some informed assumptions about which domains of Tau and TDP-43 may be involved in their interaction.

Our finding that TDP-43 suppresses Tau fibril formation suggests that TDP-43 may interact with the fibril core region of Tau, known to be involved in the formation of paired helical filaments (PHFs) (Fitzpatrick et al., 2017; Oakley et al., 2020). PHFs consist of two protofilaments of identical structure, with a core formed by specific stacking of amino acids in the R3 and R4 regions of Tau, creating cross- β packing and β -helices that generate the amyloid fibrils composed of different protofilaments (Fitzpatrick et al., 2017; Oakley et al., 2020). Thus, we suppose that TDP-43 bind to all or part of these regions, preventing Tau from adopting the structural conformation necessary to form PHFs, and ultimately inhibiting fibril development.

Interestingly, our finding on the inhibitory role of TDP-43 on Tau fibrillization aligns with a study which demonstrates that TDP-43 inhibits the early and intermediate stages of A β

fibrillization *in vitro* (Shih et al., 2020). Moreover, the N-terminal domain (NTD, amino acids 1-265) of TDP-43 seems to be involved in the A β fibrils inhibition (Shih et al., 2020). In line with this, we further hypothesize that TDP-43 might act similarly on Tau fibrillization. In fact, we observed that the NTD mainly hinders Tau fibril formation similarly to full-length TDP-43; contrarily, the C-terminal domain (CTD) is unlikely to bind Tau and interfere with this process, since long fibrils were observed when Tau was incubated with TDP-43-CTD.

Additionally, considering the structural characteristics of Tau and TDP-43 (Fig. 16), one can speculate that their binding could occur through electrostatic interactions between the two oppositely charged domains of Tau (the negatively charged NTD, and the positively charged CTD) and the alternatively positive and negative regions of TDP-43. Furthermore, the aromatic residues in the CTD of TDP-43 might bind to positively charged residues of Tau.

In conclusion, our study marks the beginning of the investigation on the interplay between Tau and TDP-43, and emphasizes the importance of further unraveling the molecular mechanisms that underlie this crucial interaction, which in the future may pave the way for novel therapeutic targets in AD.

6.6 Molecular commonalities and cellular crosstalks between Tau and TDP-43

There are several molecular commonalities of Tau and TDP-43 that could influence their interaction.

Both proteins have an intrinsically disordered nature, allowing them to undergo phase separation (Zbinden et al., 2020). Their individual condensation behaviors have already been extensively described (Ambadipudi et al., 2017; Li et al., 2018b), however, we have characterized their co-condensation *in vitro*, and have shown that both proteins can phase separate in the presence of the other, leading to the formation of multiphasic irregular Tau/TDP-43 co-condensates.

Another common aspect is their interaction with RNA and the consequent effects on their phase separation. In fact, RNA is known to promote phase separation of Tau by interacting with its positively charged domains (Lin et al., 2019; Zhang et al., 2017). TDP-43, as an RNA-binding protein, interacts with RNA, which binds to its RRM domains reducing its condensation (Mann et al., 2019), or alternatively, RNA favors TDP-43 phase separation by binding the positively charged RGG motif of TDP-43 (Conicella et al., 2016). Therefore, it would be interesting to investigate the role of RNA in Tau/TDP-43 co-condensation process; given the high RNA content present in cells, studying this effect would also offer valuable insights into the interaction of these two proteins within a cellular context.

Additionally, both Tau and TDP-43 undergo different post-translational modifications (PTMs) during normal cellular functions. However, among these PTMs, abnormal phosphorylation is a common feature of pathological Tau and TDP-43 found in inclusions of AD, ALS and FTD patients (Cracco et al., 2022; Kametani et al., 2016; Long and Holtzman, 2019).

Phosphorylation adds phosphate groups to serine, threonine and tyrosine residues, altering the charge state of the protein towards a more negative net charge. Given this significant modification that phosphorylation brings on a protein, it would be interesting to study how it affects Tau/TDP-43 interaction *in vitro*, and which are the effects of this PTM on their co-condensation and aggregation, possibly using phosphorylated or phosphomimetic variants of these proteins.

Overlapping features between Tau and TDP-43 are also evident in cellular pathways leading to their respective proteinopathies. Both proteins respond to various types of stress, are recruited to SGs, and they are involved in autophagy defects (Chornenkyy et al., 2019). All these events are considered upstream causes of neurodegeneration and may have implications for both Tau and TDP-43 pathogenesis and their co-pathologies (Chornenkyy et al., 2019).

Moreover, TDP-43 and Tau might directly or indirectly influence each other's subcellular localization and functions.

A study by Candia and colleagues revealed that when a pathological pseudophosphorylation mutant of Tau (PH-Tau) is transfected in HEK293 cells, it translocates into the nucleus. They also propose the presence of a nuclear localization signal (NLS) within Tau sequence, and identify the importin- α/β pathway as responsible for the nuclear translocation of PH-Tau (Candia et al., 2022). This process results in altered nucleocytoplasmic transport (NCT) and increased cell death, which can be prevented by blocking PH-Tau entry into the nucleus. Interestingly, PH-Tau-expressing cells exhibit disruption of the nuclear lamina and consequent mislocalization of several nuclear proteins, including TDP-43 (Candia et al., 2022).

Evidences of disruption of the NCT by Tau in AD has already been demonstrated (Eftekharzadeh et al., 2018). Moreover, alterations of NCT are also commonly observed in other neurodegenerative diseases, such as ALS and FTD (Chou et al., 2018; Hutten and Dormann, 2020); in fact, nuclear import involving importin- α and importin- β have also been associated with TDP-43 (Nishimura et al., 2010). As a consequence of this, mislocalization of both Tau and TDP-43 may lead to their encounter in unusual compartments, promoting their pathological protein-protein interaction and resulting in toxic cellular phenotypes.

There is also substantial evidence on the effect of TDP-43 on Tau mRNA and its consequences in disease conditions.

Gu and colleagues showed that the CTD of TDP-43 binds to Tau mRNA and regulates its translation in cells, specifically promoting its instability and reducing its expression. Additionally, this work demonstrated that different ALS-associated mutations on TDP-43 have different effects on Tau mRNA (Gu et al., 2017b).

The same researchers further investigated the role of TDP-43 on Tau expression, and discovered that TDP-43 promotes the inclusion of intron 10 of Tau *in vivo*, thereby increasing the production of the Tau 4R isoform (Gu et al., 2017a), which is known to be the predominant isoform of various neurodegenerative diseases (Dugger and Dickson, 2017). They concluded that the translocation of TDP-43 in the cytoplasm affects Tau alternative splicing regulation, exacerbating disease pathogenesis as results of increased TDP-43 cytoplasmic aggregation, and imbalance of Tau 3R/4R ratio (Gu et al., 2017a). This mechanism appears to involve casein

kinase I ϵ (CKI ϵ)-mediated phosphorylation of TDP-43 (Gu et al., 2020; Wu et al., 2021; Yang et al., 2023).

Taken together, different aspects of Tau and TDP-43 are critical factors that may influence their molecular interplay and cellular crosstalks, ultimately affecting each other's functions in both physiological and pathological conditions.

6.7 Future directions to study Tau/TDP-43 interaction

There are different key open questions that remain to be answered on the molecular mechanisms that underline Tau and TDP-43 interaction; in fact, several future experiments are needed to gain a deeper understanding of this protein interplay.

For instance, it would be interesting to investigate how the Tau/TDP-43 co-assemblies, which initially seem not to form aggregates, eventually transition into fibrillar structures observed in AD. Further research is needed to elucidate the conformation of the amyloids that emerge from these co-condensates, and to determine how they resemble the Tau and TDP-43 conformers that have recently been resolved by cryo-EM from patient tissue (Scheres et al., 2023). Additionally, it would also be important to resolve the structure of Tau/TDP-43 co-aggregates with such high-resolution structural methods.

Furthermore, it is crucial to characterize the molecular nature of the small *in vitro* assemblies we observed by transmission EM when we induce Tau fibrillization in the presence of full-length TDP-43 and TDP-43-NTD, respectively.

Based solely on the EM images, it is not possible to determine which protein comprises the observed assemblies, or whether they form co-assemblies made of both proteins. To address this, double immunogold staining or cryo-EM experiments are needed.

Nevertheless, we can make assumptions based on our results. When we transfected the small assemblies in the HEK biosensor cells, they exhibited lower seeding potency (even if not significant) compared to Tau fibrils. This suggests that the assemblies we observed are predominantly formed by TDP-43, as the HEK biosensor cells are highly specific to Tau seeds only (Holmes et al., 2014).

In contrast, when we transfected the HEK biosensor cells with “Tau+TDP-43-NTD” assemblies, we observed a significant increase in Tau seeding, contrary to the effect seen with full length TDP-43. This finding may indicate that the NTD of TDP-43 could bind Tau and promote its oligomerization, considering that Tau oligomers are known to be the most seeding potent species of Tau (Lasagna-Reeves et al., 2011; Takeda et al., 2015; Usenovic et al., 2015; Wegmann et al., 2016).

Supporting this hypothesis, Shih and colleagues observed that in a mouse model of AD, injection of TDP-43 promotes the formation of A β oligomers through direct interaction via the NTD (amino acids 1-256) of TDP-43 and not the CTD, increasing inflammation and ultimately exacerbating spatial memory impairment in these animals. Thus, TDP-43 might similarly promote Tau oligomerization, potentially via its NTD.

Another attractive future direction would be generating recombinant mutants of Tau and TDP-43 with known disease-associated mutations found in *TARDBP* and *MAPT*. These mutants could then be used in phase separation and aggregation assays *in vitro*, to assess how Tau/TDP-43 co-condensation and fibrillation can be affected. This approach would offer valuable insights into the role of these mutations in the interaction between Tau and TDP-43 simulating pathological conditions.

One more intriguing approach of exploration would be examining whether TDP-43 by binding to Tau affects Tau's function in promoting microtubule (MT) formation. By replicating the Tau:tubulin co-condensation assay, where Tau locally nucleates MT bundle formation by concentrating tubulin in the condensed phase (Hernández-Vega et al., 2017b; Hochmair et al., 2022), we could evaluate the role of TDP-43 in this *in vitro* assay, in order to determine whether this protein competes with tubulin for the formation of MTs, and if it ultimately disrupts the generation of MT bundles.

Finally, it would be also interesting to study whether Tau and TDP-43 directly interact in the neuronal cytoplasm, and if they co-condense or co-oligomerize in cells as we observed *in vitro*. A previous study has demonstrated that by expressing Tau in primary neurons, it is possible to observe formation of Tau droplets in the cytoplasm of these cells (Wegmann et al., 2018); thus, it would be valuable examining the effects of the addition of TDP-43 and its domains (NTD and CTD) in this context. This experiment could help determine whether co-condensation and/or promotion of co-oligomerization occur in neurons, providing further insights into the interplay between Tau and TDP-43.

7 REFERENCES

- Afroz, T., Hock, E.-M., Ernst, P., Foglieni, C., Jambeau, M., Gilhespy, L.A.B., Laferriere, F., Maniecka, Z., Plückthun, A., Mittl, P., Paganetti, P., Allain, F.H.T., Polymenidou, M., 2017. Functional and dynamic polymerization of the ALS-linked protein TDP-43 antagonizes its pathologic aggregation. *Nat. Commun.* 8, 45. <https://doi.org/10.1038/s41467-017-00062-0>
- Aguzzi, A., 2009. Cell biology: Beyond the prion principle. *Nature* 459, 924–925. <https://doi.org/10.1038/459924a>
- Alami, N.H., Smith, R.B., Carrasco, M.A., Williams, L.A., Winborn, C.S., Han, S.S.W., Kiskinis, E., Winborn, B., Freibaum, B.D., Kanagaraj, A., Clare, A.J., Badders, N.M., Bilican, B., Chaum, E., Chandran, S., Shaw, C.E., Eggan, K.C., Maniatis, T., Taylor, J.P., 2014. Axonal transport of TDP-43 mRNA granules is impaired by ALS-causing mutations. *Neuron* 81, 536–543. <https://doi.org/10.1016/j.neuron.2013.12.018>
- Alberti, S., 2017. Phase separation in biology. *Curr. Biol.* CB 27, R1097–R1102. <https://doi.org/10.1016/j.cub.2017.08.069>
- Alberti, S., Dormann, D., 2019. Liquid-Liquid Phase Separation in Disease. *Annu. Rev. Genet.* 53, 171–194. <https://doi.org/10.1146/annurev-genet-112618-043527>
- Alberti, S., Gladfelter, A., Mittag, T., 2019. Considerations and Challenges in Studying Liquid-Liquid Phase Separation and Biomolecular Condensates. *Cell* 176, 419–434. <https://doi.org/10.1016/j.cell.2018.12.035>
- Alberti, S., Hyman, A.A., 2021. Biomolecular condensates at the nexus of cellular stress, protein aggregation disease and ageing. *Nat. Rev. Mol. Cell Biol.* 22, 196–213. <https://doi.org/10.1038/s41580-020-00326-6>
- Alberti, S., Hyman, A.A., 2016. Are aberrant phase transitions a driver of cellular aging? *BioEssays News Rev. Mol. Cell. Dev. Biol.* 38, 959–968. <https://doi.org/10.1002/bies.201600042>
- Amador-Ortiz, C., Lin, W.-L., Ahmed, Z., Personett, D., Davies, P., Duara, R., Graff-Radford, N.R., Hutton, M.L., Dickson, D.W., 2007. TDP-43 immunoreactivity in hippocampal sclerosis and Alzheimer's disease. *Ann. Neurol.* 61, 435–445. <https://doi.org/10.1002/ana.21154>
- Ambadipudi, S., Biernat, J., Riedel, D., Mandelkow, E., Zweckstetter, M., 2017. Liquid-liquid phase separation of the microtubule-binding repeats of the Alzheimer-related protein Tau. *Nat. Commun.* 8, 275. <https://doi.org/10.1038/s41467-017-00480-0>
- Andreadis, A., 2005. Tau gene alternative splicing: expression patterns, regulation and modulation of function in normal brain and neurodegenerative diseases. *Biochim. Biophys. Acta* 1739, 91–103. <https://doi.org/10.1016/j.bbadis.2004.08.010>
- Apicco, D.J., Ash, P.E.A., Maziuk, B., LeBlang, C., Medalla, M., Al Abdullatif, A., Ferragud, A., Botelho, E., Ballance, H.I., Dhawan, U., Boudeau, S., Cruz, A.L., Kashy, D., Wong, A., Goldberg, L.R., Yazdani, N., Zhang, C., Ung, C.Y., Tripodis, Y., Kanaan, N.M., Ikezu, T., Cottone, P., Leszyk, J., Li, H., Luebke, J., Bryant, C.D., Wolozin, B., 2018. Reducing the RNA binding protein TIA1 protects against tau-mediated neurodegeneration in vivo. *Nat. Neurosci.* 21, 72–80. <https://doi.org/10.1038/s41593-017-0022-z>

- Arai, T., Hasegawa, M., Akiyama, H., Ikeda, K., Nonaka, T., Mori, H., Mann, D., Tsuchiya, K., Yoshida, M., Hashizume, Y., Oda, T., 2006. TDP-43 is a component of ubiquitin-positive tau-negative inclusions in frontotemporal lobar degeneration and amyotrophic lateral sclerosis. *Biochem. Biophys. Res. Commun.* 351, 602–611. <https://doi.org/10.1016/j.bbrc.2006.10.093>
- Arai, T., Hasegawa, M., Nonaka, T., Kametani, F., Yamashita, M., Hosokawa, M., Niizato, K., Tsuchiya, K., Kobayashi, Z., Ikeda, K., Yoshida, M., Onaya, M., Fujishiro, H., Akiyama, H., 2010. Phosphorylated and cleaved TDP-43 in ALS, FTLN and other neurodegenerative disorders and in cellular models of TDP-43 proteinopathy. *Neuropathol. Off. J. Jpn. Soc. Neuropathol.* 30, 170–181. <https://doi.org/10.1111/j.1440-1789.2009.01089.x>
- Arai, T., Mackenzie, I.R.A., Hasegawa, M., Nonaka, T., Niizato, K., Tsuchiya, K., Iritani, S., Onaya, M., Akiyama, H., 2009. Phosphorylated TDP-43 in Alzheimer's disease and dementia with Lewy bodies. *Acta Neuropathol. (Berl.)* 117, 125–136. <https://doi.org/10.1007/s00401-008-0480-1>
- Arseni, D., Chen, R., Murzin, A.G., Peak-Chew, S.Y., Garringer, H.J., Newell, K.L., Kametani, F., Robinson, A.C., Vidal, R., Ghetti, B., Hasegawa, M., Ryskeldi-Falcon, B., 2023. TDP-43 forms amyloid filaments with a distinct fold in type A FTLN-TDP. *Nature* 620, 898–903. <https://doi.org/10.1038/s41586-023-06405-w>
- Arseni, D., Hasegawa, M., Murzin, A.G., Kametani, F., Arai, M., Yoshida, M., Ryskeldi-Falcon, B., 2022. Structure of pathological TDP-43 filaments from ALS with FTLN. *Nature* 601, 139–143. <https://doi.org/10.1038/s41586-021-04199-3>
- Arseni, D., Nonaka, T., Jacobsen, M.H., Murzin, A.G., Cracco, L., Peak-Chew, S.Y., Garringer, H.J., Kawakami, I., Suzuki, H., Onaya, M., Saito, Y., Murayama, S., Geula, C., Vidal, R., Newell, K.L., Mesulam, M., Ghetti, B., Hasegawa, M., Ryskeldi-Falcon, B., 2024. Heteromeric amyloid filaments of ANXA11 and TDP-43 in FTLN-TDP Type C. <https://doi.org/10.1101/2024.06.25.600403>
- Asakawa, K., Handa, H., Kawakami, K., 2021. Multi-phaseted problems of TDP-43 in selective neuronal vulnerability in ALS. *Cell. Mol. Life Sci.* 78, 4453–4465. <https://doi.org/10.1007/s00018-021-03792-z>
- Ash, P.E.A., Lei, S., Shattuck, J., Boudeau, S., Carlomagno, Y., Medalla, M., Mashimo, B.L., Socorro, G., Al-Mohanna, L.F.A., Jiang, L., Öztürk, M.M., Knobel, M., Ivanov, P., Petrucelli, L., Wegmann, S., Kanaan, N.M., Wolozin, B., 2021. TIA1 potentiates tau phase separation and promotes generation of toxic oligomeric tau. *Proc. Natl. Acad. Sci. U. S. A.* 118, e2014188118. <https://doi.org/10.1073/pnas.2014188118>
- Ayala, Y.M., De Conti, L., Avendaño-Vázquez, S.E., Dhir, A., Romano, M., D'Ambrogio, A., Tollervey, J., Ule, J., Baralle, M., Buratti, E., Baralle, F.E., 2011. TDP-43 regulates its mRNA levels through a negative feedback loop. *EMBO J.* 30, 277–288. <https://doi.org/10.1038/emboj.2010.310>
- Ayala, Y.M., Pantano, S., D'Ambrogio, A., Buratti, E., Brindisi, A., Marchetti, C., Romano, M., Baralle, F.E., 2005. Human, *Drosophila*, and *C.elegans* TDP43: nucleic acid binding properties and splicing regulatory function. *J. Mol. Biol.* 348, 575–588. <https://doi.org/10.1016/j.jmb.2005.02.038>
- Ayers, J.I., Giasson, B.I., Borchelt, D.R., 2018. Prion-like Spreading in Tauopathies. *Biol. Psychiatry* 83, 337–346. <https://doi.org/10.1016/j.biopsych.2017.04.003>

- Babinchak, W.M., Haider, R., Dumm, B.K., Sarkar, P., Surewicz, K., Choi, J.-K., Surewicz, W.K., 2019. The role of liquid-liquid phase separation in aggregation of the TDP-43 low-complexity domain. *J. Biol. Chem.* 294, 6306–6317. <https://doi.org/10.1074/jbc.RA118.007222>
- Bang, J., Spina, S., Miller, B.L., 2015. Frontotemporal dementia. *Lancet Lond. Engl.* 386, 1672–1682. [https://doi.org/10.1016/S0140-6736\(15\)00461-4](https://doi.org/10.1016/S0140-6736(15)00461-4)
- Bellenguez, C., Küçükali, F., Jansen, I.E., Kleineidam, L., Moreno-Grau, S., Amin, N., Naj, A.C., Campos-Martin, R., Grenier-Boley, B., Andrade, V., Holmans, P.A., Boland, A., Damotte, V., van der Lee, S.J., Costa, M.R., Kuulasmaa, T., Yang, Q., de Rojas, I., Bis, J.C., Yaqub, A., Prokic, I., Chapuis, J., Ahmad, S., Giedraitis, V., Aarsland, D., Garcia-Gonzalez, P., Abdelnour, C., Alarcón-Martín, E., Alcolea, D., Alegret, M., Alvarez, I., Álvarez, V., Armstrong, N.J., Tsolaki, A., Antúnez, C., Appollonio, I., Arcaro, M., Archetti, S., Pastor, A.A., Arosio, B., Athanasiu, L., Bailly, H., Banaj, N., Baquero, M., Barral, S., Beiser, A., Pastor, A.B., Below, J.E., Benček, P., Benussi, L., Berr, C., Besse, C., Bessi, V., Binetti, G., Bizarro, A., Blesa, R., Boada, M., Boerwinkle, E., Borroni, B., Boschi, S., Bossù, P., Bråthen, G., Bressler, J., Bresner, C., Brodaty, H., Brookes, K.J., Brusco, L.I., Buiza-Rueda, D., Bürger, K., Burholt, V., Bush, W.S., Calero, M., Cantwell, L.B., Chene, G., Chung, J., Cuccaro, M.L., Carracedo, Á., Cecchetti, R., Cervera-Carles, L., Charbonnier, C., Chen, H.-H., Chillotti, C., Ciccone, S., Claassen, J.A.H.R., Clark, C., Conti, E., Corma-Gómez, A., Costantini, E., Custodero, C., Daian, D., Dalmaso, M.C., Daniele, A., Dardiotis, E., Dartigues, J.-F., de Deyn, P.P., de Paiva Lopes, K., de Witte, L.D., Dobbie, S., Deckert, J., del Ser, T., Denning, N., DeStefano, A., Dichgans, M., Diehl-Schmid, J., Diez-Fairen, M., Rossi, P.D., Djurovic, S., Duron, E., Düzel, E., Dufouil, C., Eiriksdottir, G., Engelborghs, S., Escott-Price, V., Espinosa, A., Ewers, M., Faber, K.M., Fabrizio, T., Nielsen, S.F., Fardo, D.W., Farotti, L., Fenoglio, C., Fernández-Fuertes, M., Ferrari, R., Ferreira, C.B., Ferri, E., Fin, B., Fischer, P., Fladby, T., Fließbach, K., Fongang, B., Fornage, M., Fortea, J., Foroud, T.M., Fostinelli, S., Fox, N.C., Franco-Macías, E., Bullido, M.J., Frank-García, A., Froelich, L., Fulton-Howard, B., Galimberti, D., García-Alberca, J.M., García-González, P., Garcia-Madrona, S., Garcia-Ribas, G., Ghidoni, R., Giegling, I., Giorgio, G., Goate, A.M., Goldhardt, O., Gomez-Fonseca, D., González-Pérez, A., Graff, C., Grande, G., Green, E., Grimmer, T., Grünblatt, E., Grunin, M., Gudnason, V., Guetta-Baranes, T., Haapasalo, A., Hadjigeorgiou, G., Haines, J.L., Hamilton-Nelson, K.L., Hampel, H., Hanon, O., Hardy, J., Hartmann, A.M., Hausner, L., Harwood, J., Heilmann-Heimbach, S., Helisalmi, S., Heneka, M.T., Hernández, I., Herrmann, M.J., Hoffmann, P., Holmes, C., Holstege, H., Vilas, R.H., Hulsman, M., Humphrey, J., Biessels, G.J., Jian, X., Johansson, C., Jun, G.R., Kastumata, Y., Kauwe, J., Kehoe, P.G., Kilander, L., Ståhlbom, A.K., Kivipelto, M., Koivisto, A., Kornhuber, J., Kosmidis, M.H., Kukull, W.A., Kuksa, P.P., Kunkle, B.W., Kuzma, A.B., Lage, C., Laukka, E.J., Launer, L., Lauria, A., Lee, C.-Y., Lehtisalo, J., Lerch, O., Lleó, A., Longstreth, W., Lopez, O., de Munain, A.L., Love, S., Löwemark, M., Luckcuck, L., Lunetta, K.L., Ma, Y., Macías, J., MacLeod, C.A., Maier, W., Mangialasche, F., Spallazzi, M., Marquié, M., Marshall, R., Martin, E.R., Montes, A.M., Rodríguez, C.M., Masullo, C., Mayeux, R., Mead, S., Mecocci, P., Medina, M., Meggy, A., Mehrabian, S., Mendoza, S., Menéndez-González, M., Mir, P., Moebus, S., Mol, M., Molina-Porcel,

- L., Montreal, L., Morelli, L., Moreno, F., Morgan, K., Mosley, T., Nöthen, M.M., Muchnik, C., Mukherjee, S., Nacmias, B., Ngandu, T., Nicolas, G., Nordestgaard, B.G., Olaso, R., Orellana, A., Orsini, M., Ortega, G., Padovani, A., Paolo, C., Papenberg, G., Parnetti, L., Pasquier, F., Pastor, P., Peloso, G., Pérez-Cordón, A., Pérez-Tur, J., Pericard, P., Peters, O., Pijnenburg, Y.A.L., Pineda, J.A., Piñol-Ripoll, G., Pisanu, C., Polak, T., Popp, J., Posthuma, D., Priller, J., Puerta, R., Quenez, O., Quintela, I., Thomassen, J.Q., Rábano, A., Rainero, I., Rajabli, F., Ramakers, I., Real, L.M., Reinders, M.J.T., Reitz, C., Reyes-Dumeyer, D., Ridge, P., Riedel-Heller, S., Riederer, P., Roberto, N., Rodriguez-Rodriguez, E., Rongve, A., Allende, I.R., Rosende-Roca, M., Royo, J.L., Rubino, E., Rujescu, D., Sáez, M.E., Sakka, P., Saltvedt, I., Sanabria, Á., Sánchez-Arjona, M.B., Sanchez-Garcia, F., Juan, P.S., Sánchez-Valle, R., Sando, S.B., Sarnowski, C., Satizabal, C.L., Scamosci, M., Scarmeas, N., Scarpini, E., Scheltens, P., Scherbaum, N., Scherer, M., Schmid, M., Schneider, A., Schott, J.M., Selbæk, G., Seripa, D., Serrano, M., Sha, J., Shadrin, A.A., Skrobot, O., Slifer, S., Snijders, G.J.L., Soininen, H., Solfrizzi, V., Solomon, A., Song, Y., Sorbi, S., Sotolongo-Grau, O., Spalletta, G., Spottke, A., Squassina, A., Stordal, E., Tartan, J.P., Tárraga, L., Tesí, N., Thalamuthu, A., Thomas, T., Tosto, G., Traykov, L., Tremolizzo, L., Tybjærg-Hansen, A., Uitterlinden, A., Ullgren, A., Ulstein, I., Valero, S., Valladares, O., Broeckhoven, C.V., Vance, J., Vardarajan, B.N., van der Lugt, A., Dongen, J.V., van Rooij, J., van Swieten, J., Vandenberghe, R., Verhey, F., Vidal, J.-S., Vogelgsang, J., Vyhnalek, M., Wagner, M., Wallon, D., Wang, L.-S., Wang, R., Weinhold, L., Wiltfang, J., Windle, G., Woods, B., Yannakouli, M., Zare, H., Zhao, Y., Zhang, X., Zhu, C., Zulaica, M., Farrer, L.A., Psaty, B.M., Ghanbari, M., Raj, T., Sachdev, P., Mather, K., Jessen, F., Ikram, M.A., de Mendonça, A., Hort, J., Tsolaki, M., Pericak-Vance, M.A., Amouyel, P., Williams, J., Frikke-Schmidt, R., Clarimon, J., Deleuze, J.-F., Rossi, G., Seshadri, S., Andreassen, O.A., Ingelsson, M., Hiltunen, M., Sleegers, K., Schellenberg, G.D., van Duijn, C.M., Sims, R., van der Flier, W.M., Ruiz, A., Ramirez, A., Lambert, J.-C., 2022. New insights into the genetic etiology of Alzheimer's disease and related dementias. *Nat. Genet.* 54, 412–436. <https://doi.org/10.1038/s41588-022-01024-z>
- Bentmann, E., Haass, C., Dormann, D., 2013. Stress granules in neurodegeneration--lessons learnt from TAR DNA binding protein of 43 kDa and fused in sarcoma. *FEBS J.* 280, 4348–4370. <https://doi.org/10.1111/febs.12287>
- Bentmann, E., Neumann, M., Tahirovic, S., Rodde, R., Dormann, D., Haass, C., 2012. Requirements for Stress Granule Recruitment of Fused in Sarcoma (FUS) and TAR DNA-binding Protein of 43 kDa (TDP-43). *J. Biol. Chem.* 287, 23079–23094. <https://doi.org/10.1074/jbc.M111.328757>
- Berger, Z., Roder, H., Hanna, A., Carlson, A., Rangachari, V., Yue, M., Wszolek, Z., Ashe, K., Knight, J., Dickson, D., Andorfer, C., Rosenberry, T.L., Lewis, J., Hutton, M., Janus, C., 2007. Accumulation of Pathological Tau Species and Memory Loss in a Conditional Model of Tauopathy. *J. Neurosci.* 27, 3650–3662. <https://doi.org/10.1523/JNEUROSCI.0587-07.2007>
- Berning, B.A., Walker, A.K., 2019. The Pathobiology of TDP-43 C-Terminal Fragments in ALS and FTL. *Front. Neurosci.* 13, 335. <https://doi.org/10.3389/fnins.2019.00335>

- Bieniek, K.F., Murray, M.E., Rutherford, N.J., Castanedes-Casey, M., DeJesus-Hernandez, M., Liesinger, A.M., Baker, M.C., Boylan, K.B., Rademakers, R., Dickson, D.W., 2013. Tau pathology in frontotemporal lobar degeneration with C9ORF72 hexanucleotide repeat expansion. *Acta Neuropathol. (Berl.)* 125, 289–302. <https://doi.org/10.1007/s00401-012-1048-7>
- Boeynaems, S., Alberti, S., Fawzi, N.L., Mittag, T., Polymenidou, M., Rousseau, F., Schymkowitz, J., Shorter, J., Wolozin, B., Van Den Bosch, L., Tompa, P., Fuxreiter, M., 2018. Protein Phase Separation: A New Phase in Cell Biology. *Trends Cell Biol.* 28, 420–435. <https://doi.org/10.1016/j.tcb.2018.02.004>
- Borcherds, W., Bremer, A., Borgia, M.B., Mittag, T., 2021. How do intrinsically disordered protein regions encode a driving force for liquid-liquid phase separation? *Curr. Opin. Struct. Biol.* 67, 41–50. <https://doi.org/10.1016/j.sbi.2020.09.004>
- Boyko, S., Qi, X., Chen, T.-H., Surewicz, K., Surewicz, W.K., 2019. Liquid-liquid phase separation of tau protein: The crucial role of electrostatic interactions. *J. Biol. Chem.* 294, 11054–11059. <https://doi.org/10.1074/jbc.AC119.009198>
- Braak, H., Braak, E., 1991. Neuropathological staging of Alzheimer-related changes. *Acta Neuropathol. (Berl.)* 82, 239–259. <https://doi.org/10.1007/BF00308809>
- Brangwynne, C.P., Eckmann, C.R., Courson, D.S., Rybarska, A., Hoege, C., Gharakhani, J., Jülicher, F., Hyman, A.A., 2009. Germline P granules are liquid droplets that localize by controlled dissolution/condensation. *Science* 324, 1729–1732. <https://doi.org/10.1126/science.1172046>
- Breijyeh, Z., Karaman, R., 2020. Comprehensive Review on Alzheimer's Disease: Causes and Treatment. *Molecules* 25, 5789. <https://doi.org/10.3390/molecules25245789>
- Brody, D.L., Holtzman, D.M., 2008. Active and Passive Immunotherapy for Neurodegenerative Disorders. *Annu. Rev. Neurosci.* 31, 175–193. <https://doi.org/10.1146/annurev.neuro.31.060407.125529>
- Brown, A.-L., Wilkins, O.G., Keuss, M.J., Hill, S.E., Zanovello, M., Lee, W.C., Bampton, A., Lee, F.C.Y., Masino, L., Qi, Y.A., Bryce-Smith, S., Gatt, A., Hallegger, M., Fagegaltier, D., Phatnani, H., Newcombe, J., Gustavsson, E.K., Seddighi, S., Reyes, J.F., Coon, S.L., Ramos, D., Schiavo, G., Fisher, E.M.C., Raj, T., Secrier, M., Lashley, T., Ule, J., Buratti, E., Humphrey, J., Ward, M.E., Fratta, P., 2022. TDP-43 loss and ALS-risk SNPs drive mis-splicing and depletion of UNC13A. *Nature* 603, 131–137. <https://doi.org/10.1038/s41586-022-04436-3>
- Brown, R.C., Lockwood, A.H., Sonawane, B.R., 2005. Neurodegenerative Diseases: An Overview of Environmental Risk Factors. *Environ. Health Perspect.* 113, 1250–1256. <https://doi.org/10.1289/ehp.7567>
- Budd Haeberlein, S., O’Gorman, J., Chiao, P., Bussi re, T., von Rosenstiel, P., Tian, Y., Zhu, Y., von Hehn, C., Gheuens, S., Skordos, L., Chen, T., Sandrock, A., 2017. Clinical Development of Aducanumab, an Anti-A β Human Monoclonal Antibody Being Investigated for the Treatment of Early Alzheimer’s Disease. *J. Prev. Alzheimers Dis.* 4, 255–263. <https://doi.org/10.14283/jpad.2017.39>
- Budini, M., Buratti, E., Morselli, E., Criollo, A., 2017. Autophagy and Its Impact on Neurodegenerative Diseases: New Roles for TDP-43 and C9orf72. *Front. Mol. Neurosci.* 10, 170. <https://doi.org/10.3389/fnmol.2017.00170>

- Buée, L., Bussi re, T., Bu e-Scherrer, V., Delacourte, A., Hof, P.R., 2000. Tau protein isoforms, phosphorylation and role in neurodegenerative disorders. *Brain Res. Rev.* 33, 95–130. [https://doi.org/10.1016/S0165-0173\(00\)00019-9](https://doi.org/10.1016/S0165-0173(00)00019-9)
- Buratti, E., 2018. TDP-43 post-translational modifications in health and disease. *Expert Opin. Ther. Targets* 22, 279–293. <https://doi.org/10.1080/14728222.2018.1439923>
- Buratti, E., Baralle, F.E., 2001. Characterization and functional implications of the RNA binding properties of nuclear factor TDP-43, a novel splicing regulator of CFTR exon 9. *J. Biol. Chem.* 276, 36337–36343. <https://doi.org/10.1074/jbc.M104236200>
- Burr , J., Sharma, M., Tsetsenis, T., Buchman, V., Etherton, M.R., S dhof, T.C., 2010. Alpha-synuclein promotes SNARE-complex assembly in vivo and in vitro. *Science* 329, 1663–1667. <https://doi.org/10.1126/science.1195227>
- Caccamo, A., Majumder, S., Deng, J.J., Bai, Y., Thornton, F.B., Oddo, S., 2009. Rapamycin rescues TDP-43 mislocalization and the associated low molecular mass neurofilament instability. *J. Biol. Chem.* 284, 27416–27424. <https://doi.org/10.1074/jbc.M109.031278>
- Candia, R.F., Cohen, L.S., Morozova, V., Corbo, C., Alonso, A.D., 2022. Importin-Mediated Pathological Tau Nuclear Translocation Causes Disruption of the Nuclear Lamina, TDP-43 Mislocalization and Cell Death. *Front. Mol. Neurosci.* 15.
- Chen, S., Townsend, K., Goldberg, T.E., Davies, P., Conejero-Goldberg, C., 2010. MAPT Isoforms: Differential Transcriptional Profiles Related to 3R and 4R Splice Variants. *J. Alzheimers Dis.* 22, 1313–1329. <https://doi.org/10.3233/JAD-2010-101155>
- Chhangani, D., Mart n-Pe a, A., Rincon-Limas, D.E., 2021. Molecular, functional, and pathological aspects of TDP-43 fragmentation. *iScience* 24, 102459. <https://doi.org/10.1016/j.isci.2021.102459>
- Chin-Chan, M., Navarro-Yepes, J., Quintanilla-Vega, B., 2015. Environmental pollutants as risk factors for neurodegenerative disorders: Alzheimer and Parkinson diseases. *Front. Cell. Neurosci.* 9, 124. <https://doi.org/10.3389/fncel.2015.00124>
- Chong, P.A., Vernon, R.M., Forman-Kay, J.D., 2018. RGG/RG Motif Regions in RNA Binding and Phase Separation. *J. Mol. Biol.* 430, 4650–4665. <https://doi.org/10.1016/j.jmb.2018.06.014>
- Chornenkyy, Y., Fardo, D.W., Nelson, P.T., 2019. Tau and TDP-43 proteinopathies: kindred pathologic cascades and genetic pleiotropy. *Lab. Invest.* 99, 993–1007. <https://doi.org/10.1038/s41374-019-0196-y>
- Chou, C.-C., Zhang, Y., Umoh, M.E., Vaughan, S.W., Lorenzini, I., Liu, F., Sayegh, M., Donlin-Asp, P.G., Chen, Y.H., Duong, D.M., Seyfried, N.T., Powers, M.A., Kukar, T., Hales, C.M., Gearing, M., Cairns, N.J., Boylan, K.B., Dickson, D.W., Rademakers, R., Zhang, Y.-J., Petrucelli, L., Sattler, R., Zarnescu, D.C., Glass, J.D., Rossoll, W., 2018. TDP-43 pathology disrupts nuclear pore complexes and nucleocytoplasmic transport in ALS/FTD. *Nat. Neurosci.* 21, 228–239. <https://doi.org/10.1038/s41593-017-0047-3>
- Chu, T.-T., Gao, N., Li, Q.-Q., Chen, P.-G., Yang, X.-F., Chen, Y.-X., Zhao, Y.-F., Li, Y.-M., 2016. Specific Knockdown of Endogenous Tau Protein by Peptide-Directed Ubiquitin-Proteasome Degradation. *Cell Chem. Biol.* 23, 453–461. <https://doi.org/10.1016/j.chembiol.2016.02.016>
- Cicardi, M.E., Marrone, L., Azzouz, M., Trotti, D., 2021. Proteostatic imbalance and protein spreading in amyotrophic lateral sclerosis. *EMBO J.* 40, e106389. <https://doi.org/10.15252/embj.2020106389>

- Clippinger, A.K., D'Alton, S., Lin, W.-L., Gendron, T.F., Howard, J., Borchelt, D.R., Cannon, A., Carlomagno, Y., Chakrabarty, P., Cook, C., Golde, T.E., Levites, Y., Ranum, L., Schultheis, P.J., Xu, G., Petrucelli, L., Sahara, N., Dickson, D.W., Giasson, B., Lewis, J., 2013. Robust cytoplasmic accumulation of phosphorylated TDP-43 in transgenic models of tauopathy. *Acta Neuropathol. (Berl.)* 126, 39–50. <https://doi.org/10.1007/s00401-013-1123-8>
- Colombrita, C., Zennaro, E., Fallini, C., Weber, M., Sommacal, A., Buratti, E., Silani, V., Ratti, A., 2009. TDP-43 is recruited to stress granules in conditions of oxidative insult. *J. Neurochem.* 111, 1051–1061. <https://doi.org/10.1111/j.1471-4159.2009.06383.x>
- Colom-Cadena, M., Davies, C., Sirisi, S., Lee, J.-E., Simzer, E.M., Tzioras, M., Querol-Vilaseca, M., Sánchez-Aced, É., Chang, Y.Y., Holt, K., McGeachan, R.I., Rose, J., Tulloch, J., Wilkins, L., Smith, C., Andrian, T., Belbin, O., Pujals, S., Horrocks, M.H., Lleó, A., Spires-Jones, T.L., 2023. Synaptic oligomeric tau in Alzheimer's disease — A potential culprit in the spread of tau pathology through the brain. *Neuron* 111, 2170–2183.e6. <https://doi.org/10.1016/j.neuron.2023.04.020>
- Conicella, A.E., Dignon, G.L., Zerze, G.H., Schmidt, H.B., D'Ordine, A.M., Kim, Y.C., Rohatgi, R., Ayala, Y.M., Mittal, J., Fawzi, N.L., 2020. TDP-43 α -helical structure tunes liquid-liquid phase separation and function. *Proc. Natl. Acad. Sci. U. S. A.* 117, 5883–5894. <https://doi.org/10.1073/pnas.1912055117>
- Conicella, A.E., Zerze, G.H., Mittal, J., Fawzi, N.L., 2016. ALS Mutations Disrupt Phase Separation Mediated by α -Helical Structure in the TDP-43 Low-Complexity C-Terminal Domain. *Struct. Lond. Engl.* 1993 24, 1537–1549. <https://doi.org/10.1016/j.str.2016.07.007>
- Couratier, P., Corcia, P., Lautrette, G., Nicol, M., Marin, B., 2017. ALS and frontotemporal dementia belong to a common disease spectrum. *Rev. Neurol. (Paris), Motor neuron diseases* 173, 273–279. <https://doi.org/10.1016/j.neurol.2017.04.001>
- Cracco, L., Doud, E.H., Hallinan, G.I., Garringer, H.J., Jacobsen, M.H., Richardson, R.M., Buratti, E., Vidal, R., Ghetti, B., Newell, K.L., 2022. Distinguishing post-translational modifications in dominantly inherited frontotemporal dementias: FTLD-TDP Type A (*GRN*) vs Type B (*C9orf72*). *Neuropathol. Appl. Neurobiol.* 48, e12836. <https://doi.org/10.1111/nan.12836>
- Dai, C.-L., Hu, W., Tung, Y.C., Liu, F., Gong, C.-X., Iqbal, K., 2018. Tau passive immunization blocks seeding and spread of Alzheimer hyperphosphorylated Tau-induced pathology in 3 \times Tg-AD mice. *Alzheimers Res. Ther.* 10, 13. <https://doi.org/10.1186/s13195-018-0341-7>
- Das, T., Zaidi, F., Farag, M., Ruff, K.M., Messing, J., Taylor, J.P., Pappu, R.V., Mittag, T., 2024. Metastable condensates suppress conversion to amyloid fibrils. *BioRxiv Prepr. Serv. Biol.* 2024.02.28.582569. <https://doi.org/10.1101/2024.02.28.582569>
- de Oliveira, G.A.P., Cordeiro, Y., Silva, J.L., Vieira, T.C.R.G., 2019. Liquid-liquid phase transitions and amyloid aggregation in proteins related to cancer and neurodegenerative diseases. *Adv. Protein Chem. Struct. Biol.* 118, 289–331. <https://doi.org/10.1016/bs.apcsb.2019.08.002>
- DeMaagd, G., Philip, A., 2015. Parkinson's Disease and Its Management. *Pharm. Ther.* 40, 504–532.

- DeTure, M.A., Dickson, D.W., 2019. The neuropathological diagnosis of Alzheimer's disease. *Mol. Neurodegener.* 14, 32. <https://doi.org/10.1186/s13024-019-0333-5>
- DeVos, S.L., Corjuc, B.T., Oakley, D.H., Nobuhara, C.K., Bannan, R.N., Chase, A., Commins, C., Gonzalez, J.A., Dooley, P.M., Frosch, M.P., Hyman, B.T., 2018. Synaptic Tau Seeding Precedes Tau Pathology in Human Alzheimer's Disease Brain. *Front. Neurosci.* 12, 267. <https://doi.org/10.3389/fnins.2018.00267>
- Dewey, C.M., Cenik, B., Sephton, C.F., Dries, D.R., Mayer, P., Good, S.K., Johnson, B.A., Herz, J., Yu, G., 2011. TDP-43 is directed to stress granules by sorbitol, a novel physiological osmotic and oxidative stressor. *Mol. Cell. Biol.* 31, 1098–1108. <https://doi.org/10.1128/MCB.01279-10>
- Dhakal, S., Mondal, M., Mirzazadeh, A., Banerjee, S., Ghosh, A., Rangachari, V., 2023. α -Synuclein emulsifies TDP-43 prion-like domain—RNA liquid droplets to promote heterotypic amyloid fibrils. *Commun. Biol.* 6, 1227. <https://doi.org/10.1038/s42003-023-05608-1>
- Dormann, D., Rodde, R., Edbauer, D., Bentmann, E., Fischer, I., Hruscha, A., Than, M.E., Mackenzie, I.R.A., Capell, A., Schmid, B., Neumann, M., Haass, C., 2010. ALS-associated fused in sarcoma (FUS) mutations disrupt Transportin-mediated nuclear import. *EMBO J.* 29, 2841–2857. <https://doi.org/10.1038/emboj.2010.143>
- Dos Passos, P.M., Hemamali, E.H., Mamede, L.D., Hayes, L.R., Ayala, Y.M., 2024. RNA-mediated ribonucleoprotein assembly controls TDP-43 nuclear retention. *PLoS Biol.* 22, e3002527. <https://doi.org/10.1371/journal.pbio.3002527>
- Dugger, B.N., Dickson, D.W., 2017. Pathology of Neurodegenerative Diseases. *Cold Spring Harb. Perspect. Biol.* 9, a028035. <https://doi.org/10.1101/cshperspect.a028035>
- Ederle, H., Dormann, D., 2017. TDP-43 and FUS en route from the nucleus to the cytoplasm. *FEBS Lett.* 591, 1489–1507. <https://doi.org/10.1002/1873-3468.12646>
- Ederle, H., Funk, C., Abou-Ajram, C., Hutten, S., Funk, E.B.E., Kehlenbach, R.H., Bailer, S.M., Dormann, D., 2018. Nuclear egress of TDP-43 and FUS occurs independently of Exportin-1/CRM1. *Sci. Rep.* 8, 7084. <https://doi.org/10.1038/s41598-018-25007-5>
- Eftekharzadeh, B., Daigle, J.G., Kapinos, L.E., Coyne, A., Schiantarelli, J., Carlomagno, Y., Cook, C., Miller, S.J., Dujardin, S., Amaral, A.S., Grima, J.C., Bennett, R.E., Tepper, K., DeTure, M., Vanderburg, C.R., Corjuc, B.T., DeVos, S.L., Gonzalez, J.A., Chew, J., Vidsensky, S., Gage, F.H., Mertens, J., Troncoso, J., Mandelkow, E., Salvatella, X., Lim, R.Y.H., Petrucelli, L., Wegmann, S., Rothstein, J.D., Hyman, B.T., 2018. Tau Protein Disrupts Nucleocytoplasmic Transport in Alzheimer's Disease. *Neuron* 99, 925–940.e7. <https://doi.org/10.1016/j.neuron.2018.07.039>
- Emmanouilidis, L., Bartalucci, E., Kan, Y., Ijavi, M., Pérez, M.E., Afanasyev, P., Boehringer, D., Zehnder, J., Parekh, S.H., Bonn, M., Michaels, T.C.T., Wiegand, T., Allain, F.H.-T., 2024. A solid beta-sheet structure is formed at the surface of FUS droplets during aging. *Nat. Chem. Biol.* 1–9. <https://doi.org/10.1038/s41589-024-01573-w>
- Fakim, H., Vande Velde, C., 2024. The implications of physiological biomolecular condensates in amyotrophic lateral sclerosis. *Semin. Cell Dev. Biol.* 156, 176–189. <https://doi.org/10.1016/j.semcdb.2023.05.006>
- Fang, M.Y., Markmiller, S., Vu, A.Q., Javaherian, A., Dowdle, W.E., Jolivet, P., Bushway, P.J., Castello, N.A., Baral, A., Chan, M.Y., Linsley, J.W., Linsley, D., Mercola, M., Finkbeiner, S., Lecuyer, E., Lewcock, J.W., Yeo, G.W., 2019. Small-Molecule

- Modulation of TDP-43 Recruitment to Stress Granules Prevents Persistent TDP-43 Accumulation in ALS/FTD. *Neuron* 103, 802-819.e11. <https://doi.org/10.1016/j.neuron.2019.05.048>
- Feiler, M.S., Strobel, B., Freischmidt, A., Helferich, A.M., Kappel, J., Brewer, B.M., Li, D., Thal, D.R., Walther, P., Ludolph, A.C., Danzer, K.M., Weishaupt, J.H., 2015. TDP-43 is intercellularly transmitted across axon terminals. *J. Cell Biol.* 211, 897–911. <https://doi.org/10.1083/jcb.201504057>
- Fein, J.A., Sokolow, S., Miller, C.A., Vinters, H.V., Yang, F., Cole, G.M., Gylys, K.H., 2008. Co-localization of amyloid beta and tau pathology in Alzheimer's disease synaptosomes. *Am. J. Pathol.* 172, 1683–1692. <https://doi.org/10.2353/ajpath.2008.070829>
- Feinstein, S.C., Wilson, L., 2005. Inability of tau to properly regulate neuronal microtubule dynamics: a loss-of-function mechanism by which tau might mediate neuronal cell death. *Biochim. Biophys. Acta* 1739, 268–279. <https://doi.org/10.1016/j.bbadis.2004.07.002>
- Feric, M., Vaidya, N., Harmon, T.S., Mitrea, D.M., Zhu, L., Richardson, T.M., Kriwacki, R.W., Pappu, R.V., Brangwynne, C.P., 2016. Coexisting Liquid Phases Underlie Nucleolar Subcompartments. *Cell* 165, 1686–1697. <https://doi.org/10.1016/j.cell.2016.04.047>
- Ferrari, L., Bauer, B., Qiu, Y., Schuschnig, M., Klotz, S., Anrather, D., Juretschke, T., Beli, P., Gelpi, E., Martens, S., 2024. Tau fibrils evade autophagy by excessive p62 coating and TAX1BP1 exclusion. *Sci. Adv.* 10, eadm8449. <https://doi.org/10.1126/sciadv.adm8449>
- Ferreira, A., Bigio, E.H., 2011. Calpain-Mediated Tau Cleavage: A Mechanism Leading to Neurodegeneration Shared by Multiple Tauopathies. *Mol. Med.* 17, 676–685. <https://doi.org/10.2119/molmed.2010.00220>
- Ferreon, J.C., Jain, A., Choi, K.-J., Tsoi, P.S., MacKenzie, K.R., Jung, S.Y., Ferreon, A.C., 2018. Acetylation Disfavors Tau Phase Separation. *Int. J. Mol. Sci.* 19, 1360. <https://doi.org/10.3390/ijms19051360>
- Fitzpatrick, A.W.P., Falcon, B., He, S., Murzin, A.G., Murshudov, G., Garringer, H.J., Crowther, R.A., Ghetti, B., Goedert, M., Scheres, S.H.W., 2017. Cryo-EM structures of tau filaments from Alzheimer's disease. *Nature* 547, 185–190. <https://doi.org/10.1038/nature23002>
- Flanagan, E.P., Duffy, J.R., Whitwell, J.L., Vemuri, P., Dickson, D.W., Josephs, K.A., 2016. Mixed tau and TDP-43 pathology in a patient with unclassifiable primary progressive aphasia. *Neurocase* 22, 55–59. <https://doi.org/10.1080/13554794.2015.1041534>
- Flavin, W.P., Bousset, L., Green, Z.C., Chu, Y., Skarpathiotis, S., Chaney, M.J., Kordower, J.H., Melki, R., Campbell, E.M., 2017. Endocytic vesicle rupture is a conserved mechanism of cellular invasion by amyloid proteins. *Acta Neuropathol. (Berl.)* 134, 629–653. <https://doi.org/10.1007/s00401-017-1722-x>
- Forman-Kay, J.D., Ditlev, J.A., Nosella, M.L., Lee, H.O., 2022. What are the distinguishing features and size requirements of biomolecular condensates and their implications for RNA-containing condensates? *RNA N. Y. N.* 28, 36–47. <https://doi.org/10.1261/rna.079026.121>
- Freeman, S.H., Spires-Jones, T., Hyman, B.T., Growdon, J.H., Frosch, M.P., 2008. TAR-DNA binding protein 43 in Pick disease. *J. Neuropathol. Exp. Neurol.* 67, 62–67. <https://doi.org/10.1097/nen.0b013e3181609361>

- Fricker, M., Tolkovsky, A.M., Borutaite, V., Coleman, M., Brown, G.C., 2018. Neuronal Cell Death. *Physiol. Rev.* 98, 813–880. <https://doi.org/10.1152/physrev.00011.2017>
- Friedrich, R.P., Tepper, K., Rönicke, R., Soom, M., Westermann, M., Reymann, K., Kaether, C., Fändrich, M., 2010. Mechanism of amyloid plaque formation suggests an intracellular basis of Abeta pathogenicity. *Proc. Natl. Acad. Sci. U. S. A.* 107, 1942–1947. <https://doi.org/10.1073/pnas.0904532106>
- Furman, J.L., Vaquer-Alicea, J., White, C.L., Cairns, N.J., Nelson, P.T., Diamond, M.I., 2017. Widespread tau seeding activity at early Braak stages. *Acta Neuropathol. (Berl.)* 133, 91–100. <https://doi.org/10.1007/s00401-016-1644-z>
- Furukawa, Y., Kaneko, K., Watanabe, S., Yamanaka, K., Nukina, N., 2011. A seeding reaction recapitulates intracellular formation of Sarkosyl-insoluble transactivation response element (TAR) DNA-binding protein-43 inclusions. *J. Biol. Chem.* 286, 18664–18672. <https://doi.org/10.1074/jbc.M111.231209>
- Gallo, J.-M., Edbauer, D., 2022. A perturbed network in neurodegeneration. *Science* 378, 28–29. <https://doi.org/10.1126/science.ade4210>
- Gan, L., Cookson, M.R., Petrucelli, L., La Spada, A.R., 2018. Converging pathways in neurodegeneration, from genetics to mechanisms. *Nat. Neurosci.* 21, 1300–1309. <https://doi.org/10.1038/s41593-018-0237-7>
- Gao, J., Wang, L., Huntley, M.L., Perry, G., Wang, X., 2018. Pathomechanisms of TDP-43 in neurodegeneration. *J. Neurochem.* 146, 7–20. <https://doi.org/10.1111/jnc.14327>
- Gao, N., Chu, T.-T., Li, Q.-Q., Lim, Y.-J., Qiu, T., Ma, M.-R., Hu, Z.-W., Yang, X.-F., Chen, Y.-X., Zhao, Y.-F., Li, Y.-M., 2017. Hydrophobic tagging-mediated degradation of Alzheimer's disease related Tau. *RSC Adv.* 7, 40362–40366. <https://doi.org/10.1039/C7RA05347A>
- Gao, N., Huang, Y.-P., Chu, T.-T., Li, Q.-Q., Zhou, B., Chen, Y.-X., Zhao, Y.-F., Li, Y.-M., 2019. TDP-43 specific reduction induced by Di-hydrophobic tags conjugated peptides. *Bioorganic Chem.* 84, 254–259. <https://doi.org/10.1016/j.bioorg.2018.11.042>
- Gasset-Rosa, F., Lu, S., Yu, H., Chen, C., Melamed, Z., Guo, L., Shorter, J., Da Cruz, S., Cleveland, D.W., 2019. Cytoplasmic TDP-43 De-mixing Independent of Stress Granules Drives Inhibition of Nuclear Import, Loss of Nuclear TDP-43, and Cell Death. *Neuron* 102, 339–357.e7. <https://doi.org/10.1016/j.neuron.2019.02.038>
- Gendron, T.F., Bieniek, K.F., Zhang, Y.-J., Jansen-West, K., Ash, P.E.A., Caulfield, T., Daugherty, L., Dunmore, J.H., Castanedes-Casey, M., Chew, J., Cosio, D.M., van Blitterswijk, M., Lee, W.C., Rademakers, R., Boylan, K.B., Dickson, D.W., Petrucelli, L., 2013. Antisense transcripts of the expanded C9ORF72 hexanucleotide repeat form nuclear RNA foci and undergo repeat-associated non-ATG translation in c9FTD/ALS. *Acta Neuropathol. (Berl.)* 126, 829–844. <https://doi.org/10.1007/s00401-013-1192-8>
- Gerson, J.E., Kaye, R., 2013. Formation and propagation of tau oligomeric seeds. *Front. Neurol.* 4, 93. <https://doi.org/10.3389/fneur.2013.00093>
- Gitler, A.D., Tsuiji, H., 2016. There has been an awakening: Emerging mechanisms of C9orf72 mutations in FTD/ALS. *Brain Res.* 1647, 19–29. <https://doi.org/10.1016/j.brainres.2016.04.004>
- Gracia, P., Polanco, D., Tarancón-Díez, J., Serra, I., Bracci, M., Oroz, J., Laurents, D.V., García, I., Cremades, N., 2022. Molecular mechanism for the synchronized electrostatic

- coacervation and co-aggregation of alpha-synuclein and tau. *Nat. Commun.* 13, 4586. <https://doi.org/10.1038/s41467-022-32350-9>
- Grujic da Silva, L.A., Simonetti, F., Hutten, S., Riemenschneider, H., Sternburg, E.L., Pietrek, L.M., Gebel, J., Dötsch, V., Edbauer, D., Hummer, G., Stelzl, L.S., Dormann, D., 2022. Disease-linked TDP-43 hyperphosphorylation suppresses TDP-43 condensation and aggregation. *EMBO J.* 41, e108443. <https://doi.org/10.15252/embj.2021108443>
- Gu, J., Chen, F., Iqbal, K., Gong, C.-X., Wang, X., Liu, F., 2017a. Transactive response DNA-binding protein 43 (TDP-43) regulates alternative splicing of tau exon 10: Implications for the pathogenesis of tauopathies. *J. Biol. Chem.* 292, 10600–10612. <https://doi.org/10.1074/jbc.M117.783498>
- Gu, J., Hu, W., Tan, X., Qu, S., Chu, D., Gong, C.-X., Iqbal, K., Liu, F., 2020. Elevation of casein kinase 1 ϵ associated with TDP-43 and tau pathologies in Alzheimer's disease. *Brain Pathol. Zurich Switz.* 30, 283–297. <https://doi.org/10.1111/bpa.12775>
- Gu, J., Wu, F., Xu, W., Shi, J., Hu, W., Jin, N., Qian, W., Wang, X., Iqbal, K., Gong, C.-X., Liu, F., 2017b. TDP-43 suppresses tau expression via promoting its mRNA instability. *Nucleic Acids Res.* 45, 6177–6193. <https://doi.org/10.1093/nar/gkx175>
- Guo, J.L., Lee, V.M.Y., 2014. Cell-to-cell transmission of pathogenic proteins in neurodegenerative diseases. *Nat. Med.* 20, 130–138. <https://doi.org/10.1038/nm.3457>
- Guo, T., Noble, W., Hanger, D.P., 2017. Roles of tau protein in health and disease. *Acta Neuropathol. (Berl.)* 133, 665–704. <https://doi.org/10.1007/s00401-017-1707-9>
- Haass, C., Kaether, C., Thinakaran, G., Sisodia, S., 2012. Trafficking and Proteolytic Processing of APP. *Cold Spring Harb. Perspect. Med.* 2, a006270. <https://doi.org/10.1101/cshperspect.a006270>
- Haj-Yahya, M., Gopinath, P., Rajasekhar, K., Mirbaha, H., Diamond, M.I., Lashuel, H.A., 2020. Site-Specific Hyperphosphorylation Inhibits, Rather than Promotes, Tau Fibrillization, Seeding Capacity, and Its Microtubule Binding. *Angew. Chem. Int. Ed Engl.* 59, 4059–4067. <https://doi.org/10.1002/anie.201913001>
- Hallegger, M., Chakrabarti, A.M., Lee, F.C.Y., Lee, B.L., Amaliotti, A.G., Odeh, H.M., Copley, K.E., Rubien, J.D., Portz, B., Kuret, K., Huppertz, I., Rau, F., Patani, R., Fawzi, N.L., Shorter, J., Luscombe, N.M., Ule, J., 2021. TDP-43 condensation properties specify its RNA-binding and regulatory repertoire. *Cell* 184, 4680-4696.e22. <https://doi.org/10.1016/j.cell.2021.07.018>
- Hasegawa, M., Arai, T., Nonaka, T., Kametani, F., Yoshida, M., Hashizume, Y., Beach, T.G., Buratti, E., Baralle, F., Morita, M., Nakano, I., Oda, T., Tsuchiya, K., Akiyama, H., 2008. Phosphorylated TDP-43 in frontotemporal lobar degeneration and amyotrophic lateral sclerosis. *Ann. Neurol.* 64, 60–70. <https://doi.org/10.1002/ana.21425>
- Henstridge, C.M., Pickett, E., Spires-Jones, T.L., 2016. Synaptic pathology: A shared mechanism in neurological disease. *Ageing Res. Rev.* 28, 72–84. <https://doi.org/10.1016/j.arr.2016.04.005>
- Hernández-Vega, A., Braun, M., Scharrel, L., Jahnel, M., Wegmann, S., Hyman, B.T., Alberti, S., Diez, S., Hyman, A.A., 2017a. Local Nucleation of Microtubule Bundles through Tubulin Concentration into a Condensed Tau Phase. *Cell Rep.* 20, 2304–2312. <https://doi.org/10.1016/j.celrep.2017.08.042>
- Hernández-Vega, A., Braun, M., Scharrel, L., Jahnel, M., Wegmann, S., Hyman, B.T., Alberti, S., Diez, S., Hyman, A.A., 2017b. Local Nucleation of Microtubule Bundles through

- Tubulin Concentration into a Condensed Tau Phase. *Cell Rep.* 20, 2304–2312. <https://doi.org/10.1016/j.celrep.2017.08.042>
- Hickman, S., Izzy, S., Sen, P., Morsett, L., El Khoury, J., 2018. Microglia in neurodegeneration. *Nat. Neurosci.* 21, 1359–1369. <https://doi.org/10.1038/s41593-018-0242-x>
- Higashi, S., Iseki, E., Yamamoto, R., Minegishi, M., Hino, H., Fujisawa, K., Togo, T., Katsuse, O., Uchikado, H., Furukawa, Y., Kosaka, K., Arai, H., 2007. Concurrence of TDP-43, tau and alpha-synuclein pathology in brains of Alzheimer's disease and dementia with Lewy bodies. *Brain Res.* 1184, 284–294. <https://doi.org/10.1016/j.brainres.2007.09.048>
- Hiji, M., Takahashi, T., Fukuba, H., Yamashita, H., Kohriyama, T., Matsumoto, M., 2008. White matter lesions in the brain with frontotemporal lobar degeneration with motor neuron disease: TDP-43-immunopositive inclusions co-localize with p62, but not ubiquitin. *Acta Neuropathol. (Berl.)* 116, 183–191. <https://doi.org/10.1007/s00401-008-0402-2>
- Hipp, M.S., Kasturi, P., Hartl, F.U., 2019. The proteostasis network and its decline in ageing. *Nat. Rev. Mol. Cell Biol.* 20, 421–435. <https://doi.org/10.1038/s41580-019-0101-y>
- Hochmair, J., Exner, C., Franck, M., Dominguez-Baquero, A., Diez, L., Brognaro, H., Kraushar, M.L., Mielke, T., Radbruch, H., Kaniyappan, S., Falke, S., Mandelkow, E., Betzel, C., Wegmann, S., 2022. Molecular crowding and RNA synergize to promote phase separation, microtubule interaction, and seeding of Tau condensates. *EMBO J.* 41, e108882. <https://doi.org/10.15252/embj.2021108882>
- Hofweber, M., Hutten, S., Bourgeois, B., Spreitzer, E., Niedner-Boblenz, A., Schifferer, M., Ruepp, M.-D., Simons, M., Niessing, D., Madl, T., Dormann, D., 2018. Phase Separation of FUS Is Suppressed by Its Nuclear Import Receptor and Arginine Methylation. *Cell* 173, 706–719.e13. <https://doi.org/10.1016/j.cell.2018.03.004>
- Hogan, D.B., Jetté, N., Fiest, K.M., Roberts, J.I., Pearson, D., Smith, E.E., Roach, P., Kirk, A., Pringsheim, T., Maxwell, C.J., 2016. The Prevalence and Incidence of Frontotemporal Dementia: a Systematic Review. *Can. J. Neurol. Sci. J. Can. Sci. Neurol.* 43 Suppl 1, S96–S109. <https://doi.org/10.1017/cjn.2016.25>
- Holmes, B.B., DeVos, S.L., Kfoury, N., Li, M., Jacks, R., Yanamandra, K., Ouidja, M.O., Brodsky, F.M., Marasa, J., Bagchi, D.P., Kotzbauer, P.T., Miller, T.M., Papy-Garcia, D., Diamond, M.I., 2013. Heparan sulfate proteoglycans mediate internalization and propagation of specific proteopathic seeds. *Proc. Natl. Acad. Sci. U. S. A.* 110, E3138–3147. <https://doi.org/10.1073/pnas.1301440110>
- Holmes, B.B., Furman, J.L., Mahan, T.E., Yamasaki, T.R., Mirbaha, H., Eades, W.C., Belaygorod, L., Cairns, N.J., Holtzman, D.M., Diamond, M.I., 2014. Proteopathic tau seeding predicts tauopathy in vivo. *Proc. Natl. Acad. Sci.* 111. <https://doi.org/10.1073/pnas.1411649111>
- Hoover, B.R., Reed, M.N., Su, J., Penrod, R.D., Kotilinek, L.A., Grant, M.K., Pitstick, R., Carlson, G.A., Lanier, L.M., Yuan, L.-L., Ashe, K.H., Liao, D., 2010. Tau mislocalization to dendritic spines mediates synaptic dysfunction independently of neurodegeneration. *Neuron* 68, 1067–1081. <https://doi.org/10.1016/j.neuron.2010.11.030>
- Hu, X., Crick, S.L., Bu, G., Frieden, C., Pappu, R.V., Lee, J.-M., 2009. Amyloid seeds formed by cellular uptake, concentration, and aggregation of the amyloid-beta peptide. *Proc. Natl. Acad. Sci. U. S. A.* 106, 20324–20329. <https://doi.org/10.1073/pnas.0911281106>

- Hutten, S., Dormann, D., 2020. Nucleocytoplasmic transport defects in neurodegeneration — Cause or consequence? *Semin. Cell Dev. Biol.* 99, 151–162. <https://doi.org/10.1016/j.semcdb.2019.05.020>
- Hyun, S., Shin, D., 2021. Chemical-Mediated Targeted Protein Degradation in Neurodegenerative Diseases. *Life Basel Switz.* 11, 607. <https://doi.org/10.3390/life11070607>
- Igaz, L.M., Kwong, L.K., Xu, Y., Truax, A.C., Uryu, K., Neumann, M., Clark, C.M., Elman, L.B., Miller, B.L., Grossman, M., McCluskey, L.F., Trojanowski, J.Q., Lee, V.M.-Y., 2008. Enrichment of C-terminal fragments in TAR DNA-binding protein-43 cytoplasmic inclusions in brain but not in spinal cord of frontotemporal lobar degeneration and amyotrophic lateral sclerosis. *Am. J. Pathol.* 173, 182–194. <https://doi.org/10.2353/ajpath.2008.080003>
- Inoue, K., 2015. Genetic Risk Factors for Neurodegenerative Diseases, in: Wada, K. (Ed.), *Neurodegenerative Disorders as Systemic Diseases*. Springer Japan, Tokyo, pp. 117–134. https://doi.org/10.1007/978-4-431-54541-5_6
- Ishizawa, T., Mattila, P., Davies, P., Wang, D., Dickson, D.W., 2003. Colocalization of tau and alpha-synuclein epitopes in Lewy bodies. *J. Neuropathol. Exp. Neurol.* 62, 389–397. <https://doi.org/10.1093/jnen/62.4.389>
- Jalihal, A.P., Schmidt, A., Gao, G., Little, S.R., Pitchiaya, S., Walter, N.G., 2021. Hyperosmotic phase separation: Condensates beyond inclusions, granules and organelles. *J. Biol. Chem.* 296, 100044. <https://doi.org/10.1074/jbc.REV120.010899>
- Jiang, L., Ash, P.E.A., Maziuk, B.F., Ballance, H.I., Boudeau, S., Abdullatif, A.A., Orlando, M., Petrucelli, L., Ikezu, T., Wolozin, B., 2019. TIA1 regulates the generation and response to toxic tau oligomers. *Acta Neuropathol. (Berl.)* 137, 259–277. <https://doi.org/10.1007/s00401-018-1937-5>
- Jiang, Q., Lee, C.Y.D., Mandrekar, S., Wilkinson, B., Cramer, P., Zelcer, N., Mann, K., Lamb, B., Willson, T.M., Collins, J.L., Richardson, J.C., Smith, J.D., Comery, T.A., Riddell, D., Holtzman, D.M., Tontonoz, P., Landreth, G.E., 2008. ApoE promotes the proteolytic degradation of Abeta. *Neuron* 58, 681–693. <https://doi.org/10.1016/j.neuron.2008.04.010>
- Jiang, S., Bhaskar, K., 2020. Degradation and Transmission of Tau by Autophagic-Endolysosomal Networks and Potential Therapeutic Targets for Tauopathy. *Front. Mol. Neurosci.* 13, 586731. <https://doi.org/10.3389/fnmol.2020.586731>
- Jinwal, U.K., Abisambra, J.F., Zhang, J., Dharia, S., O’Leary, J.C., Patel, T., Braswell, K., Jani, T., Gestwicki, J.E., Dickey, C.A., 2012. Cdc37/Hsp90 protein complex disruption triggers an autophagic clearance cascade for TDP-43 protein. *J. Biol. Chem.* 287, 24814–24820. <https://doi.org/10.1074/jbc.M112.367268>
- Jo, M., Lee, S., Jeon, Y.-M., Kim, S., Kwon, Y., Kim, H.-J., 2020. The role of TDP-43 propagation in neurodegenerative diseases: integrating insights from clinical and experimental studies. *Exp. Mol. Med.* 52, 1652–1662. <https://doi.org/10.1038/s12276-020-00513-7>
- Josephs, K.A., Dickson, D.W., Tosakulwong, N., Weigand, S.D., Murray, M.E., Petrucelli, L., Liesinger, A.M., Senjem, M.L., Spychalla, A.J., Knopman, D.S., Parisi, J.E., Petersen, R.C., Jack, C.R., Whitwell, J.L., 2017. Rates of hippocampal atrophy and presence of

- post-mortem TDP-43 in patients with Alzheimer's disease: a longitudinal retrospective study. *Lancet Neurol.* 16, 917–924. [https://doi.org/10.1016/S1474-4422\(17\)30284-3](https://doi.org/10.1016/S1474-4422(17)30284-3)
- Josephs, K.A., Murray, M.E., Tosakulwong, N., Weigand, S.D., Serie, A.M., Perkerson, R.B., Matchett, B.J., Jack, C.R., Knopman, D.S., Petersen, R.C., Parisi, J.E., Petrucelli, L., Baker, M., Rademakers, R., Whitwell, J.L., Dickson, D.W., 2019. Pathological, imaging and genetic characteristics support the existence of distinct TDP-43 types in non-FTLD brains. *Acta Neuropathol. (Berl.)* 137, 227–238. <https://doi.org/10.1007/s00401-018-1951-7>
- Josephs, K.A., Murray, M.E., Whitwell, J.L., Parisi, J.E., Petrucelli, L., Jack, C.R., Petersen, R.C., Dickson, D.W., 2014a. Staging TDP-43 pathology in Alzheimer's disease. *Acta Neuropathol. (Berl.)* 127, 441–450. <https://doi.org/10.1007/s00401-013-1211-9>
- Josephs, K.A., Whitwell, J.L., Knopman, D.S., Hu, W.T., Stroh, D.A., Baker, M., Rademakers, R., Boeve, B.F., Parisi, J.E., Smith, G.E., Ivnik, R.J., Petersen, R.C., Jack, C.R., Dickson, D.W., 2008. Abnormal TDP-43 immunoreactivity in AD modifies clinicopathologic and radiologic phenotype. *Neurology* 70, 1850–1857. <https://doi.org/10.1212/01.wnl.0000304041.09418.b1>
- Josephs, K.A., Whitwell, J.L., Tosakulwong, N., Weigand, S.D., Murray, M.E., Liesinger, A.M., Petrucelli, L., Senjem, M.L., Ivnik, R.J., Parisi, J.E., Petersen, R.C., Dickson, D.W., 2015. TAR DNA-binding protein 43 and pathological subtype of Alzheimer's disease impact clinical features. *Ann. Neurol.* 78, 697–709. <https://doi.org/10.1002/ana.24493>
- Josephs, K.A., Whitwell, J.L., Weigand, S.D., Murray, M.E., Tosakulwong, N., Liesinger, A.M., Petrucelli, L., Senjem, M.L., Knopman, D.S., Boeve, B.F., Ivnik, R.J., Smith, G.E., Jack, C.R., Parisi, J.E., Petersen, R.C., Dickson, D.W., 2014b. TDP-43 is a key player in the clinical features associated with Alzheimer's disease. *Acta Neuropathol. (Berl.)* 127, 811–824. <https://doi.org/10.1007/s00401-014-1269-z>
- Jucker, M., Walker, L.C., 2023. Alzheimer's disease: From immunotherapy to immunoprevention. *Cell* 186, 4260–4270. <https://doi.org/10.1016/j.cell.2023.08.021>
- Jucker, M., Walker, L.C., 2013. Self-propagation of pathogenic protein aggregates in neurodegenerative diseases. *Nature* 501, 45–51. <https://doi.org/10.1038/nature12481>
- Jucker, M., Walker, L.C., 2011. Pathogenic protein seeding in Alzheimer disease and other neurodegenerative disorders. *Ann. Neurol.* 70, 532–540. <https://doi.org/10.1002/ana.22615>
- Kadokura, A., Yamazaki, T., Lemere, C.A., Takatama, M., Okamoto, K., 2009. Regional distribution of TDP-43 inclusions in Alzheimer disease (AD) brains: their relation to AD common pathology. *Neuropathol. Off. J. Jpn. Soc. Neuropathol.* 29, 566–573. <https://doi.org/10.1111/j.1440-1789.2009.01017.x>
- Kametani, F., Obi, T., Shishido, T., Akatsu, H., Murayama, S., Saito, Y., Yoshida, M., Hasegawa, M., 2016. Mass spectrometric analysis of accumulated TDP-43 in amyotrophic lateral sclerosis brains. *Sci. Rep.* 6, 23281. <https://doi.org/10.1038/srep23281>
- Kanaan, N.M., Hamel, C., Grabinski, T., Combs, B., 2020. Liquid-liquid phase separation induces pathogenic tau conformations in vitro. *Nat. Commun.* 11, 2809. <https://doi.org/10.1038/s41467-020-16580-3>

- Kanouchi, T., Ohkubo, T., Yokota, T., 2012. Can regional spreading of amyotrophic lateral sclerosis motor symptoms be explained by prion-like propagation? *J. Neurol. Neurosurg. Psychiatry* 83, 739–745. <https://doi.org/10.1136/jnnp-2011-301826>
- Kim, E.-J., Brown, J.A., Deng, J., Hwang, J.-H.L., Spina, S., Miller, Z.A., DeMay, M.G., Valcour, V., Karydas, A., Ramos, E.M., Coppola, G., Miller, B.L., Rosen, H.J., Seeley, W.W., Grinberg, L.T., 2018. Mixed TDP-43 proteinopathy and tauopathy in frontotemporal lobar degeneration: nine case series. *J. Neurol.* 265, 2960–2971. <https://doi.org/10.1007/s00415-018-9086-2>
- Koehler, L.C., Grese, Z.R., Bastos, A.C.S., Mamede, L.D., Heyduk, T., Ayala, Y.M., 2022. TDP-43 Oligomerization and Phase Separation Properties Are Necessary for Autoregulation. *Front. Neurosci.* 16, 818655. <https://doi.org/10.3389/fnins.2022.818655>
- Koga, S., Zhou, X., Murakami, A., Fernandez De Castro, C., Baker, M.C., Rademakers, R., Dickson, D.W., 2022. Concurrent tau pathologies in frontotemporal lobar degeneration with TDP-43 pathology. *Neuropathol. Appl. Neurobiol.* 48, e12778. <https://doi.org/10.1111/nan.12778>
- Kokoulina, P., Rohn, T.T., 2010. Caspase-cleaved transactivation response DNA-binding protein 43 in Parkinson's disease and dementia with Lewy bodies. *Neurodegener. Dis.* 7, 243–250. <https://doi.org/10.1159/000287952>
- Kolarova, M., García-Sierra, F., Bartos, A., Ricny, J., Ripova, D., 2012. Structure and Pathology of Tau Protein in Alzheimer Disease. *Int. J. Alzheimers Dis.* 2012, 731526. <https://doi.org/10.1155/2012/731526>
- Kovacs, G.G., 2018. Chapter 21 - Concepts and classification of neurodegenerative diseases, in: Kovacs, G.G., Alafuzoff, I. (Eds.), *Handbook of Clinical Neurology, Neuropathology*. Elsevier, pp. 301–307. <https://doi.org/10.1016/B978-0-12-802395-2.00021-3>
- Langdon, E.M., Qiu, Y., Ghanbari Niaki, A., McLaughlin, G.A., Weidmann, C.A., Gerbich, T.M., Smith, J.A., Crutchley, J.M., Termini, C.M., Weeks, K.M., Myong, S., Gladfelter, A.S., 2018. mRNA structure determines specificity of a polyQ-driven phase separation. *Science* 360, 922–927. <https://doi.org/10.1126/science.aar7432>
- Lasagna-Reeves, C.A., Castillo-Carranza, D.L., Sengupta, U., Clos, A.L., Jackson, G.R., Kaye, R., 2011. Tau oligomers impair memory and induce synaptic and mitochondrial dysfunction in wild-type mice. *Mol. Neurodegener.* 6, 39. <https://doi.org/10.1186/1750-1326-6-39>
- Lashuel, H.A., Overk, C.R., Oueslati, A., Masliah, E., 2013. The many faces of α -synuclein: from structure and toxicity to therapeutic target. *Nat. Rev. Neurosci.* 14, 38–48. <https://doi.org/10.1038/nrn3406>
- Latimer, C.S., Liachko, N.F., 2021. Tau and TDP-43 synergy: a novel therapeutic target for sporadic late-onset Alzheimer's disease. *GeroScience* 43, 1627–1634. <https://doi.org/10.1007/s11357-021-00407-0>
- Latimer, C.S., Stair, J.G., Hincks, J.C., Currey, H.N., Bird, T.D., Keene, C.D., Kraemer, B.C., Liachko, N.F., 2022. TDP-43 promotes tau accumulation and selective neurotoxicity in bigenic *Caenorhabditis elegans*. *Dis. Model. Mech.* 15, dmm049323. <https://doi.org/10.1242/dmm.049323>

- Lee, E.B., Lee, V.M.-Y., Trojanowski, J.Q., 2011. Gains or losses: molecular mechanisms of TDP43-mediated neurodegeneration. *Nat. Rev. Neurosci.* 13, 38–50. <https://doi.org/10.1038/nrn3121>
- Li, H.-R., Chen, T.-C., Hsiao, C.-L., Shi, L., Chou, C.-Y., Huang, J.-R., 2018a. The physical forces mediating self-association and phase-separation in the C-terminal domain of TDP-43. *Biochim. Biophys. Acta Proteins Proteomics* 1866, 214–223. <https://doi.org/10.1016/j.bbapap.2017.10.001>
- Li, H.-R., Chiang, W.-C., Chou, P.-C., Wang, W.-J., Huang, J.-R., 2018b. TAR DNA-binding protein 43 (TDP-43) liquid-liquid phase separation is mediated by just a few aromatic residues. *J. Biol. Chem.* 293, 6090–6098. <https://doi.org/10.1074/jbc.AC117.001037>
- Li, P., Banjade, S., Cheng, H.-C., Kim, S., Chen, B., Guo, L., Llaguno, M., Hollingsworth, J.V., King, D.S., Banani, S.F., Russo, P.S., Jiang, Q.-X., Nixon, B.T., Rosen, M.K., 2012. Phase transitions in the assembly of multivalent signalling proteins. *Nature* 483, 336–340. <https://doi.org/10.1038/nature10879>
- Li, S., Sheng, Z.-H., 2022. Energy matters: presynaptic metabolism and the maintenance of synaptic transmission. *Nat. Rev. Neurosci.* 23, 4–22. <https://doi.org/10.1038/s41583-021-00535-8>
- Li, W., Li, H.-L., Wang, J.-Z., Liu, R., Wang, X., 2024. Abnormal protein post-translational modifications induces aggregation and abnormal deposition of protein, mediating neurodegenerative diseases. *Cell Biosci.* 14, 22. <https://doi.org/10.1186/s13578-023-01189-y>
- Li, X., Feng, X., Sun, X., Hou, N., Han, F., Liu, Y., 2022. Global, regional, and national burden of Alzheimer's disease and other dementias, 1990-2019. *Front. Aging Neurosci.* 14, 937486. <https://doi.org/10.3389/fnagi.2022.937486>
- Li, Y.R., King, O.D., Shorter, J., Gitler, A.D., 2013. Stress granules as crucibles of ALS pathogenesis. *J. Cell Biol.* 201, 361–372. <https://doi.org/10.1083/jcb.201302044>
- Liachko, N.F., Guthrie, C.R., Kraemer, B.C., 2010. Phosphorylation promotes neurotoxicity in a *Caenorhabditis elegans* model of TDP-43 proteinopathy. *J. Neurosci. Off. J. Soc. Neurosci.* 30, 16208–16219. <https://doi.org/10.1523/JNEUROSCI.2911-10.2010>
- Lim, K.H., 2019. Diverse Misfolded Conformational Strains and Cross-seeding of Misfolded Proteins Implicated in Neurodegenerative Diseases. *Front. Mol. Neurosci.* 12, 158. <https://doi.org/10.3389/fnmol.2019.00158>
- Lin, Y., McCarty, J., Rauch, J.N., Delaney, K.T., Kosik, K.S., Fredrickson, G.H., Shea, J.-E., Han, S., 2019. Narrow equilibrium window for complex coacervation of tau and RNA under cellular conditions. *eLife* 8, e42571. <https://doi.org/10.7554/eLife.42571>
- Ling, J.P., Pletnikova, O., Troncoso, J.C., Wong, P.C., 2015. TDP-43 repression of nonconserved cryptic exons is compromised in ALS-FTD. *Science* 349, 650–655. <https://doi.org/10.1126/science.aab0983>
- Ling, S.-C., Polymenidou, M., Cleveland, D.W., 2013. Converging mechanisms in ALS and FTD: disrupted RNA and protein homeostasis. *Neuron* 79, 416–438. <https://doi.org/10.1016/j.neuron.2013.07.033>
- Linsenmeier, M., Faltova, L., Morelli, C., Capasso Palmiero, U., Seiffert, C., Küffner, A.M., Pinotsi, D., Zhou, J., Mezzenga, R., Arosio, P., 2023. The interface of condensates of the hnRNPA1 low-complexity domain promotes formation of amyloid fibrils. *Nat. Chem.* 15, 1340–1349. <https://doi.org/10.1038/s41557-023-01289-9>

- Liu, Chia-Chen, Liu, Chia-Chan, Kanekiyo, T., Xu, H., Bu, G., 2013. Apolipoprotein E and Alzheimer disease: risk, mechanisms and therapy. *Nat. Rev. Neurol.* 9, 106–118. <https://doi.org/10.1038/nrneurol.2012.263>
- Liu, Y., Feng, W., Wang, Y., Wu, B., 2024. Crosstalk between protein post-translational modifications and phase separation. *Cell Commun. Signal.* 22, 110. <https://doi.org/10.1186/s12964-023-01380-1>
- Long, J.M., Holtzman, D.M., 2019. Alzheimer Disease: An Update on Pathobiology and Treatment Strategies. *Cell* 179, 312–339. <https://doi.org/10.1016/j.cell.2019.09.001>
- Lott, I.T., Head, E., 2019. Dementia in Down syndrome: unique insights for Alzheimer disease research. *Nat. Rev. Neurol.* 15, 135–147. <https://doi.org/10.1038/s41582-018-0132-6>
- Mackenzie, I.R., Rademakers, R., Neumann, M., 2010. TDP-43 and FUS in amyotrophic lateral sclerosis and frontotemporal dementia. *Lancet Neurol.* 9, 995–1007. [https://doi.org/10.1016/S1474-4422\(10\)70195-2](https://doi.org/10.1016/S1474-4422(10)70195-2)
- Mackenzie, I.R.A., Neumann, M., Bigio, E.H., Cairns, N.J., Alafuzoff, I., Kril, J., Kovacs, G.G., Ghetti, B., Halliday, G., Holm, I.E., Ince, P.G., Kamphorst, W., Revesz, T., Rozemuller, A.J.M., Kumar-Singh, S., Akiyama, H., Baborie, A., Spina, S., Dickson, D.W., Trojanowski, J.Q., Mann, D.M.A., 2010. Nomenclature and nosology for neuropathologic subtypes of frontotemporal lobar degeneration: an update. *Acta Neuropathol. (Berl.)* 119, 1–4. <https://doi.org/10.1007/s00401-009-0612-2>
- Madabhushi, R., Pan, L., Tsai, L.-H., 2014. DNA damage and its links to neurodegeneration. *Neuron* 83, 266–282. <https://doi.org/10.1016/j.neuron.2014.06.034>
- Mandelkow, E.-M., Mandelkow, E., 2012. Biochemistry and cell biology of tau protein in neurofibrillary degeneration. *Cold Spring Harb. Perspect. Med.* 2, a006247. <https://doi.org/10.1101/cshperspect.a006247>
- Mann, J.R., Gleixner, A.M., Mauna, J.C., Gomes, E., DeChellis-Marks, M.R., Needham, P.G., Copley, K.E., Hurtle, B., Portz, B., Pyles, N.J., Guo, L., Calder, C.B., Wills, Z.P., Pandey, U.B., Kofler, J.K., Brodsky, J.L., Thathiah, A., Shorter, J., Donnelly, C.J., 2019. RNA Binding Antagonizes Neurotoxic Phase Transitions of TDP-43. *Neuron* 102, 321–338.e8. <https://doi.org/10.1016/j.neuron.2019.01.048>
- Martin, L., Latypova, X., Terro, F., 2011. Post-translational modifications of tau protein: implications for Alzheimer's disease. *Neurochem. Int.* 58, 458–471. <https://doi.org/10.1016/j.neuint.2010.12.023>
- Masuda-Suzukake, M., Nonaka, T., Hosokawa, M., Kubo, M., Shimozawa, A., Akiyama, H., Hasegawa, M., 2014. Pathological alpha-synuclein propagates through neural networks. *Acta Neuropathol. Commun.* 2, 88. <https://doi.org/10.1186/s40478-014-0088-8>
- McAleese, K.E., Walker, L., Erskine, D., Thomas, A.J., McKeith, I.G., Attems, J., 2017. TDP-43 pathology in Alzheimer's disease, dementia with Lewy bodies and ageing. *Brain Pathol. Zurich Switz.* 27, 472–479. <https://doi.org/10.1111/bpa.12424>
- McDowell, I., 2001. Alzheimer's disease: insights from epidemiology. *Aging Milan Italy* 13, 143–162. <https://doi.org/10.1007/BF03351474>
- McKeith, I.G., Dickson, D.W., Lowe, J., Emre, M., O'Brien, J.T., Feldman, H., Cummings, J., Duda, J.E., Lippa, C., Perry, E.K., Aarsland, D., Arai, H., Ballard, C.G., Boeve, B., Burn, D.J., Costa, D., Del Ser, T., Dubois, B., Galasko, D., Gauthier, S., Goetz, C.G., Gomez-Tortosa, E., Halliday, G., Hansen, L.A., Hardy, J., Iwatsubo, T., Kalaria, R.N., Kaufer, D., Kenny, R.A., Korczyn, A., Kosaka, K., Lee, V.M.Y., Lees, A., Litvan, I.,

- Londos, E., Lopez, O.L., Minoshima, S., Mizuno, Y., Molina, J.A., Mukaetova-Ladinska, E.B., Pasquier, F., Perry, R.H., Schulz, J.B., Trojanowski, J.Q., Yamada, M., Consortium on DLB, 2005. Diagnosis and management of dementia with Lewy bodies: third report of the DLB Consortium. *Neurology* 65, 1863–1872. <https://doi.org/10.1212/01.wnl.0000187889.17253.b1>
- Medeiros, R., Baglietto-Vargas, D., LaFerla, F.M., 2010. The Role of Tau in Alzheimer's Disease and Related Disorders. *CNS Neurosci. Ther.* 17, 514–524. <https://doi.org/10.1111/j.1755-5949.2010.00177.x>
- Menéndez-González, M., 2023. Toward a new nosology of neurodegenerative diseases. *Alzheimers Dement.* 19, 3731–3737. <https://doi.org/10.1002/alz.13041>
- Meneses, A., Koga, S., O'Leary, J., Dickson, D.W., Bu, G., Zhao, N., 2021. TDP-43 Pathology in Alzheimer's Disease. *Mol. Neurodegener.* 16, 84. <https://doi.org/10.1186/s13024-021-00503-x>
- Millecamps, S., Julien, J.-P., 2013. Axonal transport deficits and neurodegenerative diseases. *Nat. Rev. Neurosci.* 14, 161–176. <https://doi.org/10.1038/nrn3380>
- Min, S.-W., Cho, S.-H., Zhou, Y., Schroeder, S., Haroutunian, V., Seeley, W.W., Huang, E.J., Shen, Y., Masliah, E., Mukherjee, C., Meyers, D., Cole, P.A., Ott, M., Gan, L., 2010. Acetylation of tau inhibits its degradation and contributes to tauopathy. *Neuron* 67, 953–966. <https://doi.org/10.1016/j.neuron.2010.08.044>
- Mitra, J., Guerrero, E.N., Hegde, P.M., Liachko, N.F., Wang, H., Vasquez, V., Gao, J., Pandey, A., Taylor, J.P., Kraemer, B.C., Wu, P., Boldogh, I., Garruto, R.M., Mitra, S., Rao, K.S., Hegde, M.L., 2019. Motor neuron disease-associated loss of nuclear TDP-43 is linked to DNA double-strand break repair defects. *Proc. Natl. Acad. Sci. U. S. A.* 116, 4696–4705. <https://doi.org/10.1073/pnas.1818415116>
- Mitreá, D.M., Mittasch, M., Gomes, B.F., Klein, I.A., Murcko, M.A., 2022. Modulating biomolecular condensates: a novel approach to drug discovery. *Nat. Rev. Drug Discov.* 21, 841–862. <https://doi.org/10.1038/s41573-022-00505-4>
- Mizuno, Y., Amari, M., Takatama, M., Aizawa, H., Mihara, B., Okamoto, K., 2006. Immunoreactivities of p62, an ubiquitin-binding protein, in the spinal anterior horn cells of patients with amyotrophic lateral sclerosis. *J. Neurol. Sci.* 249, 13–18. <https://doi.org/10.1016/j.jns.2006.05.060>
- Mohanty, P., Shenoy, J., Rizuan, A., Mercado-Ortiz, J.F., Fawzi, N.L., Mittal, J., 2023. A synergy between site-specific and transient interactions drives the phase separation of a disordered, low-complexity domain. *Proc. Natl. Acad. Sci.* 120, e2305625120. <https://doi.org/10.1073/pnas.2305625120>
- Molliex, A., Temirov, J., Lee, J., Coughlin, M., Kanagaraj, A.P., Kim, H.J., Mittag, T., Taylor, J.P., 2015. Phase separation by low complexity domains promotes stress granule assembly and drives pathological fibrillization. *Cell* 163, 123–133. <https://doi.org/10.1016/j.cell.2015.09.015>
- Mondragón-Rodríguez, S., Basurto-Islas, G., Santa-Maria, I., Mena, R., Binder, L.I., Avila, J., Smith, M.A., Perry, G., García-Sierra, F., 2008. Cleavage and conformational changes of tau protein follow phosphorylation during Alzheimer's disease. *Int. J. Exp. Pathol.* 89, 81–90. <https://doi.org/10.1111/j.1365-2613.2007.00568.x>
- Montalbano, M., McAllen, S., Cascio, F.L., Sengupta, U., Garcia, S., Bhatt, N., Ellsworth, A., Heidelman, E.A., Johnson, O.D., Doskocil, S., Kaye, R., 2020. TDP-43 and Tau

- Oligomers in Alzheimer's Disease, Amyotrophic Lateral Sclerosis, and Frontotemporal Dementia. *Neurobiol. Dis.* 146, 105130. <https://doi.org/10.1016/j.nbd.2020.105130>
- Montenigro, P.H., Corp, D.T., Stein, T.D., Cantu, R.C., Stern, R.A., 2015. Chronic traumatic encephalopathy: historical origins and current perspective. *Annu. Rev. Clin. Psychol.* 11, 309–330. <https://doi.org/10.1146/annurev-clinpsy-032814-112814>
- Mortada, I., Farah, R., Nabha, S., Ojcius, D.M., Fares, Y., Almawi, W.Y., Sadier, N.S., 2021. Immunotherapies for Neurodegenerative Diseases. *Front. Neurol.* 12, 654739. <https://doi.org/10.3389/fneur.2021.654739>
- Mukrasch, M.D., Bibow, S., Korukottu, J., Jeganathan, S., Biernat, J., Griesinger, C., Mandelkow, E., Zweckstetter, M., 2009. Structural Polymorphism of 441-Residue Tau at Single Residue Resolution. *PLOS Biol.* 7, e1000034. <https://doi.org/10.1371/journal.pbio.1000034>
- Musiek, E.S., Holtzman, D.M., 2015. Three dimensions of the amyloid hypothesis: time, space and “wingmen.” *Nat. Neurosci.* 18, 800–806. <https://doi.org/10.1038/nn.4018>
- Nachman, E., Wentink, A.S., Madiona, K., Bousset, L., Katsinelos, T., Allinson, K., Kampinga, H., McEwan, W.A., Jahn, T.R., Melki, R., Mogk, A., Bukau, B., Nussbaum-Krammer, C., 2020. Disassembly of Tau fibrils by the human Hsp70 disaggregation machinery generates small seeding-competent species. *J. Biol. Chem.* 295, 9676–9690. <https://doi.org/10.1074/jbc.RA120.013478>
- Nafe, R., Arendt, C.T., Hattingen, E., 2023. Human prion diseases and the prion protein – what is the current state of knowledge? *Transl. Neurosci.* 14, 20220315. <https://doi.org/10.1515/tnsci-2022-0315>
- Nakashima-Yasuda, H., Uryu, K., Robinson, J., Xie, S.X., Hurtig, H., Duda, J.E., Arnold, S.E., Siderowf, A., Grossman, M., Leverenz, J.B., Woltjer, R., Lopez, O.L., Hamilton, R., Tsuang, D.W., Galasko, D., Masliah, E., Kaye, J., Clark, C.M., Montine, T.J., Lee, V.M.-Y., Trojanowski, J.Q., 2007. Co-morbidity of TDP-43 proteinopathy in Lewy body related diseases. *Acta Neuropathol. (Berl.)* 114, 221–229. <https://doi.org/10.1007/s00401-007-0261-2>
- Nedelsky, N.B., Taylor, J.P., 2019. Bridging biophysics and neurology: aberrant phase transitions in neurodegenerative disease. *Nat. Rev. Neurol.* 15, 272–286. <https://doi.org/10.1038/s41582-019-0157-5>
- Nelson, P.T., Abner, E.L., Patel, E., Anderson, S., Wilcock, D.M., Kryscio, R.J., Van Eldik, L.J., Jicha, G.A., Gal, Z., Nelson, R.S., Nelson, B.G., Gal, J., Azam, M.T., Fardo, D.W., Cykowski, M.D., 2018. The Amygdala as a Locus of Pathologic Misfolding in Neurodegenerative Diseases. *J. Neuropathol. Exp. Neurol.* 77, 2–20. <https://doi.org/10.1093/jnen/nlx099>
- Neumann, M., Sampathu, D.M., Kwong, L.K., Truax, A.C., Micsenyi, M.C., Chou, T.T., Bruce, J., Schuck, T., Grossman, M., Clark, C.M., McCluskey, L.F., Miller, B.L., Masliah, E., Mackenzie, I.R., Feldman, H., Feiden, W., Kretschmar, H.A., Trojanowski, J.Q., Lee, V.M.-Y., 2006. Ubiquitinated TDP-43 in frontotemporal lobar degeneration and amyotrophic lateral sclerosis. *Science* 314, 130–133. <https://doi.org/10.1126/science.1134108>
- Ng, A.S.L., Rademakers, R., Miller, B.L., 2015. Frontotemporal dementia: a bridge between dementia and neuromuscular disease. *Ann. N. Y. Acad. Sci.* 1338, 71–93. <https://doi.org/10.1111/nyas.12638>

- Nishimura, A.L., Župunski, V., Troakes, C., Kathe, C., Fratta, P., Howell, M., Gallo, J., Hortobágyi, T., Shaw, C.E., Rogelj, B., 2010. Nuclear import impairment causes cytoplasmic trans-activation response DNA-binding protein accumulation and is associated with frontotemporal lobar degeneration. *Brain* 133, 1763–1771. <https://doi.org/10.1093/brain/awq111>
- Nonaka, T., Masuda-Suzukake, M., Arai, T., Hasegawa, Y., Akatsu, H., Obi, T., Yoshida, M., Murayama, S., Mann, D.M.A., Akiyama, H., Hasegawa, M., 2013. Prion-like Properties of Pathological TDP-43 Aggregates from Diseased Brains. *Cell Rep.* 4, 124–134. <https://doi.org/10.1016/j.celrep.2013.06.007>
- Nonaka, T., Masuda-Suzukake, M., Hasegawa, M., 2018. Molecular mechanisms of the co-deposition of multiple pathological proteins in neurodegenerative diseases. *Neuropathol. Off. J. Jpn. Soc. Neuropathol.* 38, 64–71. <https://doi.org/10.1111/neup.12427>
- Nonaka, T., Suzuki, G., Tanaka, Y., Kametani, F., Hirai, S., Okado, H., Miyashita, T., Saitoe, M., Akiyama, H., Masai, H., Hasegawa, M., 2016. Phosphorylation of TAR DNA-binding Protein of 43 kDa (TDP-43) by Truncated Casein Kinase 1 δ Triggers Mislocalization and Accumulation of TDP-43. *J. Biol. Chem.* 291, 5473–5483. <https://doi.org/10.1074/jbc.M115.695379>
- Novak, P., Kovacech, B., Katina, S., Schmidt, R., Scheltens, P., Kontsekova, E., Ropele, S., Fialova, L., Kramberger, M., Paulenka-Ivanovova, N., Smisek, M., Hanes, J., Stevens, E., Kovac, A., Sutovsky, S., Parrak, V., Koson, P., Prcina, M., Galba, J., Cente, M., Hromadka, T., Filipcik, P., Piestansky, J., Samcova, M., Prenn-Gologranc, C., Sivak, R., Froelich, L., Fresser, M., Rakusa, M., Harrison, J., Hort, J., Otto, M., Tosun, D., Ondrus, M., Winblad, B., Novak, M., Zilka, N., 2021. ADAMANT: a placebo-controlled randomized phase 2 study of AADvac1, an active immunotherapy against pathological tau in Alzheimer’s disease. *Nat. Aging* 1, 521–534. <https://doi.org/10.1038/s43587-021-00070-2>
- Nussbacher, J.K., Tabet, R., Yeo, G.W., Lagier-Tourenne, C., 2019. Disruption of RNA Metabolism in Neurological Diseases and Emerging Therapeutic Interventions. *Neuron* 102, 294–320. <https://doi.org/10.1016/j.neuron.2019.03.014>
- Oakley, S.S., Maina, M.B., Marshall, K.E., Al-Hilaly, Y.K., Harrington, C.R., Wischik, C.M., Serpell, L.C., 2020. Tau Filament Self-Assembly and Structure: Tau as a Therapeutic Target. *Front. Neurol.* 11, 590754. <https://doi.org/10.3389/fneur.2020.590754>
- Oiwa, K., Watanabe, S., Onodera, K., Iguchi, Y., Kinoshita, Y., Komine, O., Sobue, A., Okada, Y., Katsuno, M., Yamanaka, K., 2023. Monomerization of TDP-43 is a key determinant for inducing TDP-43 pathology in amyotrophic lateral sclerosis. *Sci. Adv.* 9, eadf6895. <https://doi.org/10.1126/sciadv.adf6895>
- Palop, J.J., Mucke, L., 2010. Amyloid-beta-induced neuronal dysfunction in Alzheimer’s disease: from synapses toward neural networks. *Nat. Neurosci.* 13, 812–818. <https://doi.org/10.1038/nn.2583>
- Patel, A., Lee, H.O., Jawerth, L., Maharana, S., Janel, M., Hein, M.Y., Stoyanov, S., Mahamid, J., Saha, S., Franzmann, T.M., Pozniakovski, A., Poser, I., Maghelli, N., Royer, L.A., Weigert, M., Myers, E.W., Grill, S., Drechsel, D., Hyman, A.A., Alberti, S., 2015. A Liquid-to-Solid Phase Transition of the ALS Protein FUS Accelerated by Disease Mutation. *Cell* 162, 1066–1077. <https://doi.org/10.1016/j.cell.2015.07.047>

- Peng, C., Trojanowski, J.Q., Lee, V.M.-Y., 2020. Protein transmission in neurodegenerative disease. *Nat. Rev. Neurol.* 16, 199–212. <https://doi.org/10.1038/s41582-020-0333-7>
- Pesiridis, G.S., Tripathy, K., Tanik, S., Trojanowski, J.Q., Lee, V.M.-Y., 2011. A “Two-hit” Hypothesis for Inclusion Formation by Carboxyl-terminal Fragments of TDP-43 Protein Linked to RNA Depletion and Impaired Microtubule-dependent Transport. *J. Biol. Chem.* 286, 18845–18855. <https://doi.org/10.1074/jbc.M111.231118>
- Phatnani, H., Maniatis, T., 2015. Astrocytes in neurodegenerative disease. *Cold Spring Harb. Perspect. Biol.* 7, a020628. <https://doi.org/10.1101/cshperspect.a020628>
- Pohl, C., Dikic, I., 2019. Cellular quality control by the ubiquitin-proteasome system and autophagy. *Science* 366, 818–822. <https://doi.org/10.1126/science.aax3769>
- Polymenidou, M., Cleveland, D.W., 2012. Prion-like spread of protein aggregates in neurodegeneration. *J. Exp. Med.* 209, 889–893. <https://doi.org/10.1084/jem.20120741>
- Polymenidou, M., Cleveland, D.W., 2011. The seeds of neurodegeneration: prion-like spreading in ALS. *Cell* 147, 498–508. <https://doi.org/10.1016/j.cell.2011.10.011>
- Pozzi, S., Codron, P., Soucy, G., Renaud, L., Cordeau, P.J., Dutta, K., Bareil, C., Julien, J.-P., 2020. Monoclonal full-length antibody against TAR DNA binding protein 43 reduces related proteinopathy in neurons. *JCI Insight* 5, e140420, 140420. <https://doi.org/10.1172/jci.insight.140420>
- Pozzi, S., Thammisetty, S.S., Codron, P., Rahimian, R., Plourde, K.V., Soucy, G., Bareil, C., Phaneuf, D., Kriz, J., Gravel, C., Julien, J.-P., 2019. Virus-mediated delivery of antibody targeting TAR DNA-binding protein-43 mitigates associated neuropathology. *J. Clin. Invest.* 129, 1581–1595. <https://doi.org/10.1172/JCI123931>
- Prasad, S., Katta, M.R., Abhishek, S., Sridhar, R., Valisekka, S.S., Hameed, M., Kaur, J., Walia, N., 2023. Recent advances in Lewy body dementia: A comprehensive review. *Dis. Mon., Recent Advances in Lewy Body Dementia: A Comprehensive Review* 69, 101441. <https://doi.org/10.1016/j.disamonth.2022.101441>
- Protter, D.S.W., Parker, R., 2016. Principles and Properties of Stress Granules. *Trends Cell Biol.* 26, 668–679. <https://doi.org/10.1016/j.tcb.2016.05.004>
- Prusiner, S.B., 1998. Prions. *Proc. Natl. Acad. Sci. U. S. A.* 95, 13363–13383. <https://doi.org/10.1073/pnas.95.23.13363>
- Rai, S.K., Khanna, R., Avni, A., Mukhopadhyay, S., 2023. Heterotypic electrostatic interactions control complex phase separation of tau and prion into multiphasic condensates and co-aggregates. *Proc. Natl. Acad. Sci. U. S. A.* 120, e2216338120. <https://doi.org/10.1073/pnas.2216338120>
- Ratti, A., Buratti, E., 2016. Physiological functions and pathobiology of TDP-43 and FUS/TLS proteins. *J. Neurochem.* 138 Suppl 1, 95–111. <https://doi.org/10.1111/jnc.13625>
- Rauch, J.N., Chen, J.J., Sorum, A.W., Miller, G.M., Sharf, T., See, S.K., Hsieh-Wilson, L.C., Kampmann, M., Kosik, K.S., 2018. Tau Internalization is Regulated by 6-O Sulfation on Heparan Sulfate Proteoglycans (HSPGs). *Sci. Rep.* 8, 6382. <https://doi.org/10.1038/s41598-018-24904-z>
- Rauch, J.N., Luna, G., Guzman, E., Audouard, M., Challis, C., Sibih, Y.E., Leshuk, C., Hernandez, I., Wegmann, S., Hyman, B.T., Gradinaru, V., Kampmann, M., Kosik, K.S., 2020. LRP1 is a master regulator of tau uptake and spread. *Nature* 580, 381–385. <https://doi.org/10.1038/s41586-020-2156-5>

- Riback, J.A., Katanski, C.D., Kear-Scott, J.L., Pilipenko, E.V., Rojek, A.E., Sosnick, T.R., Drummond, D.A., 2017. Stress-Triggered Phase Separation Is an Adaptive, Evolutionarily Tuned Response. *Cell* 168, 1028-1040.e19. <https://doi.org/10.1016/j.cell.2017.02.027>
- Riemenschneider, H., Simonetti, F., Sheth, U., Katona, E., Roth, S., Hutten, S., Farny, D., Michaelsen, M., Nuscher, B., Schmidt, M.K., Flatley, A., Schepers, A., Gruijs Da Silva, L.A., Zhou, Q., Klopstock, T., Liesz, A., Arzberger, T., Herms, J., Feederle, R., Gendron, T.F., Dormann, D., Edbauer, D., 2023. Targeting the glycine-rich domain of TDP-43 with antibodies prevents its aggregation in vitro and reduces neurofilament levels in vivo. *Acta Neuropathol. Commun.* 11, 112. <https://doi.org/10.1186/s40478-023-01592-z>
- Robinson, J.L., Lee, E.B., Xie, S.X., Rennert, L., Suh, E., Bredenberg, C., Caswell, C., Van Deerlin, V.M., Yan, N., Yousef, A., Hurtig, H.I., Siderowf, A., Grossman, M., McMillan, C.T., Miller, B., Duda, J.E., Irwin, D.J., Wolk, D., Elman, L., McCluskey, L., Chen-Plotkin, A., Weintraub, D., Arnold, S.E., Brettschneider, J., Lee, V.M.-Y., Trojanowski, J.Q., 2018. Neurodegenerative disease concomitant proteinopathies are prevalent, age-related and APOE4-associated. *Brain J. Neurol.* 141, 2181–2193. <https://doi.org/10.1093/brain/awy146>
- Rohrer, J.D., Guerreiro, R., Vandrovcova, J., Uphill, J., Reiman, D., Beck, J., Isaacs, A.M., Authier, A., Ferrari, R., Fox, N.C., Mackenzie, I.R.A., Warren, J.D., de Silva, R., Holton, J., Revesz, T., Hardy, J., Mead, S., Rossor, M.N., 2009. The heritability and genetics of frontotemporal lobar degeneration. *Neurology* 73, 1451–1456. <https://doi.org/10.1212/WNL.0b013e3181bf997a>
- Saberi, S., Stauffer, J.E., Schulte, D.J., Ravits, J., 2015. “Neuropathology of amyotrophic lateral sclerosis and its variants.” *Neurol. Clin.* 33, 855–876. <https://doi.org/10.1016/j.ncl.2015.07.012>
- Saito, M., Hess, D., Eglinger, J., Fritsch, A.W., Kreysing, M., Weinert, B.T., Choudhary, C., Matthias, P., 2019. Acetylation of intrinsically disordered regions regulates phase separation. *Nat. Chem. Biol.* 15, 51–61. <https://doi.org/10.1038/s41589-018-0180-7>
- Saman, Sudad, Kim, W., Raya, M., Visnick, Y., Miro, S., Saman, Sarmad, Jackson, B., McKee, A.C., Alvarez, V.E., Lee, N.C.Y., Hall, G.F., 2012. Exosome-associated tau is secreted in tauopathy models and is selectively phosphorylated in cerebrospinal fluid in early Alzheimer disease. *J. Biol. Chem.* 287, 3842–3849. <https://doi.org/10.1074/jbc.M111.277061>
- Schenk, D., Barbour, R., Dunn, W., Gordon, G., Grajeda, H., Guido, T., Hu, K., Huang, J., Johnson-Wood, K., Khan, K., Kholodenko, D., Lee, M., Liao, Z., Lieberburg, I., Motter, R., Mutter, L., Soriano, F., Shopp, G., Vasquez, N., Vandevent, C., Walker, S., Wogulis, M., Yednock, T., Games, D., Seubert, P., 1999. Immunization with amyloid-beta attenuates Alzheimer-disease-like pathology in the PDAPP mouse. *Nature* 400, 173–177. <https://doi.org/10.1038/22124>
- Scheres, S.H.W., Ryskeldi-Falcon, B., Goedert, M., 2023. Molecular pathology of neurodegenerative diseases by cryo-EM of amyloids. *Nature* 621, 701–710. <https://doi.org/10.1038/s41586-023-06437-2>
- Selkoe, D.J., 2024. The advent of Alzheimer treatments will change the trajectory of human aging. *Nat. Aging* 4, 453–463. <https://doi.org/10.1038/s43587-024-00611-5>

- Shen, Yi, Chen, A., Wang, W., Shen, Yinan, Ruggeri, F.S., Aime, S., Wang, Z., Qamar, S., Espinosa, J.R., Garaizar, A., St George-Hyslop, P., Colleparado-Guevara, R., Weitz, D.A., Vigolo, D., Knowles, T.P.J., 2023. The liquid-to-solid transition of FUS is promoted by the condensate surface. *Proc. Natl. Acad. Sci.* 120, e2301366120. <https://doi.org/10.1073/pnas.2301366120>
- Shih, Y.-H., Tu, L.-H., Chang, T.-Y., Ganesan, K., Chang, W.-W., Chang, P.-S., Fang, Y.-S., Lin, Y.-T., Jin, L.-W., Chen, Y.-R., 2020. TDP-43 interacts with amyloid- β , inhibits fibrillization, and worsens pathology in a model of Alzheimer's disease. *Nat. Commun.* 11, 5950. <https://doi.org/10.1038/s41467-020-19786-7>
- Shin, Y., Brangwynne, C.P., 2017. Liquid phase condensation in cell physiology and disease. *Science* 357, eaaf4382. <https://doi.org/10.1126/science.aaf4382>
- Smith, V.D., Bachstetter, A.D., Ighodaro, E., Roberts, K., Abner, E.L., Fardo, D.W., Nelson, P.T., 2018. Overlapping but distinct TDP-43 and tau pathologic patterns in aged hippocampi. *Brain Pathol. Zurich Switz.* 28, 264–273. <https://doi.org/10.1111/bpa.12505>
- Snead, W.T., Gladfelter, A.S., 2019. The Control Centers of Biomolecular Phase Separation: How Membrane Surfaces, PTMs, and Active Processes Regulate Condensation. *Mol. Cell* 76, 295–305. <https://doi.org/10.1016/j.molcel.2019.09.016>
- Sperling, R.A., Aisen, P.S., Beckett, L.A., Bennett, D.A., Craft, S., Fagan, A.M., Iwatsubo, T., Jack, C.R., Kaye, J., Montine, T.J., Park, D.C., Reiman, E.M., Rowe, C.C., Siemers, E., Stern, Y., Yaffe, K., Carrillo, M.C., Thies, B., Morrison-Bogorad, M., Wagster, M.V., Phelps, C.H., 2011. Toward defining the preclinical stages of Alzheimer's disease: recommendations from the National Institute on Aging-Alzheimer's Association workgroups on diagnostic guidelines for Alzheimer's disease. *Alzheimers Dement. J. Alzheimers Assoc.* 7, 280–292. <https://doi.org/10.1016/j.jalz.2011.03.003>
- Spires-Jones, T.L., Attems, J., Thal, D.R., 2017. Interactions of pathological proteins in neurodegenerative diseases. *Acta Neuropathol. (Berl.)* 134, 187–205. <https://doi.org/10.1007/s00401-017-1709-7>
- Spires-Jones, T.L., Kopeikina, K.J., Koffie, R.M., de Calignon, A., Hyman, B.T., 2011. Are tangles as toxic as they look? *J. Mol. Neurosci.* MN 45, 438–444. <https://doi.org/10.1007/s12031-011-9566-7>
- Sternburg, E.L., Gruijs da Silva, L.A., Dormann, D., 2022. Post-translational modifications on RNA-binding proteins: accelerators, brakes, or passengers in neurodegeneration? *Trends Biochem. Sci.* 47, 6–22. <https://doi.org/10.1016/j.tibs.2021.07.004>
- Stevens, C.H., Guthrie, N.J., van Roijen, M., Halliday, G.M., Ooi, L., 2019. Increased Tau Phosphorylation in Motor Neurons From Clinically Pure Sporadic Amyotrophic Lateral Sclerosis Patients. *J. Neuropathol. Exp. Neurol.* 78, 605–614. <https://doi.org/10.1093/jnen/nlz041>
- Strong, M.J., Yang, W., Strong, W.L., Leystra-Lantz, C., Jaffe, H., Pant, H.C., 2006. Tau protein hyperphosphorylation in sporadic ALS with cognitive impairment. *Neurology* 66, 1770–1771. <https://doi.org/10.1212/01.wnl.0000218161.15834.db>
- Subedi, S., Sasidharan, S., Nag, N., Saudagar, P., Tripathi, T., 2022. Amyloid Cross-Seeding: Mechanism, Implication, and Inhibition. *Molecules* 27, 1776. <https://doi.org/10.3390/molecules27061776>

- Takeda, S., Wegmann, S., Cho, H., DeVos, S.L., Commins, C., Roe, A.D., Nicholls, S.B., Carlson, G.A., Pitstick, R., Nobuhara, C.K., Costantino, I., Frosch, M.P., Müller, D.J., Irimia, D., Hyman, B.T., 2015. Neuronal uptake and propagation of a rare phosphorylated high-molecular-weight tau derived from Alzheimer's disease brain. *Nat. Commun.* 6, 8490. <https://doi.org/10.1038/ncomms9490>
- Takeda, T., 2018. Possible concurrence of TDP-43, tau and other proteins in amyotrophic lateral sclerosis/frontotemporal lobar degeneration. *Neuropathol. Off. J. Jpn. Soc. Neuropathol.* 38, 72–81. <https://doi.org/10.1111/neup.12428>
- Tamvaka, N., Manne, S., Kondru, N., Ross, O.A., 2023. Pick's Disease, Seeding an Answer to the Clinical Diagnosis Conundrum. *Biomedicines* 11, 1646. <https://doi.org/10.3390/biomedicines11061646>
- Taylor, J.P., Brown, R.H., Cleveland, D.W., 2016. Decoding ALS: from genes to mechanism. *Nature* 539, 197–206. <https://doi.org/10.1038/nature20413>
- Taylor, J.P., Hardy, J., Fischbeck, K.H., 2002. Toxic proteins in neurodegenerative disease. *Science* 296, 1991–1995. <https://doi.org/10.1126/science.1067122>
- Taylor, L.M., McMillan, P.J., Liachko, N.F., Strovast, T.J., Ghetti, B., Bird, T.D., Keene, C.D., Kraemer, B.C., 2018. Pathological phosphorylation of tau and TDP-43 by TTBK1 and TTBK2 drives neurodegeneration. *Mol. Neurodegener.* 13, 7. <https://doi.org/10.1186/s13024-018-0237-9>
- Thal, D.R., Rüb, U., Orantes, M., Braak, H., 2002. Phases of A beta-deposition in the human brain and its relevance for the development of AD. *Neurology* 58, 1791–1800. <https://doi.org/10.1212/wnl.58.12.1791>
- Thomas, D.X., Bajaj, S., McRae-McKee, K., Hadjichrysanthou, C., Anderson, R.M., Collinge, J., 2020. Association of TDP-43 proteinopathy, cerebral amyloid angiopathy, and Lewy bodies with cognitive impairment in individuals with or without Alzheimer's disease neuropathology. *Sci. Rep.* 10, 14579. <https://doi.org/10.1038/s41598-020-71305-2>
- Tittelmeier, J., Sandhof, C.A., Ries, H.M., Druffel-Augustin, S., Mogk, A., Bukau, B., Nussbaum-Krammer, C., 2020. The HSP110/HSP70 disaggregation system generates spreading-competent toxic α -synuclein species. *EMBO J.* 39, e103954. <https://doi.org/10.15252/embj.2019103954>
- Tomé, S.O., Gomes, L.A., Li, X., Vandenberghe, R., Tousseyn, T., Thal, D.R., 2021. TDP-43 interacts with pathological τ protein in Alzheimer's disease. *Acta Neuropathol. (Berl.)*. <https://doi.org/10.1007/s00401-021-02295-2>
- Tomé, S.O., Tsaka, G., Ronisz, A., Ospitalieri, S., Gawor, K., Gomes, L.A., Otto, M., Von Arnim, C.A.F., Van Damme, P., Van Den Bosch, L., Ghebremedhin, E., Laureysen, C., Sleegers, K., Vandenberghe, R., Rousseau, F., Schymkowitz, J., Thal, D.R., 2023. TDP-43 pathology is associated with increased tau burdens and seeding. *Mol. Neurodegener.* 18, 71. <https://doi.org/10.1186/s13024-023-00653-0>
- Tomé, S.O., Vandenberghe, R., Ospitalieri, S., Van Schoor, E., Tousseyn, T., Otto, M., von Arnim, C.A.F., Thal, D.R., 2020. Distinct molecular patterns of TDP-43 pathology in Alzheimer's disease: relationship with clinical phenotypes. *Acta Neuropathol. Commun.* 8, 61. <https://doi.org/10.1186/s40478-020-00934-5>
- Tremblay, C., St-Amour, I., Schneider, J., Bennett, D.A., Calon, F., 2011. Accumulation of TAR DNA Binding Protein-43 (TDP-43) in Mild Cognitive Impairment and Alzheimer

- Disease. *J. Neuropathol. Exp. Neurol.* 70, 788–798. <https://doi.org/10.1097/NEN.0b013e31822c62cf>
- Tziortzouda, P., Van Den Bosch, L., Hirth, F., 2021. Triad of TDP43 control in neurodegeneration: autoregulation, localization and aggregation. *Nat. Rev. Neurosci.* 22, 197–208. <https://doi.org/10.1038/s41583-021-00431-1>
- Uryu, K., Nakashima-Yasuda, H., Forman, M.S., Kwong, L.K., Clark, C.M., Grossman, M., Miller, B.L., Kretschmar, H.A., Lee, V.M.-Y., Trojanowski, J.Q., Neumann, M., 2008. Concomitant TAR-DNA-binding protein 43 pathology is present in Alzheimer disease and corticobasal degeneration but not in other tauopathies. *J. Neuropathol. Exp. Neurol.* 67, 555–564. <https://doi.org/10.1097/NEN.0b013e31817713b5>
- Usenovic, M., Niroomand, S., Drolet, R.E., Yao, L., Gaspar, R.C., Hatcher, N.G., Schachter, J., Renger, J.J., Parmentier-Batteur, S., 2015. Internalized Tau Oligomers Cause Neurodegeneration by Inducing Accumulation of Pathogenic Tau in Human Neurons Derived from Induced Pluripotent Stem Cells. *J. Neurosci.* 35, 14234–14250. <https://doi.org/10.1523/JNEUROSCI.1523-15.2015>
- van Dyck, C.H., Swanson, C.J., Aisen, P., Bateman, R.J., Chen, C., Gee, M., Kanekiyo, M., Li, D., Reyderman, L., Cohen, S., Froelich, L., Katayama, S., Sabbagh, M., Vellas, B., Watson, D., Dhadda, S., Irizarry, M., Kramer, L.D., Iwatsubo, T., 2023. Lecanemab in Early Alzheimer's Disease. *N. Engl. J. Med.* 388, 9–21. <https://doi.org/10.1056/NEJMoa2212948>
- Van Langenhove, T., van der Zee, J., Van Broeckhoven, C., 2012. The molecular basis of the frontotemporal lobar degeneration-amyotrophic lateral sclerosis spectrum. *Ann. Med.* 44, 817–828. <https://doi.org/10.3109/07853890.2012.665471>
- Van Schependom, J., D'haeseleer, M., 2023. Advances in Neurodegenerative Diseases. *J. Clin. Med.* 12, 1709. <https://doi.org/10.3390/jcm12051709>
- Vanderweyde, T., Apicco, D.J., Youmans-Kidder, K., Ash, P.E.A., Cook, C., Lummertz da Rocha, E., Jansen-West, K., Frame, A.A., Citro, A., Leszyk, J.D., Ivanov, P., Abisambra, J.F., Steffen, M., Li, H., Petrucelli, L., Wolozin, B., 2016. Interaction of tau with the RNA-Binding Protein TIA1 Regulates tau Pathophysiology and Toxicity. *Cell Rep.* 15, 1455–1466. <https://doi.org/10.1016/j.celrep.2016.04.045>
- Vanderweyde, T., Yu, H., Varnum, M., Liu-Yesucevitz, L., Citro, A., Ikezu, T., Duff, K., Wolozin, B., 2012. Contrasting pathology of the stress granule proteins TIA-1 and G3BP in tauopathies. *J. Neurosci. Off. J. Soc. Neurosci.* 32, 8270–8283. <https://doi.org/10.1523/JNEUROSCI.1592-12.2012>
- Varadi, M., Bertoni, D., Magana, P., Paramval, U., Pidruchna, I., Radhakrishnan, M., Tsenkov, M., Nair, S., Mirdita, M., Yeo, J., Kovalevskiy, O., Tunyasuvunakool, K., Laydon, A., Židek, A., Tomlinson, H., Hariharan, D., Abrahamson, J., Green, T., Jumper, J., Birney, E., Steinegger, M., Hassabis, D., Velankar, S., 2024. AlphaFold Protein Structure Database in 2024: providing structure coverage for over 214 million protein sequences. *Nucleic Acids Res.* 52, D368–D375. <https://doi.org/10.1093/nar/gkad1011>
- Vermunt, L., Sikkes, S.A.M., van den Hout, A., Handels, R., Bos, I., van der Flier, W.M., Kern, S., Ousset, P.-J., Maruff, P., Skoog, I., Verhey, F.R.J., Freund-Levi, Y., Tsolaki, M., Wallin, Å.K., Olde Rikkert, M., Soininen, H., Spuru, L., Zetterberg, H., Blennow, K., Scheltens, P., Muniz-Terrera, G., Visser, P.J., Alzheimer Disease Neuroimaging Initiative, AIBL Research Group, ICTUS/DSA study groups, 2019. Duration of

- preclinical, prodromal, and dementia stages of Alzheimer's disease in relation to age, sex, and APOE genotype. *Alzheimers Dement. J. Alzheimers Assoc.* 15, 888–898. <https://doi.org/10.1016/j.jalz.2019.04.001>
- Vintilescu, C.R., Afreen, S., Rubino, A.E., Ferreira, A., 2016. The Neurotoxic Tau45-230 Fragment Accumulates in Upper and Lower Motor Neurons in Amyotrophic Lateral Sclerosis Subjects. *Mol. Med.* 22, 477–486. <https://doi.org/10.2119/molmed.2016.00095>
- Wang, A., Conicella, A.E., Schmidt, H.B., Martin, E.W., Rhoads, S.N., Reeb, A.N., Nourse, A., Ramirez Montero, D., Ryan, V.H., Rohatgi, R., Shewmaker, F., Naik, M.T., Mittag, T., Ayala, Y.M., Fawzi, N.L., 2018. A single N-terminal phosphomimic disrupts TDP-43 polymerization, phase separation, and RNA splicing. *EMBO J.* 37, e97452. <https://doi.org/10.15252/embj.201797452>
- Wang, C., Terrigno, M., Li, J., Distler, T., Pandya, N.J., Ebeling, M., Tyanova, S., Hoozemans, J.J.M., Dijkstra, A.A., Fuchs, L., Xiang, S., Bonni, A., Grüninger, F., Jagasia, R., 2023. Increased G3BP2-Tau interaction in tauopathies is a natural defense against Tau aggregation. *Neuron* 111, 2660-2674.e9. <https://doi.org/10.1016/j.neuron.2023.05.033>
- Wang, J., Choi, J.-M., Holehouse, A.S., Lee, H.O., Zhang, X., Jahnel, M., Maharana, S., Lemaître, R., Pozniakovsky, A., Drechsel, D., Poser, I., Pappu, R.V., Alberti, S., Hyman, A.A., 2018. A Molecular Grammar Governing the Driving Forces for Phase Separation of Prion-like RNA Binding Proteins. *Cell* 174, 688-699.e16. <https://doi.org/10.1016/j.cell.2018.06.006>
- Wang, J., Wang, B., Zhou, T., 2022. The Advance on Frontotemporal Dementia (FTD)'s Neuropathology and Molecular Genetics. *Mediators Inflamm.* 2022, 5003902. <https://doi.org/10.1155/2022/5003902>
- Wang, Y., Balaji, V., Kaniyappan, S., Krüger, L., Irsen, S., Tepper, K., Chandupatla, R., Maetzler, W., Schneider, A., Mandelkow, E., Mandelkow, E.-M., 2017. The release and trans-synaptic transmission of Tau via exosomes. *Mol. Neurodegener.* 12, 5. <https://doi.org/10.1186/s13024-016-0143-y>
- Wang, Y., Mandelkow, E., 2016. Tau in physiology and pathology. *Nat. Rev. Neurosci.* 17, 22–35. <https://doi.org/10.1038/nrn.2015.1>
- Ward, S.M., Himmelstein, D.S., Lancia, J.K., Binder, L.I., 2012. Tau oligomers and tau toxicity in neurodegenerative disease. *Biochem. Soc. Trans.* 40, 667–671. <https://doi.org/10.1042/BST20120134>
- Wegmann, S., Eftekharzadeh, B., Tepper, K., Zoltowska, K.M., Bennett, R.E., Dujardin, S., Laskowski, P.R., MacKenzie, D., Kamath, T., Commins, C., Vanderburg, C., Roe, A.D., Fan, Z., Molliex, A.M., Hernandez-Vega, A., Muller, D., Hyman, A.A., Mandelkow, E., Taylor, J.P., Hyman, B.T., 2018. Tau protein liquid-liquid phase separation can initiate tau aggregation. *EMBO J.* 37, e98049. <https://doi.org/10.15252/embj.201798049>
- Wegmann, S., Nicholls, S., Takeda, S., Fan, Z., Hyman, B.T., 2016. Formation, release, and internalization of stable tau oligomers in cells. *J. Neurochem.* 139, 1163–1174. <https://doi.org/10.1111/jnc.13866>
- Westermarck, P., Benson, M.D., Buxbaum, J.N., Cohen, A.S., Frangione, B., Ikeda, S.-I., Masters, C.L., Merlini, G., Saraiva, M.J., Sipe, J.D., Nomenclature Committee of the International Society of Amyloidosis, 2005. Amyloid: toward terminology clarification.

- Report from the Nomenclature Committee of the International Society of Amyloidosis. *Amyloid Int. J. Exp. Clin. Investig. Off. J. Int. Soc. Amyloidosis* 12, 1–4. <https://doi.org/10.1080/13506120500032196>
- Wheeler, R.J., 2020. Therapeutics-how to treat phase separation-associated diseases. *Emerg. Top. Life Sci.* 4, 307–318. <https://doi.org/10.1042/ETLS20190176>
- Williams, D.R., Lees, A.J., 2009. Progressive supranuclear palsy: clinicopathological concepts and diagnostic challenges. *Lancet Neurol.* 8, 270–279. [https://doi.org/10.1016/S1474-4422\(09\)70042-0](https://doi.org/10.1016/S1474-4422(09)70042-0)
- Wilson, D., Heron, C.L., Anderson, T., 2021. Corticobasal syndrome: a practical guide. *Pract. Neurol.* 21, 276–285. <https://doi.org/10.1136/practneurol-2020-002835>
- Wilson, D.M., Cookson, M.R., Van Den Bosch, L., Zetterberg, H., Holtzman, D.M., Dewachter, I., 2023. Hallmarks of neurodegenerative diseases. *Cell* 186, 693–714. <https://doi.org/10.1016/j.cell.2022.12.032>
- Wilson, R.S., Yu, L., Trojanowski, J.Q., Chen, E.-Y., Boyle, P.A., Bennett, D.A., Schneider, J.A., 2013. TDP-43 Pathology, Cognitive Decline, and Dementia in Old Age. *JAMA Neurol.* 70. <https://doi.org/10.1001/jamaneurol.2013.3961>
- Winton, M.J., Igaz, L.M., Wong, M.M., Kwong, L.K., Trojanowski, J.Q., Lee, V.M.-Y., 2008. Disturbance of nuclear and cytoplasmic TAR DNA-binding protein (TDP-43) induces disease-like redistribution, sequestration, and aggregate formation. *J. Biol. Chem.* 283, 13302–13309. <https://doi.org/10.1074/jbc.M800342200>
- Wolfson, C., Gauvin, D.E., Ishola, F., Oskoui, M., 2023. Global Prevalence and Incidence of Amyotrophic Lateral Sclerosis. *Neurology* 101, e613–e623. <https://doi.org/10.1212/WNL.0000000000207474>
- Wolozin, B., Ivanov, P., 2019. Stress granules and neurodegeneration. *Nat. Rev. Neurosci.* 20, 649–666. <https://doi.org/10.1038/s41583-019-0222-5>
- Wu, R., Zhou, D., Shen, X., Chen, F., Liu, F., Gu, J., 2021. Phosphorylation of trans-active response DNA-binding protein-of 43 kDa promotes its cytoplasmic aggregation and modulates its function in tau mRNA stability and exon 10 alternative splicing. *J. Neurochem.* 158, 766–778. <https://doi.org/10.1111/jnc.15450>
- Yamashita, S., Sakashita, N., Yamashita, T., Tawara, N., Tasaki, M., Kawakami, K., Komohara, Y., Fujiwara, Y., Kamikawa, M., Nakagawa, T., Hirano, T., Maeda, Y., Hasegawa, M., Takeya, M., Ando, Y., 2014. Concomitant accumulation of α -synuclein and TDP-43 in a patient with corticobasal degeneration. *J. Neurol.* 261, 2209–2217. <https://doi.org/10.1007/s00415-014-7491-8>
- Yan, X., Kuster, D., Mohanty, P., Nijssen, J., Pombo-García, K., Rizuan, A., Franzmann, T.M., Sergeeva, A., Passos, P.M., George, L., Wang, S.-H., Shenoy, J., Danielson, H.L., Honigsmann, A., Ayala, Y.M., Fawzi, N.L., Mittal, J., Alberti, S., Hyman, A.A., 2024. Intra-condensate demixing of TDP-43 inside stress granules generates pathological aggregates. *BioRxiv Prepr. Serv. Biol.* 2024.01.23.576837. <https://doi.org/10.1101/2024.01.23.576837>
- Yang, M., Qi, R., Liu, Y., Shen, X., Zhao, Y., Jin, N., Wu, R., Liu, F., Gu, J., 2023. Casein Kinase 1 δ Phosphorylates TDP-43 and Suppresses Its Function in Tau mRNA Processing. *J. Alzheimers Dis.* 91, 1527–1539. <https://doi.org/10.3233/JAD-220985>

- Yang, W., Sopper, M.M., Leystra-Lantz, C., Strong, M.J., 2003. Microtubule-associated tau protein positive neuronal and glial inclusions in ALS. *Neurology* 61, 1766–1773. <https://doi.org/10.1212/01.wnl.0000099372.75786.f8>
- Yang, W., Strong, M.J., 2012. Widespread neuronal and glial hyperphosphorylated tau deposition in ALS with cognitive impairment. *Amyotroph. Lateral Scler. Off. Publ. World Fed. Neurol. Res. Group Mot. Neuron Dis.* 13, 178–193. <https://doi.org/10.3109/17482968.2011.622405>
- Ye, H., Han, Y., Li, P., Su, Z., Huang, Y., 2022. The Role of Post-Translational Modifications on the Structure and Function of Tau Protein. *J. Mol. Neurosci.* 72, 1557–1571. <https://doi.org/10.1007/s12031-022-02002-0>
- Yoshiyama, Y., Lee, V.M., Trojanowski, J.Q., 2001. Frontotemporal dementia and tauopathy. *Curr. Neurol. Neurosci. Rep.* 1, 413–421. <https://doi.org/10.1007/s11910-001-0100-0>
- Yuzwa, S.A., Cheung, A.H., Okon, M., McIntosh, L.P., Vocadlo, D.J., 2014. O-GlcNAc modification of tau directly inhibits its aggregation without perturbing the conformational properties of tau monomers. *J. Mol. Biol.* 426, 1736–1752. <https://doi.org/10.1016/j.jmb.2014.01.004>
- Zbinden, A., Pérez-Berlanga, M., De Rossi, P., Polymenidou, M., 2020. Phase Separation and Neurodegenerative Diseases: A Disturbance in the Force. *Dev. Cell* 55, 45–68. <https://doi.org/10.1016/j.devcel.2020.09.014>
- Zhang, P., Fan, B., Yang, P., Temirov, J., Messing, J., Kim, H.J., Taylor, J.P., 2019. Chronic optogenetic induction of stress granules is cytotoxic and reveals the evolution of ALS-FTD pathology. *eLife* 8, e39578. <https://doi.org/10.7554/eLife.39578>
- Zhang, X., Lin, Y., Eschmann, N.A., Zhou, H., Rauch, J.N., Hernandez, I., Guzman, E., Kosik, K.S., Han, S., 2017. RNA stores tau reversibly in complex coacervates. *PLoS Biol.* 15, e2002183. <https://doi.org/10.1371/journal.pbio.2002183>
- Zhang, X., Vigers, M., McCarty, J., Rauch, J.N., Fredrickson, G.H., Wilson, M.Z., Shea, J.-E., Han, S., Kosik, K.S., 2020. The proline-rich domain promotes Tau liquid-liquid phase separation in cells. *J. Cell Biol.* 219, e202006054. <https://doi.org/10.1083/jcb.202006054>
- Zhu, S., Shen, Z., Wu, X., Han, W., Jia, B., Lu, W., Zhang, M., 2024. Demixing is a default process for biological condensates formed via phase separation. *Science* 384, 920–928. <https://doi.org/10.1126/science.adj7066>

8 ACKNOWLEDGEMENTS

First of all, I would like to thank my supervisors, Dorothee Dormann and Dieter Edbauer. Doro, thank you for your precious guidance throughout my PhD journey and your immense support on every decision I have taken during this path. You taught me a lot, not only about science, but also how to combine professionalism with kindness and empathy.

Eddie, thank you for giving me the opportunity to join your lab and becoming part of your group from the very start. I have learnt a lot from you, and your valuable advice and support during crucial moments of my PhD have made significant difference.

I am deeply grateful to all the past and present members of my labs (AG Dormann and AG Edbauer), for sharing their knowledge, assistance in the lab, and all the fun outside of work have enriched my experience.

A special thanks to Saskia for her immense help, kindness, and patience throughout the whole time, even across distances. To Lara and Eszter for being my colleague mates every day, sharing both the highs and lows. To Henni and Berkcan for the big support in the lab, always with a smile, and to Annika, another talented scientist and beautiful person I met during my PhD.

A big thank to the GSN for accepting me into this remarkable PhD program, and to all the staff members for their patience and support at every step of the PhD journey.

To my dearest friends, thank you for always being there, brightening my challenging moments, but especially for creating unforgettable memories together.

To my lovely family, thank you for the constant support you are always giving me, for your fundamental help and advice in crucial situations, but mostly for trusting in me and all my decisions. I feel your love and your admiration, and this gives me the strength to make important decisions and pursue my desires.

To Robert, thank you for being by my side through everything, now and always.

I utilized OpenAI's ChatGPT to assist in improving the clarity and language of certain passages of this thesis. All content, ideas, and conclusions are my own.

9 CURRICULUM VITAE

● EDUCATION

- **PH.D. DOCTORAL DEGREE in Cellular and Molecular Neuroscience** – 09/2019 – 11/2024
Graduate School of Systemic Neurosciences (GSN), Ludwig-Maximilians-Universität (LMU), **Munich**, Germany
- **MSc, MASTER DEGREE in Neuroscience** – 10/2016 – 03/2019
Università degli Studi di Trieste, **Trieste**, Italy
Final Grade: 110/110 cum laude
- **BSc, BACHELOR DEGREE in Biotechnologies** – 10/2013 – 10/2016
Università degli Studi di Trieste, **Trieste**, Italy
Final Grade: 110/110 cum laude

● WORK EXPERIENCE

- **PH.D.** project - 09/2019 – 12/2024
Joint PhD fellowship in the research groups of Pr. Dorothee DORMANN and Dr. Dieter EDBAUER
Deutsches Zentrum für Neurodegenerative Erkrankungen (DZNE), **Munich**, Germany
- **VOLUNTARY INTERNSHIP** - 05/2019 – 08/2019
Neuromet research group of Pr. Helle S. WAAGEPETERSEN and ass. Pr. Blanca Irene ALDANA GARCIA
University of Copenhagen, **Copenhagen**, Denmark
- **MASTER THESIS INTERNSHIP** - 03/2018 – 03/2019
Neuromolecular basis of Epilepsy syndrome research group of Pr. Anna-Elina LEHESJOKI
Folkhälsan Research Center - Biomedicum Helsinki, **Helsinki**, Finland
- **VOLUNTARY INTERNSHIP** - 09/2017 – 09/2017
Clinical Neuroimmunology research group of Dr. Roberto FURLAN
Ospedale San Raffaele, **Milano**, Italy
- **BACHELOR THESIS INTERNSHIP + VOLUNTARY INTERNSHIP** - 08/2015 – 05/2017
Neurobiology research group of Dr. Fabian FEIGUIN
International Center for Genetic Engineering and Biotechnology (ICGeB), **Trieste**, Italy

● ACHIEVEMENTS AND AWARDS

- Admission at the Graduate School of Systemic Neurosciences (2021), **LMU-Munich**, Germany
- EURES-Traineeship Individual Program scholarship (2019) to work at the **University of Copenhagen**, Denmark
- ERASMUS PLACEMENT (2018) scholarship to work at the **University of Helsinki**, Finland
- EUROPEAN UNION PROGRAM (ERASMUS, 2016) to study at the **University of Gothenburg**, Sweden

● WORK MANAGEMENT SKILLS

- Project Management Professional (PMP) certification, **University of California**, Irvine (Coursera, online) – ongoing
- Fast Forward Implementation Program, **Mind Matters** (online) – final certificate obtained in May 2024
- Good Manufacturing Practice (GMP) course, **GMP Academy** (online) – final certificate obtained in November 2023
- Conflict Management workshop, DZNE, **Bonn** Germany – October 2022
- Project management, GSN, **Munich** Germany – October 2021

● PRESENTATION SKILLS

- Neurobiology of Brain Disorders Gordon Research Conference (GRC), **Barcelona**, Spain – August 2024 (poster)
- 1st Biennial Conference on TDP-43 function and dysfunction in disease, **Trieste** Italy – September 2023 (poster)
- DZNE Retreat, **Bonn** Germany – October 2022 (poster)
- CURE-ND Early Career Researchers, UK Dementia Research Institute, **London** UK - May 2022 (poster)
- GSN-LMU virtual Retreat, GSN, **Munich** Germany – December 2021 (talk)
- Molecular Neurodegeneration and Therapeutic Approaches – Wellcome Genome Campus **UK** – January 2021 (talk)

● IT SKILLS

- MS office: proficient in Word, Excel, Power Point
- Python course, DZNE, **Munich** Germany – January 2022
- Science: proficient in GraphPad Prism, ImageJ, ZEN, CLC

● LANGUAGES

- Italian, mother tongue
- English, level C1 (proficient)
- German, level B1 (basic) – ongoing course

10 LIST OF PUBLICATIONS

- Direct binding of TDP-43 and Tau drives their co-condensation and suppresses Tau fibril formation
(submitted)

Francesca Simonetti, Saskia Hutten, Lisa Marie Ramirez, Henrick Riemenschneider, Janine Hochmair, Martina Schifferer, Ali Rezaei, Ivan Urosevic, Weijia Zhong, Viktoria Ruf, Tammarny Lashley, Mikael Simons, Markus Zweckstetter, Magdalini Polymenidou, Susanne Wegmann, Dieter Edbauer, Dormann Dormann

- The new missense G376V-TDP-43 variant induces late-onset distal myopathy but not amyotrophic lateral sclerosis
Brain, Volume 147, Issue 5, May 2024, Pages 1768–1783
doi: 10.1093/brain/awad410

Julia Zibold, Lola E R Lessard, Flavien Picard, Lara Gruijs da Silva, Yelyzaveta Zadorozhna, Nathalie Streichenberger, Edwige Belotti, Alexis Osseni, Andréa Emerit, Elisabeth Errazuriz-Cerda, Laurence Michel-Calemard, Rita Menassa, Laurent Coudert, Manuela Wiessner, Rolf Stucka, Thomas Klopstock, **Francesca Simonetti**, Saskia Hutten, Takashi Nonaka, Masato Hasegawa, Tim M Strom, Emilien Bernard, Elisabeth Ollagnon, Andoni Urtizberea, Dorothee Dormann, Philippe Petiot, Laurent Schaeffer, Jan Senderek, Pascal Leblanc

- Targeting the glycine-rich domain of TDP-43 with antibodies prevents its aggregation in vitro and reduces neurofilament levels in vivo
Acta Neuropathologica Communications volume 11, Article number: 112 (2023)
doi: 10.1186/s40478-023-01592-z

Henrick Riemenschneider, **Francesca Simonetti**, Udit Sheth, Eszter Katona, Stefan Roth, Saskia Hutten, Daniel Farny, Meike Michaelsen, Brigitte Nuscher, Michael K. Schmidt, Andrew Flatley, Aloys Schepers, Lara A. Gruijs da Silva, Qihui Zhou, Thomas Klopstock, Arthur Liesz, Thomas Arzberger, Jochen Herms, Regina Feederle, Tania F. Gendron, Dorothee Dormann and Dieter Edbauer

- Disease-linked TDP-43 hyperphosphorylation suppresses TDP-43 condensation and aggregation
EMBO J (2022) 41: e108443
doi: 10.15252/embj.2021108443

Lara A Gruijs da Silva, **Francesca Simonetti**, Saskia Hutten, Henrick Riemenschneider, Erin L Sternburg, Lisa M Pietrek, Jakob Gebel, Volker Dötsch, Dieter Edbauer, Gerhard Hummer, Lukas S Stelzl & Dorothee Dormann

- Cystatin B-deficiency triggers ectopic histone H3 tail cleavage during neurogenesis
Neurobiology of disease (2021) 156:105418
doi: 10.1016/j.nbd.2021

Eduard Daura, Saara Tegelberg, Masahito Yoshihara, Christopher Jackson, **Francesca Simonetti**, Katri Aksentjeff, Sini Ezer, Paula Hakala, Shintaro Katayama, Juha Kere, Anna-Elina Lehesjoki, Tarja Joensuu

- Nuclear import receptors directly bind to arginine-rich dipeptide repeat proteins and suppress their pathological interactions
Cell Reports volume 33, issue 12, 108538, December 2020
doi: 10.1016/j.celrep.2020.108538

Saskia Hutten, Sinem Usluer, Benjamin Bourgeois, **Francesca Simonetti**, Hana M Odeh, Charlotte M Fare, Mareike Czuppa, Marian Hruska-Plochan, Mario Hofweber, Magdalini Polymenidou, James Shorter, Dieter Edbauer, Tobias Madl, Dorothee Dormann

11 DECLARATION OF AUTHOR CONTRIBUTIONS

PUBLICATION I

(Grujjs da Silva et al., 2022) 'Disease-linked TDP-43 hyperphosphorylation suppresses TDP-43 condensation and aggregation'

Lara A Grujjs da Silva, **Francesca Simonetti**, Saskia Hutten, Henrick Riemenschneider, Erin L Sternburg, Lisa M Pietrek, Jakob Gebel, Volker Dötsch, Dieter Edbauer, Gerhard Hummer, Lukas S Stelzl & Dorothee Dormann

Lara A Grujjs da Silva: Investigation; Visualization; Methodology; Writing—original draft; Writing—review and editing. **Francesca Simonetti**: Investigation; Visualization; Methodology: performed the aggregation assay, the semi-denaturing detergent agarose gel electrophoresis (SDD-AGE) and some of the experiments with primary hippocampal neurons; Writing—review and editing. Saskia Hutten: Investigation; Visualization; Methodology: performed the nuclear import and the semi-permeabilized cell assays; Writing—review and editing. Henrick Riemenschneider: Investigation; Visualization; Methodology: generated the lentiviral constructs and performed most of the experiments with primary hippocampal neurons; Writing—review and editing. Erin L Sternburg: Investigation; Visualization; Methodology: performed the electrophoretic mobility shift assay (EMSA); Writing—review and editing. Lisa M Pietrek: Methodology. Jakob Gebel: Resources; Investigation; Methodology. Volker Dötsch: Resources. Dieter Edbauer: Resources; Supervision; Methodology; Writing—review and editing. Gerhard Hummer: Resources; Methodology; Writing—review and editing. Lukas D Stelzl: Investigation; Visualization; Methodology: performed the atomistic and coarse-grained simulations; Writing—original draft; Writing—review and editing. Dorothee Dormann: Conceptualization; Supervision; Funding acquisition; Writing—original draft; Writing—review and editing.

My contribution to this publication in detail:

For this publication, I conducted the TDP-43 *in vitro* aggregation assay with WT TDP-43 and the related phosphomimetic mutants (5D, 12D and 12A), followed by imaging with a confocal microscope (Fig. 2D). Additionally, I established and executed the semi-denaturing detergent agarose gel electrophoresis (SDD-AGE) assay for WT TDP-43 and the related phosphomimetic mutants (Fig. 2E, F). Furthermore, I carried out the stress granule recruitment assay in primary neurons, performing the cellular stress experiment to induce intracellular stress granules, and acquired the final images for WT TDP-43, 12D-NLSmutant and 12A-NLSmutant (Fig. 6E). Finally, I interpreted the data, participated in project discussions, and provided feedback on the manuscript.

PUBLICATION II

(Riemenschneider et al., 2023) 'Targeting the glycine-rich domain of TDP-43 with antibodies prevents its aggregation *in vitro* and reduces neurofilament levels *in vivo*'

Henrick Riemenschneider, **Francesca Simonetti**, Udit Sheth, Eszter Katona, Stefan Roth, Saskia Hutten, Daniel Farny, Meike Michaelsen, Brigitte Nuscher, Michael K. Schmidt, Andrew Flatley, Aloys Schepers, Lara A. Gruijs da Silva, Qihui Zhou, Thomas Klopstock, Arthur Liesz, Thomas Arzberger, Jochen Herms, Regina Feederle, Tania F. Gendron, Dorothee Dormann and Dieter Edbauer

HR performed, analyzed and interpreted animal and most *in vitro* experiments with help from FS, SH, DF, MM, BN, LAGS and QZ. EK prescreened novel monoclonal TDP-43 antibodies and acquired the cytokine data. US conducted and analyzed the pTDP-43 immunoassay. SR and AL helped acquiring and analyzing flow cytometry data. MKS performed automated IHC stainings. AF, AS and RF generated novel monoclonal TDP-43 antibodies. TK contributed to the conception of the study. TA and JH provided human tissue and supervised neuropathological analysis. TFG supervised and interpreted pTDP-43 immunoassays. DD supervised and interpreted *in vitro* experiments. DE designed, supervised and interpreted the study and helped with data analysis. DE wrote the manuscript with input from all other authors. All authors read and approved the final manuscript.

My contribution to this publication in detail:

For this publication, I instructed Henrick Riemenschneider (HR, first author) how to perform fluorescent labeling of recombinant proteins and *in vitro* condensation and aggregation assays of TDP-43. I assisted him during the experiment realization and image acquisition (Fig. 7). Furthermore, I conducted the cellular uptake experiment (imaging + analysis) with pHrodo-labeled TDP-43 in presence of different monoclonal antibodies in SH-SY5Y cells, which was included in the first submitted version of the manuscript.

Finally, I interpreted the data, participated in project discussions, and provided feedback on the manuscript.

PUBLICATION III

(Simonetti et al., in submission) 'Binding of TDP-43 to the core fibrillization region of Tau drives their co-condensation and suppresses Tau fibril formation'

Francesca Simonetti, Lisa Marie Ramirez, Saskia Hutten, Henrick Riemenschneider, Janine Hochmair, Martina Schifferer, Ali Rezaei, Weijia Zhong, Viktoria Ruf, Tammaryn Lashley, Mikael Simons, Magdalini Polymenidou, Susanne Wegmann, Markus Zweckstetter, Dieter Edbauer, Dormann Dormann

Conceptualization: F.S., D.E., D.D. Methodology: F.S., L.M.R., S.H., J.H., H.R., M.S., W.Z., T.L., M.P., S.W., M.Z., D.E., D.D.; L.M.R. performed dynamic light scattering (DLS) and nuclear magnetic resonance (NMR) experiments; W.Z. performed SarkoSpin preparation on brain homogenates; M.S. took some of the final images (Fig. 5b) using the EM microscope. Software Programming: A.R. Validation: F.S., D.E., D.D. Formal Analysis: F.S., L.M.R., A.R. Investigation: F.S., L.M.R., S.H., M.S., W.Z., Resources: M.S., V.R., T.L., M.P., S.W., M.Z., D.E., D.D. Data Curation: F.S., L.M.R., A.R. Writing – Original: F.S., D.E., D.D. Writing – Review & Editing: all. Visualization: F.S., L.M.R., S.H., S.W., M.Z., D.E., D.D. Supervision: D.E., D.D. Project Administration: D.E., D.D. Funding Acquisition: D.E., D.D.

My contribution to this publication in details:

As first author of this publication, I designed, carried out and analyzed most of the experiments, created all figures and wrote and edited the manuscript under the supervision of Prof. Dr. Dorothee Dormann and Prof. Dr. Dieter Edbauer.